NEUROMECHANICAL PROPERTY IDENTIFICATION IN SPASTIC MUSCLES: PERSPECTIVES FOR INSTRUMENTED ASSESSMENT, MODELING AND INTERVENTION EVALUATION

EDITED BY: Ruoli Wang, Elena Marie Gutierrez Farewik, Le Li, Lynn Bar-On and Ping Zhou

PUBLISHED IN: Frontiers in Bioengineering and Biotechnology and Frontiers in Neuroscience

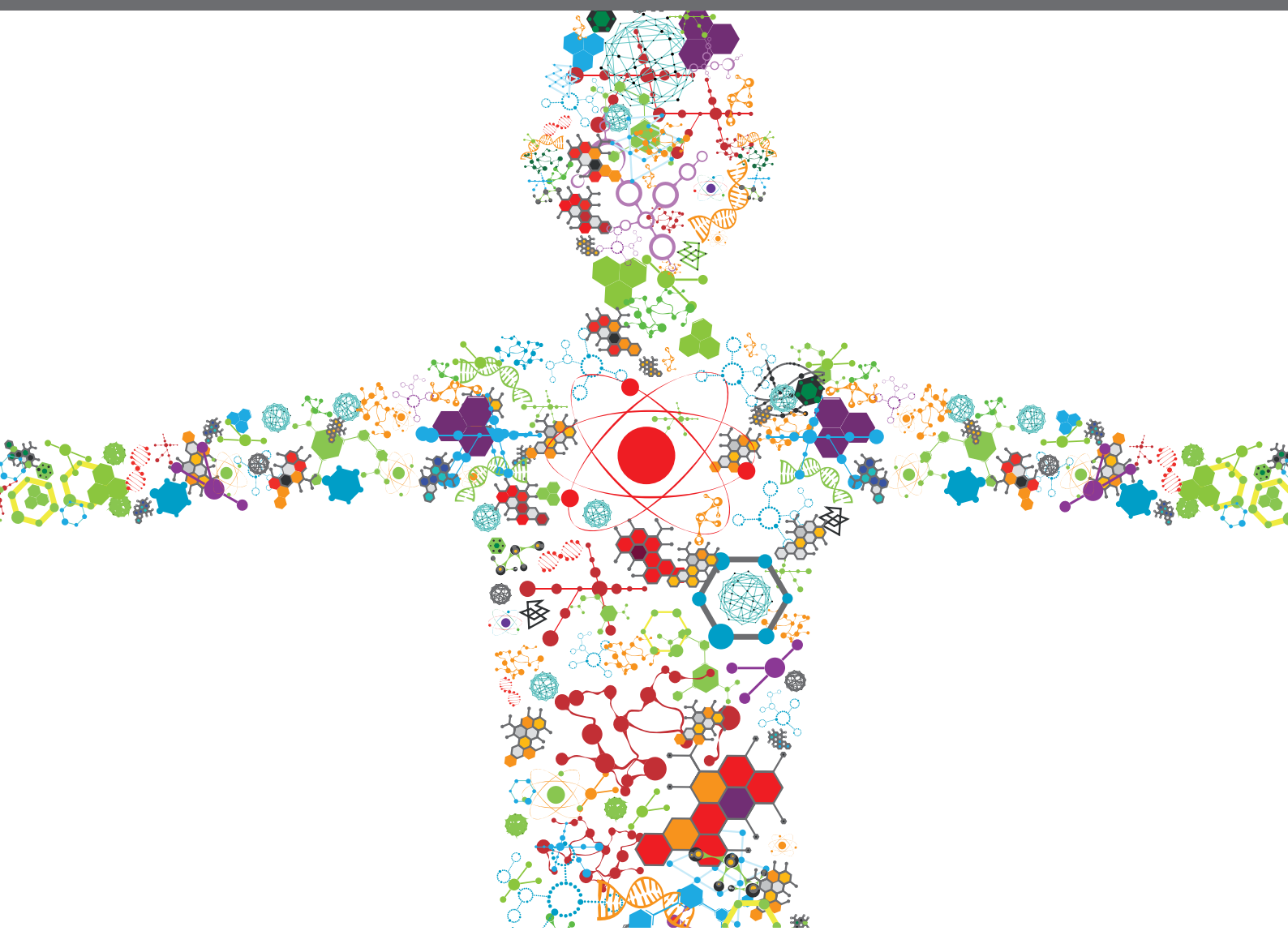

frontiers Research Topics

ISSN 1664-8714
ISBN 978-2-88971-140-6
DOI 10.3389/978-2-88971-140-6

About Frontiers

Frontiers is more than just an open-access publisher of scholarly articles: it is a pioneering approach to the world of academia, radically improving the way scholarly research is managed. The grand vision of Frontiers is a world where all people have an equal opportunity to seek, share and generate knowledge. Frontiers provides immediate and permanent online open access to all its publications, but this alone is not enough to realize our grand goals.

Frontiers Journal Series

The Frontiers Journal Series is a multi-tier and interdisciplinary set of open-access, online journals, promising a paradigm shift from the current review, selection and dissemination processes in academic publishing. All Frontiers journals are driven by researchers for researchers; therefore, they constitute a service to the scholarly community. At the same time, the Frontiers Journal Series operates on a revolutionary invention, the tiered publishing system, initially addressing specific communities of scholars, and gradually climbing up to broader public understanding, thus serving the interests of the lay society, too.

Dedication to Quality

Each Frontiers article is a landmark of the highest quality, thanks to genuinely collaborative interactions between authors and review editors, who include some of the world's best academicians. Research must be certified by peers before entering a stream of knowledge that may eventually reach the public - and shape society; therefore, Frontiers only applies the most rigorous and unbiased reviews.
Frontiers revolutionizes research publishing by freely delivering the most outstanding research, evaluated with no bias from both the academic and social point of view. By applying the most advanced information technologies, Frontiers is catapulting scholarly publishing into a new generation.

What are Frontiers Research Topics?

Frontiers Research Topics are very popular trademarks of the Frontiers Journals Series: they are collections of at least ten articles, all centered on a particular subject. With their unique mix of varied contributions from Original Research to Review Articles, Frontiers Research Topics unify the most influential researchers, the latest key findings and historical advances in a hot research area! Find out more on how to host your own Frontiers Research Topic or contribute to one as an author by contacting the Frontiers Editorial Office: frontiersin.org/about/contact

NEUROMECHANICAL PROPERTY IDENTIFICATION IN SPASTIC MUSCLES: PERSPECTIVES FOR INSTRUMENTED ASSESSMENT, MODELING AND INTERVENTION EVALUATION

Topic Editors:
Ruoli Wang, Royal Institute of Technology, Sweden
Elena Marie Gutierrez Farewik, Royal Institute of Technology, Sweden
Le Li, Northwestern Polytechnical University, China
Lynn Bar-On, Amsterdam University Medical Center, Netherlands
Ping Zhou, The University of Rehabilitation, China

Citation: Wang, R., Farewik, E. M. G., Li, L., Bar-On, L., Zhou, P., eds. (2021). Neuromechanical Property Identification in Spastic Muscles: Perspectives for Instrumented Assessment, Modeling and Intervention Evaluation. Lausanne: Frontiers Media SA. doi: 10.3389/978-2-88971-140-6

Table of Contents

frontiers in Bioengineering and Biotechnology

ORIGINAL RESEARCH
published: 09 June 2020
doi: 10.3389/fbioe.2020.00613

Intramuscular Fat in the Medial Gastrocnemius Muscle of People Who Have Had a Stroke

Arkiev D'Souza[1,2], *Bart Bolsterlee*[1,3]* *and Robert D. Herbert*[1,2]

[1] NeuRA, Randwick, NSW, Australia, [2] School of Medical Sciences, University of New South Wales, Randwick, NSW, Australia, [3] Graduate School of Biomedical Engineering, University of New South Wales, Randwick, NSW, Australia

Objective: To compare intramuscular fat fraction in people who have ankle contractures following stroke with the intramuscular fat fraction in control participants.

Design: mDixon MRI images were used to quantify intramuscular fat fractions in the medial gastrocnemius muscles of people who had experienced a hemiparetic stroke ($n = 14$, mean age 60 ± 13 years) and control participants ($n = 18$, mean age 66 ± 12 years).

Results: Intramuscular fat fractions were similar in the paretic and non-paretic sides of stroke patients (mean on paretic side 14.5%, non-paretic side 12.8%, difference 1.6%, 95% confidence interval −0.7 to 4.1%). The intramuscular fat fraction on the paretic side was higher than in the control group (mean intramuscular fat fraction in control muscles 7.6%; difference 7.8%, 95% confidence interval 4.6–10.9%). The difference between intramuscular fat fractions in non-paretic and control legs increased with age. Body mass index was similar in stroke patients and controls. There was no association between medial gastrocnemius intramuscular fat fraction and dorsiflexion range.

Conclusion: Muscles of stroke patients had elevated intramuscular fat fractions compared to muscles from control participants which were not explained by differences in body mass index. There is no clear relationship between intramuscular fat in the medial gastrocnemius muscle and dorsiflexion range of motion.

Keywords: intramuscular fat, stroke, contracture, mDixon MRI, medial gastrocnemius

OPEN ACCESS

Edited by:
Ping Zhou,
University of Texas Health Science Center at Houston, United States

Reviewed by:
Carrie Lynn Peterson,
Virginia Commonwealth University, United States
Cliff Klein,
Guangdong Province Work Injury Rehabilitation Hospital, China

***Correspondence:**
Bart Bolsterlee
b.bolsterlee@neura.edu.au

Specialty section:
This article was submitted to Biomechanics, a section of the journal Frontiers in Bioengineering and Biotechnology

Received: *12 December 2019*
Accepted: *19 May 2020*
Published: *09 June 2020*

Citation:
D'Souza A, Bolsterlee B and Herbert RD (2020) Intramuscular Fat in the Medial Gastrocnemius Muscle of People Who Have Had a Stroke. Front. Bioeng. Biotechnol. 8:613. doi: 10.3389/fbioe.2020.00613

INTRODUCTION

Contracture is a loss in joint range of motion caused by the increase in passive stiffness of muscles (Fergusson et al., 2006; Harvey et al., 2017). Contractures can severely compromise the ability to execute activities of daily living (O'Dwyer et al., 1996). People who have had a stroke often develop ankle joint contractures (Kwah et al., 2012a). It is difficult to treat contractures because the mechanisms that lead to the increased muscle stiffness are poorly understood.

In addition to contracture, stroke patients also commonly experience muscle weakness. Muscle weakness can be due to central mechanisms such as impaired descending drive to the muscle, but it may also be due to alterations at the periphery, such as reduced muscle size and physiological cross-sectional area. Alterations within the muscle, such as the infiltration of fat, reduce the cross-sectional area of muscle fibers per unit cross-sectional area of muscle, compounding to the deleterious effects of reduced muscle volume on muscle strength. Furthermore, computer

simulations suggest that the presence of intramuscular fat increases muscle stiffness (Rahemi et al., 2015), implying that the proliferation of intramuscular fat could contribute to the development of both contractures and muscle weakness.

Several studies have investigated fat content in limbs of stroke patients. People who have had a stroke tend to have more intramuscular fat than people who have not had a stroke (Akazawa et al., 2018). It has been reported that the paretic side has more fat (Iversen et al., 1989; Jorgensen and Jacobsen, 2001), or a greater proportion of intramuscular fat (Ryan et al., 2002) than the non-paretic side, although one study found more intramuscular fat in non-paretic than paretic muscles (Ryan et al., 2011). Measurements of fat have been made using dual-energy X-ray absorptiometry (DEXA) (Iversen et al., 1989; Jorgensen and Jacobsen, 2001), ultrasound (Akazawa et al., 2018), computed tomography (CT) (Ryan et al., 2002, 2011), and T1-weighted magnetic resonance imaging (MRI) (Ramsay et al., 2011). All these techniques have limitations for quantifying intramuscular fat content. While DEXA can be used to find limb-specific fat content, it cannot be used to measure muscle-specific fat content. The validity of ultrasound fat quantification has not been demonstrated. T1-weighted MRI and CT do not directly measure fat but instead classify voxels as fat based on an image intensity threshold taken from voxels which are known to be comprised of fat, such as subcutaneous tissue. This can be problematic when in-field inhomogeneities are present (Burakiewicz et al., 2017) (i.e., when there is variation in signal intensity which is not due to fat content). While CT measurements are capable of obtaining measurements from a whole muscle, studies that have investigated intramuscular fat content in people who have had a stroke have obtained measurements from a single cross-sectional slice (Ryan et al., 2002) or a few slices (Ryan et al., 2011) which may not be representative of the whole muscle.

An alternative MRI technique called mDixon imaging can also be used to measure intramuscular fat (Kovanlikaya et al., 2005b; Wren et al., 2008; Karampinos et al., 2012; Noble et al., 2014a; Burakiewicz et al., 2017). This imaging technique exploits the difference in the resonant frequencies of protons in water and lipids to measure fat fractions in each voxel. mDixon scans can accurately (Kovanlikaya et al., 2005a; Fischer et al., 2014; Noble et al., 2014b) and reliably (Ponrartana et al., 2014) quantify muscle-specific, whole-muscle fat fractions *in vivo*. This technique has already been used to quantify intramuscular fat in populations with CP (Noble et al., 2014a) and muscular dystrophy (Burakiewicz et al., 2017), but has not yet been used to investigate intramuscular fat in people who have had a stroke.

In this study, mDixon imaging was used to compare the intramuscular fat fractions in the medial gastrocnemius muscles from the paretic and non-paretic sides of people with ankle contracture following hemiparetic stroke. Comparisons were also made between people who have and have not had a stroke. The medial gastrocnemius muscle was chosen in this study because stiffness of this muscle contributes to ankle joint contractures after stroke (Kwah et al., 2012b), and because of its functional significance in locomotion.

FIGURE 1 | The custom-built electronic goniometer used to measure dorsiflexion range. The participant was placed in a supine position. An 11 cm diameter foam roller was placed under the knee. The experimenter rotated the foot through dorsiflexion until 10 Nm was reached. Dorsiflexion range was defined as the angle between an accelerometer placed on the tibia and an accelerometer placed underneath the sole of the foot at 10 Nm of torque. Ankle angles below 90° indicate plantarflexion and above 90° dorsiflexion.

MATERIALS AND METHODS

We further analyzed MRI data obtained from the legs of 14 hemiparetic stroke patients and 18 control participants. We have previously reported analyses of muscle architecture in these participants (D'Souza et al., 2020) but have not previously published analyses of intramuscular fat.

All procedures were approved by the local human research ethics committee (HC number: HC15006). Written informed consent was obtained from all participants before participation.

Participants

Participants included in this study were at least 18 years of age and had loss of ankle range of motion resulting from stroke (stroke group), or had not had a stroke (control group). Where possible, an initial assessment was conducted to identify patients with contracture, defined as having $<5^{\circ}$ passive dorsiflexion with the knee extended as measured with a goniometer by an experienced physiotherapist. In most cases it was not possible to conduct the initial assessment because participants were not referred to the study by a physiotherapist. Such participants were screened over the telephone, and were eligible for participation if they self-identified (or were identified by a carer) as having a stiff ankle as a result of stroke. Additional inclusion criteria include having no recent history of orthopedic surgery or musculoskeletal injury, and an exclusion criterion was having received a botulinum toxin injection in the 6 months prior to the experiment. Participants were not excluded based on the severity of stroke, time since stroke, or walking ability.

Range of Motion Measurement

A custom-built electronic goniometer was used to measure passive dorsiflexion range (**Figure 1**). Dorsiflexion range was defined as the ankle angle between an accelerometer on the tibia and an accelerometer underneath the sole of the foot with 10 Nm

of torque applied to the sole of the foot. Ankle angles below 90° indicate plantarflexion and above 90° dorsiflexion.

The foot was strapped in a footplate equipped with a force transducer. The experimenter applied increasing force to the sole of the foot. While speed of rotation was not controlled, the same experimenter conducted the measurement on all participants. The measurement was taken with the participant lying supine and with a foam roller (11 cm diameter) positioned under the knee. Ten preconditioning rotations were conducted to minimize history-dependent effects, followed by five recordings. The mean of the five measurements was used as the participant's dorsiflexion range.

MRI Image Acquisition

Participants were positioned supine on the MRI scanner bed. A foam wedge was placed under the knee to prevent deformation of the calf from the weight of the shank. The participant was asked to remain relaxed during the scan. The left and right lower legs were scanned in separate acquisitions within the same scanning session.

A 3-Tesla MRI scanner (Achieva TX; Philips Medical Systems, Best, The Netherlands) with a 32-channel cardiac coil was used to obtain mDixon MRI images of both lower legs. A 3D multi-echo mDixon Fast Field Echo (FFE) scan was used. Three-hundred transverse anatomical slices were obtained covering the entire cross-section of the shank from the distal end of the femur to the ankle. The settings were: 2-point 3D mDixon FFE, TR/TE1/TE2 6.1/3.5/4.6 ms, field of view 180 × 180 mm, slice thickness 2 mm (1 mm over contiguous), acquisition matrix 180 × 180 (reconstructed to 192 × 192), reconstructed voxel size 0.94 × 0.94 × 1 mm, number of signal averages (NSA) 2 and scan time 164 s.

Intramuscular Fat Calculation

The mDixon imaging technique exploits the chemical shift difference between water and fat to produce an in-phase and out-of-phase image, from which a separate fat-saturated (**Figure 2A**) and water-saturated (**Figure 2B**) image can be obtained (Dixon, 1984). A fat fraction map (**Figure 2C**) was calculated using the ratio of water and fat signal intensities within each voxel:

$$fat\ fraction = \frac{I_{fat}}{I_{fat} + I_{water}} \times 100\%$$

where I_{fat} is the signal intensity from the fat-saturated image and I_{water} is the signal intensity from the water-saturated image.

The medial gastrocnemius muscle was manually outlined on all of the slices of the mDixon scan (on the out-of-phase image) using image processing software ITK-SNAP (Yushkevich et al., 2006). Segmentations were performed by a researcher with experience in segmenting muscles of the lower leg.

The intramuscular fat fraction of the medial gastrocnemius was calculated as the average fat fraction of all voxels in the muscle. Voxels at the boundary of the muscle were excluded from calculating the average to remove potential inaccuracies from partial volume effects and small segmentation errors. For participants who have had a stroke, separate measurements were obtained for the paretic and non-paretic side. For control participants, fat fractions of the left and right muscle were averaged.

Statistical Analysis

A sample size of 32 subjects is sufficient to detect a between-group difference in intramuscular fat fractions of 1 SD with a probability of ∼80%.

In the primary analysis, linear mixed models were used to compare the differences in mean intramuscular fat fraction between the paretic, non-paretic and control muscles. Participants were assigned random intercepts and age and group were modeled as fixed effects. We also determined whether the rate of change of intramuscular fat fraction with respect to age was the same across groups by adding an age by group interaction to the model.

Linear mixed models were also used to compare the mean differences between groups for dorsiflexion range of motion. Participants were assigned random intercepts and group was modeled as a fixed effect.

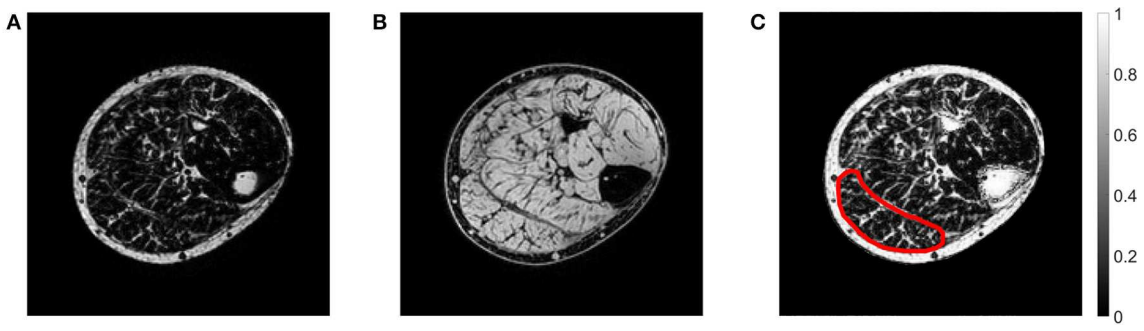

FIGURE 2 | Example of an axial mDixon image from the paretic leg of a stroke patient showing the **(A)** fat-saturated image, **(B)** water-saturated image, and **(C)** fat fraction map. In the fat fraction map, voxels with high fat fractions are white and voxels with low fat fractions are black. The slice is approximately midway between the ankle and the knee. The medial gastrocnemius muscle boundary has been outlined.

Secondary analyses explored the linear correlation between intramuscular fat fraction of the medial gastrocnemius and body mass index (BMI) and ankle dorsiflexion range. Separate correlation analyses were conducted for each group.

An additional linear mixed model was used to explore if the differences in mean intramuscular fat fraction between the paretic and non-paretic muscles varied with time since stroke. Participants were assigned random intercepts, and instead of age, time since stroke was modeled as a fixed effect along with group. We also determined whether the rate of change of intramuscular fat fraction with respect to time since stroke was the same across groups by adding a time since stroke by group interaction term to the model.

All statistical analyses were conducted using Matlab (version R2017b, The MathWorks Inc., Natick, Massachusetts, United States) statistics toolbox.

TABLE 1 | Participant characteristics.

	Stroke ($n = 14$)	Control ($n = 18$)	*P*
Age (years)	60 (13)	66 (12)	0.15
Gender (male/female)	10/4	15/3	0.42
Height (cm)	173 (7)	174 (9)	0.91
Weight (kg)	85 (18)	79 (14)	0.29
BMI (kg/m^2)	26 (7)	28 (4)	0.22
Time since stroke (years)	5 (4)	-	-
Paretic side (left/right)	7/7	-	-

Values are means (SD). An unpaired t-test was used to compare groups. A chi-square test was used to compare group differences for gender.

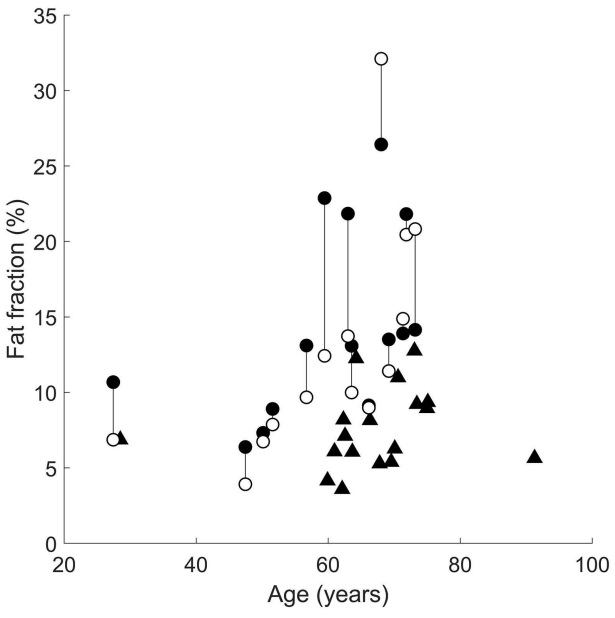

FIGURE 3 | Intramuscular fat fractions in the paretic (filled circles), non-paretic (open circles), and control (triangles) medial gastrocnemius muscles. Vertical lines join paretic and non-paretic muscles from individual stroke patients.

RESULTS

Participant Characteristics

Participant characteristics are shown in **Table 1**. No significant differences were detected between groups for age, height, weight, or BMI (unpaired *t*-test, $P > 0.05$ for all variables).

On average, the paretic, non-paretic, and control groups had 97° (*SD* 9°), 108° (8°), and 104° (7°) range of motion, respectively. On average, the paretic side of stroke patients had 11° (95% confidence interval 8–13°) less dorsiflexion range than the non-paretic side, and 7° (1–13°) less dorsiflexion range than in control participants. There was no significant difference in range of motion between the non-paretic and control legs (difference −4.0°, 95% confidence interval −9.1 to 1.2°).

Whole-Muscle Intramuscular Fat

The mean (*SD*) intramuscular fat fraction on the paretic and non-paretic sides were 14.5% (6.3%) and 12.8% (7.4%), respectively. The mean intramuscular fat fraction of the control medial gastrocnemius muscles was 7.6% (2.6%).

The following comparisons report the *absolute* difference in intramuscular fat fraction (in % of total muscle volume) of the medial gastrocnemius muscle between groups. In all but three patients, the paretic medial gastrocnemius muscle had a higher fraction of intramuscular fat than the non-paretic muscle (**Figure 3**). However, the difference in intramuscular fat fraction between the paretic and non-paretic muscles was not significant (difference 1.6%, 95% confidence interval −0.7 to 4.1%, $P = 0.2$). On average, the proportion of intramuscular fat in the paretic medial gastrocnemius muscles was 7.8% (4.6–10.9%, $P < 0.001$) higher than the control muscles (**Figure 3**). In the non-paretic versus control comparison the proportion of intramuscular fat in the non-paretic muscles was 6.5% (3.0–9.9%, $P < 0.001$) higher than the control muscles. However, in this comparison, the age by group interaction term was significant ($P = 0.01$), i.e., the difference between groups depended on age. At age 63 (the average age of all participants), the proportion of intramuscular fat in the non-paretic leg was 6.5% higher than the control leg.

In the comparison between the paretic and non-paretic groups, the interaction term was not significant, meaning that the rate of change of fat per year was the same for both groups. That is, both the paretic and non-paretic groups accumulated intramuscular fat at 0.3%/year (0.1–0.5%/year, $P = 0.01$).

Increases in intramuscular fat fraction were positively correlated with BMI in the paretic leg ($r^2 = 0.37$, $P = 0.02$), but not in the non-paretic and control leg (**Figures 4A–C** and **Table 2**). Range of motion did not correlate with intramuscular fat fraction in the paretic, non-paretic or control groups (**Figures 4D–F** and **Table 2**).

There was no effect of time since stroke on the difference in intramuscular fat fraction between the paretic and non-paretic muscles. The interaction between time since stroke and group was not significant (**Figure 5**).

DISCUSSION

The proportion of intramuscular fat in people who have had a stroke was compared to control participants using mDixon imaging. While the stroke patients had a moderate level contracture on the paretic side (Andersson and Cocchiarella, 2000), there was no difference in intramuscular fat fraction between the paretic and the non-paretic muscles of stroke patients. Muscles from both the paretic and non-paretic side had a higher proportion of intramuscular fat than the muscles from control participants. There was no difference in intramuscular fat fraction between the paretic and the non-paretic muscles of stroke patients.

Both the paretic and non-paretic muscles in the stroke group had a higher proportion of intramuscular fat than the control group. Reports of adaptations in both paretic and the non-paretic muscles after stroke are not new; Hunnicutt and Gregory showed that both sides have deficits in muscle size and strength compared to people who have not had a stroke (Hunnicutt and Gregory, 2017). It is not known why both sides undergo adaptations. One possible explanation is that decreased neural drive to the paretic side causes physical disability, and consequently, the non-paretic leg undergoes adaptation in response to disuse. This would imply that adaptations to the non-paretic side are not necessarily a direct consequence of having had a stroke, rather, it is an effect of being less mobile after stroke.

People who have had a stroke often have strength deficits. At the periphery, the physiological cross-sectional area (PCSA) of muscle will largely determine strength. The presence of intramuscular fat is likely to exacerbate muscle weakness caused by reduced muscle PCSA by reducing the proportion of the muscle cross-section composed of contractile proteins. The potential detrimental impact of intramuscular fat on muscle quality has previously been simulated (Rahemi et al., 2015). Strength was not measured here, but future studies may consider combining intramuscular fat measurements with strength tests and electromyography to identify whether muscles with higher fat fractions are less able to generate force.

Obese people tend to have more fat in their muscles (Malenfant et al., 2001) so it is possible that the increased amounts of intramuscular fat in the stroke group is due to obesity rather than stroke. However, the stroke group and control groups had a similar mean BMI (26 and 28 kg/m^2, respectively; $P = 0.68$; unpaired t-test) suggesting that the elevated intramuscular fat fractions in the stroke group are not due to obesity. In the correlation analysis of BMI with intramuscular fat, intramuscular fat fraction in the paretic muscle increased with BMI (**Figure 4A**). However, in the non-paretic muscle, BMI did not increase with fat fraction (**Figure 4B**), suggesting that factors other than

TABLE 2 | Regression coefficient [95% confidence interval] of BMI and range of motion on intramuscular fat fraction in the paretic, non-paretic, and control medial gastrocnemius muscles.

	Paretic	Non-paretic	Control
BMI	0.6 [0.1, 1.2]	0.2 [−0.4, 0.7]	0.5 [−0.2,1.2]
Range of motion	−0.2 [−1.2, 0.7]	0.08 [−0.6, 0.8]	0.7 [−0.6, 2.0]

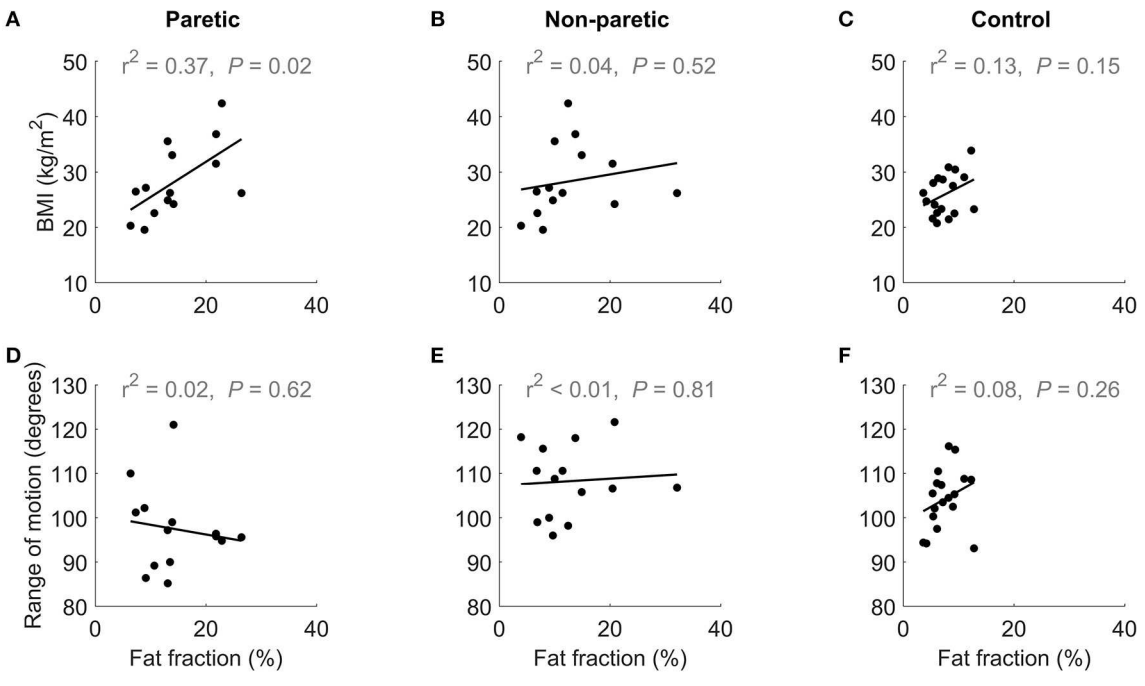

FIGURE 4 | The upper row shows the relationship between BMI and medial gastrocnemius fat fraction in the **(A)** paretic and **(B)** non-paretic muscles of stroke patients, and **(C)** control participants. The lower row shows the relationship between of dorsiflexion range of motion and medial gastrocnemius fat fraction in the **(D)** paretic and **(E)** non-paretic muscles stroke patients, and **(F)** control participants.

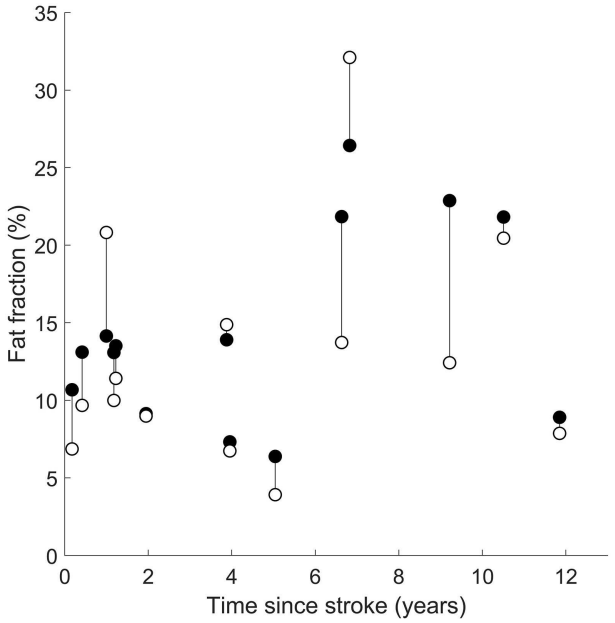

FIGURE 5 | Intramuscular fat fractions in the paretic (filled circles) and non-paretic (open circles) medial gastrocnemius muscles after a stroke. Vertical lines join paretic and non-paretic muscles from individual stroke patients.

obesity led to the increased intramuscular fat fractions in the stroke group.

In healthy populations, aging is accompanied by intramuscular fat infiltration (Marcus et al., 2010). There was no difference in the mean ages of the stroke and control group, so it is unlikely that age confounded these findings. The slopes of the linear mixed models provide an estimate for the rate of change of intramuscular fat fraction with respect to age, although a longitudinal study would be more appropriate to investigate age related changes in intramuscular fat. In all three comparisons, intramuscular fat fraction increased with respect to age, albeit slowly. These findings support the notion that intramuscular fat increases with age, but should be interpreted with caution given the cross-sectional design.

Time since stroke did not change the mean difference in intramuscular fat fraction or the rate of increase in intramuscular fat fraction between paretic and non-paretic muscles (**Figure 5**). This finding suggests that intramuscular fat infiltration on both legs is driven by similar stimuli after stroke. Intramuscular fat infiltration did not increase with respect to time since stroke, implying that the intramuscular fat infiltration occurs either rapidly around the time of stroke, or that intramuscular fat fraction was elevated prior to the stroke and did not change with time.

Muscle contracture is thought to be caused by an increase in muscle stiffness (Gao et al., 2009; Kwah et al., 2012b). Intramuscular fat could contribute to contracture by increasing muscle stiffness (Rahemi et al., 2015). While muscle stiffness was not measured directly, range of motion was measured as a surrogate measure of muscle stiffness. Medial gastrocnemius intramuscular fat fraction did not correlate with dorsiflexion range of motion (**Figures 4D–F**).

Intramuscular fat fractions should not be mistaken with the volume of fat within the muscle. Intramuscular fat fractions are a proportion (often reported as a percentage), while the fat volume is the absolute amount of fat (reported in cm^3 or mL). We investigated whether the fat volume was different between the three groups by multiplying muscle volume by intramuscular fat fraction. Fat volume in the paretic, non-paretic and control groups were 28.9 cm^3 (*SD* 14.9 cm^3), 29.4 cm^3 (19.9 cm^3), and 18.2 cm^3 (9.6 cm^3), respectively. Fat volume comparisons followed similar trends to the intramuscular fat fraction comparisons: medial gastrocnemius fat volume did not differ between the paretic and non-paretic muscles (−0.5 cm^3, −6.3 to 5.4 cm^3). The paretic muscles had 13.0 cm^3 (4.7–21.4 cm^3) more fat than the control muscles, and the non-paretic muscles had 13.5 cm^3 (3.0–24.0 cm^3) more fat than the control muscles. Thus, people who have had a stroke have both higher proportions and total volume of fat in their medial gastrocnemius compared to people who have not had a stroke. That is despite the muscles of stroke patients having, on average, 15% smaller muscle volumes (D'Souza et al., 2020).

This study demonstrates that intramuscular fat fraction and the absolute volume of fat is elevated in people who have had a stroke. While this finding is not new, the imaging modality used here can accurately and reliably quantify muscle-specific intramuscular fat across the entire muscle. Previous studies used ultrasound [which has only been minimally validated for measurements of intramuscular fat (Young et al., 2015)], DEXA scans (which cannot be used to measure muscle-specific fat fraction), and CT and T1-weighted images (which only indirectly estimate intramuscular fat fraction via reference to fatty voxels).

The measurements presented here along with the previous intramuscular fat measurements paint a consistent picture of elevated intramuscular fat in people who have had a stroke. However, more research needs be done to understand if stroke *causes* the increase in intramuscular fat, or whether the intramuscular fat was already present prior to stroke. It is possible that the stroke cohort had elevated levels of intramuscular fat which preceded, and therefore was not caused by, having had a stroke. If elevated intramuscular fat is detrimental to longevity and quality of life, therapy should be targeted toward reducing intramuscular fat. In people who have had a stroke, this may be achieved by resistance training which reduces intramuscular fat in the paretic and non-paretic lower extremities (Ryan et al., 2011).

Study Limitations

The range of motion test combines the stiffness of all structures at the ankle and does not provide muscle specific stiffness. As such, the lack of correlation between range of motion and intramuscular fat fraction should not imply that intramuscular fat fraction and muscle stiffness are unrelated. This limitation may be overcome by combining imaging modalities such as shear wave elastography with mDixon imaging to directly measure muscle-specific stiffness and quantify intramuscular fat.

Another limitation of this study is that physical activity was not measured. Physical *inactivity* has been shown to be a risk factor for stroke (O'Donnell et al., 2010) while physical *activity* can prevent infiltration of intramuscular fat in older adults

(Goodpaster et al., 2008). The participants who have had a stroke may have had elevated intramuscular fat from being less physically active (which also put them at greater risk of having a stroke). With this cross-sectional dataset, it is impossible to determine whether the elevated intramuscular fat is due to the stroke, or physical inactivity, or a combination of both. Future intramuscular fat studies should consider collecting data on physical activity prior to and after stroke, in addition to physical activity of control participants.

The time since stroke analysis revealed that adaptations do not worsen with time after stroke. This finding was inferred from a relatively small cross-sectional sample—a large longitudinal study would provide a better assessment of changes in intramuscular fat. However, if the finding of no change in intramuscular fat fractions after stroke is true, it would mean that the adaptations were present at the time of stroke and may have been present prior to the stroke. As previously highlighted, physical activity levels were not recorded, although they are likely to be related; differences in physical activity between the stroke cohort (before or after stroke) and control participants could implicate physical activity as a confounder to the elevated intramuscular fat findings. Conversely, a finding of no difference in physical activity between the stroke cohort (prior to stroke) and control participants would suggest that the elevated intramuscular fat levels in people who had a stroke were not due to physical activity levels.

DATA AVAILABILITY STATEMENT

The raw data supporting the conclusions of this article will be made available by the authors, without undue reservation, to any qualified researcher.

ETHICS STATEMENT

The studies involving human participants were reviewed and approved by the University of New South Wales human research ethics committee (HC15006). The patients/participants provided their written informed consent to participate in this study.

AUTHOR'S NOTE

The manuscript is a chapter in AD thesis. We have previously reported analyses of muscle architecture in these participants (D'Souza et al., 2020). but have not previously published analyses of intramuscular fat. Intramuscular fat measurements were presented in a poster format at the First International Motor Impairment Conference, Sydney, November 2018.

AUTHOR CONTRIBUTIONS

RH, BB, and AD conceived and designed the research. AD and BB performed the experiments. AD processed the data and prepared the first draft of the manuscript, which was read and commented on by all authors.

FUNDING

This study was supported by the Australian National Health and Medical Research Council (NHMRC; Program Grant APP1055084). RH was supported by a research fellowship from the Australian NHMRC. AD was supported by a scholarship from the Royal Freemasons Benevolent Institute.

REFERENCES

Akazawa, N., Harada, K., Okawa, N., Tamura, K., Hayase, A., and Moriyama, H. (2018). Relationships between muscle mass, intramuscular adipose and fibrous tissues of the quadriceps, and gait independence in chronic stroke survivors: a cross-sectional study. *Physiotherapy* 104, 438–445. doi: 10.1016/j.physio.2017.08.009

Andersson, G. B. J., and Cocchiarella, L. (eds.). (2000). "Chapter 17: The lower extremities," in *Guides to the Evaluation of Permanent Impairment, 5th Edn* (Chicago, IL: American Medical Association), 537.

Burakiewicz, J., Sinclair, C. D. J., Fischer, D., Walter, G. A., Kan, H. E., and Hollingsworth, K. G. (2017). Quantifying fat replacement of muscle by quantitative MRI in muscular dystrophy. *J. Neurol.* 264, 2053–2067. doi: 10.1007/s00415–017-8547–3

Dixon, W. T. (1984). Simple proton spectroscopic imaging. *Radiology* 153, 189–194. doi: 10.1148/radiology.153.1.6089263

D'Souza, A., Bolsterlee, B., and Herbert, R. D. (2020). Architecture of the medial gastrocnemius muscle in people who have had a stroke: a diffusion tensor imaging investigation. *Clin. Biomech.* 74, 27–33. doi: 10.1016/j.clinbiomech.2020.02.004

Fergusson, D., Hutton, B., and Drodge, A. (2006). The epidemiology of major joint contractures: a systematic review of the literature. *Clin. Orthop. Relat. Res* 456, 22–29. doi: 10.1097/BLO.0b013e3180308456

Fischer, M. A., Pfirrmann, C. W. A., Espinosa, N., Raptis, D. A., and Buck, F. M. (2014). Dixon-based MRI for assessment of muscle-fat content in phantoms, healthy volunteers and patients with achillodynia: comparison to visual assessment of calf muscle quality. *Eur. Radiol.* 24, 1366–1375. doi: 10.1007/s00330–014-3121–1

Gao, F., Grant, T. H., Roth, E. J., and Zhang, L. Q. (2009). Changes in passive mechanical properties of the gastrocnemius muscle at the muscle fascicle and joint levels in stroke survivors. *Arch. Phys. Med. Rehabil.* 90, 819–826. doi: 10.1016/j.apmr.2008.11.004

Goodpaster, B. H., Chomentowski, P., Ward, B. K., Rossi, A., Glynn, N. W., Delmonico, M. J., et al. (2008). Effects of physical activity on strength and skeletal muscle fat infiltration in older adults: a randomized controlled trial. *J. Appl. Physiol.* 105:8. doi: 10.1152/japplphysiol.90425.2008

Harvey, L. A., Katalinic, O. M., Herbert, R. D., Moseley, A. M., Lannin, N. A., and Schurr, K. (2017). Stretch for the treatment and prevention of contractures. *Cochrane Database Syst. Rev.* 1:Cd007455. doi: 10.1002/14651858.CD007455.pub3

Hunnicutt, J. L., and Gregory, C. M. (2017). Skeletal muscle changes following stroke: a systematic review and comparison to healthy individuals. *Top. Stroke Rehabil.* 24, 463–471. doi: 10.1080/10749357.2017.1292720

Iversen, E., Hassager, C., and Christiansen, C. (1989). The effect of hemiplegia on bone mass and soft-tissue body-composition. *Acta Neurol. Scand* 79, 155–159. doi: 10.1111/j.1600–0404.1989.tb03729.x

Jorgensen, L., and Jacobsen, B. K. (2001). Changes in muscle mass, fat mass, and bone mineral content in the legs after stroke: a 1 year prospective study. *Bone* 28, 655–659. doi: 10.1016/S8756–328200434-3

Karampinos, D. C., Baum, T., Nardo, L., Alizai, H., Yu, H., Carballido-Gamio, J., et al. (2012). Characterization of the regional distribution of skeletal muscle adipose tissue in type 2 diabetes using chemical shift-based

water/fat separation. *J. Magn. Reson. Imaging* 35:e23512. doi: 10.1002/jmri.23512

Kovanlikaya, A., Guclu, C., Desai, C., Becerra, R., and Gilsanz, V. (2005a). Fat quantification using three-point dixon technique: *in vitro* validation1. *Acad. Radiol.* 12, 636–639. doi: 10.1016/j.acra.2005.01.019

Kovanlikaya, A., Mittelman, S. D., Ward, A., Geffner, M. E., Dorey, F., and Gilsanz, V. (2005b). Obesity and fat quantification in lean tissues using three-point Dixon MR imaging. *Pediatr. Radiol.* 35, 601–607. doi: 10.1007/s00247–005-1413-y

Kwah, L. K., Harvey, L. A., Diong, J. H. L., and Herbert, R. D. (2012a). Half of the adults who present to hospital with stroke develop at least one contracture within six months: an observational study. *J. Physiother.* 58, 41–47. doi: 10.1016/S1836–955370071-1

Kwah, L. K., Herbert, R. D., Harvey, L. A., Diong, J., Clarke, J. L., Martin, J. H., et al. (2012b). Passive mechanical properties of gastrocnemius muscles of people with ankle contracture after stroke. *Arch. Phys. Med. Rehabil.* 93, 1185–1190. doi: 10.1016/j.apmr.2012.02.009

Malenfant, P., Joanisse, D. R., Theriault, R., Goodpaster, B. H., Kelley, D. E., and Simoneau, J. A. (2001). Fat content in individual muscle fibers of lean and obese subjects. *Int. J. Obes. Relat. Metab. Disord.* 25, 1316–1321. doi: 10.1038/sj.ijo.0801733

Marcus, R. L., Addison, O., Kidde, J. P., Dibble, L. E., and Lastayo, P. C. (2010). Skeletal muscle fat infiltration: impact of age, inactivity, and exercise. *J. Nutr. Health Aging* 14, 362–366. doi: 10.1007/s12603-010-0081-2

Noble, J. J., Charles-Edwards, G. D., Keevil, S. F., Lewis, A. P., Gough, M., and Shortland, A. P. (2014a). Intramuscular fat in ambulant young adults with bilateral spastic cerebral palsy. *BMC Musculoskelet. Disord.* 15:236. doi: 10.1186/1471–2474-15–236

Noble, J. J., Keevil, S. F., Totman, J., and Charles-Edwards, G. D. (2014b). *In vitro* and *in vivo* comparison of two-, three- and four-point Dixon techniques for clinical intramuscular fat quantification at 3 T. *Br. J. Radiol.* 87:20130761. doi: 10.1259/bjr.20130761

O'Donnell, M. J., Xavier, D., Liu, L. S., Zhang, H. Y., Chin, S. L., Rao-Melacini, P., et al. (2010). Risk factors for ischaemic and intracerebral haemorrhagic stroke in 22 countries (the INTERSTROKE study): a case-control study. *Lancet* 376, 112–123. doi: 10.1016/S0140–673660834-3

O'Dwyer, N. J., Ada, L., and Neilson, P. D. (1996). Spasticity and muscle contracture following stroke. *Brain* 119, 1737–1749. doi: 10.1093/brain/119.5.1737

Ponrartana, S., Andrade, K. E., Wren, T. A. L., Ramos-Platt, L., Hu, H. H., Bluml, S., et al. (2014). Repeatability of chemical-shift-encoded water-fat MRI and diffusion-tensor imaging in lower extremity muscles in children. *Am. J. Roentgenol.* 202, W567–W573. doi: 10.2214/AJR.13.11081

Rahemi, H., Nigam, N., and Wakeling, J. M. (2015). The effect of intramuscular fat on skeletal muscle mechanics: implications for the elderly and obese. *J. Royal Soc. Interface* 12:20150365. doi: 10.1098/rsif.2015.0365

Ramsay, J. W., Barrance, P. J., Buchanan, T. S., and Higginson, J. S. (2011). Paretic muscle atrophy and non-contractile tissue content in individual muscles of the post-stroke lower extremity. *J. Biomech* 44, 2741–2746. doi: 10.1016/j.jbiomech.2011.09.001

Ryan, A. S., Buscemi, A., Forrester, L., Hafer-Macko, C. E., and Ivey, F. M. (2011). Atrophy and intramuscular fat in specific muscles of the thigh: associated weakness and hyperinsulinemia in stroke survivors. *Neurorehabil. Neural. Repair* 25, 865–872. doi: 10.1177/1545968311408920

Ryan, A. S., Dobrovolny, C. L., Smith, G. V., Silver, K. H., and Macko, R. F. (2002). Hemiparetic muscle atrophy and increased intramuscular fat in stroke patients. *Arch. Phys. Med. Rehabil.* 83, 1703–1707. doi: 10.1053/apmr.2002.36399

Wren, T. A. L., Bluml, S., Tseng-Ong, L., and Gilsanz, V. (2008). Three-point technique of fat quantification of muscle tissue as a marker of disease progression in duchenne muscular dystrophy: preliminary study. *Am. J. Roentgenol.* 190, W8–W12. doi: 10.2214/AJR.07.2732

Young, H. J., Jenkins, N. T., Zhao, Q., and Mccully, K. K. (2015). Measurement of intramuscular fat by muscle echo intensity. *Muscle Nerve* 52, 963–971. doi: 10.1002/mus.24656

Yushkevich, P. A., Piven, J., Hazlett, H. C., Smith, R. G., Ho, S., Gee, J. C., et al. (2006). User-guided 3D active contour segmentation of anatomical structures: significantly improved efficiency and reliability. *Neuroimage* 31, 1116–1128. doi: 10.1016/j.neuroimage.2006.01.015

Conflict of Interest: The authors declare that the research was conducted in the absence of any commercial or financial relationships that could be construed as a potential conflict of interest.

frontiers in Bioengineering and Biotechnology

ORIGINAL RESEARCH
published: 17 July 2020
doi: 10.3389/fbioe.2020.00795

Quantitative Assessment of Traumatic Upper-Limb Peripheral Nerve Injuries Using Surface Electromyography

Weidi Tang[1], Xu Zhang[1], Yong Sun[2]*, Bo Yao[3], Xiang Chen[1], Xun Chen[1] and Xiaoping Gao[4]*

[1] School of Information Science and Technology, University of Science and Technology of China, Hefei, China, [2] Institute of Criminal Sciences, Hefei Public Security Bureau, Hefei, China, [3] Institute of Biomedical Engineering, Chinese Academy of Medical Sciences and Peking Union Medical College, Tianjin, China, [4] Department of Rehabilitation Medicine, The First Affiliated Hospital of Anhui Medical University, Hefei, China

OPEN ACCESS

Edited by:
Le Li,
First Affiliated Hospital of Sun Yat-sen University, China

Reviewed by:
Hu Xiaoling,
Hong Kong Polytechnic University, Hong Kong
Nizam Uddin Ahamed,
University of Pittsburgh, United States

***Correspondence:**
Xu Zhang
xuzhang90@ustc.edu.cn
Yong Sun
16039120@qq.com

Specialty section:
This article was submitted to Biomechanics, a section of the journal Frontiers in Bioengineering and Biotechnology

Received: *20 February 2020*
Accepted: *22 June 2020*
Published: *17 July 2020*

Citation:
Tang W, Zhang X, Sun Y, Yao B, Chen X, Chen X and Gao X (2020) Quantitative Assessment of Traumatic Upper-Limb Peripheral Nerve Injuries Using Surface Electromyography. Front. Bioeng. Biotechnol. 8:795. doi: 10.3389/fbioe.2020.00795

Background: There is a great demand for convenient and quantitative assessment of upper-limb traumatic peripheral nerve injuries (PNIs) beyond their clinical routine. This would contribute to improved PNI management and rehabilitation.

Objective: The aim of this study was to develop a novel surface EMG examination method for quantitatively evaluating traumatic upper-limb PNIs.

Methods: Experiments were conducted to collect surface EMG data from forearm muscles on both sides of seven male subjects during their performance of eight designated hand and wrist motion tasks. All participants were clinically diagnosed as unilateral traumatic upper-limb PNIs on the ulnar nerve, median nerve, or radial nerve. Ten healthy control participants were also enrolled in the study. A novel framework consisting of two modules was also proposed for data analysis. One module was first used to identify whether a PNI occurs on a tested forearm using a machine learning algorithm by extracting and classifying features from surface EMG data. The second module was then used to quantitatively evaluate the degree of injury on three individual nerves on the examined arm.

Results: The evaluation scores yielded by the proposed method were highly consistent with the clinical assessment decisions for three nerves of all 34 examined arms ($7 \times 2 + 10 \times 2$), with a sensitivity of 81.82%, specificity of 98.90%, and significate linear correlation ($p < 0.05$) in quantitative decision points between the proposed method and the routine clinical approach.

Conclusion: This study offers a useful tool for PNI assessment and helps to promote extensive clinical applications of surface EMG.

Keywords: clinical assessment, peripheral nerve injury, surface electromyography, non-invasive examination, machine learning

INTRODUCTION

The term peripheral nerve injuries (PNIs) refers to a clinical condition caused by ischemia-reperfusion or damage of the peripheral nerves, that include torso and limb sensory, motor, and nerve autonomic dysfunction. Among PNIs, traumatic upper-limb PNI is relatively common (occurring on the upper-limb after a penetrating injury, crush, stretch, ischemia, or other traumatic injuries) (Noble et al., 1998; Campbell, 2008). People with traumatic upper-limb PNI usually suffer from sensory disturbance, dyskinesia, muscle atrophy in the control area of the damaged nerves, and have a reduced quality of life (Selecki et al., 1982). For example, those with radial nerve injury typically suffer from a weakness of the wrist and finger extensor muscles and show carpoptosis (Sallomi et al., 1998). The evaluation of upper-limb PNI has great importance for clinical treatment and rehabilitation guidance, as well as social and judicative significance. For insurance claims, as an example, the amount of compensation depends on the degree of disability following the PNI. Especially in judicial expertise, the resultant degree of the PNI is an important basis for sentencing who causes the PNI.

Currently, the clinical evaluation of peripheral nerve injury relies primarily on clinical history, clinical symptoms, and physical/neurological examination (Aminoff, 2012; Zeidenberg et al., 2015). Clinical symptoms usually include neuromuscular physiology state, special body posture, motor and sensory function, and reflex issues (Sallomi et al., 1998). More objective information can be obtained by physical/neurological examination. In previous studies, many diagnostic methods have been successfully used for PNI evaluation, such as invasive/needle electromyography (EMG) examination, MRI, and high-resolution ultrasonography (HRU) (Sunderland, 1968; Chang et al., 2019). Direct imaging with MRI or HRU is successful in clearly and accurately demonstrating neural integrity. Moreover, invasive/needle EMG can detect nerve integrity by neuromuscular activities. Through electrical stimulation, the evoked motor unit action potentials (MUAPs) are recorded to reflect potential abnormality according to nerve conduction velocity, EMG amplitude, and other signal morphological features (Robinson, 2000). However, all these methods rely on invasive/painful protocols or specialized equipment to be manipulated by clinical professionals, which is a rigorous condition that hinders their pervasive applications. The strong subjectivity of the examiners involved in the interpretation of the examination results is another problem. Therefore, a convenient and practical protocol along with an automatic expert system involving intelligent data processing and machine learning algorithms is required for quantitative and objective PNI evaluation.

Compared with invasive EMG examination, surface EMG (sEMG) is an alternative approach that detects neuromuscular activities from the skin surface in a non-invasive manner. The electrode placed over the skin surface is not as selective as that of the invasive needle. Therefore, the sEMG signal appears in interference patterns due to the superposition of a large number of MUAP waveforms. This is the primary reason for restricting clinical applications of the sEMG. To take advantage of its non-invasive feature, many studies have focused on the sEMG examination of various neuromuscular diseases, including spinal cord injury (Sherwood et al., 1996; Alexander et al., 2009), stroke (Kallenberg and Hermens, 2009; Li et al., 2017), cerebral palsy (Steele et al., 2015; Tang et al., 2015; Cappellini et al., 2016), ALS (Zhang et al., 2013a), dysphagia, and odynophagia (Vaiman and Eviatar, 2009). Its advantages in both non-invasive and ease of operation make it suitable for long-term and repetitive PNI monitoring, especially toward home or community rehabilitation. In addition, besides the nerve integrity, the sEMG was reported to have the capability to evaluate motor functions, which is also of great importance for PNI assessment and management. Moreover, the fast operation property of the surface EMG approach can facilitate early judicial intervention to PNI cases for grassroots police, without waiting for transfer to the clinician or forensic experts.

Based on the above considerations, in this study, we proposed a novel framework for evaluating upper-limb traumatic PNIs using surface EMG. To our knowledge, this is the first attempt to apply the sEMG to the assessment of traumatic upper-limb PNI. The proposed method includes intelligent signal processing and machine learning procedures, which provide a new automatic and objective solution for the PNI assessment. We expect that these advances will help to expand the usability of PNI evaluation from routine medical diagnosis to many special occasions, such as home or community rehabilitation guidance and judicial intervention.

MATERIALS AND METHODS

Subjects

Seven subjects with upper-limb PNIs (labeled as S1–S7, all males, age: 24 ± 6.6 years, mean ± standard deviation, range 17–34 years) and 10 age- and gender-matched healthy control subjects (C1–C10, age: 22 ± 4 years, range 17–29 years, male) were recruited for data collection experiments in this study. The study was approved by the Medical Ethics Review Committee of The First Affiliated Hospital of Anhui Medical University. Inclusion criteria for patients include: (1) experience of a unilateral PNI caused by trauma, at either the radial nerve, median nerve, or ulnar nerve. Subjects with simultaneous injuries of multiple nerves were also included when; (2) at least 6 months had passed since the onset of the injury; (3) the patient was in a stable condition with all wounds healing; and (4) there was no history of any neuromuscular disease, except the injury. Written consent was obtained from all subjects before the experiments.

All patients were tested through a clinical, electrophysiological examination on their radial nerves, median nerves, and the ulnar nerves using needle EMG. This approach routinely reported a three-graded degree of injury for each nerve on both sides: "−" indicates no injury; "+" indicates mild injury; and "++" indicates severe injury (likely involving nerve rapture). Detailed

TABLE 1 | Physical information and clinical assessment decisions for all subjects with peripheral nerve injuries.

ID #	Age range (year)	Gender	Side of the injury	Clinical assessment decisions					
				Left			Right		
				Ulnar	Median	Radial	Ulnar	Median	Radial
S1	26–30	M	L	++	–	–	–	–	–
S2	31–35	M	R	–	–	–	+	+	+
S3	16–20	M	L	–	–	++	–	–	–
S4	16–20	M	L	++	++	–	–	–	–
S5	31–35	M	L	–	–	++	–	–	–
S6	16–20	M	R	–	–	–	++	++	–
S7	21–25	M	L	–	+	–	–	–	–

"–" indicates health; "+" indicates an injury; "++" indicates a severe injury

information of all the patients and their clinical examination reports are shown in **Table 1**.

Experiments

Fourteen surface EMG sensors were used to collect data from three hand muscles and four forearm muscles on both sides of all subjects. Each EMG sensor has two round electrode probes, with a 3-mm diameter for each probe and an 8-mm center distance between them, constituting a single-differential surface EMG data recording channel. The hand muscles include the abductor pollicis brevis (APB) muscle, the first dorsal interosseous (FDI) muscle, and the abductor digitiminimi (ADM) muscle. On each side of the forearm, four sensors were placed around the circumference of the forearm, at a position of 25% of the entire distance from the elbow to the wrist. These were equally spaced and placed over the ulnar side, the anterior side, the radial side, and the posterior side of the forearm, mainly targeting the ulnar flexor carpi, long palmar, extensor carpi radialis, and extensor of fingers, respectively (**Figure 1**). Considering the complicated structural distribution of the forearm muscles and their possible cross-talks, activities from a variety of nearby muscles could also be sensed. Since these muscles were innervated by the three nerves tested in this study, their surface EMG activities were intentionally included for the following analysis. After the skin preparation with medical alcohol, each surface EMG sensor was firmly attached to each targeted muscle/position, with its electrode pair along the direction of muscle fibers. As a reference, a round electrode was placed on the right arm fossa cubitalison.

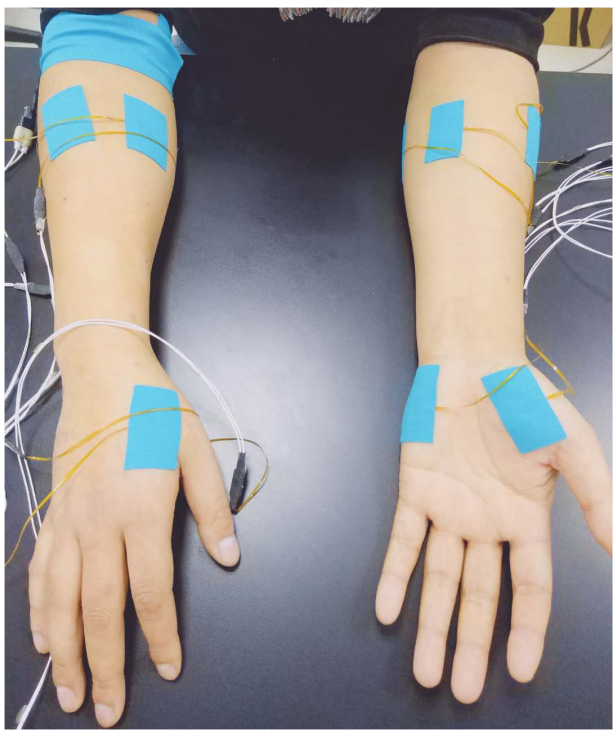

FIGURE 1 | Electrode placement for surface EMG data recording.

During the experiment, subjects were seated in a comfortable chair with their arms relaxed on a height-adjusted table. Each subject was instructed to perform eight tasks from the initial relaxation/rest state: ulnar deviation, clenching fist, stretching hand, bending of the wrist with external rotation of elbow joint and perform radial deviation, abducting the index finger, abducting the little finger, and bending of the wrist with internal rotation of elbow joint (**Figure 2**). Subjects were asked to perform these tasks with both arms/sides simultaneously. Subjects were instructed to perform each task with a maximal voluntary contraction (MVC) and to hold it as stably as possible for at least 3 s. In this study, the MVC represented a condition when the subject performed muscle contractions with maximal efforts. Although the actual muscle contraction strength/force was not precisely measured during the experiments, the surface EMG recordings were real-time monitored, and the subjects were encouraged to produce as high level of EMG intensity/amplitude as possible during their task performances, so as to ensure the quality of MVC. To gain a sufficient amount of data, each task was repeated at least three times in one trial. To avoid mental and muscular fatigue, sufficient rest was allowed between two consecutive trials.

Surface EMG data were recorded for every task with a custom-made data acquisition system supporting up to 128 EMG channels. This system has been validated and successfully applied

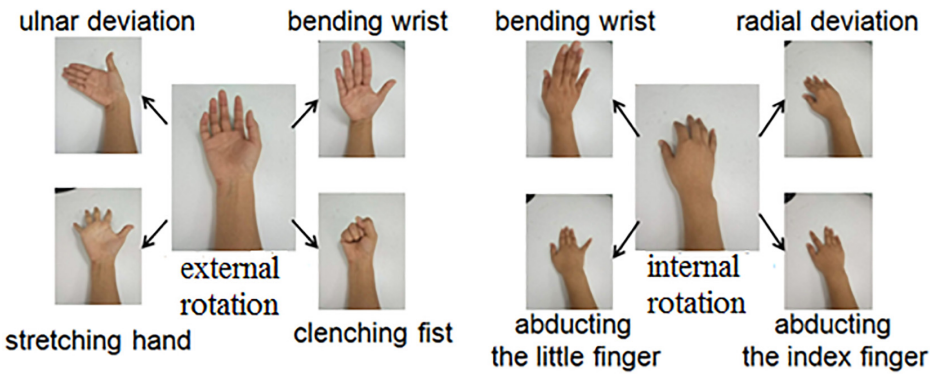

FIGURE 2 | Illustration of eight designated motion tasks.

in various neuroscience and engineering studies involving electrophysiological data recording (Tang et al., 2015, 2018). Each recorded EMG channel was amplified by a two-stage amplifier with a total gain of 52dB, band-pass filtered at 16–610 Hz, and subsequently converted into digitalized data with an 18-bit A/D converter. The sampling rate for each channel was set to 1 kHz. All recorded data were transferred into a laptop computer via a USB cable for off-line analysis in the Matlab (The Mathworks, MA, United States) environment with customized programs.

Data Preprocessing

Each channel of surface EMG was pre-processed by a zero-lag fourth-order Butterworth band-pass filter at 20–500 Hz to eliminate low-frequency motion artifacts and high-frequency interferences. If necessary, a set of second-order notch filters at the 50-Hz power line interference and its harmonics were also applied.

The recorded EMG data showed three muscular activity bursts corresponding to three repetitions of each task in one trial. This phenomenon was mainly observed from the seven EMG channels for the tested arm performing the tasks. A data segment of 3-s EMG activity was selected for each muscular activity burst, and thus three data segments were produced for each task. The EMG signals in the form of seven channels in each data segment were further divided into a series of non-overlapping analysis windows with a window length of 100 ms. We chose such a windowing approach to produce a sufficient number of data samples, while these windows were not overlapped to maintain the diversity of resultant data samples. Finally, 90 analysis windows/samples were obtained for each tested arm performing each task. These analysis windows were also considered as basic data samples in the following feature extraction and pattern classification analyses.

A great many studies have been performed for developing features to characterize the raw surface EMG data for a pattern classification purpose (Phinyomark et al., 2012). Among these, Hudgins' time-domain (TD) features (Englehart and Hudgins, 2003), autoregressive (AR) model coefficients (Zeng et al., 2019), and time-dependent power spectrum descriptors (TD-PSDs) (Altimemy et al., 2016) have been popularly used and achieved successful applications. Some studies also believe that there is little difference in the effectiveness of these features in practical use (Li et al., 2016). According to some pre-tests for these features and their combination, the set of four TD features was used in our study, including the mean absolute value (MAV), waveform length (WL), number of zero-crossings (ZC), and number of slope sign changes (SSC). Its reported effectiveness in surface EMG pattern recognition was another reason for adopting the TD feature set (Zhang et al., 2017). The four TD features were calculated separately for each sample or channel.

Subsequent data analysis consisted of two modules: Module I makes the judgment about whether the tested arm is affected by PNI. On this basis, if any nerve injury was judged, Module II evaluated injury degrees of three individual nerves (the radial nerve, median nerve, and ulnar nerve) by quantitative scores. **Figure 3** illustrates the framework for traumatic upper-limb PNI assessment using surface EMG data processing.

Module I: Arm Injury Judgment

This module was designed to make a brief judgment on whether any nerve is injured in the tested arm. Therefore, it was applied to solve a general two-class problem: normality or injury. Given the data recorded from the tested arm executing all tasks, the tested arm could be judged as being injured as long as an exception (with respect to the normality) was presented anytime and anywhere (at any channel during the performance of any task).

For each tested arm of a subject, a total of 8 (tasks) × 90 (samples per task) × 7 (channels per sample) × 4 (features per channel) features were extracted, from which only a few features needed to be selected (because the majority were believed to carry irrelevant or redundant information). It was assumed that discriminative information associated with the nerve injury could be examined from a specific location, which represents a combination of an examined muscle and a task corresponding to the muscle function. Thus, a feature selection procedure was conducted to choose a subset of features from the entire set of 224 (8 motions × 7 channels × 4 features) different kinds of features. Here, the 90 samples were viewed as 90 repetitive measures of each kind of feature. To determine the best feature subset, Fisher's class separability index (FCSI) (Englehart, 1998) was employed as

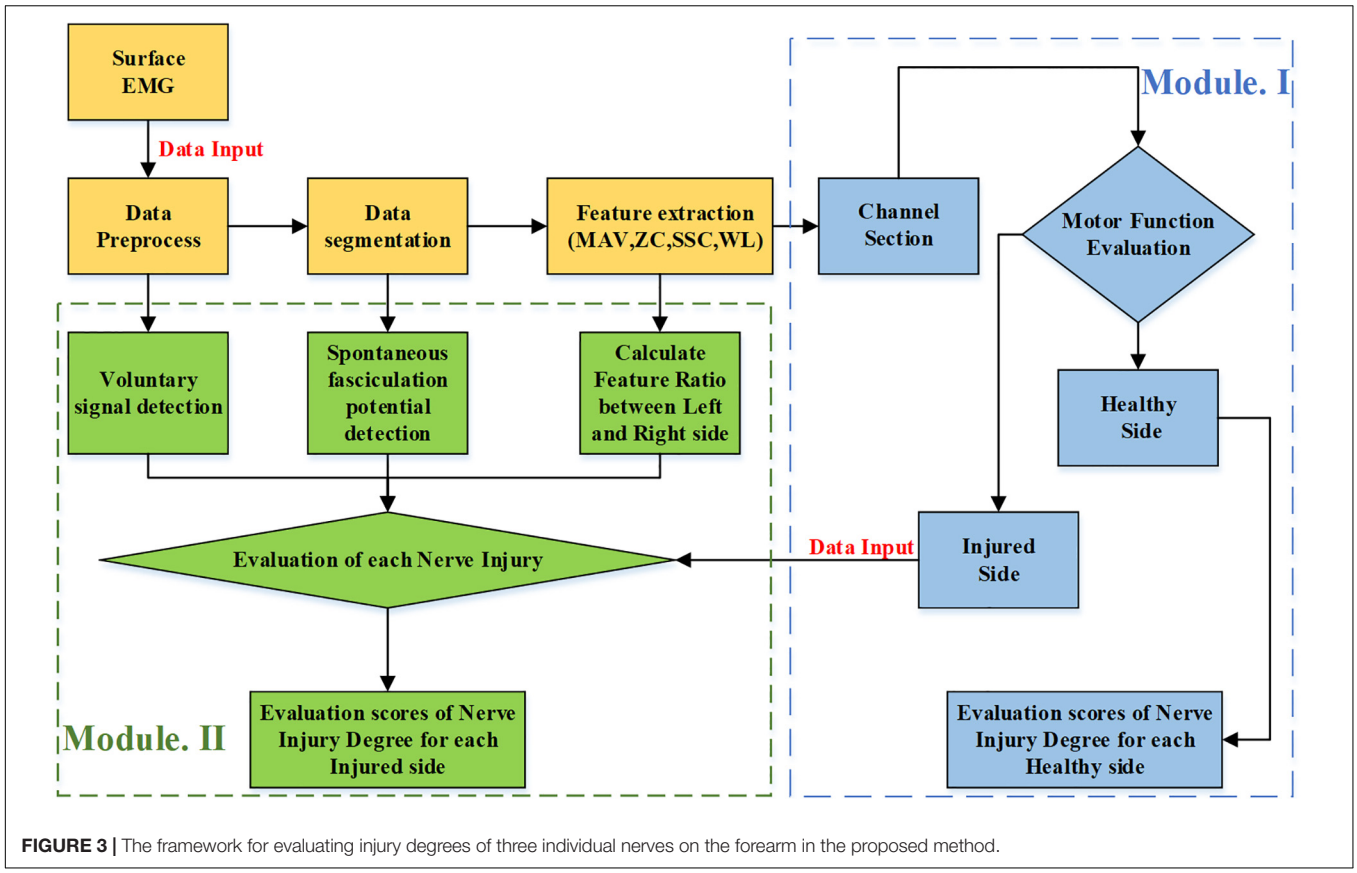

FIGURE 3 | The framework for evaluating injury degrees of three individual nerves on the forearm in the proposed method.

the discriminant measure, which is described as:

$$\mathrm{FCSI} = \sum_{a=1}^{C-1} \sum_{b=a+1}^{C} \frac{\left| \overline{m}_{j,c}^{(a)} - \overline{m}_{j,c}^{(b)} \right|^2}{\underset{1 \le i \le N_a}{\mathrm{var}} \left(x_{i,(j,k)}^{(a)} \right) + \underset{1 \le i \le N_b}{\mathrm{var}} \left(x_{i,(j,k)}^{(b)} \right)} \quad (1)$$

where *a* and *b* represent the indices of two different classes (injury or normality), and *c* represents the number of different classes. Generally, a higher value of FCSI indicates a higher degree of class separability. This feature selection algorithm is able to rank the features in descending order of their FCSI values and make it practical to choose a subset of features with top N FCSI values as being the most discriminative features (Wang et al., 2016).

After the feature selection, an N-dimensional feature vector was formed for each sample, and there were 90 samples for each tested arm. A conventional linear discriminant classifier (LDC) was used for classification between normality and injury (Smola et al., 2000; Webb, 2003; Zhang H. et al., 2013) because of its satisfactory performance and high practicability for surface EMG classification (Englehart et al., 1999). The implementation of the LDC is to construct a linear classifier by modeling the within-class density of each class as a multi-variant Gaussian distribution (Mika et al., 1999). For each tested arm, the classifier produced 90 decisions corresponding to its 90 samples. If 95% of these samples had a decision of nerve injury, we, therefore, identified a nerve injury for the tested arm; and otherwise, the tested arm was identified to be normal. Specifically, both arms of any subject with SCI were tested independently.

A leave-one-out cross-validation scheme was used to train the classifier and then to make a judgment of nerve injury for the tested arm. The data from all arms except one arm were used for determining the selected feature subset and training the classifier. Therefore, the data from the remaining arm were used for testing. This procedure was repeated 34 times (34 arms in total were tested in the experiments) so as to ensure each arm's data were considered as the testing dataset once. The performance of nerve injury judgment was evaluated by accuracy, which was defined as the percentage of correctly identified arms to all the arms tested in this study. Specifically, we intentionally adjusted the number *N* of selected subset features from 1 to 10, and *N* was finally determined to be two due to its optimal and satisfactory performance.

Module II: Evaluation of Injury Degree for Each Nerve

Given the decision of nerve injury from Module I, this module was designed to further evaluate the degree of the injury for individual nerves in the tested arms. Three nerves were considered in each tested arm: the ulnar, medial, and radial nerves. To determine their degrees of injury, we had to consider anatomical knowledge, including their dominated muscles and

muscle functions (Selecki et al., 1982; Noble et al., 1998). In detail, the ulnar nerve function can be represented by the EMG channel from ADM muscle during the performance of the task ulnar deviation (UD); the median nerve function is related to the EMG channel from APB muscle during the performance of the task radial deviation (RD); and the radial nerve function is associated with the EMG channel from the APB muscle and the radial side muscle (RM) during the performance of the task RD. Therefore, the examination of any individual nerve relied on the data from the corresponding channel/muscle and the corresponding task. The degrees of injury of these nerves were evaluated from three different aspects, including neural control command delivery to produce voluntary EMG signals, the presence of abnormal involuntary EMG activity, and comparison between arms on both sides of one subject.

We applied an accumulation deduction system to quantify the degree of injury evaluation for each nerve. Initially, each nerve has 10 points, indicating no injury and its intactness. Any phenomenon associated with a nerve injury revealed by the following three-aspect evaluation approach is marked by a deduction of points. The number of deducted points varies across reported phenomena, indicating different injury degrees. The point of one nerve can be deducted into 0, representing the severest injury and the least function.

Step 1: Examination of Sufficient Voluntary EMG Activities

The generation of sufficient EMG activities during voluntary muscle contractions is a good indication of an intact motor command delivery pathway. Such EMG generation capability might be affected by the PNI due to the hampered delivery of motor commands, further contributing to impaired motor function (Noble et al., 1998; Campbell, 2008). The examination of voluntary EMG mainly relied on the detection of its onset and offset during the performance of the designated task. Therefore, in our study, a routine approach for EMG onset/offset detection was employed and modified accordingly.

The examination of voluntary EMG activities was only performed on specific combinations of the EMG channel/muscle and task, which were designated above. Given a specific channel of EMG recorded during task performance in one trial, this examination included five steps: (1) Calculate the signal energy defined as the square of signal amplitude and filter it with a sliding window averaging using a window length of ten samples (the current sample plus nine previous samples); (2) Define an energy threshold as 5-times the quiescent baseline energy; (3) Detect the onset as the time of signal energy climbing up across the threshold; similarly, detect the offset as the time of signal energy falling below the threshold; (4) Calculate the voluntary EMG time duration by the offset time minus the onset time; and (5) Produce a decision for this examination: normality or abnormality when the duration time was more than 3-s or not, respectively.

The examination outcomes of sufficient voluntary EMG activities have to be expressed as quantitative deduction points according to the accumulation deduction system. **Table 2** clearly describes items for nerve injury judgment under various conditions. These items for revealing whether an individual nerve was injured or not were derived from anatomic knowledge regarding the muscle nerve innervation relationship and corresponding neuromuscular functions. According to **Table 2**, the nerve injury decision can be made, and the nerve with a decision of injury gets −5 points in this aspect of the examination.

TABLE 2 | The relationship between PNI decisions on individual nerves and different conditions.

Conditions		Injury Decisions	
APB muscle in RD task	**RM muscle in RD task**	**Radial nerve**	**Medial nerve**
o	o	none	none
o	x	injury	none
x	o	none	injury
x	x	injury	none
ADM muscle in UD task		**Ulnar nerve**	
o		none	
x		injury	

Step 2: Detection of Involuntary EMG Activities

The appearance of involuntary EMG has often been reported and is considered a typical pattern of abnormal EMG activities after nerve injury. These involuntary EMG activities can be grossly divided into two cases that can be detected via surface EMG. One case is spontaneous EMG activities, mainly appearing as spontaneous fasciculation potentials sporadically distributed within the quiescent baseline when the muscle is supposed to be relaxed. The fasciculation potential is regarded as an abnormal EMG pattern due to denervation of motor units or a group of muscle fibers in the examined muscle (de Carvalho and Swash, 1998). The detection of spontaneous fasciculation has been a gold-standard criterion for the diagnosis of amyotrophic lateral sclerosis (Chen and Zhou, 2014), while its occurrence has also been reported in PNI (Hermens et al., 1984). The other is spastic muscular activities, appearing as the fact that the muscle failed to be voluntarily relaxed, but its motor units continue to discharge repetitively to produce a series of relatively larger action potentials. Although spastic activities can only be attributed to the hyper-activity of upper motor neurons (muscle spasticity seldom occurs after PNI), its electrophysiological appearance in EMG data is very similar to that of spontaneous fasciculation potentials. Therefore, we used the same approach to detect either of them. Such involuntary EMG activity was evidently the case (i.e., spontaneous fasciculation potentials) in this study.

The approach for the detection of involuntary activity consisted of four steps: (1) Calculate the signal energy, which is regarded as the square of amplitude; (2) Filter the signal energy curve using a smoothing window length of 10 data points, where any sporadical spike (i.e., an involuntary action potential) was identified as a peak; (3) Detect these peaks by selecting data points with the top 3% filtered energy values. If more than one peak was located within a window of 10 ms, only the largest was regarded as the peak; (4) Confirm these sporadic peaks by comparing each

peak with nearby data points in a time deviation of 40 ms beside the peak. If the peak was 20-times larger than any of the nearby data, this peak could be confirmed. Any signal segment with more than one detected sporadic peak was regarded to be abnormal in terms of carrying involuntary EMG activities.

The examination outcomes of involuntary EMG activities have to be expressed as quantitative deduction points according to the accumulation deduction system. We used the same **Table 2** to transfer examination outcomes to decisions of injury on three examined nerves. According to **Table 2**, any nerve with a decision of injury gets −5 points in this aspect of the examination.

Step 3: Calculation of Muscle Activation Ratio Between Both Sides

Given the side dependency of PNI, an intra-subject bilateral comparison was an important indicator that helps to overcome potential cross-subject variability. It was especially useful in certain cases to reveal PNI abnormality when the above two aspects of examination failed to report any abnormality. The bilateral comparison was performed to reveal potential abnormality at the individual nerve level. We calculated the average of four features mentioned above for three segments in each trial (the four statistics were calculated from the signal in an entire segment instead of 90 analysis windows). To eliminate the influence of individual differences, we calculated the ratio of both sides (subjects were asked to perform these tasks with both arms/sides simultaneously in the experiments). For example, this ratio for the WL of APB muscle in the motion task RD was calculated as:

$$\text{R\_WL\_APB\_RD} = \frac{\text{WL\_APB\_RD on the left side}}{\text{WL\_APB\_RD on the right side}} \quad (2)$$

These ratios were supposed to be within 0 and 1. To ensure the ratio between 0 and 1, if any ratio was greater than 1, its reciprocal was used instead. Similarly, to evaluate a corresponding nerve injury, a ratio was just calculated for any designated combination of muscle and task. **Table 2** was also used to determined which nerve is injured based on the abnormality determined by the ratio. For an individual nerve, the calculated ratio had to be expressed as quantitative deduction points according to the accumulation deduction system. As a result, some minus points (from 1 to 5 minus points) were applied to an injured nerve. **Table 3** lists the different degrees of the nerve injury quantified by the minus points according to the ratio in this aspect of the examination. Please note if both the APB muscle and the RM muscle reported abnormality during the motion task RD performance (**Table 2**), the more severely affected muscle was adopted for evaluating the radial nerve injury (**Table 3**).

The proposed accumulation deduction system, consisting of the above three aspects, was used to quantify the degree of injury of each nerve. Initially, each nerve has 10 points, and no points were further deducted after reaching a 0 score. According to the three-grade clinical assessment, we also predefined three grades with our 10-point scale: the 10 points indicated *no* injury and its intactness, 7–9 points indicated a *mild* injury, and 0–6 points indicated a *severe* injury.

Performance Evaluation

The validity of the proposed method for evaluating traumatic upper limb PNI was demonstrated by comparing the evaluation decisions of the routine clinical assessment and the proposed evaluation framework. We calculated the sensitivity, specificity, positive predictive value, negative predictive value, and Youden's index for the proposed method, given the clinical assessment decisions as to the ground truth. The above indexes were described as:

$$\text{sensitivity} = \frac{\text{TP}}{\text{TP} + \text{FN}} \times 100\% \quad (3)$$

$$\text{specificity} = \frac{\text{TN}}{\text{FP} + \text{TN}} \times 100\% \quad (4)$$

$$\text{positive predictive value} = \frac{\text{TP}}{\text{TP} + \text{FP}} \times 100\% \quad (5)$$

$$\text{negative predictive value} = \frac{\text{TN}}{\text{FN} + \text{TN}} \times 100\% \quad (6)$$

$$\text{Youden's Index} = \text{sensitivity} + \text{specificity} - 1 \quad (7)$$

where TP represents the number of injured arms/nerves correctly diagnosed as injured, FP represents the number of healthy arms/nerves wrongly diagnosed as injured, FN represents the number of injured arms/nerves wrongly diagnosed as healthy, and TN represents the number of healthy arms/nerves correctly diagnosed as healthy.

We also performed a series of regression analyses to compare the injury degree of each nerve between the clinical assessment approach and the proposed method. The three-grade clinical assessment decisions ("−", "++", "++") were expressed quantitatively as 0, −1, and −2. The regression analyses between clinical assessment decisions and our evaluation points were conducted for each nerve. The level of statistical significance was set to $p < 0.05$ for all analyses. All statistical analyses were completed using SPSS software (ver. 16.0, SPSS Inc., Chicago, IL, United States).

RESULTS

Classification Results Between Arm Nerve Normality and Injury

Figure 4 shows the results for general arm injury identification for all subjects with PNIs. The proposed method yielded almost the same decisions as to the clinical assessment, except for the left arm of subject five. For healthy subjects, both sides of all ten healthy subjects were correctly determined to be normal and healthy. Therefore, when evaluating the performance of Module I in the proposed method, the sensitivity, specificity, positive predictive value, negative predictive value, and Youden's index are 85.71, 100, 100, 96.43, and 85.71%, respectively.

TABLE 3 | Deduction points according to the ratio.

Ratio(r)	$0.25 < r \leq 1$	$0.20 < r \leq 0.25$	$0.15 < r \leq 0.20$	$0.10 < r \leq 0.15$	$0.05 < r \leq 0.10$	$0 < r \leq 0.05$
Deduction points	0	−1	−2	−3	−4	−5

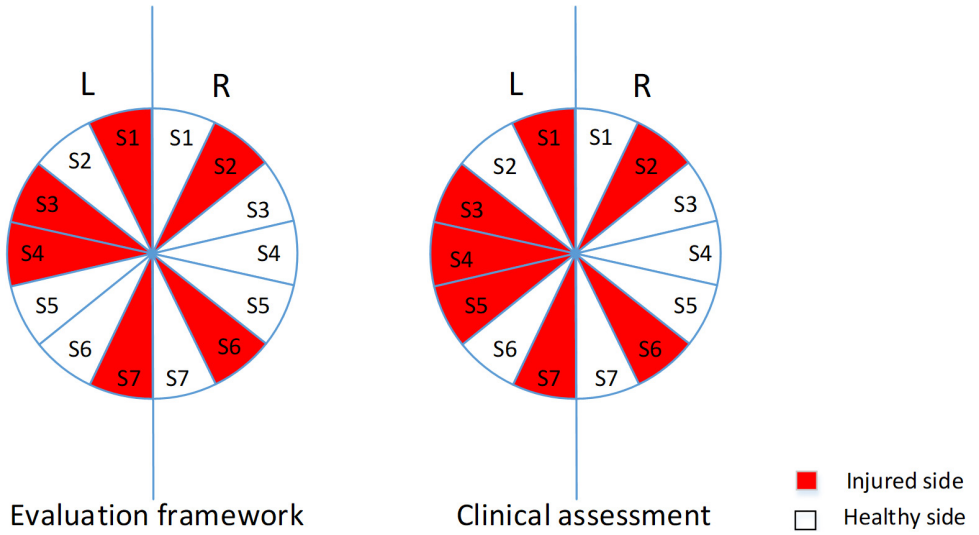

FIGURE 4 | The pie graph of evaluation decisions and clinical assessment decisions for both arms of subjects with PNIs. The left and right arms of S1–S7 were represented by a 25.71–degree fan and a fan in dark indicated that any PNI is identified on that arm.

Evaluating Injury Degrees of Individual Nerves

Evaluation Results of Each Step

The results of injured arms in each step, including the detection of voluntary EMG signals and involuntary EMG activities for selected muscles and motions, and the range of selected features' ratio, are shown in **Table 4**.

In terms of examining sufficient voluntary EMG activities, a decision of normality was given for all examined muscles and motions. Only the right ADM muscle of subject 6 in task UD was found to be abnormal, so that 5 minus points were applied to the ulnar nerve on the right arm of the subject.

When detecting involuntary EMG activities, an abnormality was reported in three cases: the left ADM muscles in motion task UD for both subject 1 and subject 4, and the left APB muscle of the subject 4. No involuntary EMG activity was found for the remaining muscles from all subjects. Therefore, corresponding deductions points were applied to the ulnar nerve of subject 1 and the ulnar and medial nerves of subject 4.

When examining the difference between both arms, the abnormality was found in most cases, and corresponding deduction points were applied (**Table 4**).

Evaluation Points and Clinical Quantitative Results

Table 5 reports the final evaluation scores derived from the proposed method and the clinical assessment decisions for individual nerves on both sides of all subjects with PNIs. Evidently, all healthy subjects were diagnosed as being "healthy" on each nerve with full points using the proposed method. From **Table 5**, we can conclude that the proposed method was mostly consistent with the clinical assessment decisions.

Given the clinical assessment decision (injury or no injury) on each nerve as the ground truth, it is also practical to calculate the five metrics for evaluating the performance of the proposed methods. When each of three individual nerves from both sides of all subjects (including all healthy subjects and subjects with PNIs) were considered independently, the sensitivity, specificity, positive predictive value, negative predictive value, and Youden's index were 81.82, 98.90, 90, 97.83, and 80.72%, respectively. Furthermore, the three-grade clinical assessment decision was quantified by scores 0, −1, and −2. Thus, in a regression analysis, the clinical assessment-derived evaluation scores and the proposed method were correlated ($p < 0.05$) when data from three nerves were pooled together. This was also true when data from each individual nerve was used ($p < 0.05$).

DISCUSSION

This paper presents a framework for quantitative evaluation of upper limb PNI using surface EMG signals in a cohort of subjects suffering from upper limb PNIs on any of the ulnar nerves, the median nerve, or the radial nerve. A protocol for surface EMG recording and intelligent data analysis was efficiently used as an examination tool for characterizing various neurological diseases, such as ALS (Chen and Zhou, 2014), stroke (Li et al., 2017), and cerebral palsy (Tang et al., 2015). In this study, we aimed to develop a non-invasive examination tool for diagnosing neurological diseases using surface EMG, which can be viewed

TABLE 4 | Results of evaluating each nerve in each step of the Module II.

Evaluation step	Muscle and task combination	S1		S2		S3		S4		S5		S6		S7	
		L	R	L	R	L	R	L	R	L	R	L	R	L	R
Step1: voluntary signal detection	ADM in UD	0	/	/	0	0	/	0	/	0	0	/	−5	0	/
	APB in RD	0	/	/	0	0	/	0	/	0	0	/	0	0	/
	RM in RD	0	/	/	0	0	/	0	/	0	0	/	0	0	/
Step2: spontaneous fasciculation detection	ADM in UD	−5	/	/	0	0	/	−5	/	0	0	/	0	0	/
	APB in RD	0	/	/	0	0	/	−5	/	0	0	/	0	0	/
	RM in RD	0	/	/	0	0	/	0	/	0	0	/	0	0	/
Step3: range of ratio	ADM in UD	−3		−3		−2		−3		0		0		0	
	APB in RD	0		−3		−4		−5		0		−5		−2	
	RM in RD	0		0		−1		0		0		0		0	

"/" indicates "not applicable".

TABLE 5 | Evaluation scores from both clinical assessment and the proposed method for all three examined nerves of all subjects.

Method	Subject #	Left			Right		
		Ulnar	Median	Radial	Ulnar	Median	Radial
Clinical Assessment	1	++	–	–	–	–	–
	2	–	–	–	+	+	+
	3	–	–	++	–	–	–
	4	++	++	–	–	–	–
	5	–	–	++	–	–	–
	6	–	–	–	++	++	–
	7	–	+	–	–	–	–
The Proposed Method	1	2	10	10	10	10	10
	2	10	10	10	7	7	10
	3	8	10	6	10	10	10
	4	2	0	10	10	10	10
	5	10	10	10	10	10	10
	6	10	10	10	5	5	10
	7	10	8	10	10	10	10

The points marked with red indicate severe injury; The points marked with blue indicate mild injury; The points without any color indicate no injury or normality.

as the first attempt to apply this to the PNI population. Its success not only facilitates PNI evaluation, but also promotes the extensive clinical use of surface EMG.

The high sensitivity and specificity in Module I demonstrated the feasibility of judging the gross arm injury as a two-classification problem, which is the prerequisite to further evaluation of injury degree for three nerves. The diversity of forearm traumatic PNI conditions is a great challenge in the design of this module. Therefore, a data-driven method was applied for mining PNI-related information using machine learning algorithms. Because of this, a general and gross judgment on whether the tested arm was injured or not can be made in this module. Unlike Module I (that uses a purely data-driven approach), Module II is largely empirical, combining anatomical and physiological knowledge. The itemized table and an accumulation deduction system did provide a quantitative evaluation of injury degrees of three individual nerves. The experimental results show that the evaluation decisions of the proposed method are highly consistent with the clinical examination results, proving the feasibility and effectiveness of the proposed method.

Some differences remain when comparing the results of the proposed method and routine clinical assessment. One arm injury (i.e., the left arm of subject 5) was wrongly judged to be normal in Module I. In addition, there were multiple cases showing slight differences in estimating nerve injury degrees by Module II as compared to clinical assessment results. For example, the left ulnar nerve of subject 3 had no injury by the clinical assessment, but our method gave it a score of eight, representing slight injury. One possible reason is the meticulous quantification process of the proposed method, which uses the more detailed ten grades than the routine clinical evaluation with only three general grades. To make a comparison between these, we had to roughly categorize the ten grades into three intervals. Therefore, there is likely to be a loss of detailed information that might account for differences in PNI evaluation. Given the rough corresponding relation, however, a higher consistency between the PNI evaluation results from both approaches was yielded

when data from all subjects were pooled together. This was also due to the large tolerance of the general three-grade scale. The different mechanisms for PNI evaluation might also explain some inconsistent decisions by these methods. The clinical, electrophysiological examination focused on the integrity of the nerve conduction pathway, while the proposed method involved the evaluation of motor functions associated with the tested nerves. Considering the complexity of neuromuscular mappings in both anatomic and functional aspects, some ambiguities or differences seem reasonable. Because of this, the proposed PNI diagnosis method conformed to the physiological essence of neuromuscular function, and the quantitative evaluation decisions were found to be closer to the subjects' motor performance, which was a better reflection of the subjects' ability during ADL.

It is worth noting that the proposed method using surface EMG is not a substitute for the traditional clinical assessment method, but it serves as a useful and complementary tool for PNI evaluation. Furthermore, given the rapid development of mobile sensing and computing technologies, miniaturized and wearable devices make it easier to collect and analyze surface EMG signals pervasively. The intelligent expert system built with advanced signal processing machine learning algorithms makes the diagnosis convenient and suitable for family and community rehabilitation. These traits contribute to the management and treatment of PNI. The universal adaptation of myoelectric data recording and processing system can also benefit the field of forensic identification. If this system is available, there is no need to wait for a professional doctor or forensic expert to give an opinion in the forensic appraisal, and this approach can be easily operated by the grassroots police instead. Thus, this enables early judicial intervention to PNI cases and facilities the mediation of associated civil disputes. It is of great significance for Chinese law enforcement officials to quickly settle some issues with the aid of this convenient PNI evaluation tool.

Although the involuntary EMG signal following PNI mainly showed spontaneous fasciculations instead of spastic muscular activities, the proposed detection method was designed according to their same characteristics, which have been previously reported (Zhang et al., 2013a,b). Thus, the proposed method could be extended for spastic EMG detection and be applied to the detection and quantitative evaluation of upper central nervous system injuries.

It should be acknowledged that the relatively small sample size remains the main limitation of the current study. As a result, a relatively simple data analysis protocol was applied with a general purpose of verifying the feasibility of the proposed framework for quantitatively evaluating the nerve injury degree in traumatic upper limb PNI. Therefore, some detailed information cannot be considered or fully investigated in this study. For example, hand dominance usually affects the motor performance of the upper limb, and it was not considered due to the limited number of recruited subjects. The validity of the current study relies on the assumption that the effect of hand dominance is limited as compared to the impact of PNI on upper-limb motor function, which is regarded to be true in general cases. Through the cross-validation strategy, the satisfactory performance of the proposed method demonstrated its good generation and usability in actual applications (to predict the degree of PNI for an unknown subject). This finding, fortunately, confirms, in part, the limited effect of the hand dominance on the PNI evaluation. However, more data needs to be collected with an enlarged sample size to promote the usability of the proposed method, and advanced machine learning algorithms are required toward improved performance of the PNI evaluation. All of these efforts are part of our planned future work.

DATA AVAILABILITY STATEMENT

The datasets generated for this study are available on request to the corresponding author.

ETHICS STATEMENT

The studies involving human participants were reviewed and approved by Medical Ethics Review Committee of The First Affiliated Hospital of Anhui Medical University. The patients/participants provided their written informed consent to participate in this study.

AUTHOR CONTRIBUTIONS

WT collected and analyzed the data, interpreted the results, and wrote the first draft of the manuscript. XZ and YS conceived the study, conducted data collection, analysis, interpretation, and substantial revision of the manuscript. BY and XiC participated in the data collection and interpretation. XuC and XG participated in data interpretation and revised the manuscript. All the authors approved the final version of the manuscript.

FUNDING

This work was supported in part by the National Natural Science Foundation of China under Grant 61771444.

REFERENCES

Alexander, M. S., Anderson, K. D., Biering-Sorensen, F., Blight, A. R., Brannon, R., Bryce, T. N., et al. (2009). Outcome measures in spinal cord injury: recent assessments and recommendations for future directions. *Spinal Cord* 47:582. doi: 10.1038/sc.2009.18

Altimemy, A. H., Khushaba, R. N., Bugmann, G., and Escudero, J. (2016). Improving the performance against force variation of EMG controlled multifunctional upper-limb prostheses for transradial amputees. *IEEE Trans. Neural. Syst. Rehabil. Eng.* 24, 650–661. doi: 10.1109/tnsre.2015.2445634

Aminoff, M. J. (2012). *Clinical Electromyography, Electrodiagnosis in Clinical Neurology*, 6th Edn, Philadelphia, PA: Churchill Livingstone.

Campbell, W. W. (2008). Evaluation and management of peripheral nerve injury. *Clin. Neurophysiol.* 119, 1951–1965. doi: 10.1016/j.clinph.2008.03.018

Cappellini, G., Ivanenko, Y. P., Martino, G., MacLellan, M. J., Sacco, A., Morelli, D., et al. (2016). Immature spinal locomotor output in children with cerebral palsy. *Front. Physiol.* 7:478. doi: 10.3389/fphys.2016.00478

Chang, K. V., Wu, W. T., and Zakar, L. (2019). Ultrasound imaging and rehabilitation of muscle disorders: part 1. traumatic injuries. *Am. J. Phys. Med. Rehabil.* 98:1.

Chen, B., and Zhou, P. (2014). "Detection of fasciculation potentials in amyotrophic lateral sclerosis using surface EMG," in *Frontier and Future Development of Information Technology in Medicine and Education*, eds S. Li, Q. Jin, X. Jiang, and J. Park (Dordrecht: Springer), 2437–2442. doi: 10.1007/978-94-007-7618-0_302

de Carvalho, M., and Swash, M. (1998). Fasciculation potentials: a study of amyotrophic lateral sclerosis and other neurogenic disorders. *Muscle Nerve* 21, 336–344. doi: 10.1002/(sici)1097-4598(199803)21:3<336::aid-mus7>3.0.co;2-b

Englehart, K. (1998). *Signal Representation For Classification Of The Transient Myoelectric Signal*. Ph.D. thesis, University of New Brunswick, Fredericton.

Englehart, K., and Hudgins, B. (2003). A robust, real-time control scheme for multifunction myoelectric control. *IEEE Trans. Biomed. Eng.* 50, 848–854. doi: 10.1109/tbme.2003.813539

Englehart, K., Hudgins, B., Parker, P. A., and Stevenson, M. (1999). Classification of the myoelectric signal using time-frequency based representations. *Med. Eng. Phys.* 21, 431–438. doi: 10.1016/s1350-4533(99)00066-1

Hermens, H. J., Boon, K. L., and Zilvold, G. (1984). The clinical use of surface EMG. *Electromyogr. Clin.* 24:243.

Kallenberg, L. A., and Hermens, H. J. (2009). Motor unit properties of biceps brachii in chronic stroke patients assessed with high-density surface EMG. *Muscle Nerve* 39, 177–185. doi: 10.1002/mus.21090

Li, Y., Zhang, X., Gong, Y., Cheng, Y., Gao, X., and Chen, X. (2017). Motor function evaluation of hemiplegic upper-extremities using data fusion from wearable inertial and surface EMG sensors. *Sensors* 17:582. doi: 10.3390/s17030582

Li, Z., Zhao, X., Han, J., and Liu, G. (2016). "Comparisons on different sEMG-features with dimension-reduction methods in hand motion recognition," in *Proceedings of the International Conference On Advanced Robotics And Mechatronics*, Macau.

Mika, S., Ratsch, G., Weston, J., Scholkopf, B., and Mullers, K. R. (1999). "Fisher discriminant analysis with kernels," in *Proceedings of the 1999 IEEE Signal Processing Society Workshop*, Madison, NJ. doi: 10.1109/NNSP.1999.788121

Noble, J., Munro, C. A., Prasad, V. S., and Midha, R. (1998). Analysis of upper and lower extremity peripheral nerve injuries in a population of patients with multiple injuries. *J. Trauma Acute Care Surg.* 45, 116–122. doi: 10.1097/00005373-199807000-00025

Phinyomark, A., Phukpattaranont, P., and Limsakul, C. (2012). Feature reduction and selection for EMG signal classification. *Expert Syst. Appl.* 39, 7420–7431. doi: 10.1016/j.eswa.2012.01.102

Robinson, L. R. (2000). Traumatic injury to peripheral nerves. *Muscle Nerve* 23, 863–873. doi: 10.1002/(sici)1097-4598(200006)23:6<863::aid-mus4>3.0.co;2-0

Sallomi, D., Janzen, D. L., Munk, P. L., Connell, D. G., and Tirman, P. F. (1998). Muscle denervation patterns in upper limb nerve injuries: MR imaging findings and anatomic basis. *Am. J. Roentgenol.* 171, 779–784. doi: 10.2214/ajr.171.3.9725316

Selecki, B. R., Ring, I. T., Simpson, D. A., Vanderfield, G. K., and Sewell, M. F. (1982). Trauma to the central and peripheral nervous systems part Ii: a statistical profile of surgical treatment new south wales 1977. *Austral. New Zeal. J. Surg.* 52, 111–116. doi: 10.1111/j.1445-2197.1982.tb06081.x

Sherwood, A. M., McKay, W. B., and Dimitrijeviæ, M. R. (1996). Motor control after spinal cord injury: assessment using surface EMG. *Muscle Nerve* 19, 966–979. doi: 10.1002/(sici)1097-4598(199608)19:8<966::aid-mus5>3.0.co;2-6

Smola, A., Bartlett, P., Schölkopf, B., and Schuurmans, D. (2000). *Linear Discriminant and Support Vector Classifiers. Advances in Large-Margin Classifiers*. Cambridge, MA: MIT Press.

Steele, K. M., Rozumalski, A., and Schwartz, M. H. (2015). Muscle synergies and complexity of neuromuscular control during gait in cerebral palsy. *Dev. Med. Child Neurol.* 57, 1176–1182. doi: 10.1111/dmcn.12826

Sunderland, S. (1968). *Nerves and Nerve In Juries*. Edinburgh: E& S Livingstone Ltd.

Tang, L., Li, F., Cao, S., Zhang, X., Wu, D., and Chen, X. (2015). Muscle synergy analysis in children with cerebral palsy. *J. Neural Eng.* 12:046017. doi: 10.1088/1741-2560/12/4/046017

Tang, X., Zhang, X., Gao, X., Chen, X., and Zhou, P. (2018). A novel interpretation of sample entropy in surface electromyographic examination of complex neuromuscular alternations in subacute and chronic stroke. *IEEE Trans. Neural. Syst. Rehabil. Eng.* 26, 1878–1888. doi: 10.1109/tnsre.2018.2864317

Vaiman, M., and Eviatar, E. (2009). Surface electromyography as a screening method for evaluation of dysphagia and odynophagia. *Head Face Med.* 5:9.

Wang, D., Zhang, X., Gao, X., Chen, X., and Zhou, P. (2016). Wavelet packet feature assessment for high-density myoelectric pattern recognition and channel selection toward stroke rehabilitation. *Front. Neurol.* 7:197. doi: 10.3389/fphys.2016.00197

Webb, A. R. (2003). *Linear Discriminant Analysis. Statistical Pattern Recognition*. Hoboken, NJ: John Wiley & Sons, Ltd.

Zeidenberg, J., Burks, S. S., Jose, J., Subhawong, T. K., and Levi, A. D. (2015). The utility of ultrasound in the assessment of traumatic peripheral nerve lesions: report of 4 cases. *Neurosurg. Focus* 39:214.

Zeng, Y., Yang, J. T., Peng, C., and Yin, Y. (2019). Evolving gaussian process autoregression based learning of human motion intent using improved energy kernel method of EMG. *IEEE Trans. Biomed. Eng.* 66, 2556–2565. doi: 10.1109/TBME.2019.2892084

Zhang, H., Zhao, Y., Yao, F., Xu, L., Shang, P., and Li, G. (2013). An adaptation strategy of using LDA classifier for EMG pattern recognition. *Conf. Proc. IEEE Eng. Med. Biol. Soc.* 2013, 4267–4270.

Zhang, X., Barkhaus, P. E., Rymer, W. Z., and Zhou, P. (2013a). Machine learning for supporting diagnosis of amyotrophic lateral sclerosis using surface electromyogram. *IEEE Trans. Neural. Syst. Rehabil. Eng.* 22, 96–103. doi: 10.1109/tnsre.2013.2274658

Zhang, X., Li, Y., Chen, X., Li, G., Rymer, W. Z., and Zhou, P. (2013b). The effect of involuntary motor activity on myoelectric pattern recognition: a case study with chronic stroke patients. *J. Neural Eng.* 10:046015. doi: 10.1088/1741-2560/10/4/046015

Zhang, S., Zhang, X., Cao, S., Gao, X., Chen, X., and Zhou, P. (2017). Myoelectric pattern recognition based on muscle synergies for simultaneous control of dexterous finger movements. *IEEE Trans. Hum. Mach. Syst.* 47, 576–582. doi: 10.1109/thms.2017.2700444

Conflict of Interest: The authors declare that the research was conducted in the absence of any commercial or financial relationships that could be construed as a potential conflict of interest.

frontiers in Bioengineering and Biotechnology

ORIGINAL RESEARCH
published: 06 August 2020
doi: 10.3389/fbioe.2020.00939

Short-Step Adjustment and Proximal Compensatory Strategies Adopted by Stroke Survivors With Knee Extensor Spasticity for Obstacle Crossing

Shang-Jun Huang[1], Xiao-Ming Yu[2], Kuan Wang[3], Le-Jun Wang[4], Xu-Bo Wu[5], Xie Wu[6] and Wen-Xin Niu[1]**

[1] Key Laboratory of Spine and Spinal Cord Injury Repair and Regeneration of Ministry of Education, Orthopaedic Department, Tongji Hospital, Tongji University School of Medicine, Shanghai, China, [2] Department of Rehabilitation, Shanghai Seventh People's Hospital, Shanghai University of Traditional Chinese Medicine, Shanghai, China, [3] Yangzhi Rehabilitation Hospital, Tongji University School of Medicine, Shanghai, China, [4] Sport and Health Research Center, Physical Education Department, Tongji University, Shanghai, China, [5] School of Rehabilitation Medicine, Shanghai University of Traditional Chinese Medicine, Shanghai, China, [6] Key Laboratory of Exercise and Health Sciences, Ministry of Education, Shanghai University of Sport, Shanghai, China

OPEN ACCESS

Edited by:
Le Li,
Sun Yat-sen University, China

Reviewed by:
Chi-Wen Lung,
Asia University, Taiwan
Fan Gao,
University of Kentucky, United States

***Correspondence:**
Xie Wu
wuxie_sus@163.com
Wen-Xin Niu
niu@tongji.edu.cn

Specialty section:
This article was submitted to Biomechanics, a section of the journal Frontiers in Bioengineering and Biotechnology

Received: *28 March 2020*
Accepted: *20 July 2020*
Published: *06 August 2020*

Citation:
Huang S-J, Yu X-M, Wang K, Wang L-J, Wu X-B, Wu X and Niu W-X (2020) Short-Step Adjustment and Proximal Compensatory Strategies Adopted by Stroke Survivors With Knee Extensor Spasticity for Obstacle Crossing. Front. Bioeng. Biotechnol. 8:939. doi: 10.3389/fbioe.2020.00939

Stroke survivors adopt cautious or compensatory strategies for safe and successful obstacle crossing. Although knee extensor spasticity is a common independent secondary sensorimotor disorder post-stroke, few studies have examined the step adjustment and compensatory strategies used by stroke survivors with knee extensor spasticity during obstacle crossing. This study aimed to compare the differences in the kinematics and kinetics during obstacle crossing between stroke survivors with and without knee extensor spasticity, and to identify knee extensor spasticity-related differences in step adjustment and compensatory strategies. Twenty stroke subjects were divided into a spasticity group [n = 11, modified Ashworth scale (MAS) $\geq$ 1] and a non-spasticity group (n = 9, MAS = 0), based on the MAS score of the knee extensor. Subjects were instructed to walk at a self-selected speed on a 10-m walkway and step over a 15 cm obstacle. A ten-camera 3D motion analysis system and two force plates were used to collect the kinematic and kinetic data. During the pre-obstacle phase, stroke survivors with knee extensor spasticity adopted a short-step strategy to approach the obstacle, while the subjects without spasticity used long-step strategy. During the affected limb swing phase, the spasticity group exhibited increased values that were significantly higher than those seen in the non-spasticity group for the following measurements: pelvic lateral tilt angle, trunk lateral tilt angle, medio-lateral distance between the ankle and ipsilateral hip joint, hip work contributions, the inclination angles between center of mass and center of pressure in anterior–posterior and medio-lateral directions. These results indicate that the combined movement of the pelvic, trunk lateral tilt, and hip abduction is an important compensatory strategy for successful obstacle crossing, but it sacrifices some balance in the sideways direction. During

the post-obstacle phase, short-step and increase step width strategy were adopted to reestablish the walking pattern and balance control. These results reveal the step adjustment and compensatory strategies for obstacle crossing and also provide insight into the design of rehabilitation interventions for fall prevention in stroke survivors with knee extensor spasticity.

Keywords: stroke, spasticity, compensatory strategy, gait, biomechanics

INTRODUCTION

Stroke often results in spasticity and associated motor impairments in the lower limbs, including muscle weakness (Li et al., 2014), proprioceptive deficit (Gorst et al., 2019), abnormal agonist-antagonist coactivation (Trumbower et al., 2010), and altered inter-joint and inter-segmental coordination (Subramanian et al., 2018; Salehi et al., 2020). In clinical rehabilitation, the spasticity and movement deficits disorders have been traditionally been considered as separate phenomena (Levin, 2016). However, spasticity is not just an independent disorder, it has a negative effect on other motor disorders. One previous study demonstrated that spasticity affects passive tissue stiffness and disrupts the agonist-antagonist activation pattern, which alters the net effect of the forces generated by the muscle groups (Singer et al., 2013). In addition, lower limb spasticity can interfere with proprioceptive inputs, inter-limb coordination, and balance control in stroke survivors (Singer et al., 2013; Singer and Mochizuki, 2015; Yang and Kim, 2015; Rahimzadeh Khiabani et al., 2017). As a result, community ambulation tasks, such as obstacle crossing, can be more challenging for stroke survivors with lower limb spasticity than for those without (Soyuer and Ozturk, 2007).

Obstacle crossing is a complex task in community ambulation (Raffegeau et al., 2019). When healthy adults step over obstacles, a 'knee strategy' is used, whereby mechanical energy is generated above the knee joint to flex both the knee and hip simultaneously (MacLellan et al., 2015). Obviously, the hip flexor (knee extensor) and knee flexor together are the main power sources for clearance and limb swing. Motor disorders after a stroke cause subjects to fall during obstacle crossing due to imbalance or tripping (Said et al., 2013; Ma et al., 2017; Punt et al., 2017). One basic motor skill of stroke survivors is the ability to initiate an appropriate movement strategy to counter the change in environmental conditions and task demands based on their functional level, including step adjustment and compensatory strategies to complete the task and maintain balance (Banina et al., 2017; Malik et al., 2017; Shafizadeh et al., 2019). Several such strategies for safe and successful obstacle crossing have been reported in stroke survivors, by comparing the obstacle crossing biomechanics of stroke survivors and age-matched healthy controls subjects, respectively (Said et al., 2008; Lu et al., 2010; Nakano et al., 2014; MacLellan et al., 2015; Chen et al., 2019; Shafizadeh et al., 2019). Experimental studies of these strategies may aid our understanding of motor control, and may help in the development of better fall prevention training programs.

During unperturbed human walking, the spatial and temporal characteristics of the steps are relatively fixed and typically show low step-to-step variability (Den Otter et al., 2005). Step modifications often involve rigorous re-parameterization of forces and require a high level of neuromuscular control (Sun et al., 2017). Consequently, stroke survivors with impaired neuromuscular functioning may be more vulnerable to perturbations of the motor task and ongoing stepping pattern (Den Otter et al., 2005). When stroke survivors approach an obstacle, the steps must be modified in due time to minimize disturbance to the gait, even in the absence of temporal constraints. Nakano et al. (2014) suggested that the short-step strategy was used by stroke survivors to approach the obstacle, which probably was intended to enhance the accuracy of swing and maintain stability. Additionally, several studies demonstrated that a "hip abduction strategy" was adopted by stroke survivors to compensate for the lack of knee flexion in crossing the obstacle successfully (Lu et al., 2010; Chen et al., 2019). Inconsistently, a previous study demonstrated that the "residual knee flexor and hip flexion strategy" is still present in the affected limb, and augmented by hip elevation and flexion (MacLellan et al., 2015). Although knee extensor spasticity is a common and independent secondary sensorimotor disorder post-stroke, few studies have examined the step adjustment and compensatory strategies used by stroke survivors with knee extensor spasticity during obstacle crossing.

Spatiotemporal parameters and joint kinematics provide information about adjustments and compensatory strategies for successful obstacle crossing and balance. One previous study reported that stroke survivors were more unstable than healthy adults (Said et al., 2005). To compensate for this instability, stroke survivors reduced the anterior–posterior (AP) speed of their center of mass (COM), shortened their step length, and shifted their COM posteriorly when the affected limb was crossing an obstacle. Chen et al. (2019) reported that the hip abduction angles and pelvic medio-lateral (ML) tilt angles of stroke survivors are larger than those of healthy subjects when the affected limbs are crossing obstacles. Additionally, recent studies have suggested that the COM-COP (center of pressure, COP) inclination angle could sensitively identify individuals with imbalance and fall risk among stroke survivors during walking and obstacle crossing (Chen and Chou, 2010; van Vugt et al., 2019). Hence, spatiotemporal parameters and joint kinematics were helpful in identifying the compensatory strategies and risk of falling during obstacle crossing.

Kinetic analysis provides insight into how to elevate lower limb to step an obstacle. As mentioned previously, the hip abduction strategy is an important compensatory strategy for successful obstacle crossing in stroke survivors. Inconsistently, MacLellan et al. (2015) studied the kinetic strategies of stroke

survivors for obstacle avoidance with either the affected or unaffected as the leading limb, and demonstrated that the residual knee flexor strategy is still present in the paretic limb, and augmented by hip elevation and flexion. Furthermore, one previous study reported that estimating the relative contribution of each joint to the total energy generated during the swing phase is a useful approach for understanding the degree of compensation strategy (Teixeira-Salmela et al., 2008). Therefore, the joint work and work contributions can be used to examine compensatory strategies for successful obstacle crossing.

The purpose of this study was to systematically examine the step adjustment and compensatory strategies used by stroke survivors with knee extensor spasticity during obstacle crossing. To achieve this goal, we compared the biomechanics of obstacle crossing between stroke survivors with and without knee extensor spasticity. A previous study suggested that the coupling of movement between the pelvic and trunk contributed to the compensatory strategy for complex tasks (Malone et al., 2016; Han et al., 2017). Therefore, we hypothesized that stroke survivors with knee extensor spasticity rely more on the trunk movement compared to those without spasticity when the affected limb is crossing an obstacle. A previous study showed that the degree of trunk movement was restricted in order to enable body stability in the early stage of motor learning and balance development (Rhee and Kim, 2015). Due to the excessive movement of the trunk and pelvic, we also hypothesized that stroke survivors with knee extensor spasticity have a higher COM-COP ML inclination angle than those without spasticity.

MATERIALS AND METHODS

Study Design

A biomechanical cross-sectional study was conducted to compare the differences in the kinematics and kinetics between stroke survivors with and without knee extensor spasticity during the crossing of 15 cm, and to identify the knee extensor spasticity-related changes in step adjustment and compensatory strategies for obstacle crossing.

Sample Size

The sample size was calculated using G*power software (v3.1.9.2) based on a comparison of the pelvic lateral tilt angle between the stroke survivors and age-matched healthy controls during obstacle crossing. A previous study showed that the means and standard deviations of the pelvic lateral tilt angle were 12.12° and 5.87°, and 8.14° and 9.38° in the stroke and healthy control groups, respectively (Chen et al., 2019). According to a prior one-way ANOVA *F*-test, with a power of 0.80 and an alpha level of 0.05, an estimated 14 participants were required for this study.

Participants

Twenty stroke subjects were recruited from the Seventh People's Hospital and community centers in the vicinity (Gaoqiao, Pudong District, Shanghai, China) using flyers, posters, and referrals from neurologists and physical therapists between October 2017 and November 2018. The basic characteristics of the subjects are shown in **Table 1**. The inclusion criteria were as follows: clinical diagnosis of cerebral hemorrhage or infarction by computed tomography/magnetic resonance imaging (CT/MRI), 30–75 years of age, ≥3 months since the stroke, a score of >24 on the Mini-Mental State Examination (MMSE), ability to walk 10 m without a gait aid or assistance, without the history of using ankle-foot orthoses, no botulinum toxin drug treatment within 3 months and ability to cross an obstacle with a height of 15 cm. The exclusion criteria included current involvement in any other clinical study or instructor-directed exercise program, vision disorders, severe hypertension or cardiopulmonary diseases, and lower limb joint or muscle injuries.

A modified Ashworth scale (MAS) was used to assess the resistance to passive movement and to indirectly measure spasticity level of the knee extensor (Ansari et al., 2008; Meseguer-Henarejos et al., 2018). The subjects were instructed to lie on a bed, with their hips and knees in extension. Behind the subject, the evaluator placed one hand just proximal to the knee to stabilize the femur, and the other hand grasped the leg just proximal to the ankle. The subject's knee was flexed from a position of maximal possible extension to maximal possible flexion over a duration of approximately 1 s (Blackburn et al., 2002). Only one movement was allowed to determine the resistance to passive movement (Ansari et al., 2008). A single physical therapist with many years of assessment experience performed all evaluations, in order to eliminate extraneous variability in the assessment results and to ensure accuracy. Twenty stroke subjects were divided into two groups: subjects with spasticity (n = 11, MAS ≥ 1) and a control group of stroke subjects without spasticity (n = 9, MAS = 0), according to the MAS score of the knee extensor. This study was approved by the institutional review board of Shanghai Seventh People's Hospital (2018-IRBQYYS-012). Informed consent was obtained from all participants enrolled in the study.

TABLE 1 | Basic characteristics of study subjects.

Characteristics	Spasticity group	Non-spasticity group	F/χ^2	*P*
Age (years)	60.02 (54.09–65.91)	61.33 (55.54–67.12)	0.129	0.724
Height (m)	1.72 (1.66–1.75)	1.69 (1.66–1.72)	0.799	0.383
Mass (kg)	73.81 (69.67–77.93)	67.39 (64.28–70.50)	4.316	0.052
Time post-stroke (months)	11.39 (7.44–15.34)	9.35 (4.54–14.16)	0.562	0.463
Sex (female/male)	9/2	6/3	0.617	0.396
Type of stroke (Isc/Hem)	9/2	5/4	0.336	0.217
Affected side (left/right)	6/5	4/5	0.000	1.000
MAS (score)	1.45 (1.14–1.77)	0.00 (0.00–0.00)	84.637	0.000
MMSE (score)	27.55 (26.19–28.90)	28.11 (26.17–30.05)	0.311	0.584
FMA (score)	25.82 (22.20–31.25)	28.44 (26.09–30.35)	1.201	0.288
BBS (score)	45.73 (45.51–51.40)	48.89 (47.75–51.59)	3.519	0.077

A score of 1+ on the modified Ashworth scale was entered as 1.5. Isc, ischemic stroke; Hem, hemorrhagic stroke; MAS, modified Ashworth scale; MMSE, mini-mental state examination; FMA, Fugl-Meyer assessment; BBS, Berg Balance Scale.

Apparatus

A total of 50 spherical 14-mm infrared-reflective markers were fastened to each subject's body according to the Vicon Plug-in-Gait model. A 10-camera 3D motion analysis system (Vicon Motion Systems, Oxford, United Kingdom) recorded the marker trajectory data at a sampling frequency of 100 Hz. Two force plates (900 mm × 600 mm × 140 mm, Kistler Instruments AG Corp., Switzerland) recorded the kinetic data at a sampling frequency of 1,000 Hz. The data from the 3D motion analysis system and force plates were systematically synchronized using the terminal box of an Analog/Digital converter. The obstacle consisted of two upright stands with a lightweight crossbar of adjustable height. The obstacle was placed in the middle of the two force plates. Two markers were attached to the obstacle to mark the relative position between the obstacle and the subject.

Procedure

Lower limb function (Fugl-Meyer Assessment, FMA), balance function (Berg Balance Scale, BBS), and cognitive level (MMSE) of all subjects were evaluated by an experienced physiotherapist before measuring each subject's biomechanics. The results of the clinical tests are provided in **Table 1**.

The subjects wore loose-fitting shorts and walking shoes. The obstacle height was set to 15 cm, which is equal to the typical height stairs in the community. A previous study demonstrated that a self-selected walking speed is a good indicator of overall gait performance and is commonly used to assess locomotor ability (Teixeira-Salmela et al., 2008). Therefore, subjects were instructed to walk at a self-selected speed on a 10 m walkway and step over the 15 cm obstacle without contacting it or losing balance. The subjects were instructed to use their affected leg as the leading limb for obstacle crossing (i.e., the first limb to cross the obstacle). Before data collection, the subjects performed five trials at a comfortable speed to familiarize themselves with the experimental environment and action. Data for each subject were then collected from three successive trials. Subjects were instructed to perform the task within their limits of safety and stop if they felt at risk. For security, a therapist walked alongside each subject to assist them, if required. A trial was excluded from analysis if the participant required the therapist's assistance to maintain balance or tripped over the obstacle.

Data Processing

Vicon Nexus (Version 1.8.5) and Visual 3D (C-Motion, Inc., United States) were used for kinematic and kinetic data processing. Trajectory data were filtered offline using a dual-pass, 4th-order Butterworth filter with a cutoff frequency of 6 Hz (MacLellan et al., 2015). From these data, a 15-segment biomechanical model (head, trunk, pelvic, 2 forearms, 2 upper arms, 2 hands, 2 thighs, 2 shanks, and 2 feet) was created, based on Visual 3D software. A crossing cycle was defined as the period beginning with the unaffected limb's heel contact before the obstacle to its next heel contact after crossing the obstacle (Chen et al., 2019). The crossing cycle was divided into four phases: a pre-obstacle double-support phase, an affected-limb swing phase, a middle-crossing double-support phase, and an unaffected-limb swing phase.

Spatiotemporal parameters provide information about step adjustment strategies for successful obstacle crossing and balance. The obstacle crossing was divided into pre-obstacle and post-obstacle phases according to the relative distance between the COM and the marker on the obstacle in AP direction. Step length was measured from heel to heel in the AP direction, and step width was measured from heel to heel in the ML direction during the pre-obstacle and post-obstacle phases. The step-to-step length variability was calculated for each step number during the pre-obstacle and post-obstacle phases (Eq. 1) (Laessoe and Voigt, 2013). Affected and unaffected swing times were calculated from the toe-off to the ipsilateral heel-contact (vertical ground reaction force $\geq$ 10 N). Two double-support phases were measured: the first from the heel contact of the unaffected limb heel to the toe-off of the affected limb during the pre-obstacle phase (DST1) and the second from the heel contact of the affected limb to the toe-off of the unaffected limb during middle-crossing (DST2). In addition, we examined three distances between the lower limb and the obstacle. The toe-obstacle distance is the horizontal distance between the unaffected-toe marker and the obstacle during the pre-obstacle phase; the heel-obstacle distance (HOD) is the horizontal distance between the heel marker of the affected limb and the obstacle during the post-obstacle phase; the toe-obstacle clearance is the vertical distance between the toe of the swing limb and the obstacle when the toe marker was above the obstacle.

$$Step\ length\ variability\ = \frac{Step_{post} - Step_{pre}}{Step_{pre}} \times 100\% \quad (1)$$

The kinematics of the lower limb joint, pelvic, and trunk were calculated to examine the compensatory strategies for successful obstacle crossing. Because the affected side differed among subjects, we defined the direction of tilt and rotation of the contralateral side as [+] and the ipsilateral side as [−] to understand the compensatory strategy better. COM position data were calculated as the weighted sum of each body segment using the whole-body model. The COP is derived from data collected from the two force plates. The averaged AP COM velocity was calculated during the pre-obstacle phase. Instantaneous COM AP and ML velocity were examined when the swing limb toe marker was above the obstacle (i.e., the affected limb, COMV1; the unaffected limb, COMV2). The moment was determined by the smallest distance between the toe marker and the obstacle in AP direction. A previous study demonstrated that the instantaneous COM-COP inclination angles provided information about balance control and fall risk (**Figure 1**) (Chen and Chou, 2010). Therefore, we calculated instantaneous COM-COP AP and ML inclination angles during the swing phases of the affected and unaffected limbs.

The joint work and joint work contributions provides insight into how to elevate lower limb to step an obstacle (Teixeira-Salmela et al., 2008). Therefore, the joint work (W), total work of limb [W_{total}, Eq. (2)], and contributions to the total work [$Cont_{\text{hip}}$, Eq. (3); $Cont_{\text{knee}}$, Eq. (4)] were calculated during the affected- and unaffected-limb swing phases in this study. The

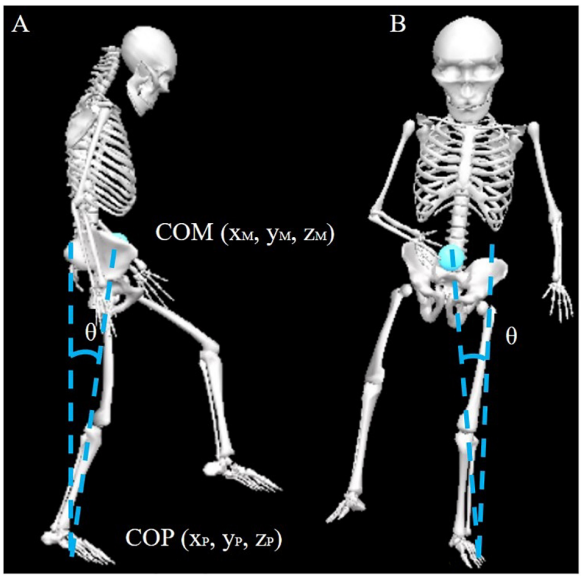

FIGURE 1 | Diagram of COM-COP inclination angles in the sagittal **(A)** and frontal planes **(B)**. COM, center of mass; COP, center of pressure.

biomechanical outcomes from the three trials for each subject were then averaged for subsequent statistical analysis.

$$W_{total} = |W_{ankle}| + |W_{knee}| + |W_{hip}| \quad (2)$$

$$Cont_{hip} = \frac{|W_{hip}|}{|W_{total}|} \quad (3)$$

$$Cont_{knee} = \frac{|W_{knee}|}{|W_{total}|} \quad (4)$$

Statistical Analysis

All statistical analyses were performed using IBM SPSS, version 20.0 (SPSS Inc., Chicago, IL, United States). All the calculated variables for both groups were first subjected to a Shapiro–Wilk test. Some variables did not show a normal distribution, and the Mann–Whitney *U* test was applied to test the group-differences. Other continuous variables showing a normal distribution were tested using one-way ANOVA, and the chi-square test was used for categorical variables. The significance level was set at 0.05.

RESULTS

Except for MAS, no significant differences were observed in the basic characteristics and clinical test results between the two groups (**Table 1**). A schematic diagram of typical trials in the spasticity group and the non-spasticity group during obstacle crossing was shown in **Figure 2**. Additionally, none of the participants exhibited contracture at any of the joints of the lower-limb during the biomechanical test.

Spatiotemporal Parameters During Obstacle Crossing

Spatiotemporal parameters during obstacle crossing for the two groups were presented in **Table 2**. Compared to the non-spasticity group, the spasticity group exhibits significantly slower COM AP velocity, slower $COMV1_{AP}$, slower $COMV2_{AP}$, shorter step length, longer DST1 and smaller toe-obstacle distance during the pre-obstacle phase. An increased step width and a decreased step length were observed in the spasticity group relative to the non-spasticity group during the post-obstacle phase. However, there were no significant differences between the two groups for other spatiotemporal parameters during obstacle crossing.

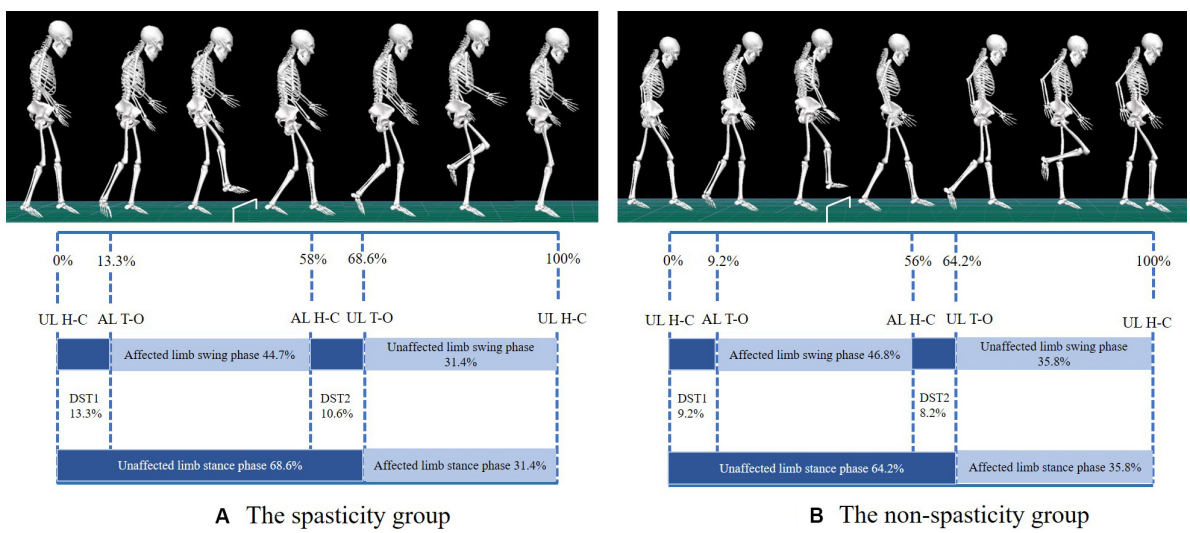

FIGURE 2 | Schematic diagram of typical trials in spasticity group **(A)** and non-spasticity group **(B)** during obstacle crossing. UL, unaffected limb; AL, affected limb; H-C, heel contact; T-O, toe-off; DST1, time between unaffected-limb heel contact and affected-limb toe-off during the pre-obstacle phase; DST2, time between affected-limb heel contact and unaffected-limb toe-off during middle crossing.

TABLE 2 | Comparison of spatiotemporal parameters by study group.

Parameters	Spasticity group	Non-spasticity group	F/χ^2	*P*
COM AP velocity (m/s)**	0.38 (0.32–0.40)	0.58 (0.41–0.77)	12.816	0.002
$COMV1_{AP}$ (m/s)**	0.25 (0.19–0.32)	0.47 (0.34–0.60)	12.542	0.002
$COMV1_{ML}$ (m/s)	0.022 (−0.01–0.025)	0.019 (0.02–0.025)	0.082	0.778
$COMV2_{AP}$ (m/s)**	0.35 (0.27–0.42)	0.53 (0.41–0.64)	10.006	0.005
$COMV2_{ML}$ (m/s)	0.041 (0.01–0.05)	0.036 (0.02–0.05)	0.098	0.758
SL_{PRE} (m)**	0.26 (0.23–0.30)	0.43 (0.37–0.47)	35.100	0.000
Cross step length (m)**	0.43 (0.39–0.47)	0.56 (0.51–0.61)	22.075	0.000
SL_{POST} (m)*	0.28 (0.21–0.34)	0.45 (0.36–0.54)	13.666	0.002
SW_{PRE} (m)	0.10 (0.07–0.13)	0.08 (0.03–0.13)	0.608	0.446
SW_{POST} (m)*	0.15 (0.13–0.18)	0.11 (0.08–0.15)	4.533	0.047
DST1 (%)*	13.34 (10.08–16.59)	9.23 (7.45–11.02)	5.381	0.032
DST2 (%)	10.60 (7.68–13.52)	8.18 (6.26–10.10)	1.031	0.157
Affected swing time (%)	44.67 (41.41–47.93)	46.79 (43.43–50.15)	2.180	0.323
Unaffected swing time (%)	31.40 (0.26–0.36)	35.80 (0.30–0.42)	1.681	0.211
TOD (m)**	0.12 (0.10–0.15)	0.22 (0.16–0.28)	13.456	0.002
TOC (m)	0.11 (0.06–0.17)	0.13 (0.09–0.16)	0.211	0.651
HOD (m)	0.07 (0.03–0.10)	0.10 (0.06–0.14)	1.905	0.184

*COM AP velocity, anterior–posterior velocity of COM during the pre-obstacle phase; $COMV1_{AP}$, anterior–posterior velocity of COM when the affected-limb toe marker is above the obstacle; $COMV1_{ML}$, medio-lateral velocity of COM when the affected-limb toe marker is above the obstacle; $COMV2_{AP}$, anterior–posterior velocity of COM when the unaffected-limb toe marker is above the obstacle; $COMV2_{ML}$, medio-lateral velocity of COM when the unaffected-limb toe marker is above the obstacle; SL, step length; SW, step width; DST1, time between unaffected-limb heel contact and affected-limb toe-off during the pre-obstacle phase; DST2, time between affected-limb heel contact and unaffected-limb toe-off during obstacle crossing; TOD, horizontal distance between the unaffected-limb toe marker and the obstacle during the pre-obstacle phase; HOD, horizontal distance between the affected-limb heel marker and the obstacle during the post-obstacle phase; TOC, vertical distance between the toe of the swing limb and the obstacle when the toe marker is above the obstacle. *$P < 0.05$, **$P < 0.01$.*

Figure 3 shows the step adjustment among the two groups during obstacle crossing. Compared to the non-spasticity group, an additional shortened step was observed in the spasticity group during the pre-obstacle phase, in front of the obstacle, prior to the actual crossing maneuver. Between steps −2 and −1, a negative and positive change percentage of the step length was observed in the spasticity group (−38.32 percentage points; 95% CI, 20.44. 56.20) and the non-spasticity group (48.56 percentage points; 95% CI, 9.02. 88.10), respectively. During the post-obstacle phase, an additional shortened step was also observed in the spasticity group prior to restoring step length between steps 1 and 3. Between cross step and step 1, a negative change in the percentage of the step length was found in the spasticity group (−53.98 percentage points; 95% CI, 28.61. 79.35) and the non-spasticity group (−39.37 percentage points; 95% CI, 15.98. 62.76), respectively. However, no significant difference was observed between the two groups ($F = 0.877$, $P = 0.361$). Additionally, a positive change in the percentage of the step length was found in the spasticity group between steps 2 and 3 (106.06 percentage points; 95% CI, 13.82. 198.29), and a positive change in the percentage of the step length was found in the non-spasticity group between steps 1 and 2 (91.79% percentage points; 95% CI, 9.28. 174.3). No significant group-differences were found ($F = 0.065$, $P = 0.802$).

Kinematics of Trunk, Pelvic, Lower Limb Joint, and COM-COP Inclination Angle During Swing Phases

Figure 4 shows the kinematics of the trunk and pelvic during obstacle crossing. Compared to the non-spasticity group, the trunk lateral tilt, pelvic lateral tilt, and pelvic rotation angles were higher in the spasticity group when the affected limb toe was above the obstacle (**Table 3A**). The trunk lateral tilt angle was higher in the spasticity group relative to the non-spasticity group when the unaffected-limb toe was above the obstacle (**Table 3B**).

Figure 5 shows the kinematics of the affected-limb hip, knee, and ankle during obstacle crossing. During the affected-limb swing phase, the hip rotation, knee flexion, and ankle dorsiflexion values were lower in the spasticity group relative to the non-spasticity group when the affected-limb toe was above the obstacle (**Table 3A**). No significant difference was observed between the two groups for toe-obstacle clearance (**Table 2**).

Figure 6 shows the kinematics of the unaffected-limb hip, knee, and ankle during obstacle crossing. However, no significant differences were observed between the two groups for all kinematic parameters during the unaffected-limb swing phase (**Tables 2**, **3**).

Figure 7 shows the COM-COP AP and ML inclination angles during the affected-limb swing phase and the unaffected-limb swing phase. During the swing phase of the affected limb, the COM-COP AP inclination angle was larger in the spasticity group (14.95°; 95% CI, 13.12. 16.77) than that in the non-spasticity group (2.45°; 95% CI, 1.53. 3.37) when the affected-limb toe marker was above the obstacle ($F = 772.378$, $P = 0.000$). Furthermore, the COM-COP ML inclination angle was larger in the spasticity group (9.29°; 95% CI, 4.08. 14.50) than that in the non-spasticity group (3.57°; 95% CI, 2.69. 4.46) when the affected-limb toe marker was above the obstacle ($F = 4.754$, $P = 0.043$). No significant differences were observed in the COM-COP AP and ML inclination angles between the two groups during the unaffected-limb swing phase.

Work and Work Contributions of Joints During Swing Phases

Table 4 shows the joints work and work contributions of the swing limb during the affected-limb and the unaffected-limb swing phases. During the swing phase of the affected-limb, the lower knee work, lower knee work contributions and higher hip work contributions were observed in the spasticity group than in the non-spasticity group. However, no significant differences were observed in work and work contributions between the two groups during the unaffected-limb swing phase.

DISCUSSION

The purpose of this study was to systematically examine the step adjustment and compensatory strategies used by stroke

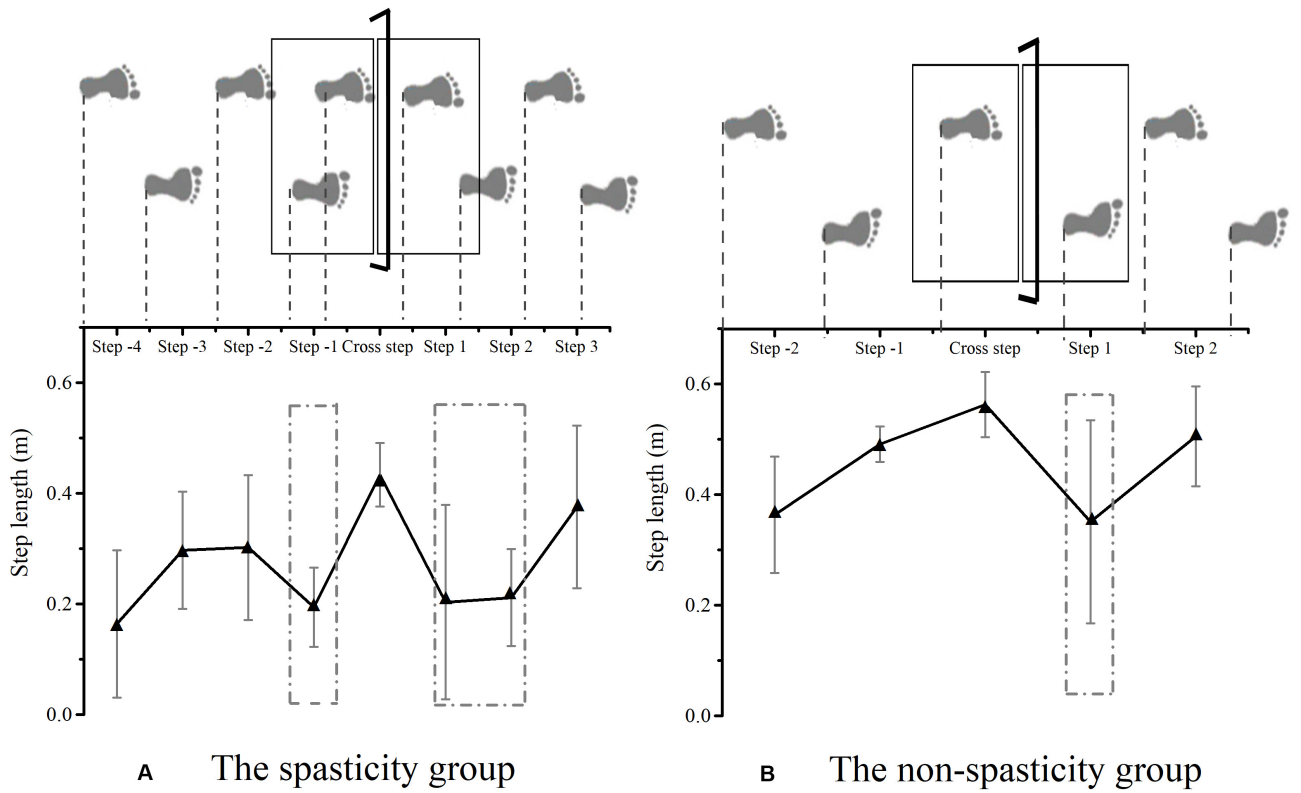

FIGURE 3 | Schematic explanation of step adjustments strategy among the spasticity group **(A)** and the non-spasticity group **(B)** during obstacle crossing. **(A)** The spasticity group; **(B)** the non-spasticity group; Mean values and standard deviation for each step in the two groups were plotted as black and gray lines, respectively. The dash-dotted rectangular area represents the location of step adjustment.

survivors with knee extensor spasticity during obstacle crossing. In the present study, we compared kinematics and kinetics of a spasticity group versus a non-spasticity group during the crossing of a 15 cm obstacle and identified knee extensor spasticity-related differences in step adjustment and compensatory strategies. Our results demonstrate that stroke survivors with knee spasticity use different step adjustment and compensatory strategies during the different phases of the obstacle crossing. As expected, the coupling of movement between the pelvic and trunk is an important compensatory strategy for successful obstacle crossing, but it sacrifices some balance in the sideways direction (Rhee and Kim, 2015; van Vugt et al., 2019). These results revealed the step adjustment and compensatory strategies for obstacle crossing and also provide insight into the design of rehabilitation interventions for fall prevention in stroke survivors with knee extensor spasticity.

When the stroke survivors approach the obstacle, the steps must be modified in due time to minimize disturbance to the gait, even in the absence of temporal constraints (Nakano et al., 2014). Step adjustment strategies are necessary to cross the obstacle successfully and maintain balance during complex community ambulation (Laessoe and Voigt, 2013). Several studies reported that the step length and COM AP velocity were significantly smaller in stroke survivors than in healthy controls (healthy controls reference value, 0.69 m, 1.05 m/s) (Said et al., 2008). Therefore, we expected a shorter step length and slower COM AP velocity in the spasticity group than the non-spasticity group, due to the knee extensor spasticity. As expected, a shorter step length and slower COM AP velocity were observed in the spasticity group relative to the non-spasticity group during the pre-obstacle phase in the present study. This finding was consistent with comparisons between stroke and healthy subjects in previous studies (Said et al., 2008; Nakano et al., 2014; Chen et al., 2019). Nakano et al. (2014) suggested that the short-step strategy was used by stroke survivors to step over the obstacle, which probably intended to enhance the accuracy of swing and maintain stability. The smaller step length positions the COP closer to the COM, which could result in smaller moment arms for bodyweight of the stance limb, and requires less muscular effort to maintain balance (Chou et al., 2003; Said et al., 2008). In addition, the slower COM AP velocity has the potential advantage of easily regaining stability (Said et al., 2008). More importantly, the spasticity group added an additional shortened step between step −2 and cross step prior to the actual crossing maneuver. Successful community ambulation depends on the ability to adapt gait to the environment and to diverse behavioral goals (Malone et al., 2016). A possible explanation for this finding might be that the spasticity group integrates the available sensory and environmental information to initiate an appropriate or cautious

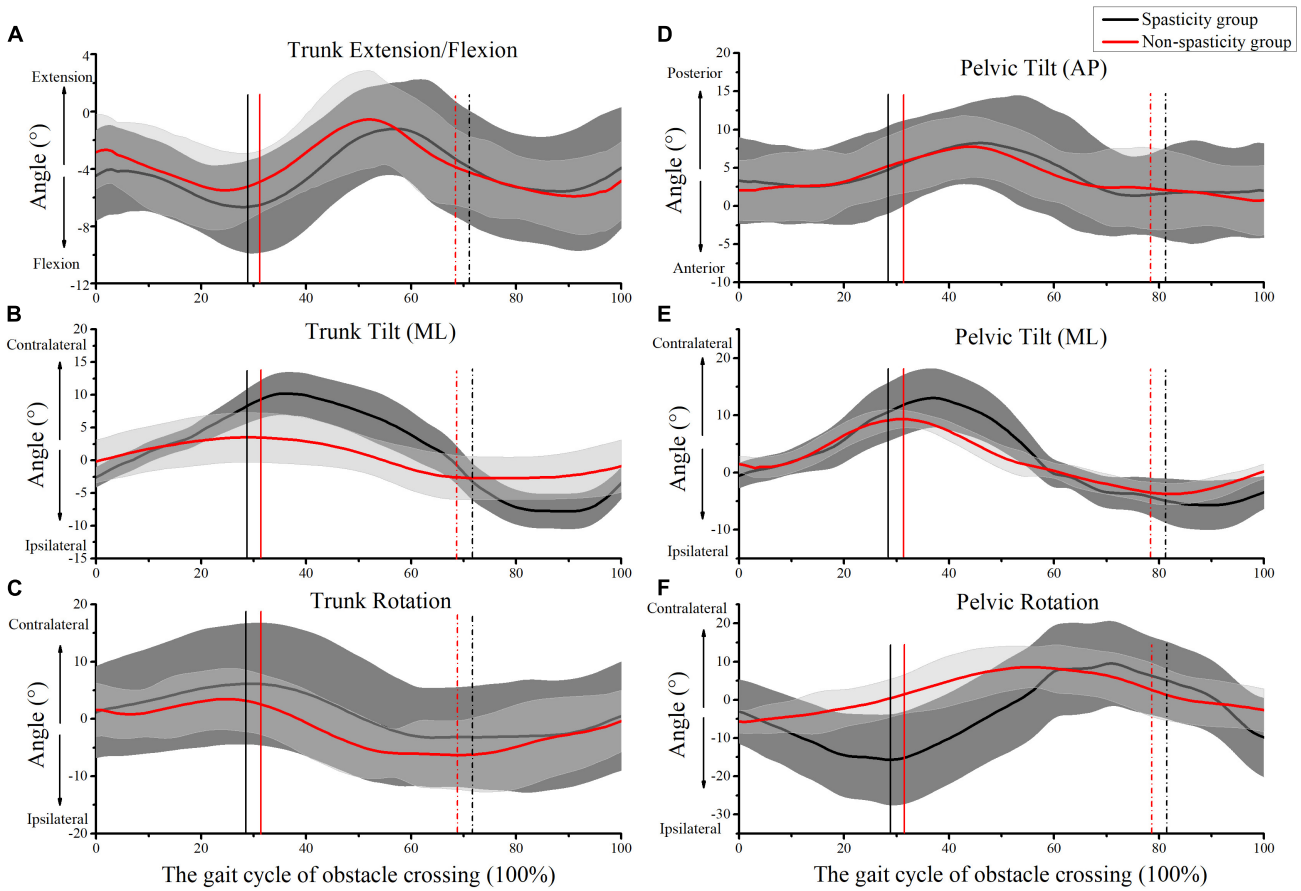

FIGURE 4 | Kinematics of trunk and pelvic during obstacle crossing. **(A)** Trunk extension/flexion; **(B)** trunk medio-lateral (ML) tilt; **(C)** trunk rotation; **(D)** pelvic anterior–posterior (AP) tilt; **(E)** pelvic ML tilt; **(F)** pelvic rotation. The mean times that the affected-limb was above the obstacle in the spasticity group (29.12 ± 4.44%) and the non-spasticity group (30.38 ± 2.48%) were plotted as black and red vertical lines, respectively. The mean times that the unaffected-limb toe was above the obstacle in the spasticity group (81.61 ± 5.62%) and the non-spasticity group (78.68 ± 5.29%) were plotted as black and red vertical dash-dot lines, respectively.

movement strategy, based on their functional level and knee extensor spasticity.

Den Otter et al. (2005) reported that stroke survivors generally preferred a lengthening of the step to cross the obstacle under a time constraint. They concluded that the ability to adequately modify the stepping pattern in response to imposed spatiotemporal constraints is impaired in patients with stroke, especially when modifications must be performed under time pressure. A previous study reported that stroke survivors adopted a short-step strategy to step over the obstacle in the absence of time constraints (Nakano et al., 2014). However, the non-spasticity group lengthened their steps during pre-obstacle in the present study without time constraints. The potential explanation for the step lengthening is that the crossing limb will be in a leading position and that visual information on the crossing limb will be available continuously. In contrast, the shortened step will generally result in a situation in which the crossing limb will be in a trailing position, so that visual information will not, or will only partially, be available. This may make a lengthened step easier to implement, especially for stroke survivors who are more dependent on visual information (Den Otter et al., 2005; Laessoe and Voigt, 2013; Watanabe et al., 2016). The differences in the basic characteristics of subjects may be being the reason why the present study is inconsistent with Nakano et al. (2014). In the present study, the sample was composed of mild compromised post-stroke individuals. Additionally, the present findings on long-step strategy are in line with results obtained in healthy elderly (Den Otter et al., 2005). Therefore, the step adjustment strategy may be related to the functional level of the subjects.

Our analysis of the toe-obstacle distance, cross step length and heel-obstacle distance data supports the proposal that the spasticity group utilized the above-mentioned short-step strategy for successful obstacle crossing. A previous study suggested that the short-step strategy was used to approach the obstacle in stroke survivors, which probably intended to enhance the accuracy of swing and maintain stability (Nakano et al., 2014). Therefore, we expected that the shorter toe-obstacle distance in the spasticity group than in the non-spasticity group (healthy controls reference value, 0.20 m) (MacLellan et al., 2015). The spasticity disrupts the pattern of agonist-antagonist activation and alters the net effect of the forces generated by muscle groups,

TABLE 3 | Mean joint angle (95% confidence intervals) of the swing limb when the affected-limb toe or unaffected-limb toe was above the obstacle.

	(A) Affected limb swing				(B) Unaffected limb swing			
Crossing angle (°)	**Spasticity group**	**Non-spasticity group**	***F***	***P***	**Spasticity group**	**Non-spasticity group**	***F***	***P***
Trunk flexion (−)/extension (+)	−6.45 (−8.95–−3.95)	−5.19 (−7.10–−3.27)	0.756	0.396	−5.12 (−8.05–−2.18)	−6.00 (−7.84–−4.17)	0.296	0.593
Trunk lateral tilt Contra (+)/Ipsi (−) **,#	8.72 (6.43–11.01)	3.63 (0.55–6.71)	9.464	0.007	−5.08 (−6.70–−3.46)	−1.86 (−1.97–−2.06)	8.115	0.011
Trunk rotation Contra (+)/Ipsi (−)	5.10 (3.60–6.59)	3.03 (0.24–5.83)	2.448	0.135	−2.64 (−6.87–1.58)	−4.64 (−8.83–−0.46)	−0.266	0.790
Pelvic tilt anterior (−)/posterior (+)	5.54 (2.49–8.59)	5.77 (2.57–8.96)	0.013	0.912	1.61 (−3.19–6.41)	2.37 (−1.78–6.54)	0.071	0.793
Pelvic lateral tilt Contra (+)/Ipsi (−)*	10.77 (9.14–12.40)	7.98 (6.32–9.62)	7.264	0.015	−4.65 (−9.32–0.02)	−1.68 (−4.53–1.16)	1.322	0.265
Pelvic rotation Contra (+)/Ipsi (−)**	−15.56 (−19.47–−11.65)	−0.79 (−5.13–−3.55)	32.717	0.000	6.59 (5.06–8.13)	4.42 (0.63–9.46)	1.070	0.315
Hip flexion (+)/extension (−)	37.50 (31.17–43.83)	43.12 (35.48–50.53)	1.632	0.218	27.41 (19.17–35.65)	26.38 (16.81–35.94)	0.035	0.855
Hip abduction (+)/adduction (−)	9.29 (5.46–13.13)	6.16 (2.36–9.95)	−1.709	0.087	8.64 (2.27–15.01)	10.67 (3.59–17.74)	0.233	0.635
Hip rotation internal (+)/external (−)*	7.95 (7.48–13.16)	17.33 (10.07–26.81)	−2.165	0.030	12.16 (7.77–16.56)	17.29 (11.48–23.10)	2.646	0.121
Knee flexion (−)/extension (+)*	−58.84 (−68.98–−48.69)	−74.61 (−87.81– −61.42)	4.780	0.042	−93.81 (−102.62–−85.02)	−96.48 (−105.99–−86.97)	0.215	0.649
Ankle DF (+)/PF (−)*	5.18 (0.44–9.90)	11.72 (7.19–16.24)	4.937	0.039	14.04 (8.18–19.88)	17.73 (13.09–22.35)	1.158	0.296

*DF, dorsiflexion; PF, plantarflexion; Contra, contralateral; Ipsi, ipsilateral; *reflects a significant difference between the two groups when the affected-limb toe was above the obstacle ($P < 0.05$); **reflects $P < 0.01$; #reflects a significant difference between the two groups when the unaffected-limb toe was above the obstacle ($P < 0.05$).*

as confirmed by a previous study (Singer et al., 2013). We further expected the smaller cross step length and heel-obstacle distance in the spasticity group compared to the non-spasticity group (healthy controls reference value, 0.78 and 0.22 m) (Said et al., 2008; Chen et al., 2019). In the present study, our results showed that the toe-obstacle distance was shorter in the spasticity group, while no group-differences were observed in cross step length and heel-obstacle distance between the two groups. The usage the short-step strategy by the spasticity group may provide two advantages for obstacle crossing (Nakano et al., 2014). One is foot placement accuracy, the other is safety. A shorter toe-obstacle distance may be the result of the short-step adjustment strategy, to shorten the distance between the swing limb and the effective swing-foot position. Furthermore, the slower COM AP velocity may provide time to modify the swing-foot position and easily regain stability (Said et al., 2008; Mizusawa et al., 2017). Although a shorter toe-obstacle distance provides an advantage in successfully crossing obstacles, it may also reduce the space of the swing limb and increase the risk of tripping over the obstacle. A previous study reported that the shorter heel-obstacle distance in stroke survivors compared with healthy controls might place stroke survivors at risk of actual contact with or tripping over the obstacle (Said et al., 2005; Chen et al., 2019). However, no significant difference was found in the cross step length and heel-obstacle distance between the spasticity and the non-spasticity groups in the present study. A potential explanation is that the spasticity group used the short-step strategy during the pre-obstacle phase to obtain a similar cross step length as the non-spasticity group.

Stroke survivors may face difficulty in muscle recruitment and knee motion range, and knee extensor spasticity may further exacerbate this negative effect (Singer et al., 2013). Therefore, we expected the lower knee flexion angle and knee work contributions occur in the spasticity group compared to non-spasticity group (healthy controls reference value, 97.46°) (Chen et al., 2019). Due to a lack of knee flexion, a "hip abduction strategy" is typically used by stroke survivors for limb elevation during obstacle crossing (Lu et al., 2010; Chen et al., 2019). We further expected greater hip abduction angle and hip work contributions in the spasticity group compared to the non-spasticity group (healthy controls reference value, 0.14°) (Chen et al., 2019). As expected, the spasticity group exhibited lower knee flexion when the affected-limb toe was above the obstacle. However, no significant difference was found in hip abduction between the two groups when the affected-limb toe was above the obstacle. This finding is inconsistent with the results of a previous study (Chen et al., 2019). A possible explanation for this inconsistency might be that in the present study the hip kinematics were calculated relative to the pelvic, and the angle of pelvic tilt in the frontal plane was higher in the spasticity group than the non-spasticity group in our study. This may lead to underestimation of the true hip abduction in the global coordinate system. Therefore, we calculated the relative ML distance between the ankle and ipsilateral hip joint when the affected-limb toe was above the obstacle. Our results showed the higher ML distance between the ankle and ipsilateral hip joint in the spasticity group (0.102 m; 95% CI, 0.061. 0.145) than the non-spasticity group (0.048 m; 95% CI, 0.025. 0.071)

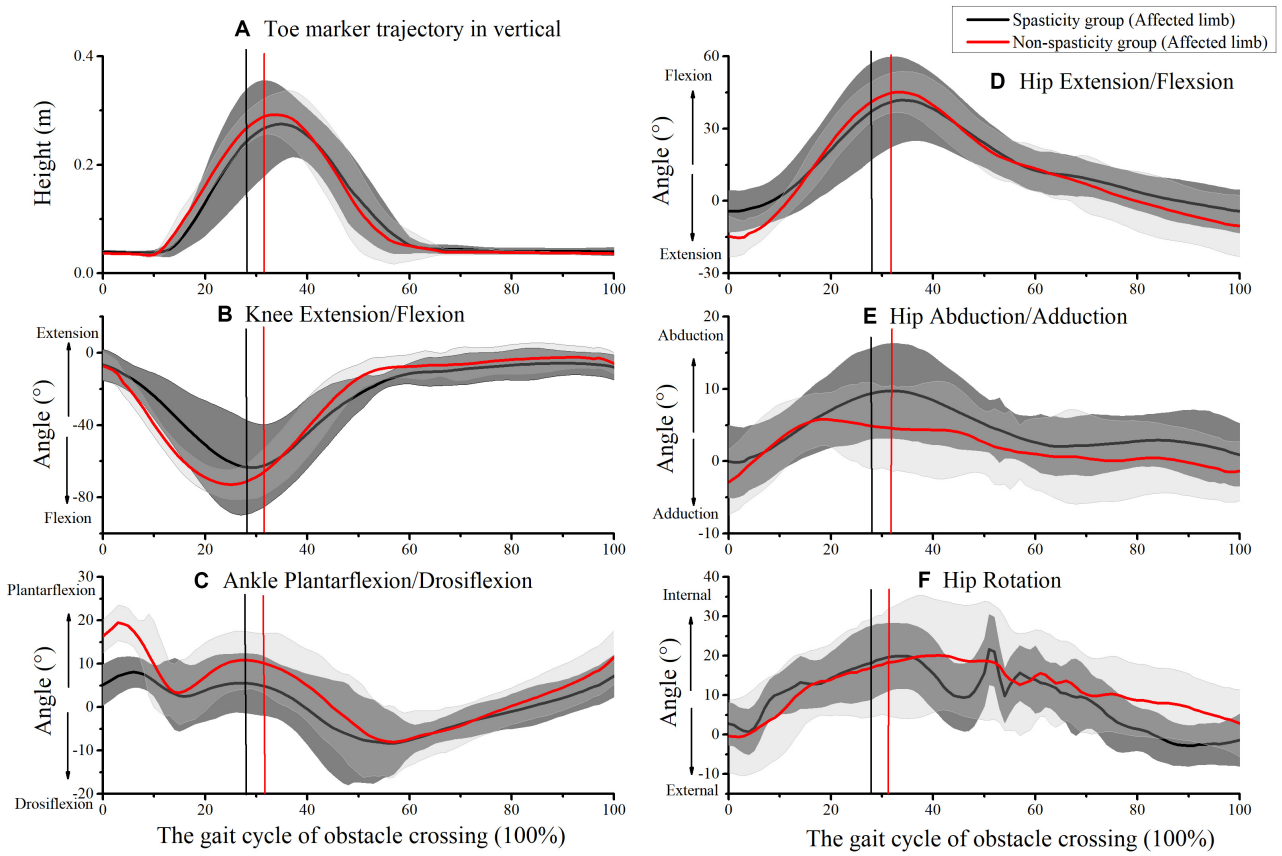

FIGURE 5 | Kinematics of affected-limb joints during obstacle crossing. **(A)** Toe marker vertical trajectory; **(B)** knee extension/flexion; **(C)** ankle plantarflexion/dorsiflexion; **(D)** hip extension/flexion; **(E)** hip abduction/adduction; **(F)** hip rotation. The mean times that the affected-limb toe was above the obstacle in the spasticity group (29.12 ± 4.44%) and the non-spasticity group (30.38 ± 2.48%) were plotted as black and red vertical lines, respectively.

when the affected-limb toe was above the obstacle (F = 5.56, P = 0.030). Additionally, the results showed that hip work contributions were higher and knee work contributions were lower in the spasticity group than in the non-spasticity group. These results indicate that the hip may be a key component of limb elevation.

The coupling of movement between the pelvic and trunk contributed to the compensatory strategy for complex tasks. Han et al. (2017) and Chen et al. (2019) reported that the pelvic and trunk lateral tilt angles were larger in stroke survivors than in healthy controls (healthy controls reference value, 4.5°). Our results suggest that the coupling of movement between the pelvic and the trunk is an important compensatory strategy in the spasticity group during obstacle crossing. As we hypothesized, the pelvic and trunk lateral tilt angles in the spasticity group were indeed larger than those in the non-spasticity group. This finding was similar to that of a previous study (Han et al., 2017; Chen et al., 2019; van Vugt et al., 2019). In the current study, the spasticity group initially shifted their weight to the unaffected side, then laterally tilted the pelvic and trunk toward the unaffected side and abducted the hip to elevate the swing foot. By adopting this proximal movement compensatory strategy, the spasticity group was able to cross the obstacle successfully.

Chen and Chou (2010) suggested that the COM-COP inclination angle could sensitively identify individuals with imbalance and fall risk among stroke survivors during walking and obstacle crossing. A previous study reported that after using the pelvic lateral tilt strategy, stroke survivors showed greater instability in the ML direction during the push-off and landing phases (Chen et al., 2019). Therefore, we expected the COM-COP ML inclination angle would be larger in the spasticity group than in the non-spasticity group (healthy controls reference value, 4.09°) (Lee and Chou, 2006). As expected, we observed that the COM-COP ML inclination angle was larger in the spasticity group than in the non-spasticity group when the affected-limb toe was above the obstacle. In addition, the COM-COP AP inclination angle was larger in the spasticity group when the affected-limb toe was above the obstacle. Although a proximal movement compensatory strategy may improve obstacle crossing, it sacrifices some balance in the sideways direction. Even though the relation between COM-COP ML can be related to balance disruption, this can also be a compensatory strategy to complete the task. Similar results were found in posture control during gait in adults with hereditary spastic paraparesis (van Vugt et al., 2019). The adults with hereditary spastic paraparesis had slower walking velocity, more time spent

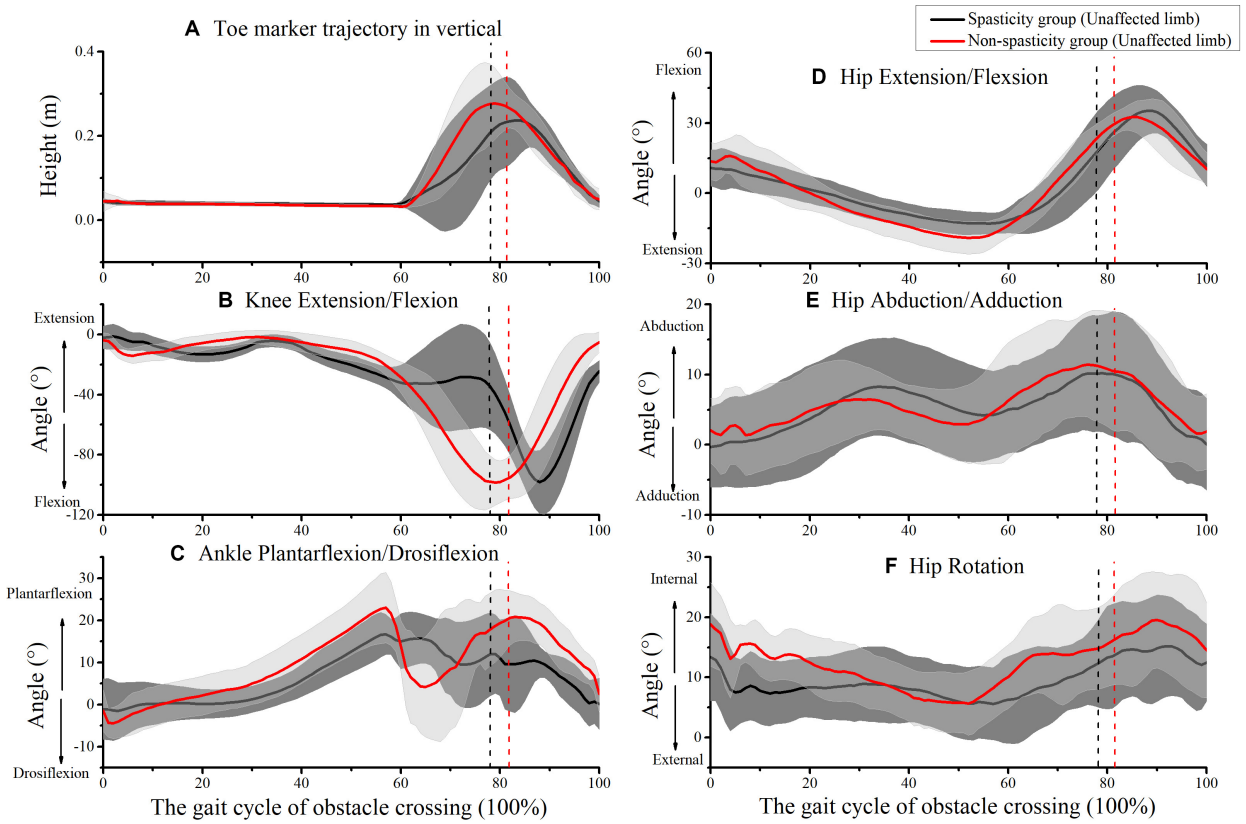

FIGURE 6 | Kinematics of unaffected-limb joints during obstacle crossing. **(A)** Toe marker vertical trajectory; **(B)** knee extension/flexion; **(C)** ankle plantarflexion/dorsiflexion; **(D)** hip extension/flexion; **(E)** hip abduction/adduction; **(F)** hip rotation. The mean times that the unaffected-limb toe was above the obstacle in the spasticity group (81.61 ± 5.62%) and the non-spasticity group (78.68 ± 5.29%) were plotted as black and red vertical dash-dot lines, respectively.

in double stance, larger step widths, and greater trunk lateral tilt than the healthy controls. These results suggest that the individuals with hereditary spastic paraparesis adjust their gait to minimize the instability arising from their impairments but have residual deficits in ML stability.

Spatiotemporal parameters measured after obstacle crossing provided information about the reestablish of a walking pattern and balance control. Said et al. (2008) demonstrated that a reduction in step length after the obstacle could represent a reestablishment of the gait pattern. Therefore, we expected a smaller step length in the spasticity group than in the non-spasticity group (healthy controls reference value, 0.69 m) (Said et al., 2008). As expected, our results show that the step length was indeed smaller in the spasticity group than in the non-spasticity group. Interestingly, an additional shortened step was observed prior to restoring step length between step 1 and step 3 in the spasticity group. Furthermore, we observed that the step width in the spasticity group was longer than that in the non-spasticity group. This indicates that a short-step and increase step width strategy was adopted to reestablish the walking pattern and balance control because the affected limb is less capable of providing single support.

In the present study, the sample size was calculated using parametric methods before the biomechanics test while some measures were tested using non-parametric methods. In our results, the heel-obstacle distance, step width in pre-obstacle and trunk rotation angle were not showed normal distributions, and using Mann–Whitney *U* test to test the group-differences. However, no significant differences was found between the two groups. The central limit theorem essentially demonstrated that even though the distribution of individual observations is not normal, with an increasing sample size, the distribution of a mean becomes more normal (Divine et al., 2013). Additionally, the number of subjects actually recruited ($n = 20$) is greater than the result of the sample size calculations ($n = 14$). Therefore, this discrepancy may be not affecting the results and conclusions of the present study.

Experimental studies on the step adjustment and compensatory strategies for obstacle crossing in stroke survivors with knee extensor spasticity may help in the development of better fall preventive training programs. In the present study, our results demonstrate that the trunk and pelvic movement compensatory strategies may improve obstacle crossing, but it sacrifices some balance in the sideways direction. A previous study suggested that the degree of trunk movement was restricted to enable body stability during the early stage of motor learning and balance development (Rhee and Kim, 2015). When trunk control must respond to external disturbances

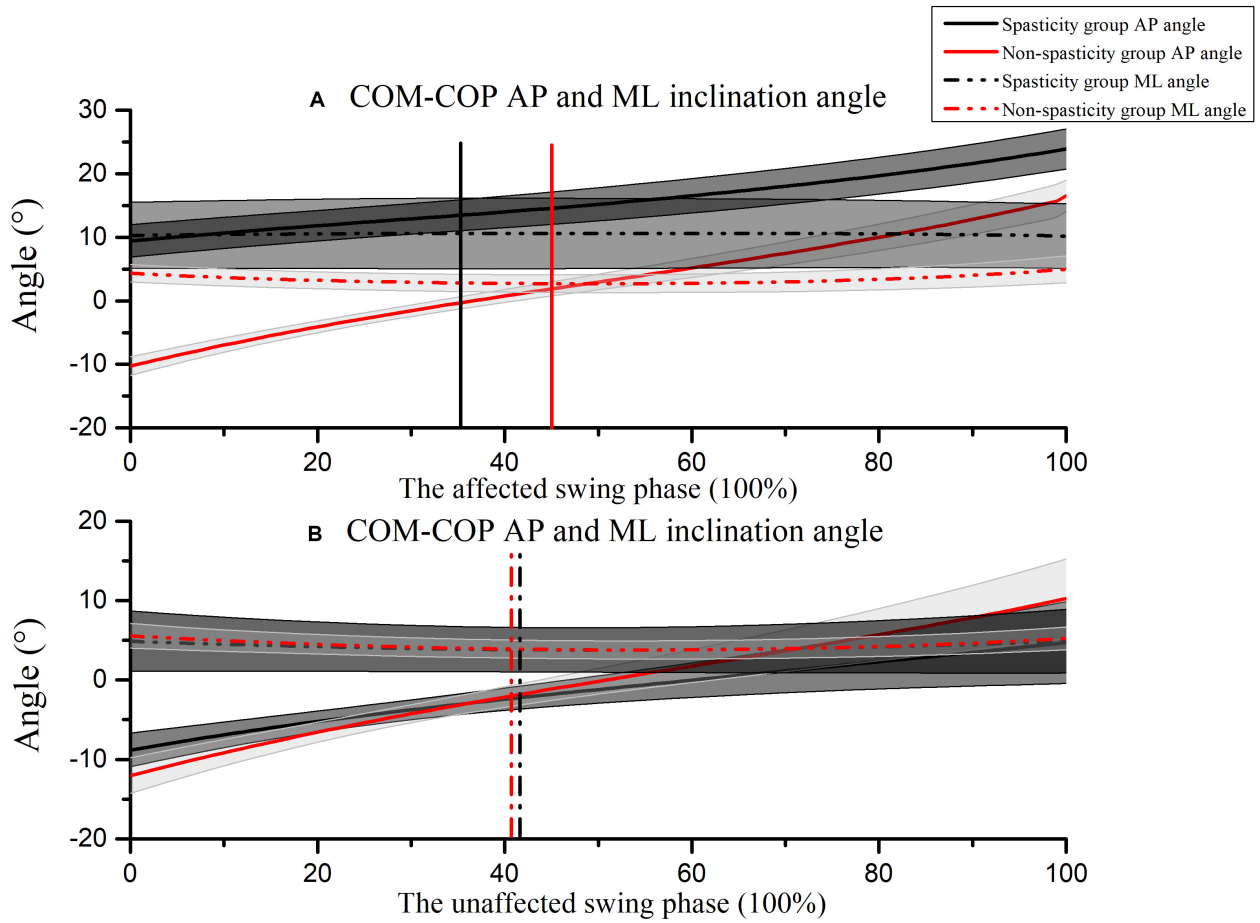

FIGURE 7 | COM-COP inclination angles during **(A)** the affected-limb swing phase, and **(B)** the unaffected-limb swing phase. Positive values indicate that the COM is in front of the COP. Toe-off and heel contact are indicated as 0 and 100%, respectively. The mean time that the affected-limb toe was above the obstacle in the spasticity group (35.47 ± 7.49%) and the non-spasticity group (45.41 ± 3.53%) were plotted as black and red vertical lines, respectively. The mean time that the unaffected-limb toe was above the obstacle in the spasticity group (41.08 ± 8.09%) and the non-spasticity group (40.96 ± 4.71%) were plotted as black and red vertical dash-dot lines, respectively.

TABLE 4 | Mean joint work (95% confidence intervals) of the swing limb during the affected-limb swing phase **(A)** or unaffected-limb swing phase **(B)**.

Joint work and work contributions	(A) Affected limb swing				(B) Unaffected limb swing			
	Spasticity group	Non-spasticity group	*F*	*P*	Spasticity group	Non-spasticity group	*F*	*P*
Ankle work (J)	0.13 (0.05–0.21)	0.19 (0.11–0.27)	1.329	0.264	0.49 (0.37–0.62)	0.61 (0.50–0.72)	2.636	0.124
Knee work (J)*	1.06 (0.64–1.48)	2.08 (1.05–3.11)	5.072	0.037	28.71 (23.45–33.95)	30.41 (22.55–38.27)	0.188	0.670
Hip work (J)	2.98 (1.94–4.02)	2.75 (1.71–3.79)	0.122	0.731	19.19 (11.97–26.41)	20.04 (12.09–27.98)	0.033	0.859
Limb total work (J)	4.18 (2.79–5.56)	5.02 (3.39–6.65)	0.811	0.380	48.39 (36.31–60.47)	51.05 (36.06–66.07)	0.105	0.750
Hip work contributions (%)**	71.05 (65.56–76.54)	55.77 (46.14–65.40)	10.820	0.004	38.02 (33.05–43.00)	38.37 (32.50–44.24)	0.011	0.918
Knee work contributions (%)**	25.16 (19.60–30.71)	33.43 (23.93–42.93)	8.815	0.008	60.92 (56.07–65.76)	60.29 (54.72–65.87)	0.038	0.848

**Reflects a significant difference between the two groups during the affected-limb swing phase ($P < 0.05$). **Reflects $P < 0.01$.*

or to compensatory movement of other joints, the risk of falling may be increased. This indicates that trunk stabilization exercises or core muscle strength enhancement in early stage of rehabilitation may play an important role in fall prevention for stroke survivors (Shin and Don Kim, 2016; Lee et al., 2018). Additionally, recent clinical studies found that trunk stabilization exercises influence the muscle tone of the distal part, which can be explained as a decrease in spasticity because the excitation of the spinal cord motor neurons decreased after the trunk stabilization exercise (Rhee and Kim, 2015). Furthermore, in the present study, in the absence of time pressure, stroke survivors with knee extensor spasticity preferred short-step adjustment

strategies, which is differed than the non-spasticity group. A previous study demonstrated that the ability to adequately "on-line" modify the stepping pattern in response to imposed spatiotemporal constraints is impaired for stroke and older adults, especially when modifications must be performed under time pressure (Den Otter et al., 2005). Therefore, trunk stabilization exercises and repeated obstacle avoidance exercises under time constraint may be an effective intervention to prevent falls (Chien and Hsu, 2018).

This study has several limitations. First, considering the insufficient strength and spasticity of the affected limb during the stance phase, we did not instruct the subjects to step over the obstacle with their unaffected side due to safety issues. Therefore, we collected data only when the affected limb was the leading limb during obstacle crossing, but this does not influence the results and conclusions of this study. Second, the obstacle height was set at 15 cm, which is equal to the height between stairs in the community. We did not assess the biomechanics of crossing obstacles of different heights (e.g., the percentage of leg length). A previous study demonstrated that stair climbing is a critical factor for restoring independent daily living to stroke survivors (Morone et al., 2018). Although obstacle crossing is not identical to stair climbing, the compensatory strategies of affected-limb elevation during obstacle crossing are still applicable to limb elevation during stair climbing because the height of the obstacle is the same. Third, the spasticity of the other lower limb muscles (e.g., hip adductors, ankle dorsiflexors, and ankle plantar flexors) was not assessed in the present study. In future work, this should be combined with EMG analysis to investigate compensatory strategies used by stroke survivors with single and multiple spasticity muscle groups, which has important theoretical value in rehabilitation treatment and fall prevention for stroke survivors with spasticity.

CONCLUSION

During the pre-obstacle phase, stroke survivors with knee extensor spasticity adopted a short-step strategy to approach the obstacle, while stroke survivors without knee extensor spasticity used long-step strategy. During the affected-limb swing phase, the combined movement of the pelvic, and trunk lateral tilt and hip abduction is an important compensatory strategy for successful obstacle crossing, but it sacrifices some balance in the sideways direction. During the post-obstacle phase, short-step and increase step width strategies were adopted to reestablish the walking pattern and balance control. Trunk stabilization exercises and repeated obstacle avoidance exercises under time constraints may be an effective intervention to prevent falls.

DATA AVAILABILITY STATEMENT

The raw data supporting the conclusions of this article will be made available by the authors, without undue reservation, to any qualified researcher.

ETHICS STATEMENT

The studies involving human participants were reviewed and approved by Ethics Committee of Shanghai Seventh People's Hospital. The patients/participants provided their written informed consent to participate in this study.

AUTHOR CONTRIBUTIONS

S-JH, X-MY, X-BW, and W-XN conceived and designed the study. S-JH and X-MY recruited subjects and collected the basic characteristics of subjects. X-BW performed clinical assessment. S-JH, X-MY, and KW performed the experiments. S-JH, L-JW, and XW made a contribution to data analysis. S-JH and W-XN wrote this manuscript. All authors had read and approved the manuscript.

FUNDING

This study was supported by National Natural Science Foundation of China (11732015) and National Key Research and Development Program of China (2020YFC2004200).

ACKNOWLEDGMENTS

The authors acknowledge Yan Lu, Jun Qiao, and Hai-Chen Xu for the recruitment of study participants; Qian Liu, Wei Zhuang, Zheng-Liang Xia, and Xiao-Le Sun for assistance with biomechanical experiments; Ya-Qi Li helps for grammar modification in the manuscript. The authors would like to thank all the participants of this study.

REFERENCES

Ansari, N. N., Naghdi, S., Younesian, P., and Shayeghan, M. (2008). Inter- and intrarater reliability of the modified modified ashworth scale in patients with knee extensor poststroke spasticity. *Physiother. Theory Pract.* 24, 205–213. doi: 10.1080/09593980701523802

Banina, M. C., Mullick, A. A., McFadyen, B. J., and Levin, M. F. (2017). Upper limb obstacle avoidance behavior in individuals with stroke. *Neurorehabil. Neural Repair.* 31, 133–146. doi: 10.1177/1545968316662527

Blackburn, M., van Vliet, P., and Mockett, S. P. (2002). Reliability of measurements obtained with the modified Ashworth scale in the lower extremities of people with stroke. *Phys. Ther.* 82, 25–34. doi: 10.1093/ptj/82.1.25

Chen, C. J., and Chou, L. S. (2010). Center of mass position relative to the ankle during walking: a clinically feasible detection method for gait imbalance. *Gait Posture* 31, 391–393. doi: 10.1016/j.gaitpost.2009.11.010

Chen, N., Xiao, X., Hu, H., Chen, Y., Song, R., and Li, L. (2019). Identify the alteration of balance control and risk of falling in stroke survivors during obstacle crossing based on kinematic analysis. *Front. Neurol.* 10:813. doi: 10.3389/fneur.2019.00813

Chien, J. E., and Hsu, W. L. (2018). Effects of dynamic perturbation-based training on balance control of community-dwelling older adults. *Sci. Rep.* 8:17231. doi: 10.1038/s41598-018-35644-35645

Chou, L. S., Kaufman, K. R., Hahn, M. E., and Brey, R. H. (2003). Medio-lateral motion of the center of mass during obstacle crossing distinguishes elderly individuals with imbalance. *Gait Posture* 18, 125–133. doi: 10.1016/s0966-6362(02)00067-x

Den Otter, A. R., Geurts, A. C., de Haart, M., Mulder, T., and Duysens, J. (2005). Step characteristics during obstacle avoidance in hemiplegic stroke. *Exp. Brain Res.* 161, 180–192. doi: 10.1007/s00221-004-2057-2050

Divine, G., Norton, H. J., Hunt, R., and Dienemann, J. (2013). Statistical grand rounds: a review of analysis and sample size calculation considerations for Wilcoxon tests. *Anesth. Analg.* 117, 699–710. doi: 10.1213/ANE.0b013e31827f53d7

Gorst, T., Rogers, A., Morrison, S. C., Cramp, M., Paton, J., Freeman, J., et al. (2019). The prevalence, distribution, and functional importance of lower limb somatosensory impairments in chronic stroke survivors: a cross sectional observational study. *Disabil. Rehabil.* 41, 2443–2450. doi: 10.1080/09638288.2018.1468932

Han, J. T., Lee, J. H., and Fell, D. W. (2017). Kinematic head and trunk strategies used by hemiplegic stroke patients crossing over obstacles of different heights. *J. Phys. Ther. Sci.* 29, 109–111. doi: 10.1589/jpts.29.109

Laessoe, U., and Voigt, M. (2013). Step adjustments among young and elderly when walking toward a raised surface. *Aging Clin. Exp. Res.* 25, 299–304. doi: 10.1007/s40520-013-0038-35

Lee, H. J., and Chou, L. S. (2006). Detection of gait instability using the center of mass and center of pressure inclination angles. *Arch. Phys. Med. Rehabil.* 87, 569–575. doi: 10.1016/j.apmr.2005.11.033

Lee, N. G., You, J. S. H., Yi, C. H., Jeon, H. S., Choi, B. S., Lee, D. R., et al. (2018). Best core stabilization for anticipatory postural adjustment and falls in hemiparetic stroke. *Arch. Phys. Med. Rehabil.* 99, 2168–2174. doi: 10.1016/j.apmr.2018.01.027

Levin, M. F. (2016). Principles of motor recovery after neurological injury based on a motor control theory. *Adv. Exp. Med. Biol.* 957, 121–140. doi: 10.1007/978-3-319-47313-0_7

Li, S., Liu, J., Bhadane, M., Zhou, P., and Rymer, W. Z. (2014). Activation deficit correlates with weakness in chronic stroke: evidence from evoked and voluntary EMG recordings. *Clin. Neurophysiol.* 125, 2413–2417. doi: 10.1016/j.clinph.2014.03.019

Lu, T. W., Yen, H. C., Chen, H. L., Hsu, W. C., Chen, S. C., Hong, S. W., et al. (2010). Symmetrical kinematic changes in highly functioning older patients post-stroke during obstacle-crossing. *Gait Posture* 31, 511–516. doi: 10.1016/j.gaitpost.2010.02.012

Ma, C., Chen, N., Mao, Y., Huang, D., Song, R., and Li, L. (2017). Alterations of muscle activation pattern in stroke survivors during obstacle crossing. *Front. Neurol.* 8:70. doi: 10.3389/fneur.2017.00070

MacLellan, M. J., Richards, C. L., Fung, J., and McFadyen, B. J. (2015). Comparison of kinetic strategies for avoidance of an obstacle with either the paretic or non-paretic as leading limb in persons post stroke. *Gait Posture* 42, 329–334. doi: 10.1016/j.gaitpost.2015.06.191

Malik, R. N., Cote, R., and Lam, T. (2017). Sensorimotor integration of vision and proprioception for obstacle crossing in ambulatory individuals with spinal cord injury. *J. Neurophysiol.* 117, 36–46. doi: 10.1152/jn.00169.2016

Malone, A., Kiernan, D., French, H., Saunders, V., and O'Brien, T. (2016). Obstacle crossing during gait in children with cerebral palsy: cross-sectional study with kinematic analysis of dynamic balance and trunk control. *Phys. Ther.* 96, 1208–1215. doi: 10.2522/ptj.20150360

Meseguer-Henarejos, A. B., Sanchez-Meca, J., Lopez-Pina, J. A., and Carles-Hernandez, R. (2018). Inter- and intra-rater reliability of the Modified Ashworth Scale: a systematic review and meta-analysis. *Eur. J. Phys. Rehabil. Med.* 54, 576–590. doi: 10.23736/S1973-9087.17.04796-4797

Mizusawa, H., Jono, Y., Iwata, Y., Kinoshita, A., and Hiraoka, K. (2017). Processes of anticipatory postural adjustment and step movement of gait initiation. *Hum. Mov. Sci.* 52, 1–16. doi: 10.1016/j.humov.2017.01.003

Morone, G., Matamala-Gomez, M., Sanchez-Vives, M. V., Paolucci, S., and Iosa, M. (2018). Watch your step! Who can recover stair climbing independence after stroke? *Eur. J. Phys. Rehabil. Med.* 54, 811–818. doi: 10.23736/S1973-9087.18.04809-4808

Nakano, W., Sakamoto, R., and Ohashi, Y. (2014). How patients with stroke adjust their step length to step over obstacles. *Int. J. Rehabil. Res.* 37, 34–39. doi: 10.1097/MRR.0b013e3283646bca

Punt, M., Bruijn, S. M., Wittink, H., van de Port, I. G., Wubbels, G., and van Dieen, J. H. (2017). Virtual obstacle crossing: reliability and differences in stroke survivors who prospectively experienced falls or no falls. *Gait Posture* 58, 533–538. doi: 10.1016/j.gaitpost.2017.09.013

Raffegeau, T. E., Kellaher, G. K., Terza, M. J., Roper, J. A., Altmann, L. J., and Hass, C. J. (2019). Older women take shorter steps during backwards walking and obstacle crossing. *Exp. Gerontol.* 122, 60–66. doi: 10.1016/j.exger.2019.04.011

Rahimzadeh Khiabani, R., Mochizuki, G., Ismail, F., Boulias, C., Phadke, C. P., and Gage, W. H. (2017). Impact of spasticity on balance control during quiet standing in persons after Stroke. *Stroke Res. Treat.* 2017:6153714. doi: 10.1155/2017/6153714

Rhee, M. H., and Kim, L. J. (2015). Muscle tone changes in the lower limbs of stroke patients induced by trunk stabilization exercises. *J. Phys. Ther. Sci.* 27, 2663–2664. doi: 10.1589/jpts.27.2663

Said, C. M., Galea, M. P., and Lythgo, N. (2013). People with stroke who fail an obstacle crossing task have a higher incidence of falls and utilize different gait patterns compared with people who pass the task. *Phys. Ther.* 93, 334–344. doi: 10.2522/ptj.20120200

Said, C. M., Goldie, P. A., Culham, E., Sparrow, W. A., Patla, A. E., and Morris, M. E. (2005). Control of lead and trail limbs during obstacle crossing following stroke. *Phys. Ther.* 85, 413–427. doi: 10.1093/ptj/85.5.413

Said, C. M., Goldie, P. A., Patla, A. E., Culham, E., Sparrow, W. A., and Morris, M. E. (2008). Balance during obstacle crossing following stroke. *Gait Posture* 27, 23–30. doi: 10.1016/j.gaitpost.2006.12.009

Salehi, R., Mofateh, R., Mehravar, M., Negahban, H., Tajali, S., and Monjezi, S. (2020). Comparison of the lower limb inter-segmental coordination during walking between healthy controls and people with multiple sclerosis with and without fall history. *Mult. Scler. Relat. Disord.* 41:102053. doi: 10.1016/j.msard.2020.102053

Shafizadeh, M., Wheat, J., Kelley, J., and Nourian, R. (2019). Stroke survivors exhibit stronger lower extremity synergies in more challenging walking conditions. *Exp. Brain Res.* 237, 1919–1930. doi: 10.1007/s00221-019-05560-5569

Shin, J. W., and Don Kim, K. (2016). The effect of enhanced trunk control on balance and falls through bilateral upper extremity exercises among chronic stroke patients in a standing position. *J. Phys. Ther. Sci.* 28, 194–197. doi: 10.1589/jpts.28.194

Singer, J. C., Mansfield, A., Danells, C. J., McIlroy, W. E., and Mochizuki, G. (2013). The effect of post-stroke lower-limb spasticity on the control of standing balance: inter-limb spatial and temporal synchronisation of centres of pressure. *Clin. Biomech.* 28, 921–926. doi: 10.1016/j.clinbiomech.2013.07.010

Singer, J. C., and Mochizuki, G. (2015). Post-stroke lower limb spasticity alters the interlimb temporal synchronization of centre of pressure displacements across multiple timescales. *IEEE Trans. Neural Syst. Rehabil. Eng.* 23, 786–795. doi: 10.1109/TNSRE.2014.2353636

Soyuer, F., and Ozturk, A. (2007). The effect of spasticity, sense and walking aids in falls of people after chronic stroke. *Disabil. Rehabil.* 29, 679–687. doi: 10.1080/09638280600925860

Subramanian, S. K., Feldman, A. G., and Levin, M. F. (2018). Spasticity may obscure motor learning ability after stroke. *J. Neurophysiol.* 119, 5–20. doi: 10.1152/jn.00362.2017

Sun, R., Cui, C., and Shea, J. B. (2017). Aging effect on step adjustments and stability control in visually perturbed gait initiation. *Gait Posture* 58, 268–273. doi: 10.1016/j.gaitpost.2017.08.013

Teixeira-Salmela, L. F., Nadeau, S., Milot, M. H., Gravel, D., and Requiao, L. F. (2008). Effects of cadence on energy generation and absorption at lower extremity joints during gait. *Clin. Biomech.* 23, 769–778. doi: 10.1016/j.clinbiomech.2008.02.007

Trumbower, R. D., Ravichandran, V. J., Krutky, M. A., and Perreault, E. J. (2010). Contributions of altered stretch reflex coordination to arm impairments following stroke. *J. Neurophysiol.* 104, 3612–3624. doi: 10.1152/jn.00804.2009

van Vugt, Y., Stinear, J., Claire Davies, T., and Zhang, Y. (2019). Postural stability during gait for adults with hereditary spastic paraparesis. *J. Biomech.* 88, 12–17. doi: 10.1016/j.jbiomech.2019.03.001

Watanabe, T., Ishida, K., Tanabe, S., and Nojima, I. (2016). Preparatory state and postural adjustment strategies for choice reaction step initiation. *Neuroscience* 332, 140–148. doi: 10.1016/j.neuroscience.2016.06.055

Yang, J. M., and Kim, S. Y. (2015). Correlation of knee proprioception with muscle strength and spasticity in stroke patients. *J. Phys. Ther. Sci.* 27, 2705–2708. doi: 10.1589/jpts.27.2705

Conflict of Interest: The authors declare that the research was conducted in the absence of any commercial or financial relationships that could be construed as a potential conflict of interest.

frontiers in Bioengineering and Biotechnology

ORIGINAL RESEARCH
published: 07 August 2020
doi: 10.3389/fbioe.2020.00920

Movement History Influences Pendulum Test Kinematics in Children With Spastic Cerebral Palsy

Jente Willaert[1], Kaat Desloovere[2,3], Anja Van Campenhout[3,4,5], Lena H. Ting[6,7] and Friedl De Groote[1]*

[1] Department of Movement Sciences, Katholieke Universiteit Leuven, Leuven, Belgium, [2] Department of Rehabilitation Sciences, Katholieke Universiteit Leuven, Leuven, Belgium, [3] Clinical Motion Analysis Laboratory, Universitair Ziekenhuis Leuven, Leuven, Belgium, [4] Department of Development and Regeneration, Katholieke Universiteit Leuven, Leuven, Belgium, [5] Department of Orthopedics, Universitair Ziekenhuis Leuven, Leuven, Belgium, [6] Wallace H. Coulter Department of Biomedical Engineering, Emory University and Georgia Institute of Technology, Atlanta, GA, United States, [7] Division of Physical Therapy, Department of Rehabilitation Medicine, Emory University, Atlanta, GA, United States

The pendulum test assesses quadriceps spasticity by dropping the lower leg of a relaxed patient from the horizontal position and observing limb movement. The first swing excursion (FS) decreases with increasing spasticity severity. Our recent simulation study suggests that the reduced initial swing results from muscle short-range stiffness and its interaction with reflex hyper-excitability. Short-range stiffness emerges from the thixotropic behavior of muscles where fiber stiffness upon stretch increases when the muscle is held isometric. Fiber stiffness might thus be higher during the first swing of the pendulum test than during consecutive swings. In addition, it has recently been suggested that muscle spindle firing reflects fiber force rather than velocity and therefore, reflex activity might depend on fiber stiffness. If this hypothesized mechanism is true, we expect to observe larger first swing excursions and reduced reflex muscle activity when the leg is moved rather than kept isometric before release, especially in patients with increased reflex activity. We performed the pendulum test in 15 children with cerebral palsy (CP) and 15 age-matched typically developing (TD) children in two conditions. In the hold condition, the leg was kept isometric in the extended position before release. In the movement condition, the leg was moved up and down before release to reduce the contribution of short-range stiffness. Knee kinematics and muscle activity were recorded. Moving the leg before release increased first swing excursion ($p < 0.001$) and this increase was larger in children with CP (21°) than in TD children (8°) ($p < 0.005$). In addition, pre-movement delayed reflex onset by 87 ms ($p < 0.05$) and reduced reflex activity as assessed through the area under the curve of rectus femoris electromyography ($p < 0.05$) in children with CP. The movement history dependence of pendulum kinematics and reflex activity supports our hypothesis that muscle short-range stiffness and its interaction with reflex hyper-excitability contribute to joint hyper-resistance in spastic CP. Our results have implications for standardizing movement history in clinical tests of spasticity and for understanding the role of spasticity in functional movements, where movement history differs from movement history in clinical tests.

Keywords: stretch reflex, hyperreflexia, thixotropy, instrumented assessment of spasticity, rectus femoris muscle, joint hyper-resistance

OPEN ACCESS

Edited by:
Ruoli Wang,
KTH Royal Institute of Technology, Sweden

Reviewed by:
Joshua Thomas Morgan,
University of California, Riverside, United States
Massimiliano Zingales,
University of Palermo, Italy

****Correspondence:***
Jente Willaert
jente.willaert@kuleuven.be

Specialty section:
This article was submitted to Biomechanics, a section of the journal Frontiers in Bioengineering and Biotechnology

Received: *30 March 2020*
Accepted: *16 July 2020*
Published: *07 August 2020*

Citation:
Willaert J, Desloovere K, Van Campenhout A, Ting LH and De Groote F (2020) Movement History Influences Pendulum Test Kinematics in Children With Spastic Cerebral Palsy. Front. Bioeng. Biotechnol. 8:920. doi: 10.3389/fbioe.2020.00920

INTRODUCTION

Spasticity is a common symptom in patients with cerebral palsy (CP) or stroke, but the underlying mechanisms are poorly understood. Spasticity is traditionally defined as "a velocity-dependent increase in tonic stretch reflex resulting from hyper-excitability of the stretch reflex" (Lance, 1980). Clinical tests of spasticity, such as the Modified Ashworth Scale (MAS) or Tardieu Scale, assess the resistance of the joint to imposed movement at different speeds. In this paper, we will use the terms spasticity and joint hyper-resistance against movement interchangeable. These clinical tests give little insight in the underlying mechanisms of increased resistance to movement, which might explain why the contribution of spasticity to walking impairments is only poorly understood (Papageorgiou et al., 2019). There is growing consensus that it is important to distinguish different contributions to joint hyper-resistance, i.e., non-neural originating from passive tissue properties, and neural originating from background muscle activity and stretch hyperreflexia (van den Noort et al., 2017). Our recent simulation study of the pendulum test of spasticity suggests that background muscle activity interacts with stretch hyperreflexia through muscle short-range stiffness that is dependent on movement history (De Groote et al., 2018). Hence, interactions between neural contributions and history-dependent muscle mechanics might be a crucial determinant of joint hyper-resistance to stretch in movement impairments. Yet, we currently lack experimental evidence for the movement history dependence of joint hyper-resistance.

During the pendulum test, an examiner drops the leg of a seated and relaxed patient from the horizontal position and the lower leg then swings freely under the influence of gravity (Fowler et al., 2000; **Figure 1A**). Upon release of the leg, the quadriceps muscles are stretched. In healthy individuals, the lower leg behaves like a damped pendulum. With increasing levels of spasticity, (1) the amplitude of the first swing excursion (FS) decreases, (2) the number of oscillations (NO) decreases, and (3) the position of the lower leg when it comes to rest, described by the resting angle (RA), is less vertical (**Figure 1B**). The first swing excursion has been found to be the strongest predictor of spasticity severity (Fowler et al., 2000; Szopa et al., 2014).

We performed a simulation study to test the neuro-mechanical mechanisms underlying altered pendulum test kinematics in children with spastic CP and found that modeling muscle tone, i.e., background muscle activity, and transient short-range stiffness were crucial to simulate decreased first swing excursion and non-vertical first swing excursion (De Groote et al., 2018). Short-range stiffness emerges from the thixotropic behavior of muscles where fiber stiffness upon stretch depends on movement history with stiffness increasing when the muscle is held at a constant length (Campbell and Lakie, 1998). When a muscle fiber is consecutively stretched and released multiple times, the increase in force is significantly higher during the first stretch than during the later stretches. Short-range stiffness leads to a sharp and rapid increase in force upon stretch of an isometric muscle until a force plateau is reached at the critical stretch of the muscle (Campbell and Moss, 2002). Both the initial rate of force development and force plateau depend on the level of isometric force before the stretch (Campbell and Moss, 2002), and therefore on the level of background muscle activity and through the muscle's force-length relationship on isometric fiber length (Gordon and Ridgway, 1987; Herzog and ter Keurs, 1988). The isometric period before releasing the leg in the pendulum test and the high prevalence of increased background muscle activity in CP (Fee and Miller, 2004; Freeman, 2005) might therefore lead to large contributions from short-range stiffness during the first swing limiting leg excursion. In addition, background muscle activity of the quadriceps might also contribute to the non-vertical resting angle.

Furthermore, our simulation study suggested an interaction between muscle short-range stiffness and reflex activity. The reduction in the number of oscillations was best reproduced by simulating stretch reflex activity in terms of force, and not velocity, feedback (De Groote et al., 2018). Our model of reflex activity was based on prior experimental work in cats in which sensory signals from muscle spindles are transiently increased in response to muscle stretch after being held at a constant length. Spindle firing was strongly correlated with muscle short-range stiffness force and force rate, i.e., yank (Blum et al., 2017; Lin et al., 2019). Similarly, short-range stiffness might interact with hyperactive stretch reflexes during the pendulum test in individuals with spastic CP to reduce first swing excursion and thereby the number of subsequent oscillations.

Here, we tested the hypothesis that short-range stiffness due to increased muscle tone and its interaction with reflexes contribute to abnormal pendulum test kinematics in spastic CP. To this aim, we performed the pendulum test in different conditions that were designed to alter the contribution of short-range stiffness in children with spastic CP and age-matched typically developing (TD) children. In the isometric condition, the leg was held still for at least five seconds prior to release whereas in the pre-movement condition, the leg was moved up and down prior to release to decrease the contribution of short-range stiffness. If short-range stiffness indeed contributes to abnormal pendulum test kinematics in spastic CP, pre-movement should normalize pendulum test kinematics by increasing the first swing excursion and number of oscillations. However, pre-movement is not expected to alter the resting angle, which is assumed to be determined by muscle tone and passive muscle properties, and thus not altered by movement history. In addition, if short-range stiffness indeed interacts with reflex activity, pre-movement of the leg should reduce reflex activity (Blum et al., 2017). More precisely, we expect the slower build-up of force, due to decreased short-range stiffness in the pre-movement condition, to reduce and delay the peak in reflex activity. Finally, we tested the dependency of joint hyper-resistance on active muscle force by altering the pose of the subjects from sitting to supine, which increases rectus femoris length. The muscle's force–length relationship predicts a decrease in active force due to muscle

Abbreviations: AUC, area under the curve; CP, cerebral palsy; FS, first swing excursion; GMFCS, Gross Motor Function Classification Scale; HR, hold and release; IA, initial angle; MAS, Modified Ashworth Scale; MR, movement and release; NO, number of oscillations; RA, resting angle; RF, rectus femoris; sEMG, surface electromyography; TD, typically developing.

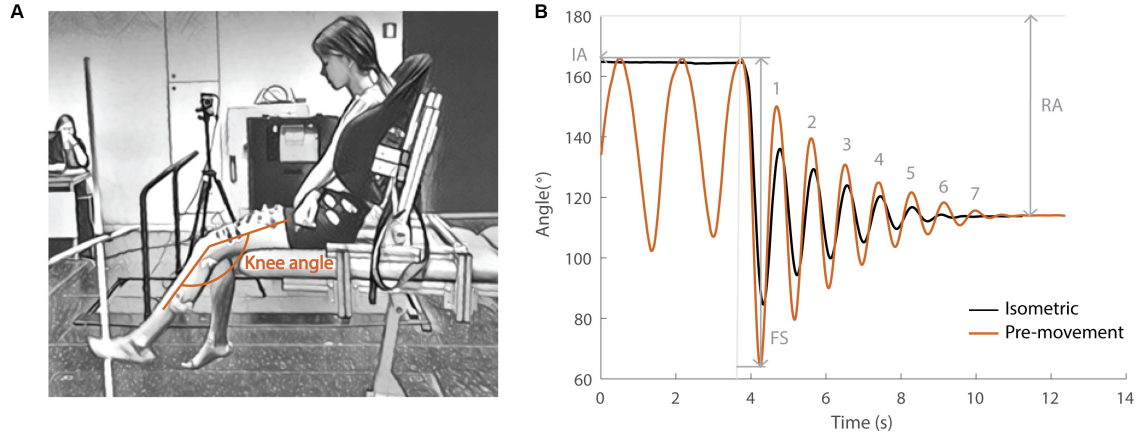

FIGURE 1 | Pendulum test set-up and definition of kinematic outcome parameters. **(A)** Subject leaned against a custom-made backrest in the seated position. The knee angle of the swinging leg is indicated in orange. **(B)** Knee angle trajectory during an isometric (HR) trial in black and a pre-movement (MR) trial in orange in the sitting position with indication of kinematic outcome parameters. IA, initial angle; FS, first swing excursion; RA, resting angle; numbers indicate the number of oscillations for the orange trajectory. The vertical gray line indicates release of the leg.

tone and an increase in passive force when a muscle is stretched beyond its optimal length (Gordon and Ridgway, 1987; Herzog and ter Keurs, 1988). As short-range stiffness is proportional to active force, we expect the effect of pre-movement to be smaller in the supine than in the sitting position. Since TD children have lower muscle tone and reflexes than children with CP when relaxed (Freeman, 2005; Dietz and Sinkjaer, 2007), we expect a smaller effect of pre-movement in TD children.

MATERIALS AND METHODS

Subjects

Thirty children (20 boys and 10 girls) participated in this study. Fifteen children with spastic CP were recruited through the clinical motion analysis laboratory at the University Hospital of Leuven (Belgium). Measurements were planned following the clinical gait analysis that was part of the routine clinical follow-up for children with CP. All patients were diagnosed as having spastic CP confirmed by a neuro-pediatrician. Following inclusion criteria were used: (1) age between 5 and 17 years; (2) Gross Motor Function Classification Scale (GMFCS) level I–III; (3) no orthopedic or neurological surgery in the previous year; and (4) no Botulinum toxin injections at least 6 months before the measurements of this study. The CP group consisted of children with unilateral (N = 3) and bilateral (N = 12) spasticity. Eight of them had GMFCS level I, five GMFCS level II and two GMFCS level III. Four children had spasticity in both the quadriceps and hamstring muscles, nine children had spasticity only in the hamstring muscles and two children had no hamstrings or quadriceps spasticity as measured by the MAS (**Supplementary Table S1**). Fifteen TD children, which were recruited through colleagues and friends, volunteered as controls. All children (CP and TD) were aged between 5 and 14 years old and groups were age matched (**Table 1**). For children with CP, the most affected leg was tested, while for TD children one leg was randomly selected.

Materials

Children with spastic CP were tested in the clinical motion analysis laboratory at the University hospital of Leuven (Belgium). Typically developing children were tested in the Movement and Posture analysis Laboratory Leuven (MALL, Belgium). Both labs are equipped with a Vicon camera system (Vicon, Oxford Metrics, United Kingdom, 100 Hz). Kinematics were measured by placing reflective markers that could be detected by infrared cameras on specific anatomic landmarks on the participant (for details on marker placement, see **Supplementary Figure S1**). Muscle activity was measured simultaneously by a wireless surface electromyography system (sEMG) (CP: Wave Wireless EMG, Biometrics, United Kingdom, 1000 Hz; TD: ZeroWire EMG Aurion, Cometa, Italy, 1000 Hz) with silver-chloride, pre-gelled bipolar electrodes (CP: Nutrode, Xsanatec, Belgium; TD: Ambu Blue Sensor, Ballerup, Denmark). Muscle activity was measured for four lower limb muscles (m. rectus femoris, m. vastus lateralis, m. semitendinosus, and m. biceps femoris). All electrodes were placed according to SENIAM guidelines (Hermens et al., 2000). A custom-made backrest was built to provide back support during the pendulum test. This chair allowed us to control and standardize the hip angle between subjects and trials. The pendulum test was performed in two positions: a sitting and supine position. On average, the hip was

TABLE 1 | Demographic data of the participants.

	CP		TD	
	Mean	**SD**	**Mean**	**SD**
Female/male	3/12		7/8	
Age (years)	9.7	2.8	10.0	2.5
Length (cm)	138	18	142	15
Weight (kg)	33.4	12.1	33.6	10.0

28° (±11°) into flexion for the sitting position and 8° (±8°) into extension for the supine position.

Protocol

The protocol was approved by the Ethical Committee of UZ Leuven/KU Leuven (s61641). A legal representative of the participant signed the informed consent and participants older than 12 years signed informed assent in accordance with the Declaration of Helsinki before measurements were started. For every subject, age and anthropometrics (length and weight) were collected and sEMG electrodes and markers were placed. Children with CP had a clinical examination and clinical gait analysis before the pendulum test was performed. Rest in between measurements was provided when needed.

During the pendulum test, the child was asked to sit relaxed on the table with back support (**Figure 1A**). The examiner extended the leg to a horizontal position (initial angle) and then dropped the leg. The leg was then allowed to swing freely under the influence of gravity until it came to rest. Kinematic trajectories and sEMG signals were recorded during the test. In each position (sit and supine), the pendulum test was performed in two different conditions; (1) with the leg isometric prior to release (hold and release – HR) and (2) with pre-movement of the leg prior to release (movement and release – MR). For the sitting position, the back support was used to assure a relaxed position. By flexing the hip, the possible effect of hamstring muscle tightness was minimized. In the supine position, no backrest was used and children were lying in their natural supine position on the table. During the HR condition, the leg was held as close to horizontal as soft tissues allowed for at least 5 s prior to release [presented in all figures in black (sit) or gray (supine)]. In the MR condition, small oscillatory movements away from and back to the horizontal position were made with the leg prior to release [presented in all figures in orange (sit) or yellow (supine)]. Every condition (HR/MR) was repeated five times or until at least three trials during which the subject was relaxed were obtained with the subject both sitting and supine. Relaxation of the subjects was assessed during the test by real-time visual inspection of the sEMG signals. All trials and subjects were measured by the same examiner.

Data Processing and Analysis

Marker trajectories from Nexus (Version 2.8.5, Oxford Metrics, United Kingdom) were processed using OpenSim 3.3 to calculate knee joint angles (Delp et al., 2007; Seth et al., 2018). Key kinematic parameters, first swing excursion, and resting angle (**Figure 1B**), were calculated using Matlab (R2018b, Mathworks, United States). Raw sEMG data were band-pass filtered using a fourth order Butterworth filter between 10 and 450 Hz followed by signal rectification. Finally, a fourth order Butterworth low-pass filter with 20 Hz cut-off was applied (De Luca et al., 2010).

Key kinematic parameters were defined following Fowler et al. (2000) (**Figure 1B**). First swing excursion was calculated as the difference between the initial knee joint angle (180° corresponds to full extension) and the knee joint angle at the first reversal of the swinging limb. The initial angle was the position at which the examiner released the participant's heel. We defined release onset as the first frame with angular velocity of the knee <-0.01 rad/s. The number of oscillations was determined by counting the maxima of the sinusoidal waves produced by the swinging limb after the heel was released. The criterion for each oscillation was a displacement of at least 3° toward extension. The resting angle was the lower leg orientation relative to horizontal when the lower leg came to rest after the oscillatory movement. The initial angle was standardized during data collection within each position and subject by placing a visual reference point next to the subject. There was no difference in initial angle observed between the HR and MR condition in the sitting position. However, the leg was on average 1.6° (max: 7.1°) and 2.1° (max: 6.4°) closer to horizontal in respectively children with CP and TD children in the MR condition with respect to the HR condition in the supine position.

Reflex activity was assessed using three outcome parameters: (1) the occurrence of reflex activity, (2) reflex onset, and (3) reflex magnitude. The occurrence of reflex activity was expressed as the percentage of trials that showed reflex activity. The presence of muscle reflex activity was determined by evaluating whether sEMG after release of the leg exceeded average baseline muscle activation in the two seconds prior to release by eight times the standard deviation. We chose a threshold of eight times standard deviation, since lower thresholds resulted in a lot of false positive cases based on visual inspection of the sEMG signal. When reflex activity was observed, the onset was defined as the first frame where muscle activity exceeded baseline muscle activation by four times the standard deviation. We could use a lower threshold here as the higher threshold used for detection prevented false detection of reflex activity. The change in reflex magnitude between conditions was assessed based on the area under the curve (AUC) of the baseline subtracted sEMG signal from release onset until 500 ms after release onset. Since the magnitude of sEMG signals cannot be compared between subjects, we used a relative measure of the change in AUC between conditions. The relative difference in AUC between the HR and MR conditions was calculated as the ratio of the difference between the AUC of the HR and MR condition, and the AUC of the HR condition. For subject 4 of the CP group, no sEMG signals were collected during the sitting position for the HR condition due to technical issues and this patient was therefore omitted from sEMG analyses in this condition.

All trials were checked for voluntary activity by visual inspection of the sEMG and kinematic signals. Trials were excluded from further analysis based on sEMG (1) when muscle activity was higher prior to than after release of the leg or (2) when the increase in muscle activity after release of the leg could not be attributed to reflexes based on the criterion that reflexes occurred during muscle stretch and not shortening. Trials were excluded based on kinematic signals (1) when the amplitude of the oscillations increased over time (not taking into account the first swing amplitude) or (2) when the leg came to an abrupt stop. When the child was relaxed during the beginning of the trial but not afterward according to the above criteria, we still included the trial to analyze outcome parameters that were not affected

by voluntary activation in later parts of the trial (e.g., first swing excursion).

Statistical Analysis

Key kinematic parameters (first swing excursion, number of oscillations, and resting angle) and reflex outcomes (occurrence of reflex activity, onset of reflex activity, and reflex magnitude between conditions) were averaged across trials within each condition and subject. Normality was tested using the Shapiro Wilk test. An unpaired *t*-test was used to compare key kinematic and reflex outcomes between children with CP and TD children. A paired *t*-test was used to compare outcome parameters between the HR and MR conditions to investigate the influence of movement history. Further, a paired *t*-test was used to compare outcome parameters between the sitting and supine positions to investigate the influence of position.

We also assessed correlations between outcome parameters that are dependent on the same underlying deficits according to the hypothesized mechanism. First, we assessed the correlation between first swing excursion and resting angle in the isometric condition as both reduced first swing excursion and less vertical resting angle could be explained by increased muscle tone in our model. Second, we calculated the correlation between first swing excursion and reflex activity in the isometric condition as both reduced first swing excursion and increased reflex activity resulted from short-range stiffness in our model. All correlations were calculated using Pearson's correlations. An alpha level of 0.05 was chosen as cut-off for all statistical comparisons. All statistical analyses were performed using IBM SPSS software version 22 (SPSS Inc., Chicago, IL, United States).

RESULTS

Information on Included Trials

All recruited children (15 CP and 15 TD) finished the full test battery. After excluding trials with voluntary muscle activity prior to or during the first swing (see section "Materials and Methods"), 274 trials (mean: 4.56 trials per condition) were retained for children with CP and 258 (mean: 4.3 trials per condition) trials were retained for TD children to analyze first swing excursion (range 2–8 trials per subject and condition) (**Table 2**). For number of oscillations and resting angle, 75.9% (CP) and 74.8% (TD) of these trials (range 1–7 trials) were used. To analyze reflex activity, 97.8% (CP) and 99.6% (TD) of these trials (range 2–7 trials) were used (**Table 2**).

TABLE 2 | Information on the number of included trials.

			CP			TD		
			#	Mean	Range	#	Mean	Range
IA	Sit	HR	69	4.6	3–8	64	4.3	3–5
		MR	65	4.3	3–5	62	4.3	2–5
	Supine	HR	72	4.8	2–6	66	4.4	2–5
		MR	68	4.5	3–6	66	4.4	2–5
FS	Sit	HR	69	4.6	3–8	64	4.3	3–5
		MR	65	4.3	3–5	62	4.3	2–5
	Supine	HR	72	4.8	2–6	66	4.4	2–5
		MR	68	4.5	3–6	66	4.4	2–5
NO	Sit	HR	55	3.7	1–5	48	3.2	1–5
		MR	48	3.2	1–5	46	3.1	1–5
	Supine	HR	59	3.9	2–7	51	3.4	1–5
		MR	46	3.1	1–5	48	3.2	1–5
RA	Sit	HR	55	4.7	1–5	48	3.2	1–5
		MR	48	3.2	1–5	46	3.1	1–5
	Supine	HR	59	3.9	2–7	51	3.4	1–5
		MR	46	3.1	1–5	48	3.2	1–5
Reflex	Sit	HR	65	4.3	2–8	64	4.3	3–5
		MR	65	4.3	2–5	62	4.1	2–5
	Supine	HR	72	4.8	2–7	66	4.4	2–6
		MR	66	4.4	3–6	65	4.3	2–5

IA, initial angle; FS, first swing excursion; NO, number of oscillations; RA, resting angle; HR, hold and release; MR, movement and release.

Key Kinematic Differences Between Children With CP and TD Children for the Isometric Condition

In agreement with previous studies, the first swing excursion and first swing excursion were smaller in children with CP than in TD children (**Figures 2A,B** and **Supplementary Table S2**). However, the resting angle was only different between children with CP and TD children in the supine and not in the sitting position (**Figure 2C**). In the sitting position (**Figure 2**, column 1–2), the first swing excursion in children with CP was 51° smaller than in TD children ($p < 0.001$, CP: 62° ± 30°; TD: 113° ± 8°). Further, the number of oscillations was 2.7 smaller in children with CP compared to TD children ($p < 0.001$, CP: 3.7 ± 2.0; TD: 6.4 ± 1.4). Finally, the resting angle was not different between the two groups (CP: 64° ± 7°; TD: 66° ± 7°). In the supine position (**Figure 2**, column 3–4), the first swing excursion in children with CP was 43° smaller than in TD children ($p < 0.001$, CP: 61° ± 29°; TD: 105° ± 8°). The number of oscillations was 1.5 smaller in children with CP compared to TD children ($p < 0.05$, CP: 4.2 ± 1.8; TD: 5.7 ± 1.6). In contrast to the sitting position, in the supine position the resting angle was 6° less vertical in children with CP than in TD children ($p < 0.05$, CP: 53° ± 9°; TD: 59° ± 6°).

Influence of Position on Key Kinematic Parameters

The resting angle was less vertical in the supine position than in the sitting position for both groups of children ($p < 0.001$, CP: 64° ± 7° sitting versus 53° ± 9° supine; TD: 66° ± 7° sitting versus 59° ± 6° supine), (**Figure 2C** and **Supplementary Table S2**). Further, the first swing excursion in TD children was 8° smaller in the supine position than in the sitting position ($p < 0.001$, sitting: 113° ± 8°; supine: 105° ± 8°), (**Figure 2A**). No other differences were observed between the sitting and supine position.

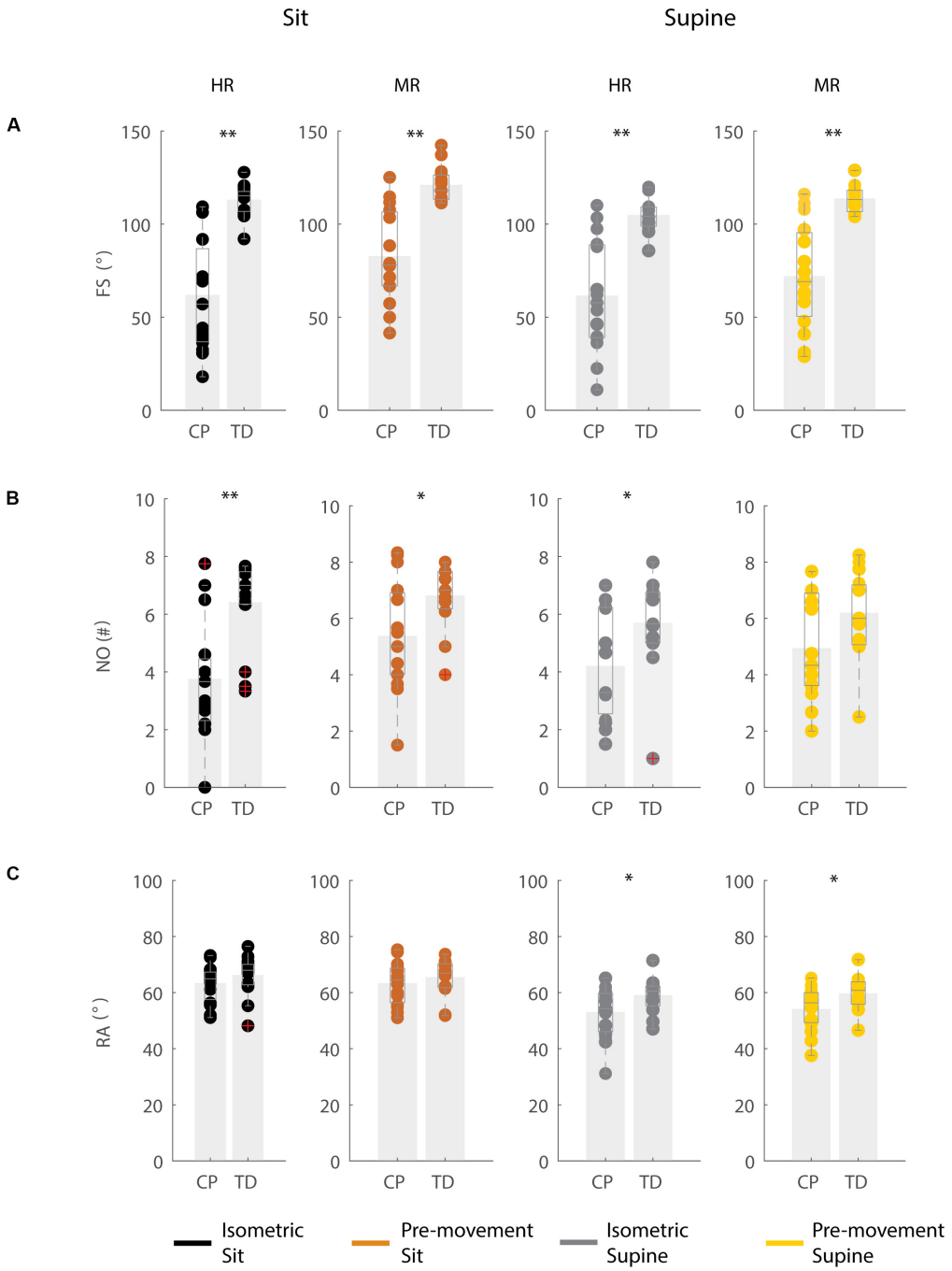

FIGURE 2 | Key kinematic outcomes in children with CP and TD children. **(A)** First swing excursion FS; **(B)** number of oscillations NO; **(C)** resting angle RA. Dots represent the average value over all trials for each child, light gray bars represent mean values over all children within a group. Significant differences between children with CP and TD children are indicated with $*p < 0.05$ and $**p < 0.01$. Black = isometric (HR) – sitting; orange = pre-movement (MR) – sitting; gray = isometric (HR) – supine; yellow = pre-movement (MR) – supine.

Movement History Alters First Swing Excursion and Number of Oscillations but Not Resting Angle

When the leg was moved prior to release (MR), the first swing excursion and number of oscillations increased while the resting angle did not change (**Figures 3–5** and **Supplementary Table S3**) and the observed increases in first swing excursion and number of oscillations were larger in children with CP than in TD children. In the sitting position, the first swing excursion increased on average by 21° ($p < 0.001$, ±12°) for children with CP (**Figures 3, 5A**) and by 8° ($p < 0.001$, ±7°) for TD children

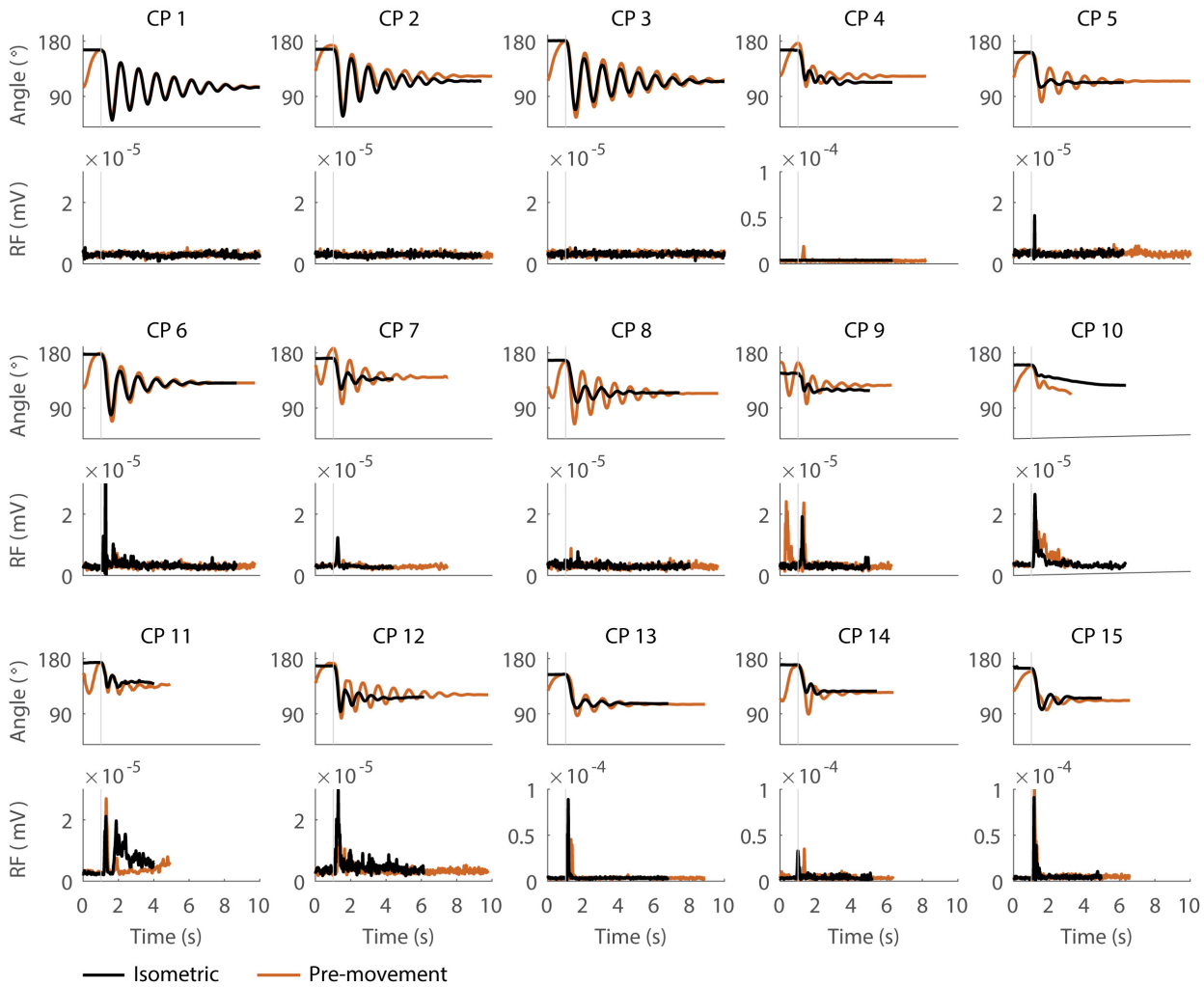

FIGURE 3 | Pendulum trajectories and rectus femoris (RF) muscle activity (sEMG) of children with CP in the sitting position. A representative knee angle trajectory is shown for the isometric (black) and pre-movement (orange) conditions. Children are numbered from low reflex activity to high reflex activity based on number of trials with reflex activity (occurrence of reflexes). An increase in first swing excursion and number of oscillations is seen in the movement condition in orange as compared to the isometric condition in black.

(**Figures 4**, **5A**). This increase was higher ($p < 0.01$) in children with CP than in TD children (**Figure 5A**, column 1). The number of oscillations increased on average by 2 oscillations ($p < 0.001$, ± 1.1) for children with CP (**Figures 3**, **5B**) and by 0.4 oscillations ($p < 0.01$, ± 0.4) for TD children (**Figures 4**, **5B**). The increase in number of oscillations was higher ($p < 0.001$) in children with CP than in TD children (**Figure 5B**, column 1). Movement history did not influence the resting angle (**Figure 5C**, column 1).

Also in the supine position, the first swing excursion and number of oscillations increased with pre-movement (MR), but the increase was not different between children with CP and TD children. First swing excursion increased on average by 10° ($p < 0.001$, $\pm 7°$) for children with CP and by 9° ($p < 0.001$, $\pm 5°$) for TD children (**Figure 5A**, column 2). Further, the number of oscillations increased on average by one oscillation ($p < 0.01$, ± 0.8) for children with CP and by 0.5 oscillations ($p < 0.05$, ± 0.7) for TD children (**Figure 5B**, column 2). The increases observed in first swing excursion and number of oscillations were not different between children with CP and TD children. Also in the supine position, there was no influence of movement history on the resting angle (**Figure 5C**, column 2).

The Effect of Movement History on Pendulum Kinematics Is More Variable in Children With CP Than in TD Children

First swing excursion was more variable in children with CP than in TD children for both the sitting and supine position ($p < 0.001$) (**Figure 2A**). Also the variability in the

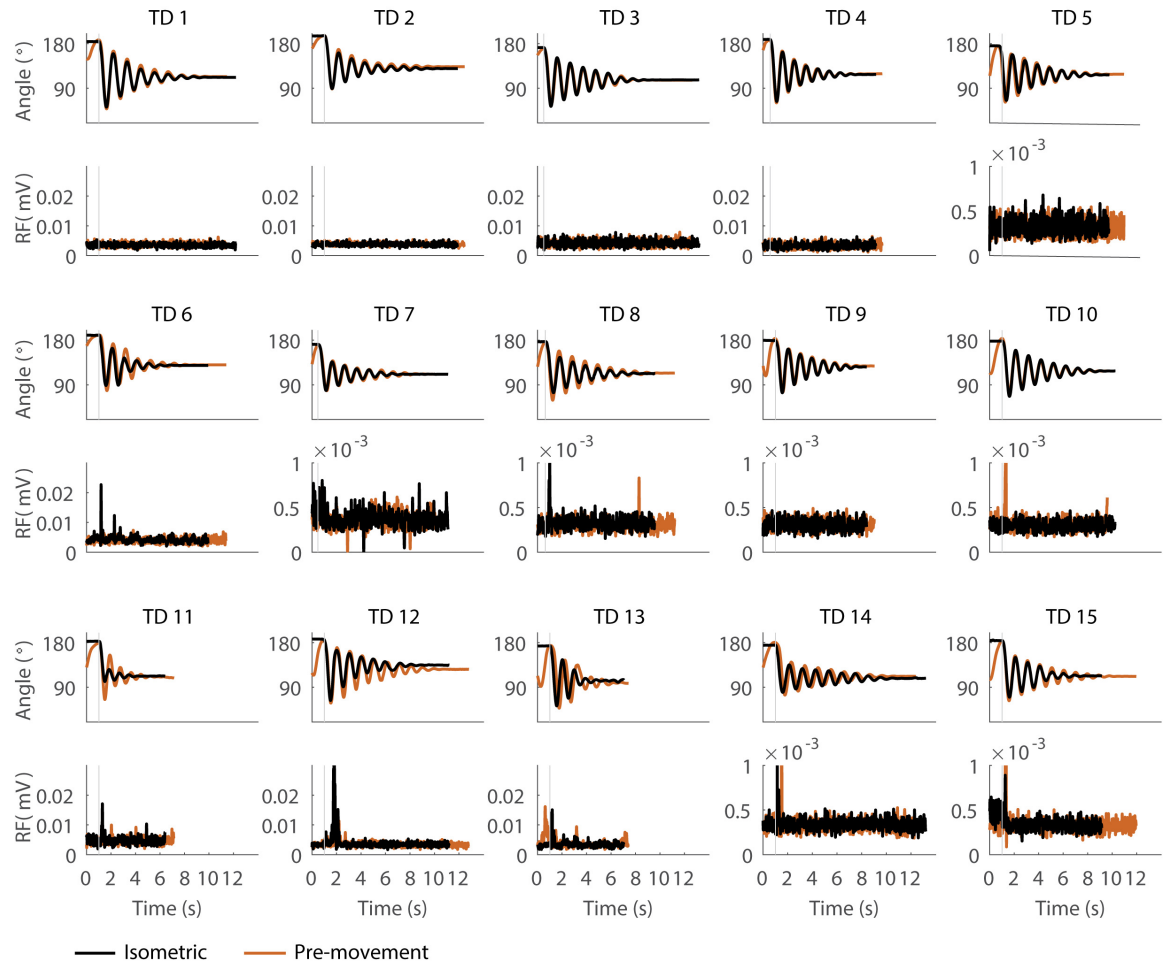

FIGURE 4 | Pendulum trajectories and rectus femoris (RF) muscle activity (sEMG) of TD children in the sitting position. A representative knee angle trajectory is shown for the isometric (black) and pre-movement (orange) conditions. Children are numbered from low reflex activity to high reflex activity based on number of trials with reflex activity (occurrence of reflexes). An increase in first swing excursion and number of oscillations is seen in the movement condition in orange as compared to the isometric condition in black.

increase in first swing excursion ($p < 0.01$) and number of oscillations ($p < 0.001$) when moving the leg before releasing it was higher in children with CP than in TD children in the sitting position, but not in the supine position (**Figures 5A,B**). Notwithstanding this high variability across children with CP, the first swing excursion and number of oscillations increased in all children with pre-movement (**Figures 3**, **5A,B**). Given this high variability, we explored whether a smaller first swing excursion in the isometric condition was related to a larger increase in first swing excursion in the pre-movement versus isometric condition in children with CP. However, we did not find such relation (**Supplementary Figure S2**). Children that had similar first swing excursions in the isometric condition (HR), presented different responses in the pre-movement condition (MR) (**Figure 3** and **Supplementary Figure S2**).

Higher Occurrence and Earlier Onset of Reflexes in Children With CP Than in TD Children

We observed reflex activity more often in children with CP than in TD children during the first swing and reflexes occurred sooner after release of the leg in children with CP than in TD children (**Figure 6** and **Supplementary Table S4**).

In the sitting position, the occurrence of reflex activity was higher in children with CP than in TD children ($p < 0.05$, CP: 73.9%; TD: 42.2%) when the leg was held isometric (HR) but not when the leg was moved prior to release (MR) (**Figure 6A** bottom). When reflexes were observed, reflex onset was 70 ms earlier in children with CP than in TD children ($p < 0.05$, 142 ± 30 ms in CP versus 212 ± 78 ms in TD) in the isometric condition (HR), but reflex onset was not different

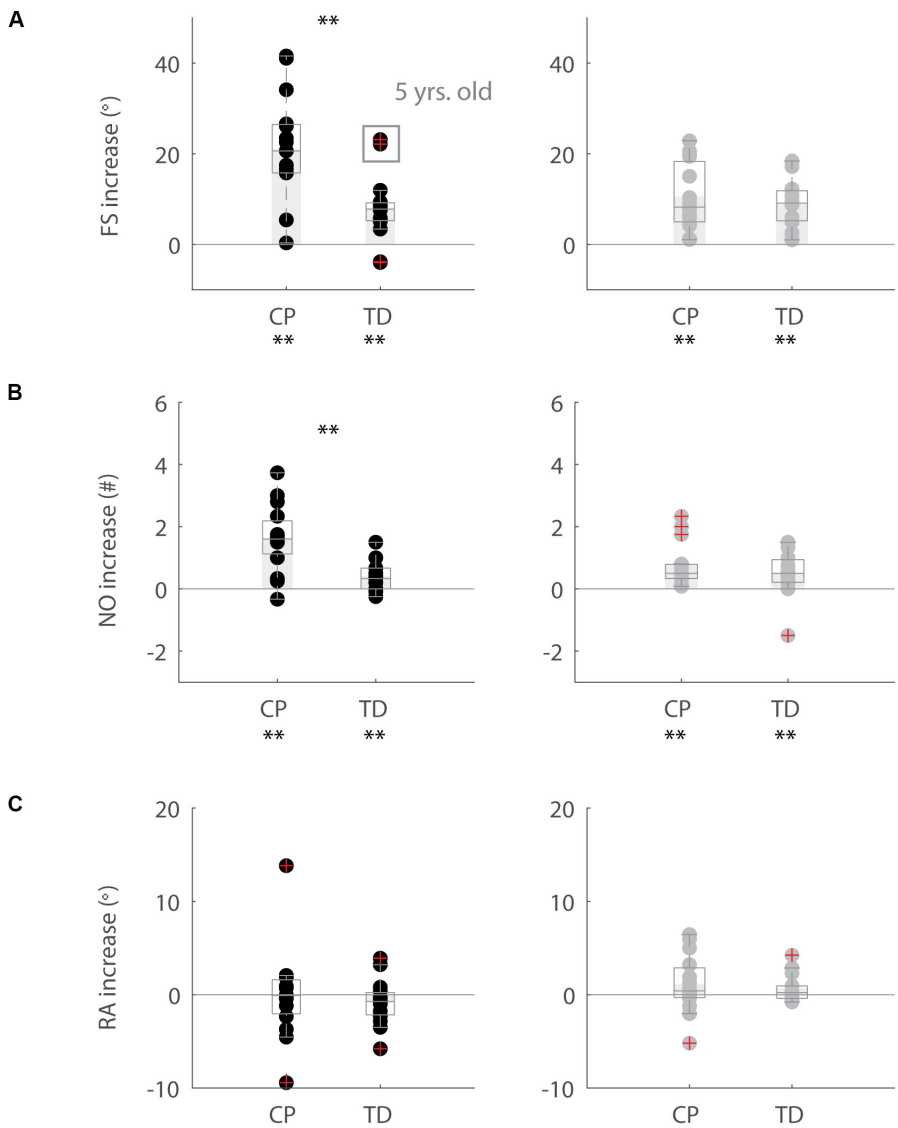

FIGURE 5 | Influence of movement history on key kinematic outcomes. **(A)** First swing excursion FS; **(B)** number of oscillations NO; **(C)** resting angle RA. We computed the difference in outcome parameters by subtracting outcomes in the isometric (HR) condition from outcomes in the pre-movement (MR) condition. Dots represent the average value over all trials for each child, light gray bars represent mean value over all children within a group. Significant differences between conditions are indicated with $^{*}p < 0.05$ and $^{**}p < 0.01$ below the graph, significant differences between children with CP and TD children are indicated by $^{*}p < 0.05$ and $^{**}p < 0.01$ above and in between graphs. Black = sitting position; gray = supine position.

between children with CP and TD children in the pre-movement condition (MR) (**Figure 6A** top).

In the supine position, the occurrence of reflexes was higher in children with CP than in TD children in both the HR and MR conditions ($p < 0.05$, HR: 63.2% in CP versus 29.2% in TD; MR: 59.3% in CP versus 27.3% in TD), (**Figure 6B** bottom). When reflexes were observed, reflex onset was 170 ms earlier in children with CP than in TD children ($p < 0.001$, CP: 165 ± 77 ms; TD: 294 ± 124 ms) in the isometric condition (HR), but reflex onset was not different between children with CP and TD children in the pre-movement condition (MR) (**Figure 6B** top).

Movement History Influences the Onset of Reflex Activity in Children With CP

Moving the leg instead of keeping it isometric prior to release did not alter the occurrence of reflex activity but delayed the onset of reflex activity by 87 ms ($p < 0.05$) while sitting and by 78 ms ($p < 0.001$) while supine in children with CP (**Figure 6**: black

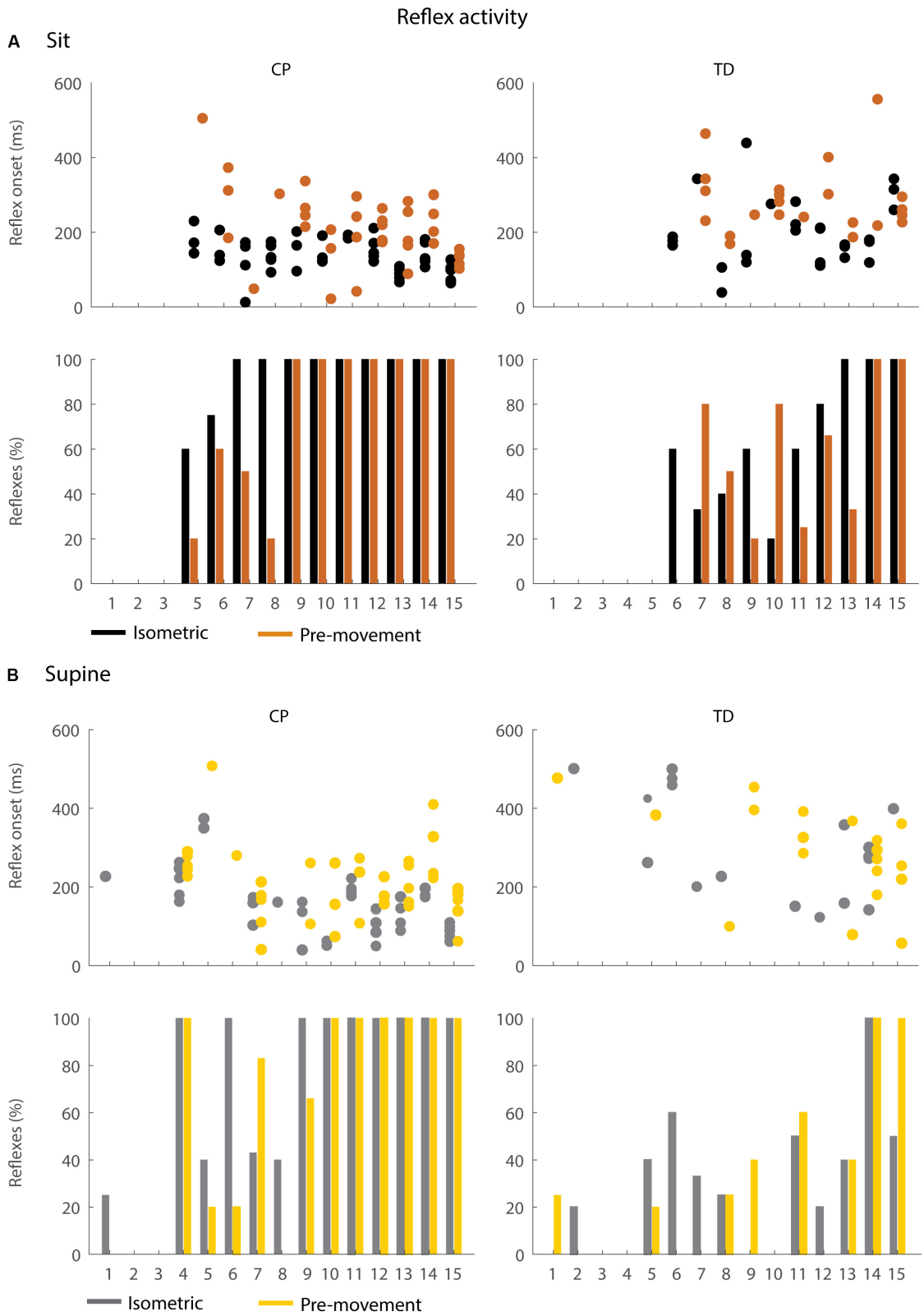

FIGURE 6 | Occurrence and timing of reflex activity in the sitting **(A)** and supine **(B)** position. The dots represent reflex onset with respect to release of the leg, only for trials in which reflex activity was observed. The bars represent the percentage of trials with reflex activity. Black = isometric (HR) – sitting; orange = pre-movement (MR) – sitting; gray = isometric (HR) – supine; yellow = pre-movement (MR) – supine.

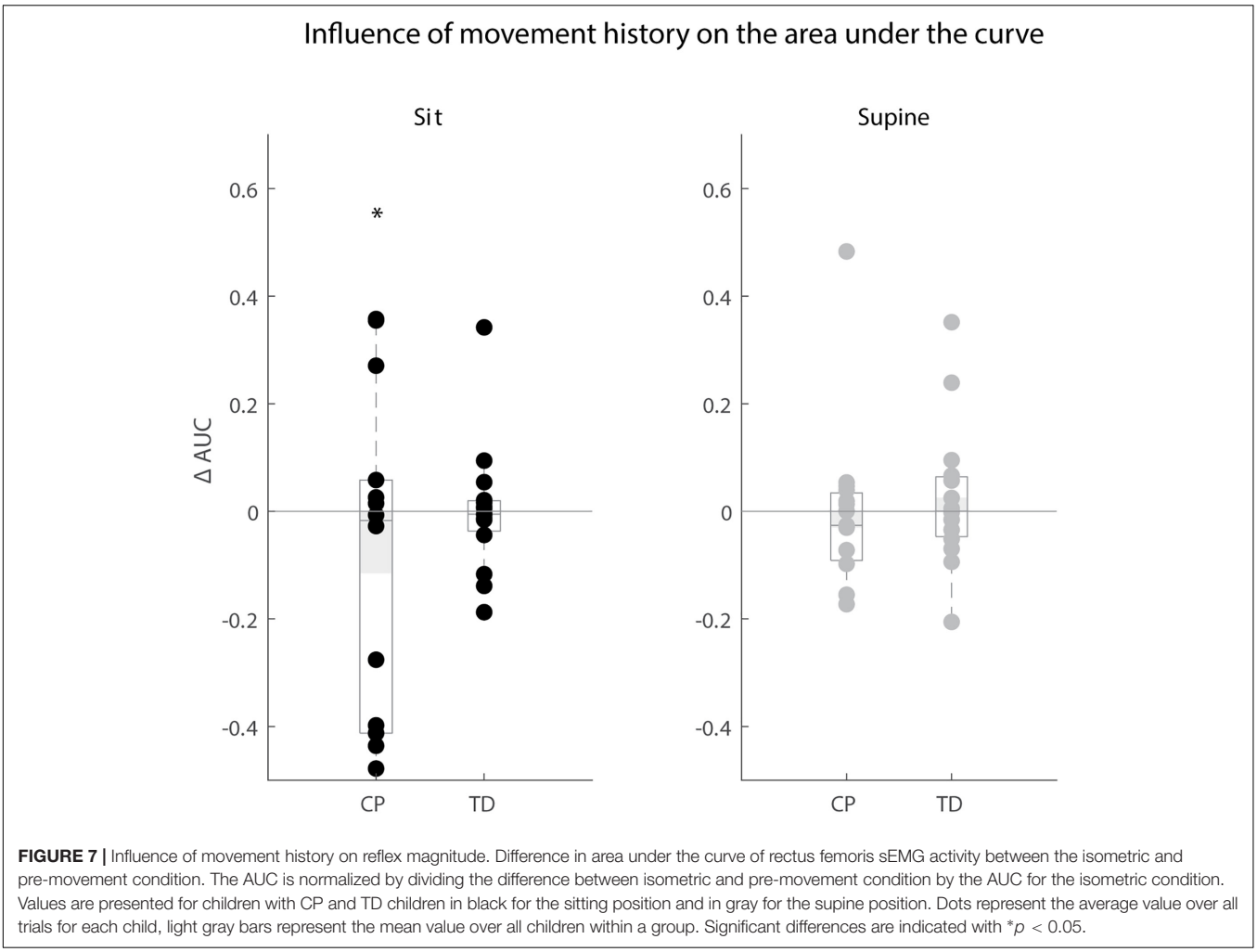

FIGURE 7 | Influence of movement history on reflex magnitude. Difference in area under the curve of rectus femoris sEMG activity between the isometric and pre-movement condition. The AUC is normalized by dividing the difference between isometric and pre-movement condition by the AUC for the isometric condition. Values are presented for children with CP and TD children in black for the sitting position and in gray for the supine position. Dots represent the average value over all trials for each child, light gray bars represent the mean value over all children within a group. Significant differences are indicated with $*p < 0.05$.

versus orange and gray versus yellow, **Supplementary Table S5**). No differences in occurrence of reflex activity and in reflex onset were observed in TD children.

Movement history only altered reflex magnitude of the rectus femoris for children with CP in the sitting position. The AUC decreased when the leg was moved instead of kept isometric prior to release ($p < 0.05$), but we observed large variability in the responses between children with CP. The AUC decreased in the MR condition in six children, whereas it did not change in six other children and increased in two others. There was no influence of movement history on reflex magnitude for TD children (sit and supine position) and children with CP in the supine position (**Figure 7**).

First Swing Excursion Was Correlated With Resting Angle and Occurrence of Reflex Activity

Resting Angle

In the supine, but not in the sitting position, children with a larger first swing excursion also had a more vertical resting angle (CP: $p < 0.001$, $r = 0.84$; TD: $p < 0.01$, $r = 0.66$), (**Figure 8A** and **Supplementary Table S6**).

Occurrence of Reflex Activity

In both the sitting and supine position, the first swing excursion was smaller in children with CP that had a higher occurrence of reflex activity (sit: $p < 0.001$, $r = -0.82$; supine: $p < 0.001$, $r = -0.87$), (**Figure 8B** and **Supplementary Table S6**). First swing excursion and occurrence of reflex activity were not related in TD children.

DISCUSSION

The current study showed that movement history alters key kinematic features of the pendulum test that are related to joint hyper-resistance. When moving the leg prior to releasing it instead of keeping it still, pendulum kinematics in children with CP became more similar to pendulum kinematics in TD children. In particular, the first swing excursion and number of oscillations, two key kinematic features that are sensitive to the presence and severity of spasticity, increased (Fowler et al., 2000).

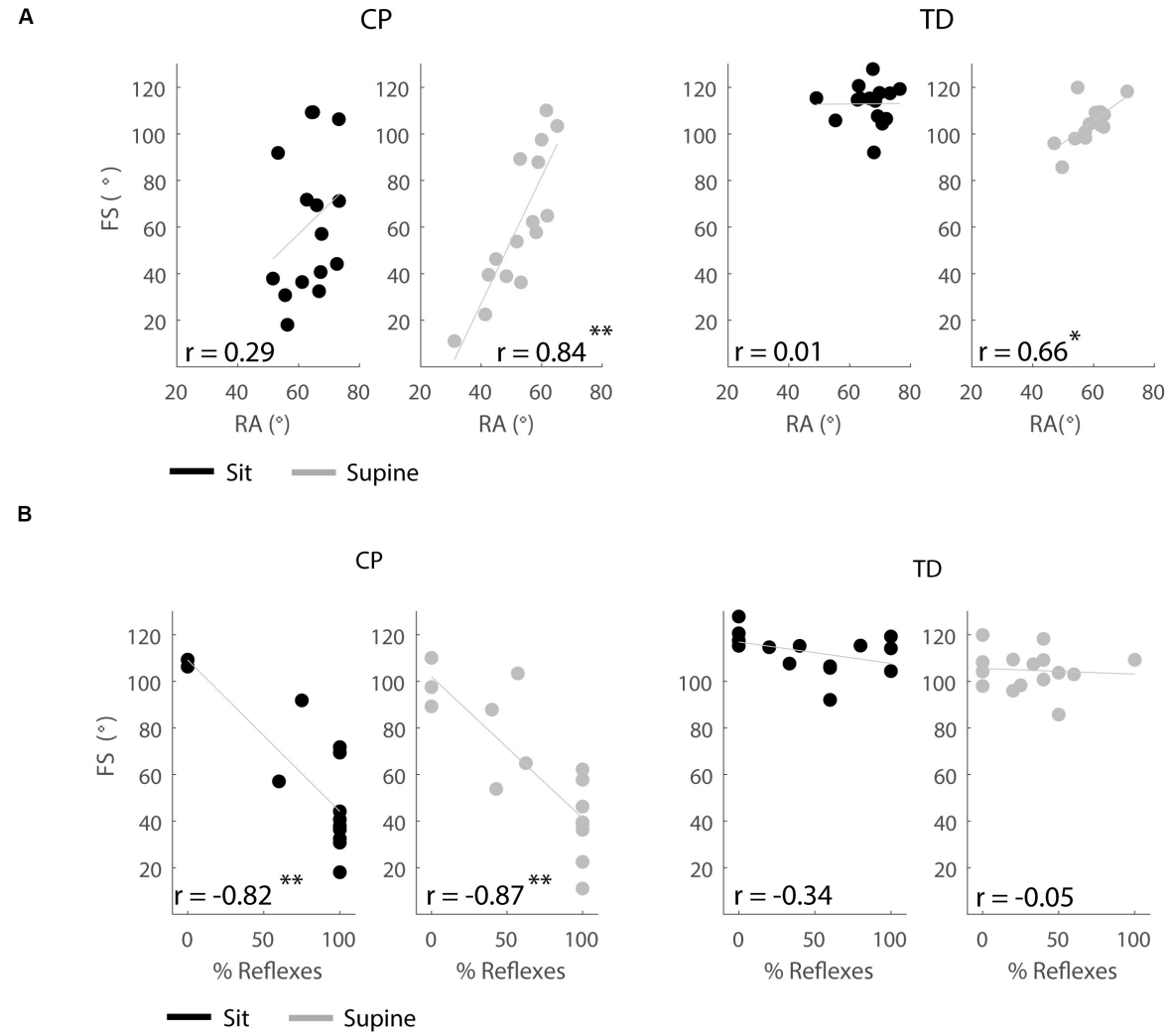

FIGURE 8 | Correlations between outcome parameters. **(A)** First swing excursion and resting angle are positively correlated in the supine position but not in the sitting position. **(B)** First swing excursion is negatively correlated with occurrence of reflexes in children with CP but not in TD children. Significant correlations are indicated with $^{*}p < 0.05$ and $^{**}p < 0.01$.

Further, reflex activity was delayed. As pre-movement will reduce muscle short-range stiffness, our observations are consistent with the hypothesis that muscle short-range stiffness, due to its interaction with muscle tone and reflex activity, contributes to increased resistance against stretch. Our work has implications for standardizing the pendulum test as an assessment of spasticity and for understanding the role of spasticity in functional movements, where movement history differs from movement history in clinical tests.

The movement history dependence of pendulum test kinematics suggests that short-range stiffness contributes to the decreased first swing excursion and number of oscillations in individuals with spastic CP. Pre-movement decreases short-range stiffness upon stretch in isolated muscle fibers (Campbell and Moss, 2002). Therefore, moving the leg prior to releasing it is expected to decrease short-range stiffness in the knee extensors, thereby reducing the resistance against movement. The increase in first swing excursion and number of oscillations when the leg was moved prior to release compared to the isometric condition in both children with CP and TD is thus in agreement with a reduced contribution from short-range stiffness.

Short-range stiffness is proportional to isometric force prior to the stretch (Campbell and Moss, 2002) and therefore the high prevalence of background muscle activity in CP (Freeman, 2005) might explain why pre-movement had a larger effect on pendulum test kinematics in children with CP. We were not able to directly confirm the role of background muscle activity, since the magnitude of the sEMG signal also depends on the conductance of the underlying soft tissues and therefore does not provide a quantitative measure of muscle activity. Although our previous modeling study suggested that background extensor muscle activity contributes to both reduced first swing excursion and less vertical resting angle (De Groote et al., 2018), we did not find a correlation between decreased first swing excursion

and less vertical resting angle in the sitting position. Possibly, this is due to other factors independently influencing first swing excursion and resting angle. For example, reflex hyper-excitability might mainly influence first swing excursion whereas background flexor activity might mainly influence resting angle, indicating that more factors should be taken into account.

We were able to test the dependency of joint hyper-resistance on active muscle force by altering the pose of the subjects. Assuming that changing the subject's position from sitting to supine would stretch rectus femoris beyond its optimal length, we expected a decrease in active muscle force and an increase in passive force. Since short-range stiffness is proportional to active force (Campbell and Moss, 2002; Blum et al., 2019), we therefore expected a smaller influence of short-range stiffness in the supine position compared to the sitting position. Indeed, we found that pre-movement had a smaller influence on first swing excursion and first swing excursion in the supine compared to the sitting position. In addition, the resting angle was less vertical in children with CP compared to TD children in the supine position but not in the sitting position, in agreement with the assumed increased contribution from passive muscle force (Gordon and Ridgway, 1987; Herzog and ter Keurs, 1988).

The decreased and delayed reflex activity with pre-movement suggests that the interaction between reflex hyperactivity and history-dependent short-range stiffness force contributes to joint hyper-resistance. The decrease in reflex activity with increased first swing excursion due to reduced short-range stiffness is in agreement with muscle spindles being encoders of force and yank, i.e., time derivative of force, during passive stretch conditions after being held isometric rather than fiber length and velocity (Blum et al., 2017; Falisse et al., 2018). If muscle spindle firing would reflect changes in length and velocity, reflexes would increase and happen sooner with pre-movement due to the larger and faster muscle stretch. The interaction between short-range stiffness and reflex activity was further confirmed by the correlation between a smaller first swing excursion and a larger number of trials with reflex activity in children with CP. However, reflex activity and the influence of movement history on reflex activity varied largely across children with CP. This might be explained by differential contributions of muscle tone versus reflex activity to joint hyper-resistance in our heterogeneous group of children with CP.

Movement history dependence of joint hyper-resistance calls for standardization of movement before applying stretch in clinical tests of spasticity and suggests pre-movement as an experimental manipulation to distinguish different neural and non-neural contributions to joint hyper-resistance. Failure to standardize movement prior to muscle stretch in spasticity might introduce large variability in joint hyper-resistance, which might have contributed to the low repeatability of commonly used tests of spasticity (van den Noort et al., 2017). Based on single fiber experiments, a rest period of five seconds between two consecutive stretches restores most of the SRS force (Campbell and Moss, 2002). Therefore, holding the starting position for at least five seconds before applying joint rotations might improve repeatability of clinical tests of spasticity including the pendulum test and MAS. In agreement with literature, we found reduced first swing excursions in children with CP that have no spasticity according to MAS scores for the quadriceps muscle (**Supplementary Table S1**), confirming the higher sensitivity of the pendulum test as compared to MAS (Brown et al., 1988; Fowler et al., 2000). We believe that performing the pendulum test in both the hold and pre-movement condition might further improve assessment of spasticity. Since pre-movement affects short-range stiffness, which interacts with neural factors (e.g., background muscle activity and hyperreflexia) but not with increased resistance due to altered non-contractile tissue properties, our results suggest that the effect of pre-movement will be larger when joint hyper-resistance results from neural factors rather than from non-neural factors.

Therefore, multiple test conditions might enable better discrimination between neural and non-neural contributions to joint hyper-resistance (van den Noort et al., 2017). Although the observation that first swing excursion depends on movement history was very robust across children with CP and TD children, the magnitude of the effect varied widely in our heterogeneous (based on clinical scores including MAS, GMFCS, and range of motion) group of children. A supplementary analysis showed that the variability in the effect of movement history on first swing excursion could not be explained by differences in first swing excursion in the isometric condition in children with CP (**Supplementary Figure S3**). Children with similar first swing excursions in the isometric condition responded differently to pre-movement. This suggests that differential contributions of neural and non-neural factors between subjects might contribute to the variability in the effect of movement history. Note that we also observed two outliers with higher increases in first swing excursion in the more homogenous group of TD children (**Figure 5A**). Remarkably, these outliers were the two youngest children, which were only 5 years old at the time of the test. Reflex excitability might be higher in TD children up to the age of six years than in older children (O'Sullivan et al., 1991). Indeed, both children had a high occurrence of reflexes in the hold trials that decreased with pre-movement (**Figure 6**, TD11 and 13).

Assessing the effect of movement history on joint hyper-resistance might also be important to further increase our understanding of the role of spasticity in functional movements, where movement history is typically different from clinical tests. Our results suggest that joint hyper-resistance as measured during clinical tests might not be representative for the hyper-resistance during tasks requiring non-isometric muscle contractions but the discrepancy in hyper-resistance in clinical tests of spasticity and functional movements might be highly subject-specific given the high variability of the effect of movement history on first swing excursion.

Despite the fact that we tried to control the initial angle between trials and conditions, the leg was on average 1.6° (CP – max: 7.1°) and 2.1° (TD – max: 6.4°) closer to horizontal in the pre-movement than in the isometric condition. However, this difference alone cannot explain the difference in first swing excursion between conditions. We simulated lower leg kinematics based on different initial angles (De Groote et al., 2018).

The simulated difference in first swing excursion due to altered initial angles was 1.5° and 4° for a difference of 2° (observed average) and 7° (observed maximum) in initial angle, respectively (**Supplementary Figure S3**). These differences in first swing excursion due to altered initial angles were both smaller than the observed differences between conditions (CP mean: 10.5°; TD mean: 8.8°). In addition, we corrected the increase in first swing excursion with the simulated difference in first swing excursion due to the difference in initial angle and repeated the statistical analysis based on the corrected values. Our results and conclusions did not change.

Collecting direct *in vivo* evidence for the proposed hypothesis is not possible in humans. We therefore indirectly tested the potential contribution of SRS through evaluating the effect of pre-movement, which is known to reduce SRS *in vitro* (Campbell and Moss, 2002). Our experimental set-up only required a small modification to the pendulum test and was easy to perform in a clinical gait lab. There are no reliable methods to assess muscle tone across individuals. While near infrared spectroscopy may provide a measure of baseline muscle oxygen metabolism before the drop, it has not been validated against a gold standard, and its reliability at low levels of muscle activation, as expected during the pendulum test, is not known (Shang et al., 2017). Human micro-neurography provides a direct measure of muscle spindle firing rates but its use is limited to movements with small joint ranges of motion (Day et al., 2017). In addition, the invasiveness of the technique makes it unsuitable for testing in children.

CONCLUSION

Our study supports a novel hypothesis about the mechanism of joint hyper-resistance derived from a previously published computational model of the pendulum test of spasticity. The movement history dependence of pendulum kinematics and reflex activity supports our hypothesis that muscle short-range stiffness and its interaction with increased background muscle activity and reflex hyper-excitability contribute to joint hyper-resistance in spastic CP. Our results suggest that movement history should be taken into account when assessing joint hyper-resistance and when studying its contribution to movement impairments. We demonstrate that the period of rest before stretching the muscle in clinical tests of spasticity is critical for the following response. Therefore, the period of rest before imposing the stretch should be standardized. In addition, the response to muscle stretch in a relaxed patient might be very different from the response to muscle stretch in the same patient performing functional movements as both movement history and background muscle activity will be different in both conditions. Assessing the effect of movement history in clinical tests of spasticity might be a first step toward a better understanding of the role of joint hyper-resistance in movement impairments. Our results suggest that there might be large variability in the effect of pre-movement between patients that present with the same clinical score, which might necessitate a more personalized treatment of hyper-resistance problems.

DATA AVAILABILITY STATEMENT

The raw data supporting the conclusions of this article will be made available by the authors, without undue reservation.

ETHICS STATEMENT

The studies involving human participants were reviewed and approved by Ethical Committee of UZ Leuven/KU Leuven. Written informed consent to participate in this study was provided by the participants' legal guardian/next of kin. Written informed consent was obtained from the minor(s)' legal guardian/next of kin for the publication of any potentially identifiable images or data included in this article.

AUTHOR CONTRIBUTIONS

LT and FD: conceptualization. JW and AV: recruitment. JW: data collection and curation. JW, LT, and FD: methodology and funding acquisition. JW and FD: formal analysis and visualization. All authors contributed to the interpretation of the results and in writing the manuscript.

FUNDING

This study was funded by the Flemish agency for scientific research (FWO-Vlaanderen) through a research fellowship to JW (1192320N) and by the National Institute of Health (NIH) research grant R01 HD090642 to LT.

ACKNOWLEDGMENTS

We would like to thank Sistania Bong for designing the back rest and all our participants for participating in this study.

SUPPLEMENTARY MATERIAL

The Supplementary Material for this article can be found online at: https://www.frontiersin.org/articles/10.3389/fbioe.2020.00920/full#supplementary-material

FIGURE S1 | Marker set-up used to measure kinematics during the pendulum test in children with CP and TD children.

FIGURE S2 | Relation between first swing excursion in the isometric condition and the increase in first swing excursion in the pre-movement with respect to the isometric condition for children with CP in the sitting position.

FIGURE S3 | Simulated pendulum movement for three different initial angles: 0° (gray), –5° (purple), –7° (pink). Only minor differences are observed in the first swing excursion between trials. Curves are shifted horizontally for clarity.

Kinematic trajectories were simulated based on the model described by De Groote et al. (2018). The model with short-range stiffness, but without reflex activity was used, since the largest differences based on initial angle were expected in this configuration. Muscle tone was set on 0.4 Nm. We used values for mass (2.4 kg), length (0.26 m), and inertia (0.21 kg/m^2) that were representative for the subjects in our database.

TABLE S1 | Spasticity scores as measured by the Modified Ashworth Scale for children with CP.

TABLE S2 | (a) Key kinematic outcomes (mean and standard deviation). **(b)** *p*-values for the comparisons between subject groups (CP and TD) and positions (sitting and supine).

TABLE S3 | (a) Influence of movement history on key kinematic outcomes (mean and standard deviation). **(b)** *p*-values for the comparison between conditions (isometric vs. pre-movement). **(c)** *p*-values for the comparison of the influence of pre-movement on the key kinematic outcomes between groups (CP vs TD) for the outcomes that were influenced by pre-movement.

TABLE S4 | (a) EMG-based outcomes describing rectus femoris reflex activity (occurrence of reflex activity (%), onset of reflexes (ms) AUC, mean and standard deviation). **(b)** *p*-values for the comparisons between subject groups (CP and TD) and positions (sitting and supine).

TABLE S5 | (a) Influence of movement history on EMG-based outcomes describing rectus femoris reflex activity (mean and standard deviations). **(b)** *p*-values for the comparison between conditions (isometric and pre-movement). **(c)** *p*-values for the comparison between groups for parameters that were influenced by pre-movement.

TABLE S6 | (a) Correlations between first swing excursion and resting angle in the isometric (HR) condition. **(b)** Correlations between first swing excursion and occurrence of reflexes in the isometric (HR) condition.

REFERENCES

Blum, K. P., Lamotte, D., Incamps, B., Zytnicki, D., and Ting, L. H. (2017). Force encoding in muscle spindles during stretch of passive muscle. *PLoS Comput. Biol.* 13:e1005767. doi: 10.1371/journal.pcbi.1005767

Blum, K. P., Nardelli, P., Cope, T. C., and Ting, L. H. (2019). Elastic tissue forces mask muscle fiber forces underlying muscle spindle Ia afferent firing rates in stretch of relaxed rat muscle. *J. Exp. Biol.* 222:jeb196287. doi: 10.1242/jeb.196287

Brown, R. A., Lawson, D. A., Leslie, G. C., MacArthur, A., MacLennan, W. J., McMurdo, M. E., et al. (1988). Does the Wartenberg pendulum test differentiate quantitatively between spasticity and rigidity? A study in elderly stroke and Parkinsonian patients. *J. Neurol. Neurosurg. Psychiatry* 51, 1178–1186. doi: 10.1136/jnnp.51.9.1178

Campbell, K. S., and Lakie, M. (1998). A cross-bridge mechanism can explain the thixotropic short-range elastic component of relaxed frog skeletal muscle. *J. Physiol.* 510, 941–962. doi: 10.1111/j.1469-7793.1998.941bj.x

Campbell, K. S., and Moss, R. L. (2002). History-dependent mechanical properties of permeabilized rat soleus muscle fibers. *Biophys. J.* 82, 929–943. doi: 10.1016/s0006-3495(02)75454-4

Day, J., Bent, L. R., Birznieks, I., Macefield, V. G., and Cresswell, A. G. (2017). Muscle spindles in human tibialis anterior encode muscle fascicle length changes. *J. Neurophysiol.* 117, 1489–1498. doi: 10.1152/jn.00374.2016

De Groote, F., Blum, K. P., Horslen, B. C., and Ting, L. H. (2018). Interaction between muscle tone, short-range stiffness and increased sensory feedback gains explains key kinematic features of the pendulum test in spastic cerebral palsy: a simulation study. *PLoS One* 13:e0205763. doi: 10.1371/journal.pone.0205763

De Luca, C. J., Gilmore, L. D., Kuznetsov, M., and Roy, S. H. (2010). Filtering the surface EMG signal: movement artifact and baseline noise contamination. *J. Biomech.* 43, 1573–1579. doi: 10.1016/j.jbiomech.2010.01.027

Delp, S. L., Anderson, F. C., Arnold, A. S., Loan, P., Habib, A., John, C. T., et al. (2007). OpenSim: open-source software to create and analyze dynamic simulations of movement. *IEEE Trans. Biomed. Eng.* 54, 1940–1950. doi: 10.1109/tbme.2007.901024

Dietz, V., and Sinkjaer, T. (2007). Spastic movement disorder: impaired reflex function and altered muscle mechanics. *Lancet Neurol.* 6, 725–733. doi: 10.1016/s1474-4422(07)70193-x

Falisse, A., Bar-On, L., Desloovere, K., Jonkers, I., and De Groote, F. (2018). A spasticity model based on feedback from muscle force explains muscle activity during passive stretches and gait in children with cerebral palsy. *PLoS One* 13:e0208811. doi: 10.1371/journal.pone.0208811

Fee, J. W., and Miller, F. (2004). The Leg Drop Pendulum Test performed under general anesthesia in spastic cerebral palsy. *Dev. Med. Child Neurol.* 46, 273–281. doi: 10.1111/j.1469-8749.2004.tb00482.x

Fowler, E., Nwigwe, A., and Ho, T. (2000). Sensitivity of the pendulum test for assessing spasticity in persons with cerebral palsy. *Dev. Med. Child Neurol.* 42, 182–189. doi: 10.1017/s0012162200000323

Freeman, M. (2005). *Cerebral Palsy [Online]*. Cham: Spirnger. Available online at: https://www.springer.com/gp/book/9783319745572

Gordon, A. M., and Ridgway, E. B. (1987). Extra calcium on shortening in barnacle muscle. Is the decrease in calcium binding related to decreased cross-bridge attachment, force, or length? *J. Gen. Physiol.* 90, 321–340. doi: 10.1085/jgp.90.3.321

Hermens, H. J., Freriks, B., Disselhorst-Klug, C., and Rau, G. (2000). Development of recommendations for SEMG sensors and sensor placement procedures. *J. Electromyogr. Kinesiol. Off. J. Int. Soc. Electrophysiol. Kinesiol.* 10, 361–374. doi: 10.1016/s1050-6411(00)00027-4

Herzog, W., and ter Keurs, H. E. D. J. (1988). Force-length relation of in-vivo human rectus femoris muscles. *Pflüg Arch.* 411, 642–647. doi: 10.1007/bf00580860

Lance, J. W. (1980). "Pathophysiology of spasticity and clinical experience with Baclofen," in *Spasticity: Disordered Motor Control, Year Book* (Chicago, IL), 185–204.

Lin, D. C., McGowan, C. P., Blum, K. P., and Ting, L. H. (2019). Yank: the time derivative of force is an important biomechanical variable in sensorimotor systems. *J. Exp. Biol.* 222:jeb180414. doi: 10.1242/jeb.180414

O'Sullivan, M., Eyre, J., and Miller, S. (1991). Radiation of phasic stretch reflex in biceps brachii to muscles of the arm in man and its restriction during development. *J. Physiol.* 439, 529–543. doi: 10.1113/jphysiol.1991.sp018680

Papageorgiou, E., Simon-Martinez, C., Molenaers, G., Ortibus, E., Van Campenhout, A., and Desloovere, K. (2019). Are spasticity, weakness, selectivity, and passive range of motion related to gait deviations in children with spastic cerebral palsy? A statistical parametric mapping study. *PLoS One* 14:e0223363. doi: 10.1371/journal.pone.0223363

Seth, A., Hicks, J. L., Uchida, T. K., Habib, A., Dembia, C. L., Dunne, J. J., et al. (2018). OpenSim: simulating musculoskeletal dynamics and neuromuscular control to study human and animal movement. *PLoS Comput. Biol.* 14:e1006223. doi: 10.1371/journal.pcbi.1006223

Shang, Y., Li, T., and Yu, G. (2017). Clinical applications of near-infrared diffuse correlation spectroscopy and tomography for tissue blood flow monitoring and imaging. *Physiol. Meas.* 38, R1–R26.

Szopa, A., Domagalska-Szopa, M., Kidoñ, Z., and Syczewska, M. (2014). Quadriceps femoris spasticity in children with cerebral palsy: measurement with the pendulum test and relationship with gait abnormalities. *J. Neuroeng. Rehabil.* 11:166. doi: 10.1186/1743-0003-11-166

van den Noort, J. C., Bar-On, L., Aertbeliën, E., Bonikowski, M., Braendvik, S. M., Broström, E. W., et al. (2017). European consensus on the concepts and measurement of the pathophysiological neuromuscular responses to passive muscle stretch. *Eur. J. Neurol.* 24:981-e38.

Conflict of Interest: The authors declare that the research was conducted in the absence of any commercial or financial relationships that could be construed as a potential conflict of interest.

frontiers in Bioengineering and Biotechnology

ORIGINAL RESEARCH
published: 18 August 2020
doi: 10.3389/fbioe.2020.01007

Muscle Fatigue Enhance Beta Band EMG-EMG Coupling of Antagonistic Muscles in Patients With Post-stroke Spasticity

Le-Jun Wang[1,2], Xiao-Ming Yu[3], Qi-Neng Shao[1], Ce Wang[1], Hua Yang[1], Shang-Jun Huang[2] and Wen-Xin Niu[2]**

[1] *Physical Education Department, Sport and Health Research Center, Tongji University, Shanghai, China,* [2] *Key Laboratory of Spine and Spinal Cord Injury Repair and Regeneration of Ministry of Education, Orthopaedic Department, Tongji Hospital, Tongji University School of Medicine, Shanghai, China,* [3] *Department of Rehabilitation, Shanghai Seventh People's Hospital, Shanghai University of Traditional Chinese Medicine, Shanghai, China*

OPEN ACCESS

Edited by:
Ruoli Wang, KTH Royal Institute of Technology, Sweden

Reviewed by:
Francesco Cenni, University of Jyväskylä, Finland
Hu Xiaoling, Hong Kong Polytechnic University, Hong Kong

***Correspondence:**
Xiao-Ming Yu
278828225@qq.com
Wen-Xin Niu
niu@tongji.edu.cn

Specialty section:
This article was submitted to Biomechanics, a section of the journal Frontiers in Bioengineering and Biotechnology

Received: *30 March 2020*
Accepted: *31 July 2020*
Published: *18 August 2020*

Citation:
Wang L-J, Yu X-M, Shao Q-N, Wang C, Yang H, Huang S-J and Niu W-X (2020) Muscle Fatigue Enhance Beta Band EMG-EMG Coupling of Antagonistic Muscles in Patients With Post-stroke Spasticity. Front. Bioeng. Biotechnol. 8:1007. doi: 10.3389/fbioe.2020.01007

There is a significant influence of muscle fatigue on the coupling of antagonistic muscles while patients with post-stroke spasticity are characterized by abnormal antagonistic muscle coactivation activities. This study was designed to verify whether the coupling of antagonistic muscles in patients with post-stroke spasticity is influenced by muscle fatigue. Ten patients with chronic hemipare and spasticity and 12 healthy adults were recruited to participate in this study. Each participant performed a fatiguing isometric elbow flexion of the paretic side or right limb at 30% maximal voluntary contraction (MVC) level until exhaustion while surface electromyographic (sEMG) signals were collected from the biceps brachii (BB) and triceps brachii (TB) muscles during the sustained contraction. sEMG signals were divided into the first (minimal fatigue) and second halves (severe fatigue) of the contraction. The power and coherence between the sEMG signals of the BB and TB in the alpha (8–12 Hz), beta (15–35 Hz), and gamma (35–60 Hz) frequency bands associated with minimal fatigue and severe fatigue were calculated. The coactivation ratio of the antagonistic TB muscle was also determined during the sustained fatiguing contraction. The results demonstrated that there was a significant decrease in maximal torque during the post-fatigue contraction compared to that during the pre-fatigue contraction in both stroke and healthy group. In the stroke group, EMG-EMG coherence between the BB and TB in the alpha and beta frequency bands was significantly increased in severe fatigue compared to minimal fatigue, while coactivation of antagonistic muscle increased progressively during the sustained fatiguing contraction. In the healthy group, coactivation of the antagonistic muscle showed no significant changes during the fatiguing contraction and no significant coherence was found in the alpha, beta and gamma frequency bands between the first and second halves of the contraction. Therefore, the muscle fatigue significantly increases the coupling of antagonistic muscles in patients with post-stroke spasticity,

which may be related to the increased common corticospinal drive from motor cortex to the antagonistic muscles. The increase in antagonistic muscle coupling induced by muscle fatigue may provide suggestions for the design of training program for patients with post-stroke spasticity.

Keywords: antagonist muscle, coactivation, EMG, muscle fatigue, post-stroke spasticity

INTRODUCTION

The ability of the central nervous system to appropriately control agonistic and antagonistic muscles is a key mechanism to maintain body coordination during human voluntary movements and postural adjustments, which can be damaged by post-stroke spasticity (Tamburella et al., 2017). Spasticity is a common complication of stroke and affects up to 40% of patients with hemiplegia (Wissel et al., 2013). It results from the decreased inhibition or facilitation of hypertonia after stroke as a result of motor impairment (Wang et al., 2018). The decreased inhibitory input to the motor unit leads to uncoordinated activities of antagonist muscles during volitional movement (Turpin et al., 2017; Levin et al., 2018).

Neuromuscular fatigue has the tendency to arise when performing physical activities after stroke, which has received little attention in clinical rehabilitation research (Boudarham et al., 2014). It can be defined as a reversible reduction in the neuromuscular system's capacity to generate force or power (Vollestad, 1997), which encompasses a number of changes occurring at both the central and peripheral levels (Enoka et al., 2011; Wang et al., 2017). The relationship between agonist and antagonist muscles during muscle fatigue has been focused on, and significant muscle fatigue-induced interaction changes have been reported previously (Duchateau and Baudry, 2014; Arellano et al., 2016). Particularly, previous studies have revealed an increased interconnection between synchronized cortical neurons and the motoneuron pool of antagonist muscles as a result of fatigue (Wang et al., 2015). However, whether neuromuscular fatigue influences the control of antagonist muscles in patients with post-stroke spasticity remains unclear.

Frequency-based electromyography (EMG) assessment has been used as an effective tool to explore the motor control strategy of movement. In particular, EMG–EMG coherence analysis is a method of reflecting the similarity of two signals in frequency domain and has been applied to evaluate the common synaptic input to co-contracting muscles or to two parts of the same muscle from branches of last order neurons to spinal motoneurons (De Luca and Mambrito, 1987; Keen et al., 2012). Previous researches have suggested that inter- and intramuscular coherence in beta (15–35 Hz) and gamma (35–60 Hz) bands are predominantly driven by the motor cortex (Baker et al., 1997), whereas coherence in the alpha (8–12 Hz) band is influenced by multifactors (McKiernan et al., 2000). In previous research, EMG-EMG coherence analysis has been widely used to reflect neuromuscular control mechanisms of movement and to gauge the functional integrity of corticomotor tracts while patients with stroke complete motor tasks (Lodha et al., 2017; Wang et al., 2019).

Based on these studies, we wondered whether the coupling and controlling strategies of antagonistic muscles in patients with post-stroke spasticity can be influenced by muscle fatigue. The current study was designed to verify this hypothesis. EMG activities of the biceps brachii (BB) and triceps brachii (TB) were recorded from both patients with post-stroke spasticity and healthy subjects during fatiguing isometric elbow flexion contraction. The amount of antagonist activation and EMG-EMG coherence between the BB and TB were compared between the first (stage 1 with minimal fatigue) and second halves (stage 2 with severe fatigue) of the contraction.

MATERIALS AND METHODS

Participants

Twelve healthy adults (12 men; age: 21.1 ± 3.4 years; height: 177.6 ± 7.7 cm; weight: 66.25 ± 9.5 kg) and 10 patients with chronic hemiparesis (7 men and 3 women; age: 60.5 ± 9.1 years; height: 169.9 ± 8.8 cm; weight: 69.9 ± 11.3 kg) participated in this study. All healthy subjects reported no known neuromusculoskeletal impairments and were right-handed. The inclusion criteria for the patients with stroke were as follows: (1) hemiplegia secondary to an ischemic or hemorrhagic stroke, (2) at least 6 months post-stroke, (3) residual voluntary elbow flexion force, (4) spastic hypertonia in elbow flexors of the impaired side, rated as Modified Ashworth Scale (MAS) less than 3, and (5) able to understand and follow instructions related to the experiment. All subjects were fully informed of all procedures and risks associated with the experimental tests before providing their informed written consent to participate. The experiment was approved by the Ethics Committee of Tongji University.

Experimental Tasks

The experiment consisted of three motor tasks. First, participants performed isometric maximal elbow flexion contraction test for three times with 5 min rest after each test, in order to acquire the maximal isometric elbow flexion torque of each subject without muscle fatigue. Second, after 5-min rest, each participant performed a sustained elbow flexion fatiguing contraction at 30% maximal elbow flexion force for as long time as possible. Lastly, as soon as the fatiguing elbow flexion contraction task was complete, the subjects were instructed to perform another isometric maximal elbow flexion contraction test. All motor tasks were finished with the affected limb.

In the experiment, the participants sat with the upper arm vertically placed, and the elbow angle was maintained at 90°. The right forearm was positioned parallel to the ground and

supinated. The participants were instructed to maintain their posture by flexing the elbow with the elbow joint maintained as close as possible to 90° until they experienced exhaustion and were no longer able to continue the contraction. The participants were verbally vigorously encouraged to continue the sustained contraction for as long as possible. During the sustained contraction, surface EMG signals of the BB and TB muscles of the affected limb were recorded. The experimental setup has been depicted in **Figure 1**.

Data Collection

The elbow flexion torque was measured using a torque sensor (TRS-500, Transducer Techniques, Temecula, CA). The sensor was located in line with the center of the rotation of the active elbow joint. Surface electromyographic signals were recorded by bipolar surface electrodes of NeuroScan system (NeuroScan Inc., El Paso, TX). Two pairs of electrodes were placed over the belly of the right BB and TB muscles with a center-to-center inter-electrode distance of 2 cm. A common reference electrode was placed to the left of the processus mastoideus. The skin was shaved and cleaned with alcohol wipes before filling the electrodes with conducting gel and fixing. Medical adhesive tape and plastic casts were applied to fix the electrodes. The EMG signals were amplified, band-pass filtered (3–1000 Hz), digitized (2000 samples/s), and acquired by using the NeuroScan system.

Data Analysis

Data were analyzed off-line by custom-written programs using MATLAB R2016a software (Mathworks Inc., Natick, MA).

Data Preprocessing

The raw EMG signals recorded from both the BB and TB muscles were band-pass filtered offline at 5–500 Hz using a fourth order zero-phase-shift Butterworth filter. Then, the filtered surface EMG (sEMG) signals of both the BB and TB muscles were further full-wave rectified using the Hilbert transform according to the research of Farina et al. (2013). Filtered and rectified EMG signals were adopted in the latter coherence analysis process, while filtered-only EMG were used when calculating EMG median frequency, power and coactivation ratio.

EMG Median Frequency, Power, and Coactivation Ratio

The EMG median frequency and power spectrum based on Fourier transform of filtered-only EMG signals were calculated for non-overlapping 2.048-s epochs during the sustained fatiguing contraction and were averaged for each epoch during

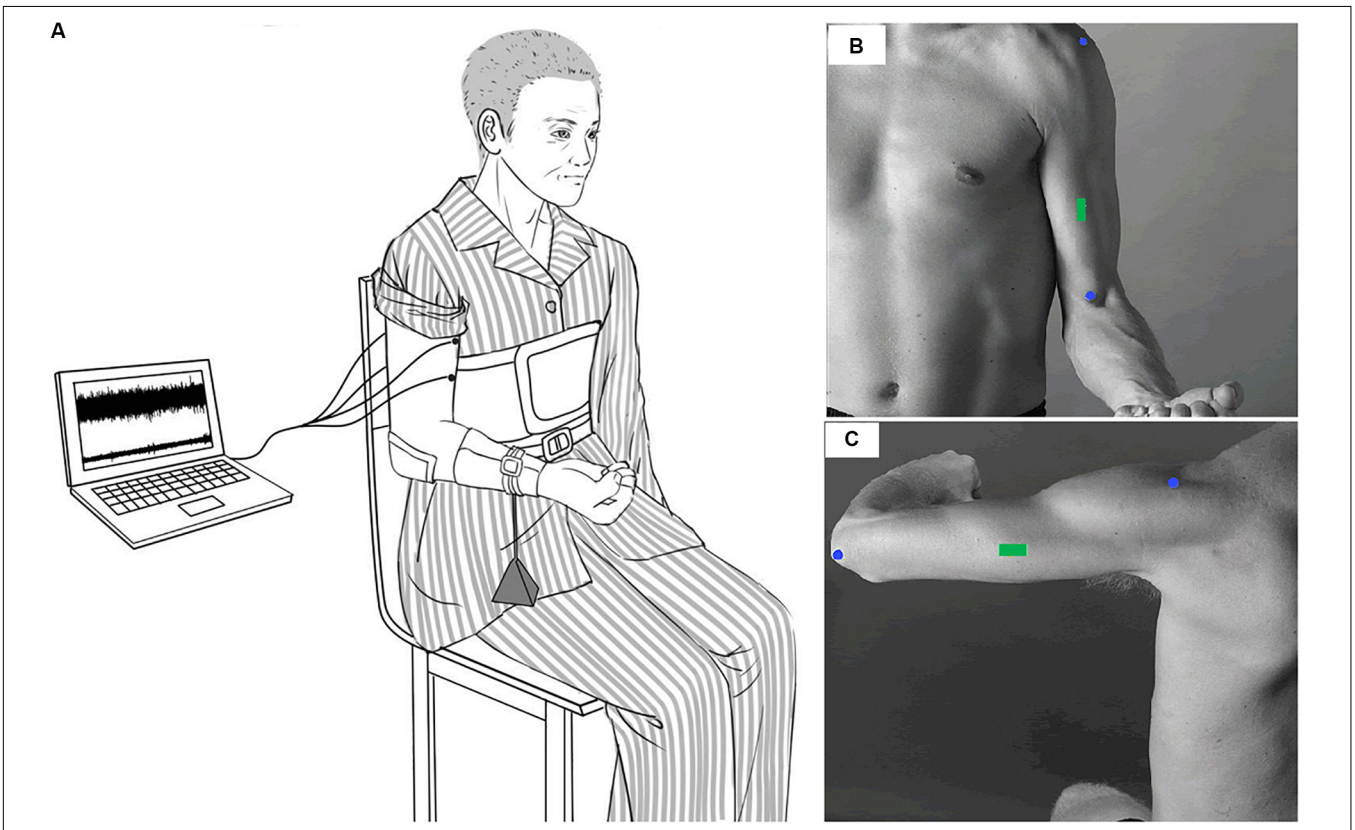

FIGURE 1 | Experimental setup. Participants sat with the upper arm vertically placed and the elbow angle keeping in 90°. The right forearm was positioned parallel to the ground and supinated. During the sustained elbow flexion contraction, a weight was suspended from the distal part of the right forearm so as to produce a target force of 30% maximal elbow flexion force **(A)**. Surface EMG signals were recorded from the BB and TB of the affected side. The EMG sensors of the BB and TB were placed on the green rectangle of **(B,C)** according to SENIAM recommendations.

the first and second halves of the sustained elbow flexion contraction. The EMG power in the alpha (8–12 Hz), beta (15–35 Hz), and gamma (35–60 Hz) frequency bands were acquired during the first and second halves of the sustained elbow flexion contraction.

The coactivation ratio of the antagonistic TB muscle, described as the quotient of the TB EMG amplitude divided by the sum of the BB and TB EMG amplitudes, was also calculated for non-overlapping 2.048-s epochs during the sustained fatiguing contraction and time normalized to 20 points for each subject and then averaged for all subjects.

EMG-EMG Coherence

The filtered and rectified sEMG signals of each participant were equally divided into two segments: the first and second halves of the contraction. Coherence analysis was conducted on each half segment between EMG signals recorded from the BB and TB muscles. The coherence was calculated for a segment length of 2048 samples with 50% overlap, using a Hanning window, as suggested by previous research.

The magnitude squared coherence, Cxy(f) between the two EMG signals (rectified EMG signals) recorded from the BB and TB muscles, x(t) and y(t), for a given frequency f was calculated as follows:

$$C_{xy}(f) = \frac{|S_{xy}(f)|^2}{S_{xx}(f) . S_{yy}(f)} \quad (1)$$

where Sxy(f) is the cross spectrum and Sxx(f) and Syy(f) are the auto spectra of x(t) and y(t), respectively.

The significance level of the coherence spectrum was calculated based on the methods described by Terry and Griffin (2008). The coherence areas in the alpha, beta and gamma bands greater than the upper 95% confidence interval of the coherence spectrum were computed.

Statistical Analysis

Statistical analysis was performed using IBM SPSS 20.0 (SPSS Inc., Chicago, IL). Normality was tested using the Kolmogorov–Smirnov test. A repeated-measures general linear model was used to determine the difference between the maximal torque

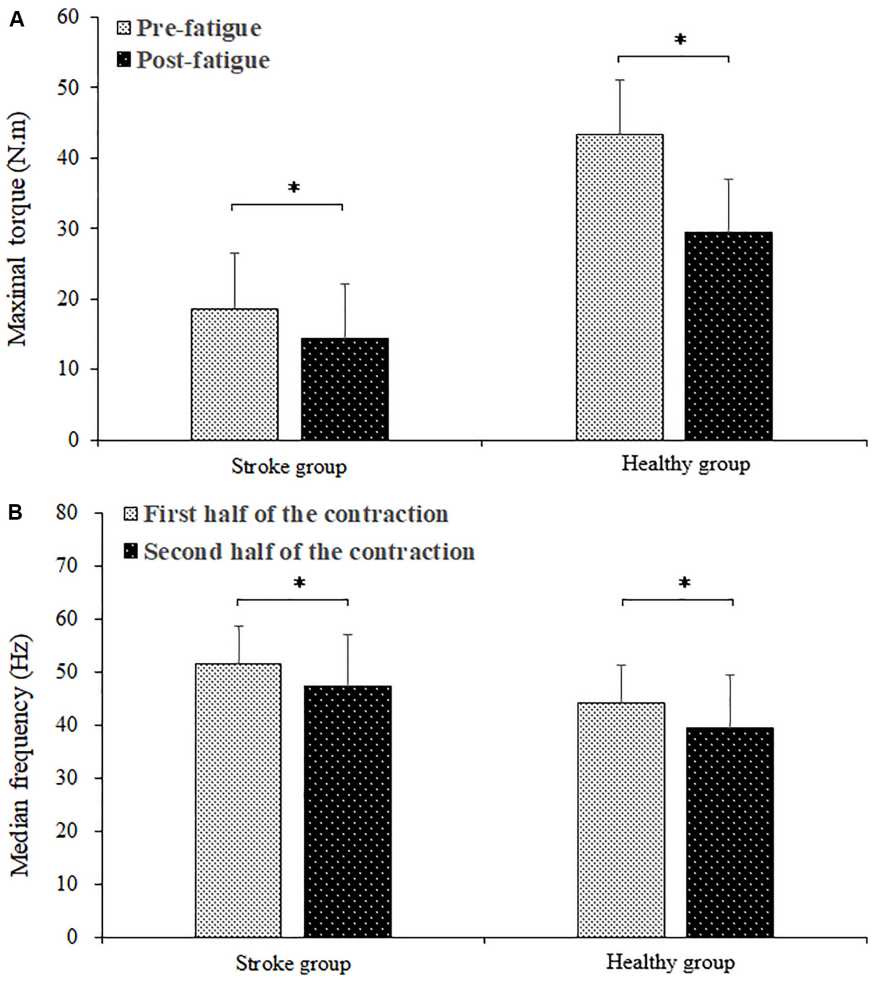

FIGURE 2 | Comparison of maximal torque between the pre- and post-fatigue **(A)** and the BB EMG median frequency between the first and second halves **(B)** of the fatiguing contraction. * demonstrated a significant difference of observed index between the pre- and post-fatigue conditions.

and median frequency. Pearson's cross-correlation analysis was employed to determine the relationship between the coactivation ratio of antagonistic muscles and the contraction duration time. The non-parametric Wilcoxon test was adopted to test the difference in EMG power and coherence between the first and second halves of the contraction. All significance thresholds were set at $\alpha = 0.05$.

RESULTS

Maximal Torque, Median Frequency, and Antagonist Muscle Coactivation

The fatiguing contraction times of the stroke group and healthy group subjects were averages of 220.66 ± 109.19 s and 258.58 ± 51.13 s, respectively. There was no significant difference between the fatiguing contraction times of the stroke and healthy group subjects ($P = 0.296$). **Figure 2** shows the comparison of maximal torque between pre- and post-fatigue and EMG median frequency of the BB muscle between the first and second halves of the fatiguing contraction of the stroke and healthy group subjects. The maximal torques of the healthy group subjects were significantly higher than those of the stroke group subjects ($F = 30.758$, $P = 0.000$). A significant group by fatigue interaction was found ($F = 35.771$, $P = 0.000$). For both the stroke and healthy group subjects, there was a significant decrease in the maximal torque during post-fatigue contractions compared to that during pre-fatigue contractions (stroke group: $P = 0.000$; healthy group: $P = 0.000$). The median frequency decreased significantly during the second half of the fatiguing contraction compared to that during the first half contraction ($F = 46.332$, $P = 0.000$). A higher median frequency was found in the stroke group than in the healthy group subjects ($F = 8.050$, $P = 0.010$). No significant group by fatigue interaction was present ($F = 0.096$, $P = 0.760$).

Changes in the average coactivation ratio among stroke and healthy subjects for each 5% duration times are shown in **Figure 3**. In the stroke group, the coactivation ratio was 0.222 ± 0.085 in the first 5% of the contraction duration and increased progressively during the sustained fatiguing contraction, reaching 0.301 ± 0.079 in the last 5% contraction duration. In the healthy group, the coactivation ratios were 0.087 ± 0.052 in the first 5% contraction duration and 0.082 ± 0.036 in the last 5% of contraction duration. Pearson's correlation analysis was used to observe the correlation between coactivation ratio and contraction duration, and a significant increasing tendency of the contraction ratio with the change in contraction duration was found in the stroke group ($r = 0.183$, $P = 0.010$), while no significant correlation was found between the contraction ratio and contraction duration in the healthy group ($r = -0.011$, $P = 0.868$).

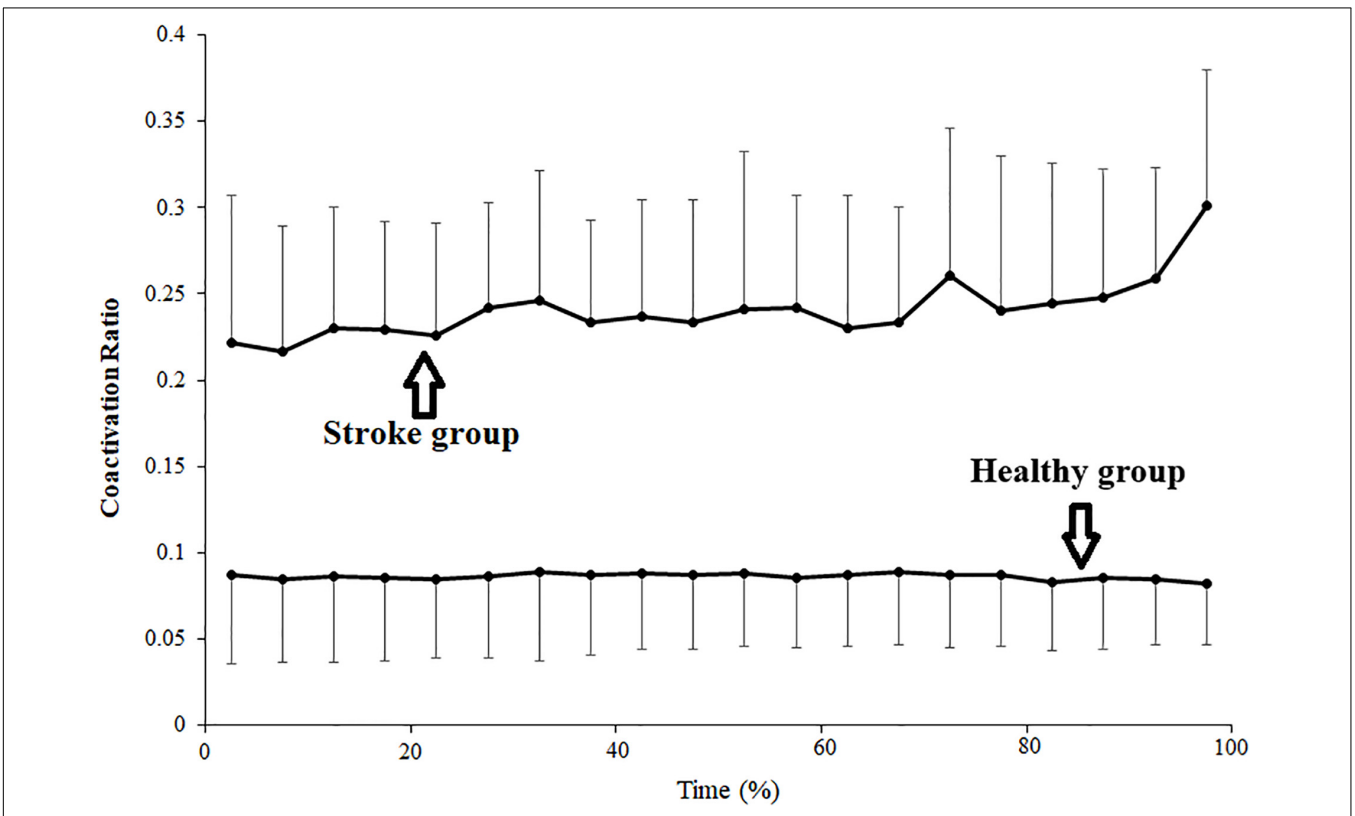

FIGURE 3 | Changes of average coactivation ratio plotted as a percentage of contraction time during the sustained fatiguing contraction. The coactivation ratio was calculated as quotient of the antagonistic muscle TB EMG amplitude divided by the sum of agonistic muscle BB EMG amplitude and TB EMG amplitude.

EMG Power of Agonist and Antagonist Muscles

The average EMG power of the BB and TB muscles in the alpha, beta and gamma frequency bands during the first and second halves of the contraction in the stroke and healthy group were presented in **Figure 4**. In the stroke group, the power of the TB muscle in the beta frequency band was significantly higher during the second half of the contraction than during the first half of contraction (P = 0.046). In the healthy group, the powers of both the BB and TB muscles in the alpha, beta and gamma frequency bands showed significant increases during the second half of the contraction compared to those during the first half of contraction (For BB, alpha: P = 0.000, beta: P = 0.000, gamma: P = 0.006; For TB: alpha: P = 0.016, beta: P = 0.016, gamma: P = 0.010).

Coherence Analysis

In order to present the characteristics of the coherence spectra and provide clues to verify the impact level of cross-talk on the results, representative coherence spectra of two subjects as well as pooled coherence spectra of all the subjects in the stroke and healthy group were presented in **Figure 5**. It can be seen from the figure that in the stroke group, significant intermuscular coherence was found in distinct frequency bands rather than in a broadband spectrum. Significant coherence was mainly appeared in beta frequency band in the pooled coherence spectrum and was higher in the second half of contraction compared to the first half contraction. In the healthy group, significant coherence was observed across a broad range of frequencies and prominent peak coherence values were found around 10 Hz during the first and second halves of contraction. The coherence spectra showed had very similar values between the first and second halves of the contraction at the same frequency point in the healthy group.

Comparisons of significant coherence integral in the alpha, beta, and gamma frequency bands during the first and second halves of the fatiguing contraction were presented in **Figure 6**. The wilcoxon test was used to compare the differences in the significant coherence integrals, and the results revealed that significant coherence integral results in both the alpha (P = 0.018) and beta (P = 0.005) frequency bands were significantly higher during the second half of the fatiguing contraction compared to those during the first half of the contraction. No significant difference was found between the first and second halves of the fatiguing contraction in the gamma

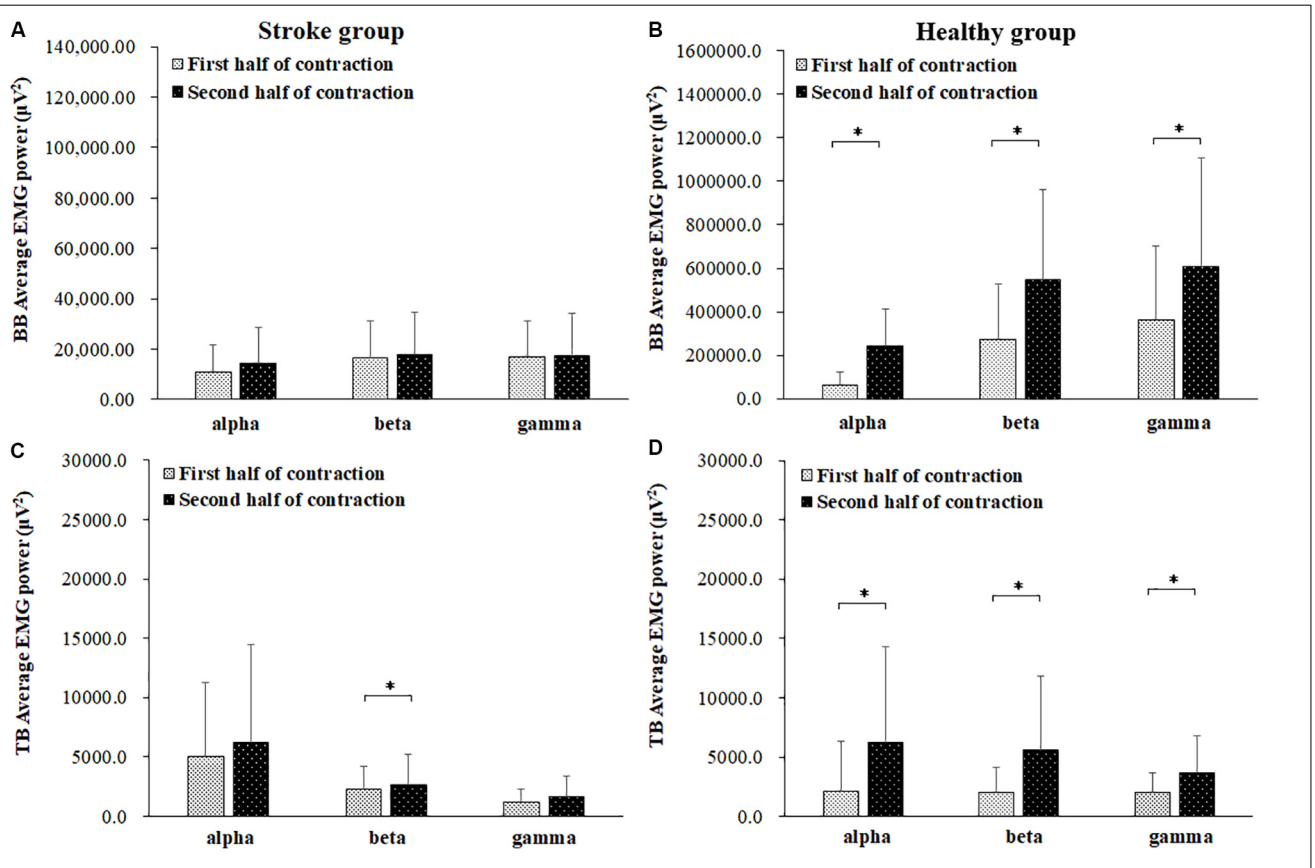

FIGURE 4 | Comparisons of the average EMG power of BB **(A,B)** and TB **(C,D)** muscles of the stroke **(A,C)** and healthy **(B,D)** groups. in the alpha (8–12 Hz), beta (15–35 Hz), and gamma (35–60 Hz) frequency bands between the first (light bar) and second (dark bar) halves of the fatiguing contraction. A significant increase of EMG power was found at BB muscle in the alpha frequency band and TB muscle in beta frequency band. * demonstrated a significant difference of observed index between the first and second half of contraction.

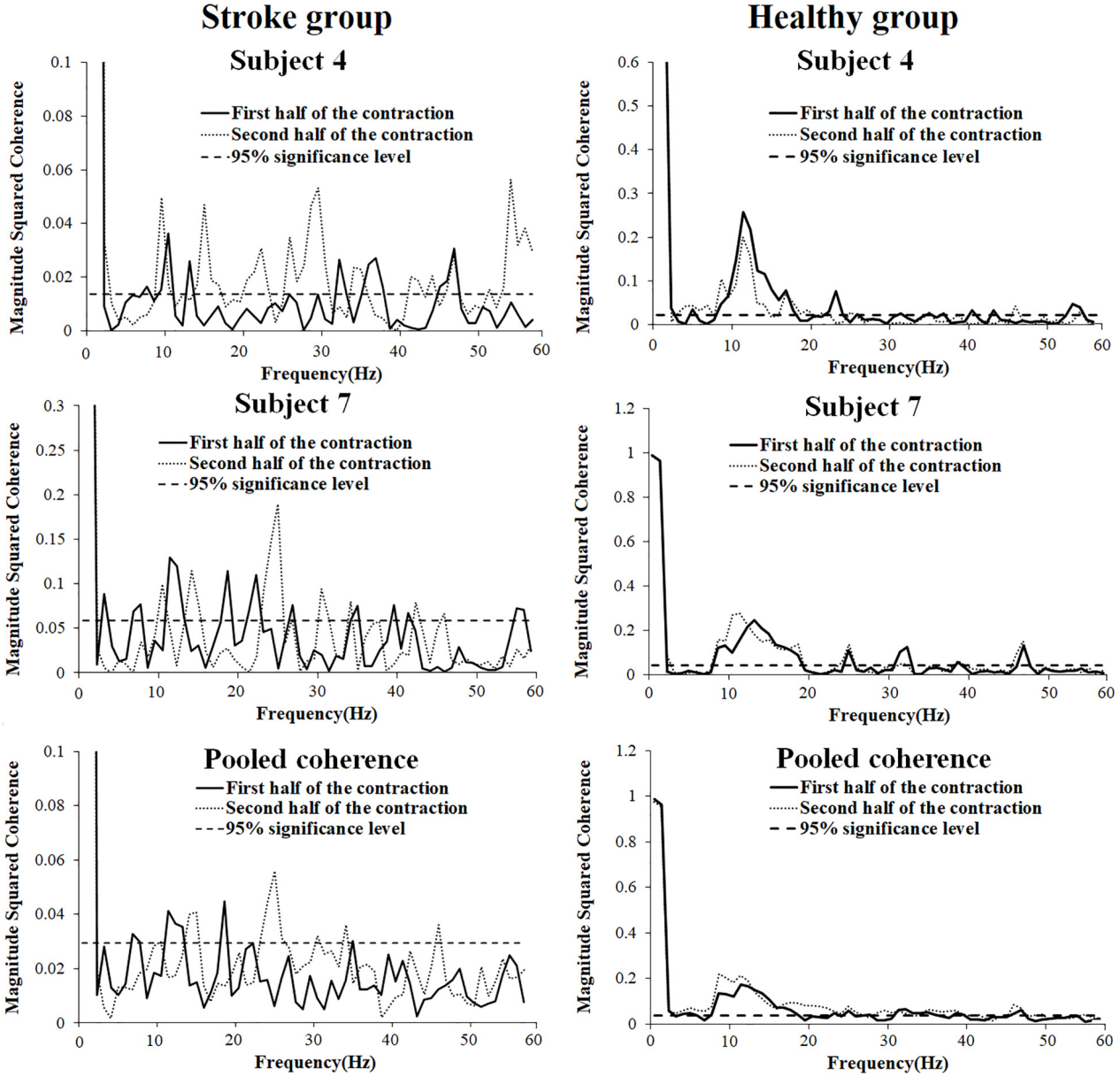

FIGURE 5 | Representative (subject 4, 7, and 10) and pooled coherence spectra of the BB and TB sEMG signals during the first (thick line) and second (thin line) halves of the fatiguing contraction.

band (P = 0.241) among the stroke group and in the alpha (P = 0.158), beta (P = 0.480), and gamma (P = 0.814) bands among the healthy group.

DISCUSSION

In the present study, we examined the influence of fatigue on the antagonistic muscle coupling of limbs with spasticity induced by stroke. The sEMG activation and coherence between antagonist muscles were compared between the first and second halves of the 30% maximal-level sustained fatiguing isometric elbow flexion contraction between patients with post-stroke spasticity and healthy adults. We found that the intermuscular coherences between the antagonistic BB and TB muscles in the alpha and beta frequency bands were significantly increased during the second half of the contraction compared to those during the first half of the contraction in the stroke group. As far as we know, this is the first study conducted to examine the effect of fatigue on antagonistic muscle coupling of limbs with stroke-induced spasticity.

It may be argued that the reliability of the results may have been reduced by cross-talk contamination, which has been widely studied in relevant studies of antagonist muscle coactivation

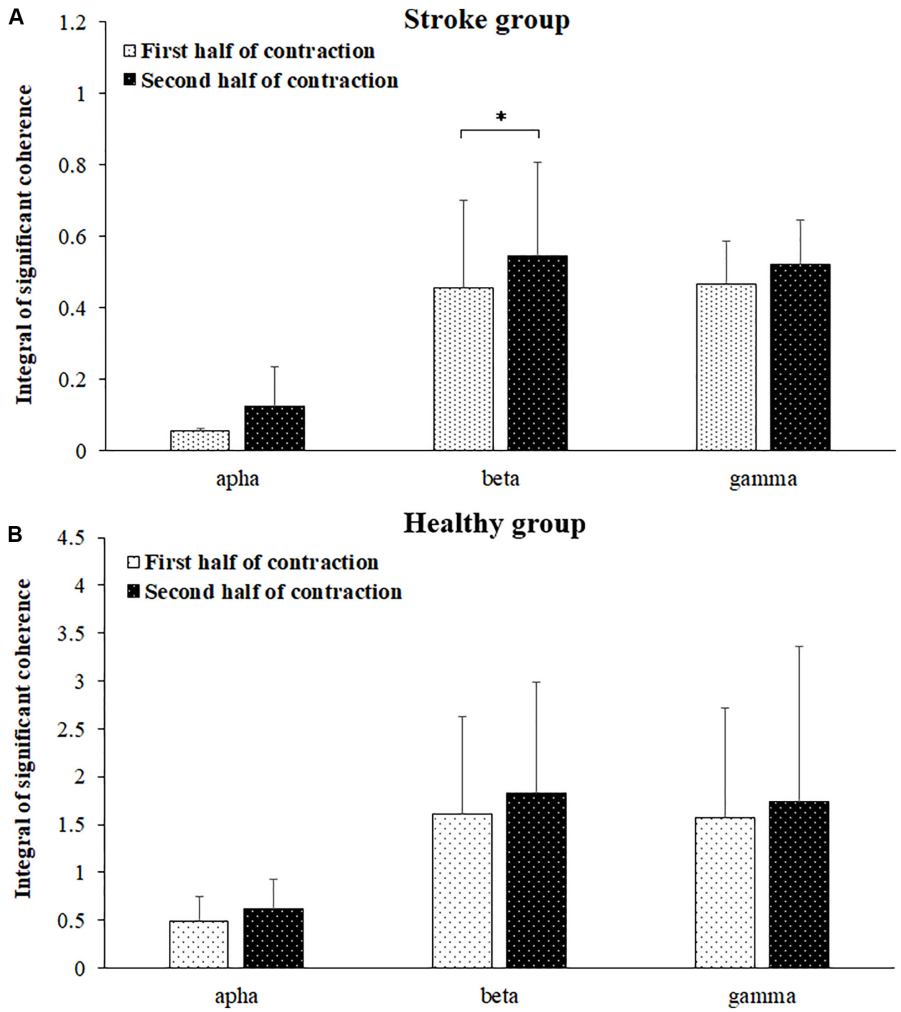

FIGURE 6 | Comparisons of significant coherence integral for the stroke **(A)** and healthy **(B)** groups in the alpha, beta, and gamma frequency bands between the first and second halves of the fatiguing contraction. The data has been averaged over all subjects. Coherence in the beta band was significantly increased during the second half of the contraction compared to that during the first half of contraction.

activities (Lowery et al., 2003; Farina et al., 2004; Wu et al., 2017). In the current research, we adopted an isometric low-force muscle contraction with only a 30% maximal voluntary contraction (MVC), which may be helpful in reducing cross-talk (Farmer et al., 2007). In addition, the size of the electrode adopted in this study was much smaller (with a diameter of 6 mm and area of 28 mm^2) than the most commonly used electrode (with a diameter of 10 mm and area of 79 mm^2), which has been suggested to reduce cross-talk (Jaskolska et al., 2006). In addition, EMG rectification has been conducted before coherence analysis according to the recommendation of previous studies, and thus, the influence of cross-talk can be restrained (Farina et al., 2013). EMG–EMG crosstalk, when present, produces high levels of coherence across a wide range of frequencies (1–250 Hz) (Farmer et al., 2007). In the current study, in the stroke group, significant coherence values were found in distinct frequency bands mainly below 60 Hz rather than across a wide range of frequencies. In the healthy group, coherence spectra were mainly discovered below 60 Hz and had very similar values between the first and second halves of the contraction at the same frequency point, which is consistent with the results of previous research (Wang et al., 2015). Therefore, it seems that the results in the current study were not significantly influenced by cross-talk.

In this study, the maximal torque of elbow flexion decreased significantly during the post-fatigue contraction compared to that during the pre-fatigue contraction, while the EMG median frequency of the BB muscle during the second half of the contraction showed a significant reduction compared to that during the first half of the contraction. This demonstrated that muscle fatigue of the agonist muscle BB occurred during the sustained elbow flexion contraction. In previous researches, it has been found that post-stroke spasticity increased force inaccuracy and variability and thus increase the movement instability (Carlyle and Mochizuki, 2018). As a result, the cocontraction level of antagonistic muscles showed a significant increased than healthy subjects, which is consistent with this study. In

the stroke group, fatigue seemed to increase the activity of the antagonist muscle rather than that of the agonist muscle in post-stroke spasticity group subjects as the coactivation and EMG power of the TB muscle in the beta frequency band showed significant fatigue-related increases, while the EMG power of the BB muscle showed no significant increase in any frequency bands.

EMG-EMG coherence in the beta band has been suggested to be closely related to the common corticospinal drive from the motor cortex to the muscles (Chen et al., 2018), whereas coherence in the alpha band is influenced by multiple factors such as the stretch-reflex, mechanical resonance, and cortical drives (McAuley and Marsden, 2000). In this study, increased coherence in the beta frequency bands between the antagonistic elbow muscles was observed during the second half of the contraction compared to that during the first half of the contraction in the stroke group, indicating a fatigue-related increase in beta band coherence between the antagonistic elbow muscles during the sustained isometric elbow flexion exercise. The enhanced coherence in the beta bands in the stroke group is considered to reflect increased common neural inputs and stronger coupling between motor cortical neurons and the motor units of co-contracted muscles (Keenan et al., 2012). This result is consistent with the findings of previous research involving healthy young men (Wang et al., 2015). This result may indicate increased coupling between synchronized cortical neurons and the motoneuron pool of the BB and TB.

However, no significant coherence was found between the first and second halves of the fatiguing contraction in healthy adults in the current study, which is inconsistent with the results acquired in sustained isometric fatiguing contraction with 20% MVC force level in previous research (Wang et al., 2015). The higher force level of sustained isometric contraction leads to a higher proportion of peripheral fatigue and lower proportion of central fatigue (Gandevia, 2001; Sogaard et al., 2006). On the other hand, the fatigue of the stroke group may be mainly attributed to central fatitue as the low efficiency of motor control attributed to motor impairment, as well as the low force level for peripheral muscle capacity. Therefore, the results of this study seemed to indicate that fatigue-related changes of antagonistic muscles EMG coupling may have close relationship with the degree of central fatigue.

In this study, we have mainly focused on the fatigue-related EMG coupling properties of antagonistic muscles in the population of patients with post-stroke spasticity. As a limitation of this study, the stroke survivors without spasticity have not been acquired and compared. This makes it hard to explicitly demonstrate the direct correlation between spasticity and muscle coupling. Actually, the results in the current study may be close related to cortically originated muscular discoordination, or motor recruitment, rather than spasticity in passive motion. Therefore, whether spasticity may significant influence EMG coupling of antagonistic muscles in stroke patients still need further research.

EMG synchrony within the Piper frequency band is considered a biomarker of functional corticomotor integrity (Clark et al., 2013; Lodha et al., 2017). A number of prior studies have shown that central nervous system disease and functional deficits are linked to reduced EMG synchrony within the Piper frequency band (Petersen et al., 2013; Willerslev-Olsen et al., 2015). Patients with post-stroke spasticity are expected to have diminished EMG synchrony within the Piper frequency band during motor tasks due to the damage of descending corticomotor pathways (Lodha et al., 2017). Therefore, an enhancement in EMG-EMG coherence may indicate better functional integrity of corticomotor tracts during motor tasks for patients with post-stroke spasticity. In previous research, fatigue has been suggested as a training stimulus to promote exercise performance (Gabriel et al., 2001). Therefore, the increase in antagonistic muscle coupling induced by muscle fatigue may provide suggestions for the design of training programs for patients with post-stroke spasticity.

CONCLUSION

A significant increase in intermuscular coherence in the beta frequency band between the antagonistic elbow muscles was observed during the second half of the 30% maximal-level sustained isometric contraction compared to that during the first half of the contraction, indicating that muscle fatigue significantly increases the coupling of antagonistic muscles in patients with post-stroke spasticity, which may be related to the increased common corticospinal drive from the motor cortex to the antagonistic muscles. The increase in antagonistic muscle coupling induced by muscle fatigue may provide suggestions for the design of training programs for patients with post-stroke spasticity.

DATA AVAILABILITY STATEMENT

The raw data supporting the conclusions of this article will be made available by the authors, without undue reservation.

ETHICS STATEMENT

The studies involving human participants were reviewed and approved by the Ethics Committee of the Tongji University. The patients/participants provided their written informed consent to participate in this study.

AUTHOR CONTRIBUTIONS

L-JW, X-MY, and W-XN conceived and designed the study. S-JH and X-MY recruited the subjects and collected the basic characteristics of the subjects. X-MY performed the clinical assessment. L-JW, Q-NS, CW, and HY performed the experiments. L-JW, S-JH, X-MY, and W-XN made a contribution

to the data analysis. L-JW wrote this manuscript. All authors contributed to the article and approved the submitted version.

FUNDING

This work was supported by the Research and Construction Project of Teaching Reform in the Tongji University, Science & Technology Project Foundation of Shanghai Sports Bureau (20C005), and the National Natural Science Foundation of China (61761166002).

ACKNOWLEDGMENTS

We acknowledge Yan Lu and Honglin Wang for the recruitment of study participants; Fanhui Zheng for assistance with EEG experiments. We would like to thank all the participants of this study.

REFERENCES

Arellano, C. J., Caha, D., Hennessey, J. E., Amiridis, I. G., Baudry, S., and Enoka, R. M. (2016). Fatigue-induced adjustment in antagonist coactivation by old adults during a steadiness task. *J. Appl. Physiol.* 120, 1039–1046. doi: 10.1152/japplphysiol.00908.2015

Baker, S. N., Olivier, E., and Lemon, R. N. (1997). Coherent oscillations in monkey motor cortex and hand muscle EMG show task-dependent modulation. *J. Physiol.* 501, 225–241. doi: 10.1111/j.1469-7793.1997.225bo.x

Boudarham, J., Roche, N., Teixeira, M., Hameau, S., Robertson, J., Bensmail, D., et al. (2014). Relationship between neuromuscular fatigue and spasticity in chronic stroke patients: a pilot study. *J. Electromyogr. Kinesiol.* 24, 292–299. doi: 10.1016/j.jelekin.2013.11.006

Carlyle, J. K., and Mochizuki, G. (2018). Influence of post-stroke spasticity on EMG-force coupling and force steadiness in biceps brachii. *J. Electromyogr. Kinesiol.* 38, 49–55. doi: 10.1016/j.jelekin.2017.11.005

Chen, Y., Li, S., Magat, E., Zhou, P., and Li, S. (2018). Motor overflow and spasticity in chronic stroke share a common pathophysiological process: analysis of Within-Limb and Between-Limb EMG-EMG coherence. *Front. Neurol.* 9:795. doi: 10.3389/fneur.2018.00795

Clark, D. J., Kautz, S. A., Bauer, A. R., Chen, Y., and Christou, E. A. (2013). Synchronous EMG activity in the piper frequency band reveals the corticospinal demand of walking tasks. *Ann. Biomed. Eng.* 41, 1778–1786. doi: 10.1007/s10439-013-0832-4

De Luca, C. J., and Mambrito, B. (1987). Voluntary control of motor units in human antagonist muscles - coactivation and reciprocal activation. *J. Neurophysiol.* 58, 525–542. doi: 10.1152/jn.1987.58.3.525

Duchateau, J., and Baudry, S. (2014). The neural control of coactivation during fatiguing contractions revisited. *J. Electromyogr. Kinesiol.* 24, 780–788. doi: 10.1016/j.jelekin.2014.08.006

Enoka, R. M., Baudry, S., Rudroff, T., Farina, D., Klass, M., and Duchateau, J. (2011). Unraveling the neurophysiology of muscle fatigue. *J. Electromyogr. Kinesiol.* 21, 208–219. doi: 10.1016/j.jelekin.2010.10.006

Farina, D., Merletti, R., Indino, B., and Graven-Nielsen, T. (2004). Surface EMG crosstalk evaluated from experimental recordings and simulated signals - Reflections on crosstalk interpretation, quantification and reduction. *Method Inform.* 43, 30–35. doi: 10.1055/s-0038-1633419

Farina, D., Negro, F., and Jiang, N. (2013). Identification of common synaptic inputs to motor neurons from the rectified electromyogram. *J. Physiol.* 591, 2403–2418. doi: 10.1113/jphysiol.2012.246082

Farmer, S. F., Gibbs, J., Halliday, D. M., Harrison, L. M., James, L. M., Mayston, M. J., et al. (2007). Changes in EMG coherence between long and short thumb abductor muscles during human development. *J. Physiol.* 579, 389–402. doi: 10.1113/jphysiol.2006.123174

Gabriel, D. A., Basford, J. R., and An, K. N. (2001). Neural adaptations to fatigue: implications for muscle strength and training. *Med. Sci. Sport Exerc.* 33, 1354–1360. doi: 10.1097/00005768-200108000-00017

Gandevia, S. C. (2001). Spinal and supraspinal factors in human muscle fatigue. *Physiol. Rev.* 81, 1725–1789. doi: 10.1152/physrev.2001.81.4.1725

Jaskolska, A., Kisiel-Sajewicz, K., Brzenczek-Owczarzak, W., Yue, G. H., and Jaskolski, A. (2006). EMG and MMG of agonist and antagonist muscles as a function of age and joint angle. *J. Electromyogr. Kinesiol.* 16, 89–102. doi: 10.1016/j.jelekin.2005.05.003

Keen, D. A., Chou, L., Nordstrom, M. A., and Fuglevand, A. J. (2012). Short-term synchrony in diverse motor nuclei presumed to receive different extents of direct cortical input. *J. Neurophysiol.* 108, 3264–3275. doi: 10.1152/jn.01154.2011

Keenan, K. G., Massey, W. V., Walters, T. J., and Collins, J. D. (2012). Sensitivity of EMG-EMG coherence to detect the common oscillatory drive to hand muscles in young and older adults. *J. Neurophysiol.* 107, 2866–2875. doi: 10.1152/jn.01011.2011

Levin, M. F., Solomon, J. M., Shah, A., Blanchette, A. K., and Feldman, A. G. (2018). Activation of elbow extensors during passive stretch of flexors in patients with post-stroke spasticity. *Clin. Neurophysiol.* 129, 2065–2074. doi: 10.1016/j.clinph.2018.07.007

Lodha, N., Chen, Y., McGuirk, T. E., Fox, E. J., Kautz, S. A., Christou, E. A., et al. (2017). EMG synchrony to assess impaired corticomotor control of locomotion after stroke. *J. Electromyogr. Kinesiol.* 37, 35–40. doi: 10.1016/j.jelekin.2017.08.007

Lowery, M. M., Stoykov, N. S., and Kuiken, T. A. (2003). A simulation study to examine the use of cross-correlation as an estimate of surface EMG cross talk. *J. Appl. Physiol.* 94, 1324–1334. doi: 10.1152/japplphysiol.00698.2002

McAuley, J. H., and Marsden, C. D. (2000). Physiological and pathological tremors and rhythmic central motor control. *Brain* 123, 1545–1567. doi: 10.1093/brain/123.8.1545

McKiernan, B. J., Marcario, J. K., Karrer, J. L., and Cheney, P. D. (2000). Correlations between corticomotoneuronal (CM) cell postspike effects and cell-target muscle covariation. *J. Neurophysiol.* 83, 99–115. doi: 10.1152/jn.2000.83.1.99

Petersen, T. H., Farmer, S. F., Kliim-Due, M., and Nielsen, J. B. (2013). Failure of normal development of central drive to ankle dorsiflexors relates to gait deficits in children with cerebral palsy. *J. Neurophysiol.* 109, 625–639. doi: 10.1152/jn.00218.2012

Sogaard, K., Gandevia, S. C., Todd, G., Petersen, N. T., and Taylor, J. L. (2006). The effect of sustained low-intensity contractions on supraspinal fatigue in human elbow flexor muscles. *J. Physiol.* 573, 511–523. doi: 10.1113/jphysiol.2005.103598

Tamburella, F., Moreno, J. C., Iosa, M., Pisotta, I., Cincotti, F., Mattia, D., et al. (2017). Boosting the traditional physiotherapist approach for stroke spasticity using a sensorized ankle foot orthosis: a pilot study. *Top. Stroke Rehabil.* 24, 447–456. doi: 10.1080/10749357.2017.1318340

Terry, K., and Griffin, L. (2008). How computational technique and spike train properties affect coherence detection. *J. Neurosci. Methods* 168, 212–223. doi: 10.1016/j.jneumeth.2007.09.014

Turpin, N. A., Feldman, A. G., and Levin, M. F. (2017). Stretch-reflex threshold modulation during active elbow movements in post-stroke survivors with spasticity. *Clin. Neurophysiol.* 128, 1891–1897. doi: 10.1016/j.clinph.2017.07.411

Vollestad, N. K. (1997). Measurement of human muscle fatigue. *J. Neurosci. Methods* 74, 219–227. doi: 10.1016/S0165-0270(97)02251-6

Wang, L., Lu, A., Zhang, S., Niu, W., Zheng, F., and Gong, M. (2015). Fatigue-related electromyographic coherence and phase synchronization analysis between antagonistic elbow muscles. *Exp. Brain Res.* 233, 971–982. doi: 10.1007/s00221-014-4172-x

Wang, L., Ma, A., Wang, Y., You, S., and Lu, A. (2017). Antagonist muscle prefatigue increases the intracortical communication between contralateral motor cortices during elbow extension contraction. *J. Healthc. Eng.* 2017:8121976. doi: 10.1155/2017/8121976

Wang, L., Niu, W., Wang, K., Zhang, S., Li, L., and Lu, T. (2019). Badminton players show a lower coactivation and higher beta band intermuscular interactions of ankle antagonist muscles during isokinetic exercise. *Med. Biol. Eng. Comput.* 57, 2407–2415. doi: 10.1007/s11517-019-02040-8

Wang, R., Gaverth, J., and Herman, P. A. (2018). Changes in the neural and non-neural related properties of the spastic wrist flexors after treatment with botulinum toxin a in post-stroke subjects: an optimization study. *Front. Bioeng. Biotechnol.* 6:73. doi: 10.3389/fbioe.2018.00073

Willerslev-Olsen, M., Petersen, T. H., Farmer, S. F., and Nielsen, J. B. (2015). Gait training facilitates central drive to ankle dorsiflexors in children with cerebral palsy. *Brain* 138, 589–603. doi: 10.1093/brain/awu399

Wissel, J., Manack, A., and Brainin, M. (2013). Toward an epidemiology of poststroke spasticity. *Neurology* 802, S13–S19. doi: 10.1212/WNL.0b013e3182762448

Wu, R., Delahunt, E., Ditroilo, M., Lowery, M. M., and De Vito, G. (2017). Effect of knee joint angle and contraction intensity on hamstrings coactivation. *Med. Sci. Sport Exerc.* 49, 1668–1676. doi: 10.1249/MSS.0000000000001273

Conflict of Interest: The authors declare that the research was conducted in the absence of any commercial or financial relationships that could be construed as a potential conflict of interest.

frontiers in Bioengineering and Biotechnology

ORIGINAL RESEARCH
published: 16 November 2020
doi: 10.3389/fbioe.2020.589321

Increased Muscle Activity Accompanying With Decreased Complexity as Spasticity Appears: High-Density EMG-Based Case Studies on Stroke Patients

*Tian Xie[1], Yan Leng[2], Yihua Zhi[1], Chao Jiang[1], Na Tian[1], Zichong Luo[3], Hairong Yu[1] and Rong Song[1]**

[1] Key Laboratory of Sensing Technology and Biomedical Instrument of Guangdong Province, School of Biomedical Engineering, Sun Yat-sen University, Guangzhou, China, [2] Department of Rehabilitation Medicine, Guangdong Engineering Technology Research Center for Rehabilitation Medicine and Clinical Translation, The First Affiliated Hospital, Sun Yat-sen University, Guangzhou, China, [3] Department of Electromechanical Engineering, Faculty of Science and Technology, University of Macau, Macau, China

OPEN ACCESS

Edited by:
Ping Zhou,
The University of Rehabilitation, China

Reviewed by:
Xu Zhang,
University of Science and Technology of China, China
Maoqi Chen,
Guangdong Provincial Work Injury Rehabilitation Hospital, China

***Correspondence:**
Rong Song
songrong@mail.sysu.edu.cn

Specialty section:
This article was submitted to Biomechanics, a section of the journal Frontiers in Bioengineering and Biotechnology

Received: *30 July 2020*
Accepted: *28 October 2020*
Published: *16 November 2020*

Citation:
Xie T, Leng Y, Zhi Y, Jiang C, Tian N, Luo Z, Yu H and Song R (2020) Increased Muscle Activity Accompanying With Decreased Complexity as Spasticity Appears: High-Density EMG-Based Case Studies on Stroke Patients. Front. Bioeng. Biotechnol. 8:589321. doi: 10.3389/fbioe.2020.589321

Spasticity is a major contributor to pain, disabilities and many secondary complications after stroke. Investigating the effect of spasticity on neuromuscular function in stroke patients may facilitate the development of its clinical treatment, while the underlying mechanism of spasticity still remains unclear. The aim of this study is to explore the difference in the neuromuscular response to passive stretch between healthy subjects and stroke patients with spasticity. Five healthy subjects and three stroke patients with spastic elbow flexor were recruited to complete the passive stretch at four angular velocities (10°/s, 60°/s, 120°/s, and 180°/s) performed by an isokinetic dynamometer. Meanwhile, the 64-channel electromyography (EMG) signals from biceps brachii muscle were recorded. The root mean square (RMS) and fuzzy entropy (FuzzyEn) of EMG recordings of each channel were calculated, and the relationship between the average value of RMS and FuzzyEn over 64-channel was examined. The two groups showed similar performance from results that RMS increased and FuzzyEn decreased with the increment of stretch velocity, and the RMS was negatively correlated with FuzzyEn. The difference is that stroke patients showed higher RMS and lower FuzzyEn during quick stretch than the healthy group. Furthermore, compared with the healthy group, distinct variations of spatial distribution within the spastic muscle were found in the EMG activity of stroke patients. These results suggested that a large number of motor units were recruited synchronously in the presence of spasticity, and this recruitment pattern was non-uniform in the whole muscle. Using a combination of RMS and FuzzyEn calculated from high-density EMG (HD-EMG) recordings can provide an innovative insight into the physiological mechanism underlying spasticity, and FuzzyEn could potentially be used as a new indicator for spasticity, which would be beneficial to clinical intervention and further research on spasticity.

Keywords: spasticity, entropy, HD-EMG, stroke, stretch reflex

INTRODUCTION

Spasticity, one of the positive features of the upper motor neuron syndrome (UMNS) after stroke or other central nervous system diseases, is a velocity-dependent increase in muscle tone caused by an exaggeration of stretch reflex (Lance, 1980). The prevalence of spasticity ranges from 25 to 40% within the year after the first-ever stroke (Watkins et al., 2002; Sommerfeld et al., 2004; Urban et al., 2010; Wissel et al., 2010). Spasticity contributes significantly to motor impairments and activity limitations for stroke patients. Not only does it cause pain and many secondary complications, such as urinary incontinence, pressure ulcers and contractures, but it can also interfere with walking, sitting and voluntary movements of limbs, seriously affecting the quality of life (QoL) of patients (Hsu et al., 2003; Duncan et al., 2005; Welmer et al., 2006; Francisco and McGuire, 2012; Ward, 2012). Effective and targeted intervention for spasticity is critical for neurorehabilitation after stroke. A clear understanding of the pathophysiology of spasticity may facilitate the development of its clinical management.

An accurate and objective assessment tool is a reliable guarantee for investigating the underlying mechanism of spasticity. In order to make up for the subjectivity and poor reliability of commonly used clinical scales, such as the Ashworth Scale (AS) and Modified Ashworth Scale (MAS), some studies used the isokinetic dynamometer to assess the spasticity by quantifying the resistance of a joint to passive stretch (Kim et al., 2005; Starsky et al., 2005; Damiano et al., 2007). Matching the velocity-dependent characteristics, this biomechanical measure can standardize the subject's range of motion (ROM) to carry out passive stretch at a predefined constant angular velocity. Compared with the use of clinical scales, using this method is not only objective and accurate, but also has better reliability and validity (Pierce et al., 2006; Sin et al., 2019). However, the resistance is composed of two parts, namely the neural component of the tonic stretch reflex and the non-neural component of the soft tissue characteristics (Fleuren et al., 2010; Li et al., 2017). After UMN lesions, the non-neural component also changes and depends on the stretch velocity (Lindberg et al., 2011). Hence this quantification is difficult to specifically distinguish the contribution of the velocity-response of stretch reflex to the increased resistance. On the other hand, the electrophysiological measure, which is not affected by mechanical components, has superiority in representing the velocity-dependent reflex components to assess spasticity (Kim et al., 2005; Zhang et al., 2019). On the basis of electromyography (EMG), the reflex muscle activity in response to passive stretch can be well reflected (Kim et al., 2005; Voerman et al., 2005; Wood et al., 2005; Sorinola et al., 2009). Recently, the innovation of high-density EMG (HD-EMG) recording the EMG signals in a wide area with dense electrodes of 2D arrays, has the potential to provide spatial features in addition to temporal features of muscle activity to study the neuromuscular function (Rojas-Martínez et al., 2012). The spatial distribution can describe the activation of different portions within regions of a muscle, which increases the possibility of capturing the motor units' (MUs) characteristics (Drost et al., 2006; Gallina and Botter, 2013). The additional ability enhances the discrimination power of differences of action potentials between two MUs, which is more sensitive than intramuscular electrodes. As a result, it is feasible to extract individual MU property from surface EMG (Zhou et al., 2011). By constructing the activation map obtained from 2D arrays recordings, the HD-EMG technique is able to track the spatial heterogeneity of muscle activity during different tasks (Castroflorio et al., 2012; Hu et al., 2014, 2015). The heterogeneous activation underlines the inhomogeneous distribution and recruitment of MUs in the muscle area (Farina et al., 2008). A recent study revealed that after injection of botulinum toxin, the muscle activity of a stroke patient with spasticity was not homogeneous during voluntary elbow flexion tasks (Afsharipour et al., 2018), indicating possible changes in spatial recruitment patterns within the spastic muscle. However, it is unclear whether the activation pattern of involuntary muscle activity changes in the generation of spasticity. The spatial distribution can identify changes in muscle activity during passive stretch under the influence of spasticity, which provides a unique perspective for understanding its underlying mechanism. Applying the combination of isokinetic dynamometer and HD-EMG in the measurement, we can not only reliably assess the muscular reflex response to passive stretch, but also explore possible alterations in the spatial distribution of reflex activation due to spasticity.

In addition, considering that the EMG signals are complex, different types of entropy indexes have been developed to capture its non-linear features. Compared with the approximate entropy (ApEn) and sample entropy (SampEn), fuzzy entropy (FuzzyEn) has advantages in robustness and data length dependence, which could characterize the regularity of the neuromuscular system more reasonably in noisy and shorter signals (Chen et al., 2007; Wu et al., 2018; Tian and Song, 2019). As a complexity indicator, a small entropy value is associated with small complexity and great regularity. Studies have shown that the complexity of EMG signals changes in stroke patients with spasticity during voluntary contraction (Dash et al., 2019), and the entropy-based method can reliably and precisely detect the stretch reflex onset (Hu et al., 2018).

Few studies have made an effort on the changes in EMG complexity and spatial distribution of muscle activity when the spasticity is induced. The purpose of this study is to investigate possible alterations in complexity and spatial activation pattern of muscle activity caused by spasticity in comparison with healthy subjects. The combination of HD-EMG amplitude and complexity to study the underlying mechanism of spasticity will provide useful clinical information to give a basis for better therapies and further research on spasticity.

MATERIALS AND METHODS

Participants

Five healthy subjects (three males and two females, 23.6 $\pm$ 0.5 years) and three stroke patients participated in this study. The dominant side of all subjects was the right side. The stroke patients with spastic elbow flexor were recruited from The First Affiliated Hospital of Sun Yat-sen University. **Table 1** showed the basic information of three stroke patients. The

inclusion criteria including: (1) to have hemiplegic elbow flexor spasticity in the range of MAS scores 1–2, (2) to have the ability to perform voluntary elbow flexion, (3) to have sufficient passive ROM of elbow joint, (4) to have intact cognition, auditory and visual sense to understand and follow the experimental instructions, (5) to have no any other orthopedic diseases to impede the neuromuscular function, (6) to have not taken medication for spasticity. This study was approved by the Ethics Committee of The First Affiliated Hospital of Sun Yat-sen University. All subjects signed the informed consent prior to the experiments.

HD-EMG Recording

An isokinetic dynamometer system (CSMi, HUMACNORM, United States) was used to perform the passive movement and record the torque at a sampling frequency of 100 Hz. The monopolar HD-EMG signals of both heads of biceps brachii (BB) muscle of the dominant side of healthy subjects or the affected side of stroke patients were acquired simultaneously by the REFA system (TMSi, REFA, Netherlands) at a sampling frequency of 2000 Hz. The 8 × 8 electrode array consisted of 64 separate channels with an electrode's diameter of 2 mm and an interelectrode distance of 12 mm in both directions, as shown in **Figure 1A**. Following the columns of the array along with the muscle fiber, the center of the electrode array was placed on the line between the medial acromion and the fossa cubit at one-third from the fossa cubit, and a reference electrode was placed on the styloid process of ulna according to the recommendation of SENIAM. **Figure 1B** showed the relative position of the electrode array to the body. In order to ensure the signal quality, the conducting gel was applied on the surface of each electrode, and the electrode array was fixed with the aid of an elastic bandage. Before the placement of the electrode array, the skin was abraded and cleaned with abrasive cream and alcohol to reduce noise. For eliminating the influence of gravity, a custom-built fixture holder was used to support the forearm on the anti-gravity position with a foam pad at the bottom of the elbow, as shown in **Figure 1C**. The forearm was fastened to the dynamometer rig with an elastic belt, which was approximately 3 cm above the wrist. The rotation axis of the dynamometer aligned with the movement axis of the elbow joint.

Experimental Procedure

The subject sat comfortably on the chair of the isokinetic dynamometer system with the dominant forearm or affected forearm fixed on the custom-built equipment. The initial position of the subject was with the shoulder abduction and elbow flexion in 90°, and the forearm, wrist and fingers were kept in a neutral position. Two straps were crossed in front of the chest and one strap was tied at the waist to stabilize the trunk. Then the subject was familiarized with the whole experimental process before the formal test, including passive movement, and maximal isometric voluntary contraction (MIVC).

In the first stage, the range of elbow passive movement from the starting position was first measured manually. The range of all subjects was 90°, except the patient 1 was 80° because of discomfort, but the angle was not crucial to results. The subject was asked to relax as much as possible, then his/her forearm was passively moved along with the custom-built equipment within the predefined range at four constant angular velocities with this order: 10°, 60°, 120°, and 180°/s. If the velocity is below a certain threshold, the stretch reflex response would not be observed (Wang et al., 2019), so the slow baseline velocity of 10°/s can represent a quiet state of no reflex response. One measuring trial consisted of moving back and forth twice between the predefined range. The process from the starting position to the end position of passive movement was referred to as the passive stretch of BB. When one trial was finished, the subject was relaxed with a 10 s interval time. Three trials were performed at each velocity with a 60 s break before velocity changing. After all velocities were completed, the subject was allowed to take a 3 min rest, then moving on to the next stage.

In the second stage, the MIVC of elbow flexion was performed at an elbow joint angle of 90° flexion. The subject was asked to push the machine with the maximal force for 4 s and was encouraged verbally to ensure maximal contraction. Three trials were performed with a 1 min break between each trial.

Data Analysis

For the HD-EMG signals recorded in the experiment, a 6th-order Butterworth band-pass filter from 20 to 500 Hz and a 40th-order 50 Hz notch filter were applied to remove the interference noise and power-line interference. After that, the HD-EMG recordings of the first passive stretch of BB were cut out separately according to each stretch velocity task. Then the trial that had the maximum number of effective channels for each velocity was chosen to calculate the feature values:

(1) Root mean square (RMS), the RMS value is used to quantify the intensity of muscle activity. The 2D RMS activation map AM with a dimension of 8 × 8 was calculated to visualize the spatial distribution of muscle activity as follows:

$$AM_{ij} = \frac{\frac{1}{M}\sum_{m=1}^{M} RMS_m(x_{ij})}{MIVC} \quad (1)$$

TABLE 1 | Basic information of stroke patients.

ID	Gender	Age (years)	Time since stroke (months)	Affected side	MAS scores	MMT scores
Patient 1	Male	59	3	Right	1+	3
Patient 2	Male	71	1	Right	1	3
Patient 3	Male	44	3	Right	1	4

MAS, Modified Ashworth Scale; MMT, Manual Muscle Test.

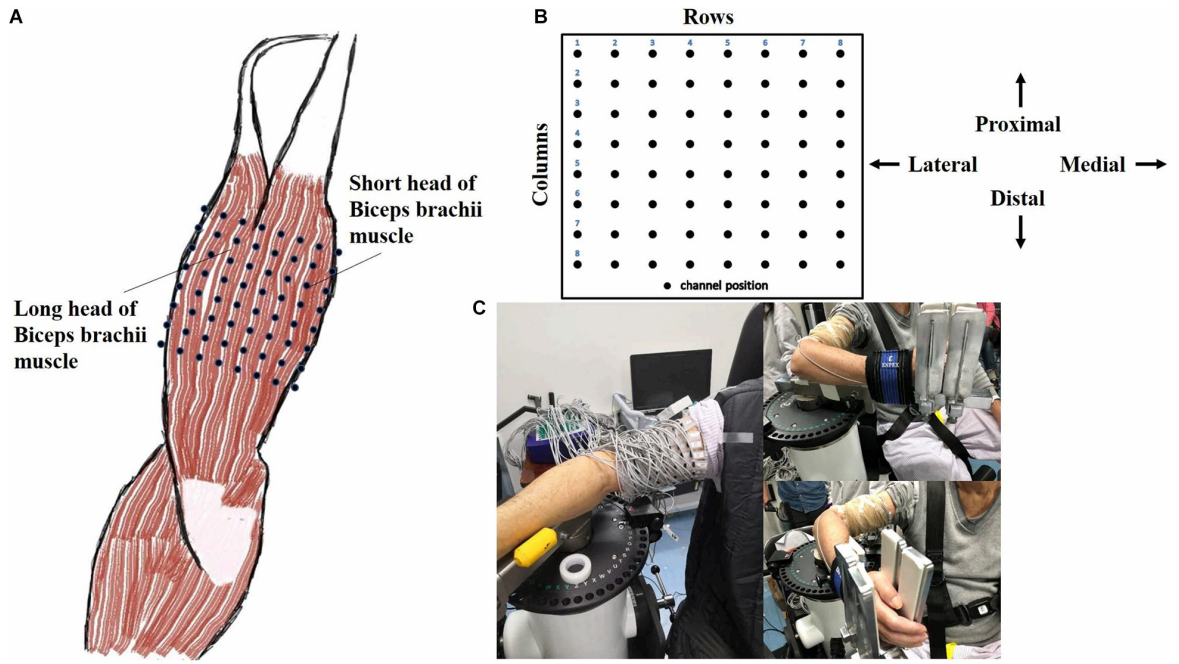

FIGURE 1 | Electrode placement and experimental apparatus. **(A)** A 8 × 8 EMG electrode array was placed over both long and short head of biceps brachii muscle (Right). **(B)** The relative position of the array to the body was presented. **(C)** The experimental apparatus was illustrated in reality operation.

where $RMS_m(x_{ij}) = \sqrt{\frac{1}{N}\sum_{n=1}^{N} x_{ij}^2(n)}$ as used to calculate the RMS value of the m-th segment, HD-EMG recordings were divided into M segments with a non-overlapping window length of 200 ms in each task, N corresponded to the total number of samples in a window length, x_{ij} as the EMG signal from the channel located at row i and column j of the electrode array, here channel (1,1) corresponding to the upper left corner of **Figure 1B**. The maximum RMS value of all non-overlapped windows in three trials was considered as the MIVC amplitude. The amplitude of each pixel in the map represented the normalized activation intensity of the corresponding channel of the electrode array. The yellow color (bright) referred to the maximum activation of the channel while the blue color (dark) referred to the minimum activation of the channel.

(2) Fuzzy entropy (FuzzyEn), the FuzzyEn values of 64-channel were computed as follows (Chen et al., 2009):

Given an N samples time series $\{u(1), u(2), \ldots, u(N)\}$, define m to reconstruct the vector:

$$X_i^m = \{\, u(i),\ u(i+1)\ ,\ \ldots\ ,\ u(i+m-1)\,\} - \bar{u}(i) \qquad (2)$$

where $\bar{u}(i) = \frac{1}{m}\sum_{k=0}^{m-1} u(i+k)$, $i = 1, 2, \ldots, N\text{-}m{+}{+}1$.

For a certain X_i^m the d_{ij}^m is the maximum absolute difference of X_i^m and $X_j^m j = 1, 2, \ldots, N\text{-}m{+}1; j \neq i$.

$$d_{ij}^m = d\left[X_i^m, X_j^m\right]$$

$$= \max_{p \in (0, m-1)} \left|\left(u(i+p) - \bar{u}(i)\right) - \left(u(j+p) - \bar{u}(j)\right)\right| \qquad (3)$$

For the given n and r, the similarity degree S_{ij}^m of X_i^m and $X_j^m$is calculated:

$$S_{ij}^m = \exp\left(-\left(\frac{d_{ij}^m}{r}\right)^n\right), \quad n = 2 \qquad (4)$$

Define the function C_i^m as:

$$C_i^m(r) = \frac{1}{N-m+1}\sum_{j=1, j\neq i}^{N-m+1} S_{ij}^m \qquad (5)$$

Then get the Φ^m(r):

$$\Phi^m(r) = \frac{1}{N-m+1}\sum_{i=1}^{N-m+1} ln(C_i^m(r)) \qquad (6)$$

Finally, we can define the FuzzyEn function as:

$$FuzzyEn(m,\ r) = \lim_{N\to\infty}\left[ln\ \Phi^m(r) - ln\ \Phi^{m+1}(r)\right] \qquad (7)$$

That, for finite datasets, can be estimated by the statistic:

$$FuzzyEn(m, r, N) = \ln \Phi^m(r) - \ln \Phi^{m+1}(r) (8)$$

In this study, $m = 2$, $r = 0.2$ * STD of the HD-EMG signals.

The same as above, the 2-D FuzzyEn maps would be acquired to visualize the topographic distribution of the complexity of

EMG signals for each velocity. What's more, the average value of RMS and FuzzyEn over 64-channel was calculated, respectively. The data of five healthy subjects were averaged as the healthy group to compare with stroke patients. A linear correlation between the average value of RMS and FuzzyEn of the healthy group and three stroke patients was analyzed, respectively.

RESULTS

Figure 2 showed the curve of the average value of RMS over 64-channel with the velocity of the healthy group and three stroke patients. The trends of RMS average value in different velocity were different between the healthy group and stroke patients. It was obvious that the RMS value of stroke patients increased linearly with the velocity. The RMS average value of quick stretch (60°/s, 120°/s, and 180°/s) were much greater than that of slow baseline (10°/s) of stroke patients. However, the RMS value of the healthy group did not increase linearly but gradually trends gently. Furthermore, **Figure 3** illustrated that the RMS activation maps of the healthy group and three stroke patients at four velocities. The position of the RMS map relative to the body is the same as the position of the electrode array relative to the body. As the increase of velocity, the RMS maps of the healthy group were always kept the dark state. Different from the healthy group, the activation region of stroke patients was expanded with the increasing velocity and the activation was heterogeneous within the muscle. It was noteworthy that the activation areas of the three stroke patients were different.

Figure 4 showed the curve of the average value of FuzzyEn over 64-channel with the velocity of the healthy group and three stroke patients. There was a decreasing trend in FuzzyEn value with increasing velocity of the healthy group as well as three stroke patients. But the extent of reduction of stroke patients was greater than that of the healthy group, especially from the slow baseline of 10°/s to quick stretch of 60°/s. **Figure 5** illustrated that the FuzzyEn maps of the healthy group and three stroke patients at four velocities, with the same relative position to the body as above. It was clear that the complexity of stroke patients decreased sharply in a large area as the velocity progressed. On the contrary, the complexity of the healthy group decreased slowly in a smaller area.

As shown in **Figure 6**, although the RMS value was negatively correlated with the FuzzyEn value in the healthy group and three stroke patients, their rate of change was different. When the quick stretch was carried out, the changes of the stroke patients were greater both for the RMS and FuzzyEn value compared with the healthy group, especially from the 10°/s to 60°/s. In addition, although three patients showed similar trend lines, there were some differences among the three of them in response to the increased stretch velocity. The most obvious reduction in FuzzyEn values was from the slow baseline of 10°/s to a quick stretch of 60°/s for all of them. But in terms of the most obvious increase in RMS values was from 10°/s to 60°/s for patient 1, 120°/s to 180°/s for patient 2, and 60°/s to 120°/s for patient 3.

DISCUSSION

In order to study the dysfunctional muscle activity resulted from spasticity, case studies of three stroke patients were reported by comparison with healthy subjects. Benefited from the HD-EMG technique, the spatial heterogeneous activation was

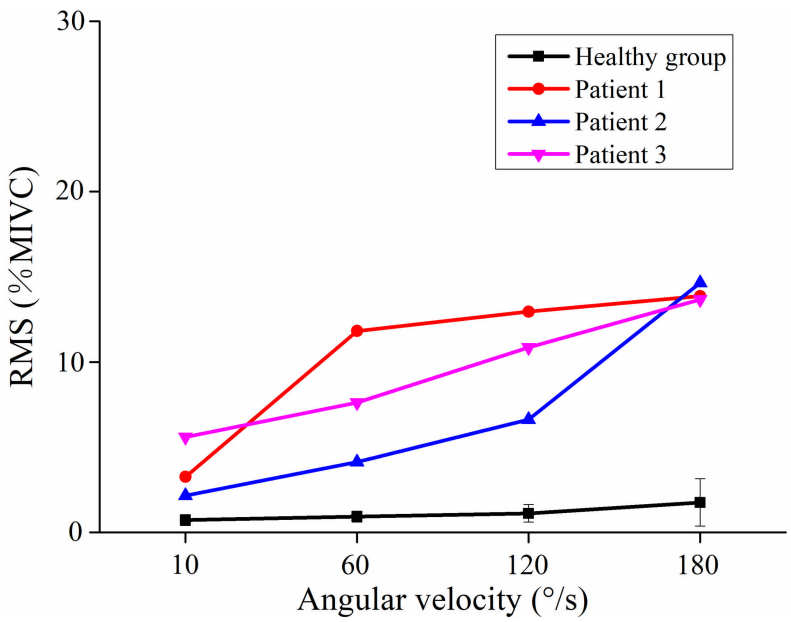

FIGURE 2 | The relationship between the angular velocity of passive stretch and the average value of root mean square (RMS) of the healthy group (healthy group: the average of five healthy subjects) and each stroke patient.

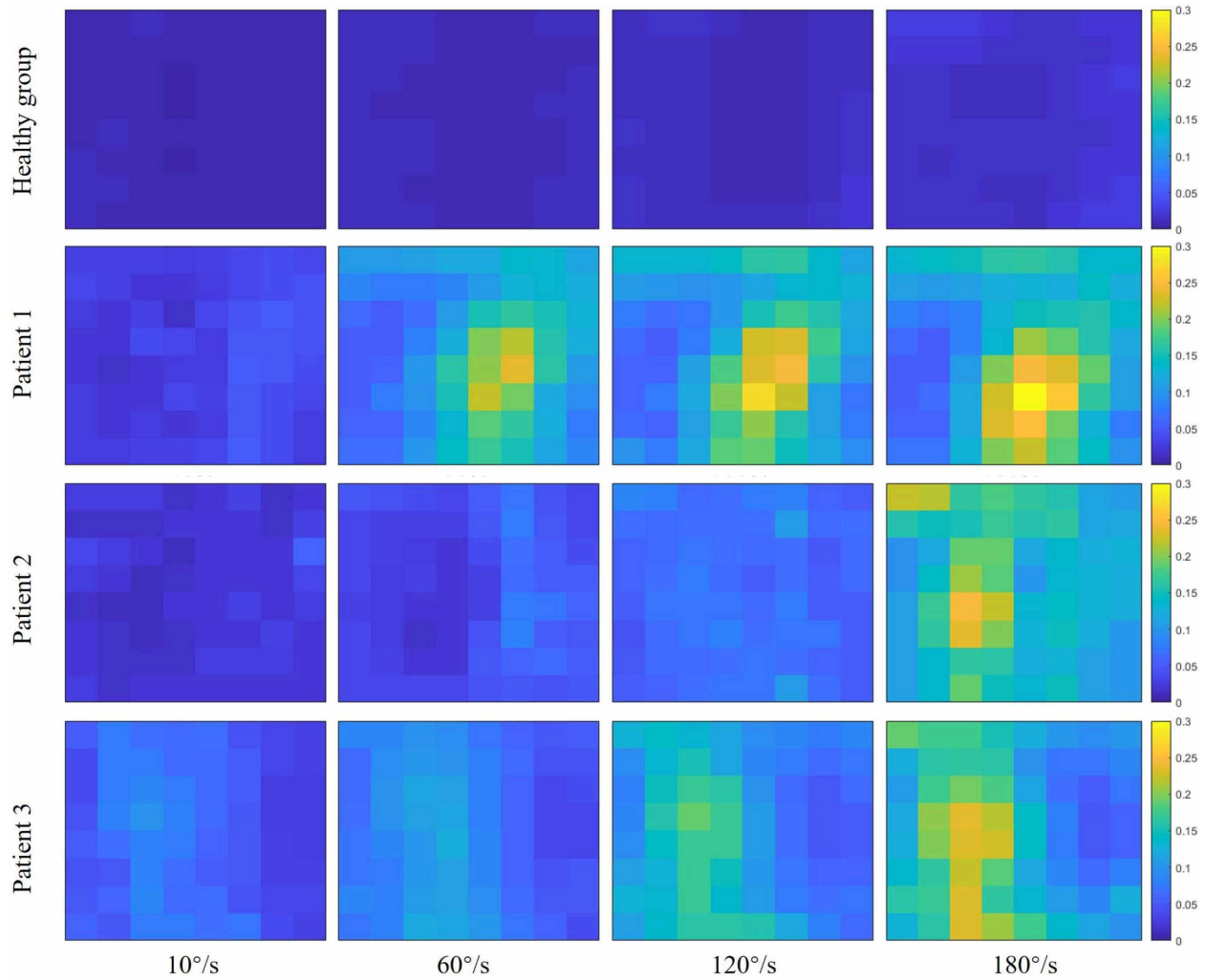

FIGURE 3 | Root mean square (RMS) maps of passive stretch at four angular velocities of the healthy group (healthy group: the average of five healthy subjects) and each stroke patient.

found within the spastic muscle due to spasticity. Besides, by using FuzzyEn index, it was found that the EMG complexity decreased in response to incremental stretch velocity. The changes in amplitude and complexity may be associated with the high degree of synchronization caused by high MUs recruitment with the emergency of spasticity. The muscle activity was heterogeneous and the activation area was gradually expanded as the velocity progressed, which indicated that the spatial recruitment pattern of MUs was non-uniform in the spastic muscle and this MUs recruitment increased with the reflex response.

The EMG Amplitude and Spatial Distribution

Compared with the healthy group, the reflex EMG amplitude of stroke patients exhibited a linear increase during the quick passive stretch. The increased reflex response of stroke patients indicated that their excitability of stretch reflex was enhanced pathologically. The previous study showed a velocity of 35°/s is fast enough to induce significant EMG activity in spastic elbow flexor (Lee et al., 2002). The EMG activity of stroke patients increased with the stretch velocity, which was consistent with the definition of spasticity, which was muscle overactivity caused by the velocity-dependent exaggeration of the stretch reflex (Ward, 2012). The stroke patients with spasticity failed to regulate the stretch reflex due to the alterations in the sensitivity of muscle spindle and supraspinal command (Gracies, 2005; Sheean and McGuire, 2009). Therefore, the excessive reflex response to quick stretch resulted in the involuntary activity of spastic muscle. Similar results were reported in previous researches using conventional bipolar EMG, that is, the stretch reflex response of stroke patients was positively correlated with stretch velocity (Kim et al., 2005; Sorinola et al., 2009). However, there have been few articles investigating the spatial distribution of muscle activity during passive

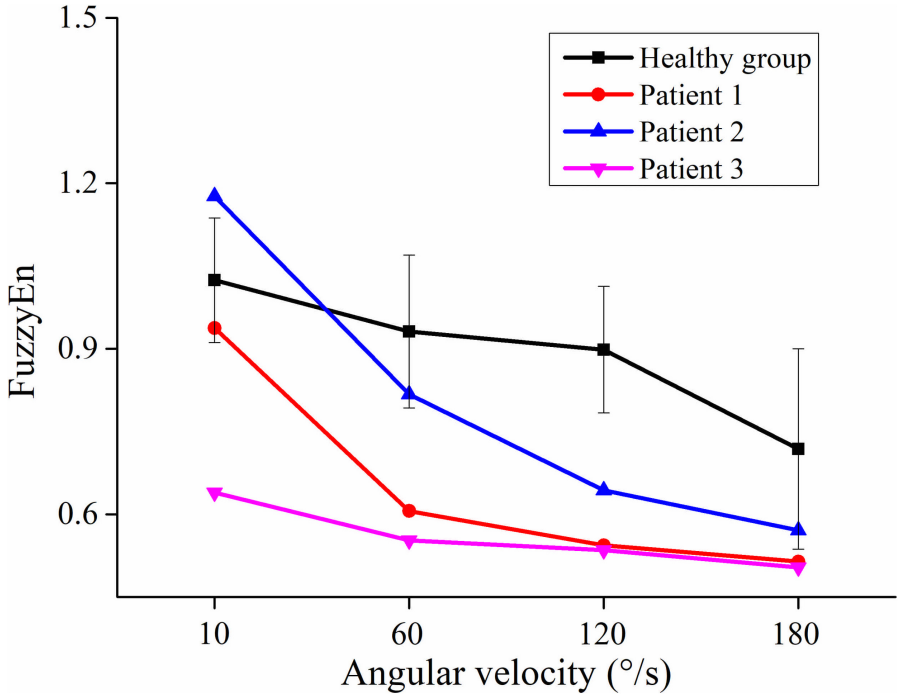

FIGURE 4 | The relationship between the angular velocity of passive stretch and the average value of fuzzy entropy (FuzzyEn) of the healthy group (healthy group: the average of five healthy subjects) and each stroke patient.

stretch. In this study, the spatial inhomogeneous activation and expanding activation area were found in stroke patients by the HD-EMG technique. Distinct areas were activated differentially during passive stretch revealed that the MUs recruitment resulted from spasticity is non-uniform within the spastic muscle. The spatial distribution of muscle activity is related to the distribution and recruitment strategy of MUs within a muscle (Holtermann et al., 2005; Rojas-Martínez et al., 2013; Abboud et al., 2018). The high-threshold MUs degenerated after stoke so that the MUs recruitment caused by the stretch reflex was mainly to recruit the smaller low-threshold MUs (Kallenberg and Hermens, 2011). Thus, the modulation of MUs recruitment could be associated with heterogeneities in muscle activation. Meanwhile, the gradually broadening activation area indicated that the number of recruited MUs would increase with the increase of velocity. In the three stroke patients, the activation area was different indicated that the spatial activation pattern of a spastic muscle might vary between individuals. A previous study showed that the MUs recruitment pattern resulted from the stretch reflex changed depending on the level of spasticity (Hu et al., 2018).

The Complexity of HD-EMG Recordings

In the process of increasing stretch velocity, the EMG complexity of stroke patients decreased more than that of the healthy group. The induced stretch reflex is accompanied by the recruitment of MUs (Kallenberg and Hermens, 2011; Kosar et al., 2012). It has been confirmed that the MUs were activated by the same reflex mechanism that would result in the synchronism of EMG signals (Evans et al., 1983). Therefore, the decrease in complexity may be the result of the increased synchronization of EMG due to stretch reflex. In addition, researches had shown that the motoneurons were synchronized when they were recruited by the stretch reflex (Schuurmans et al., 2009; Finley et al., 2013), which would also lead to the synchronous activation of MUs. Studies have shown that the balance between the inhibitory and excitatory tract that controls the stretch reflex is disrupted after a UMN lesion resulting in a disinhibition of stretch reflex, and only the origin of the inhibitory track is under the control of the cortex (Ward, 2012; Trompetto et al., 2014). In consequence, the exaggerated reflex response of stroke patients would recruit more MUs leading to higher synchronization. The faster the stretch velocity, the more synchronization, so the complexity is sensitive to the stretch velocity. On the other hand, it could be speculated that the reduction in the complexity of stroke patients was also related to the decreased information from the cerebral cortex to the spinal cord. Due to pathological reasons, there is less information from the cerebral cortex to the spinal cord, so the information from the spinal cord to the muscles is also reduced. Some researchers reported that the neural drive to muscles was positively correlated with the complexity of EMG (Kamavuako et al., 2012; Dash et al., 2019). It was interesting to note that the complexity of patient 1 and patient 2 decreased rapidly when the stretch velocity changed from the baseline of 10°/s to a quick stretch of 60°/s, and much slower from 120°/s to 180°/s, while the opposite phenomenon occurred in

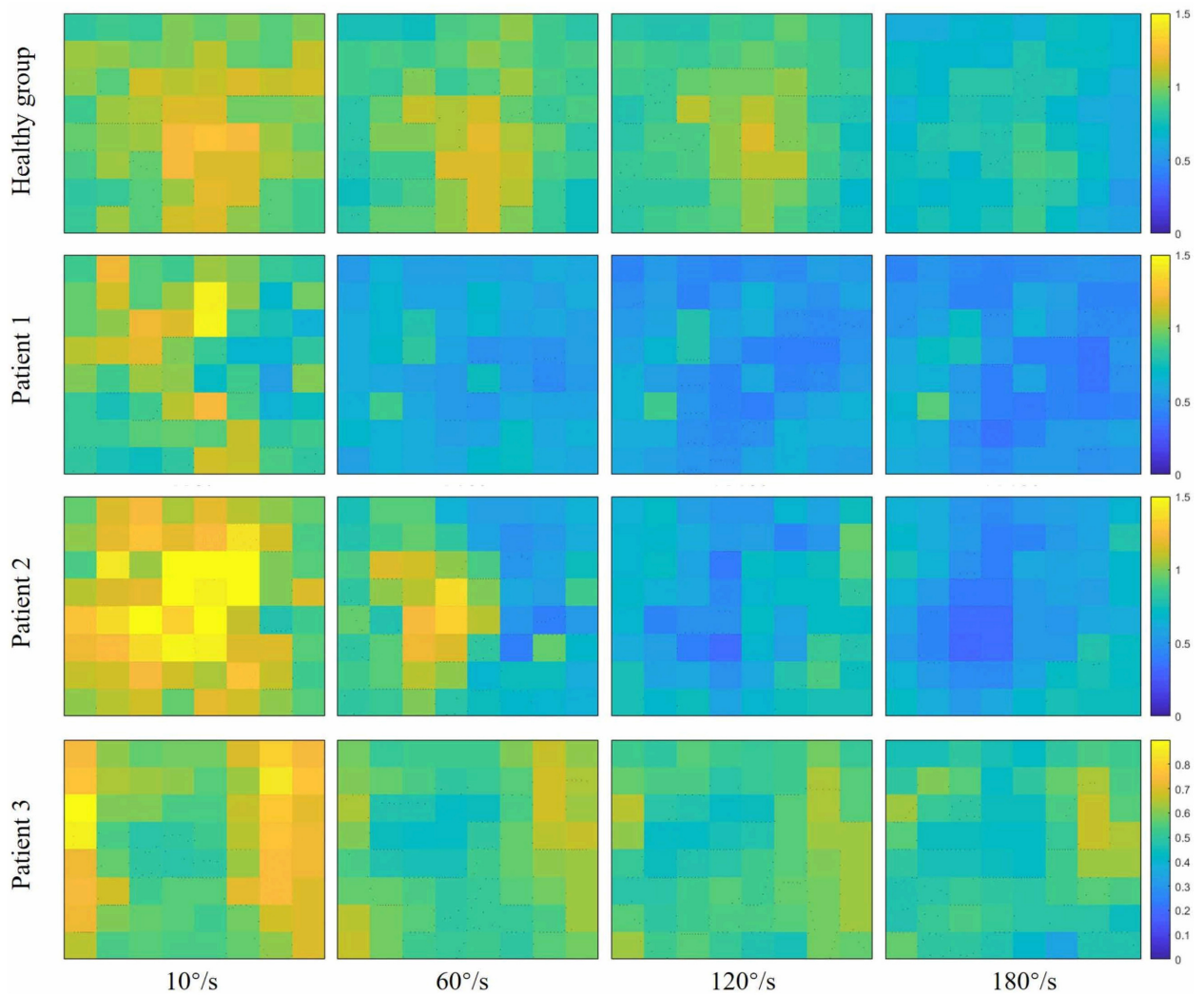

FIGURE 5 | Fuzzy entropy (FuzzyEn) maps of passive stretch at four different angular velocities of the healthy group (healthy group: the average of five healthy subjects) and each stroke patient.

the healthy group. Different from the healthy group, stroke patients were sensitive to the stretch velocity. Once the quick stretch was performed, the stretch reflex was induced to cause a large amount of EMG synchronization, so the complexity from the baseline to quick stretch decreased rapidly. However, the change of patient 3 from baseline to quick stretch was slower than them. It might be due to the lower level of spasticity, causing lower sensitivity to quick stretch. For different quick stretch velocities, the difference was only in the degree of induced spasticity, so the much slower decrease from 120°/s to 180°/s may be due to the limited number and firing rate of recruited MUs. On the contrary, the change from 120°/s to 180°/s was most obvious for the healthy group, which may be because the velocity was too fast and exceeded the threshold at which healthy subjects can control their stretch reflex. When the BB was stretched faster, the complexity of stroke patients decreased rapidly in a clearly large area. The brightest areas of RMS maps corresponded to the darkest areas of FuzzyEn maps, so it might be hypothesized that the spatial heterogeneity of complexity is associated with the spatial distribution of muscle activation.

In comparison with the healthy group, stroke patients showed evident differences in RMS and FuzzyEn when the fast velocity was used. The negative correlation between them implied that the higher amplitude was associated with lower complexity. Moreover, the different responses of the three stroke patients to the increased stretch velocity suggested that patients may have different sensitivity to stretch velocity due to the different levels of the hyperexcitability of the stretch reflex. To our knowledge, this is a prospective study showing that the exaggeration of the stretch reflex is accompanied by an increase in the recruitment and synchronization of MUs. The application of the HD-EMG technique can provide rich spatial information to facilitate

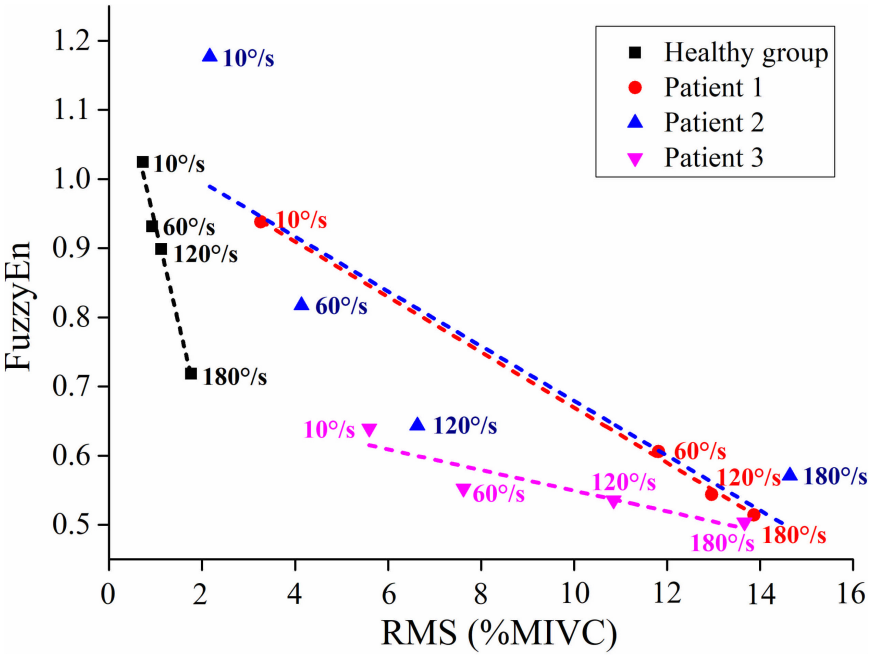

FIGURE 6 | The relationship between the average value of root mean square (RMS) and fuzzy entropy (FuzzyEn) of the healthy group (healthy group: the average of five healthy subjects) and each stroke patient.

understanding the physiological mechanism underlying spasticity on the level of MUs.

Limitations

Three cases might not be sufficient for all stroke patients with different severity of spasticity, and the ages of stroke patients and healthy subjects were not exactly matched. Further research is needed to increase the data of stroke patients with various levels of spasticity and the date of age-matched healthy subjects to obtain more comprehensive information and to further better investigate the physiological mechanisms underlying the spasticity. Meanwhile, the normalization of RMS is related to the results of EMG amplitude. In addition, the HD-EMG decomposition technique would help to provide direct evidence regarding the underlying mechanism of spasticity on the MUs level (Holobar and Zazula, 2007; Chen and Zhou, 2016). From this point of view, the findings in our current work can provide guidance for HD-EMG decomposition, which will be completed in the future.

CONCLUSION

The neuromuscular response to passive stretch of stroke patients with spasticity is different from that of healthy subjects, which is reflected in the increased amplitude and decreased complexity of EMG activity. Furthermore, the involuntary muscle activity due to spasticity is not only manifested in the EMG amplitude, but also in spatial distribution. It would be beneficial to further pathological research and clinical management of spasticity.

DATA AVAILABILITY STATEMENT

The raw data supporting the conclusions of this article will be made available by the authors, without undue reservation.

ETHICS STATEMENT

The studies involving human participants were reviewed and approved by the Ethics Committee of The First Affiliated Hospital of Sun Yat-sen University. The patients/participants provided their written informed consent to participate in this study. Written informed consent was obtained from the individual(s) for the publication of any potentially identifiable images or data included in this article.

AUTHOR CONTRIBUTIONS

TX, YL, YZ, and ZL collected the data. TX, CJ, and NT analyzed the data and drafted the manuscript. HY and RS revised and determined the final manuscript.

ACKNOWLEDGMENTS

The authors would like to thank Liming Zhao and Chenglin Xie for their support with the experiments, and thank all the volunteers who participated in this experiment.

REFERENCES

Abboud, J., Daneau, C., Nougarou, F., Dugas, C., and Descarreaux, M. (2018). Motor adaptations to trunk perturbation: Effects of experimental back pain and spinal tissue creep. *J. Neurophysiol.* 120, 1591–1601. doi: 10.1152/jn.00207.2018

Afsharipour, B., Chandra, S., Son, J., Rymer, W. Z., and Suresh, N. L. (2018). Effect of Botulinum Toxin on the Spatial Distribution of Biceps Brachii EMG Activity Using a Grid of Surface Electrodes: A Case Study. *Proc. Ann. Int. Conf.* 2018, 4693–4696. doi: 10.1109/EMBC.2018.8513125

Castroflorio, T., Falla, D., Wang, K., Svensson, P., and Farina, D. (2012). Effect of experimental jaw-muscle pain on the spatial distribution of surface EMG activity of the human masseter muscle during tooth clenching. *J. Oral Rehabil.* 39, 81–92. doi: 10.1111/j.1365-2842.2011.02246.x

Chen, M., and Zhou, P. (2016). A novel framework based on FastICA for high density surface EMG decomposition. *IEEE Transact. Neural Sys. Rehabil. Engin.* 24, 117–127. doi: 10.1109/TNSRE.2015.2412038

Chen, W., Wang, Z., Xie, H., and Yu, W. (2007). Characterization of surface EMG signal based on fuzzy entropy. *IEEE Transact. Neural Sys. Rehabil. Engin.* 15, 266–272. doi: 10.1109/TNSRE.2007.897025

Chen, W., Zhuang, J., Yu, W., and Wang, Z. (2009). Measuring complexity using FuzzyEn, ApEn, and SampEn. *Med. Engin. Phys.* 31, 61–68. doi: 10.1016/j.medengphy.2008.04.005

Damiano, D. L., Quinlivan, J. M., Owen, B. F., Payne, P., Nelson, K. C., and Abel, M. F. (2007). What does the Ashworth scale really measure and are instrumented measures more valid and precise? *Devel. Med. Child Neurol.* 44, 112–118. doi: 10.1111/j.1469-8749.2002.tb00296.x

Dash, A., Dutta, A., and Lahiri, U. (2019). Quantification of grip strength with complexity analysis of surface electromyogram for hemiplegic post-stroke patients. *NeuroRehabilit.* 45, 45–56. doi: 10.3233/NRE-192734

Drost, G., Stegeman, D. F., van Engelen, B. G. M., and Zwarts, M. J. (2006). Clinical applications of high-density surface EMG: A systematic review. *J. Electromyogr. Kinesiol.* 16, 586–602. doi: 10.1016/j.jelekin.2006.09.005

Duncan, P. W., Zorowitz, R., Bates, B., Choi, J. Y., Glasberg, J. J., Graham, G. D., et al. (2005). Management of Adult Stroke Rehabilitation Care: a clinical practice guideline. *J. Cerebr. Circulat.* 36, 100–143e. doi: 10.1161/01.STR.0000180861.54180.FF

Evans, C. M., Fellows, S. J., Rack, P. M., Ross, H. F., and Walters, D. K. (1983). Response of the normal human ankle joint to imposed sinusoidal movements. *J. Physiol.* 344, 483–502. doi: 10.1113/jphysiol.1983.sp014953

Farina, D., Leclerc, F., Arendt-Nielsen, L., Buttelli, O., and Madeleine, P. (2008). The change in spatial distribution of upper trapezius muscle activity is correlated to contraction duration. *J. Electromyogr. Kinesiol.* 18, 16–25. doi: 10.1016/j.jelekin.2006.08.005

Finley, J. M., Dhaher, Y. Y., and Perreault, E. J. (2013). Acceleration dependence and task-specific modulation of short- and medium-latency reflexes in the ankle extensors. *Physiol. Rep.* 1, 1–12. doi: 10.1002/phy2.51

Fleuren, J. F. M., Voerman, G. E., Erren-Wolters, C. V., Snoek, G. J., Rietman, J. S., Hermens, H. J., et al. (2010). Stop using the Ashworth Scale for the assessment of spasticity. *J. Neurol. Neurosur. Psych.* 81, 46–52. doi: 10.1136/jnnp.2009.177071

Francisco, G. E., and McGuire, J. R. (2012). Poststroke spasticity management. *Stroke* 43, 3132–3136. doi: 10.1161/STROKEAHA.111.639831

Gallina, A., and Botter, A. (2013). Spatial localization of electromyographic amplitude distributions associated to the activation of dorsal forearm muscles. *Front. Physiol.* 4:1–8. doi: 10.3389/fphys.2013.00367

Gracies, J. M. (2005). Pathophysiology of spastic paresis. II: Emergence of muscle overactivity. *Muscle Nerve* 31, 552–571. doi: 10.1002/mus.20285

Holobar, A., and Zazula, D. (2007). Multichannel blind source separation using convolution Kernel compensation. *IEEE Transact. Sign. Proces.* 55, 4487–4496. doi: 10.1109/TSP.2007.896108

Holtermann, A., Roeleveld, K., and Karlsson, J. S. (2005). Inhomogeneities in muscle activation reveal motor unit recruitment. *J. Electromyogr. Kinesiol.* 15, 131–137. doi: 10.1016/j.jelekin.2004.09.003

Hsu, A. L., Tang, P. F., and Jan, M. H. (2003). Analysis of impairments influencing gait velocity and asymmetry of hemiplegic patients after mild to moderate stroke. *Archiv. Phys. Med. Rehabilit.* 84, 1185–1193. doi: 10.1016/S0003-9993(03)00030-3

Hu, B., Zhang, X., Mu, J., Wu, M., Zhu, Z., Liu, Z., et al. (2018). Spasticity Measurement Based on the HHT Marginal Spectrum Entropy of sEMG Using a Portable System: A Preliminary Study. *IEEE Transact. Neural Sys. Rehabil. Engin.* 26, 1424–1434. doi: 10.1109/TNSRE.2018.2838767

Hu, X., Suresh, N. L., Xue, C., and Rymer, W. Z. (2015). Extracting extensor digitorum communis activation patterns using high-density surface electromyography. *Front. Physiol.* 6, 1–9. doi: 10.3389/fphys.2015.00279

Hu, Y., Kwok, J. W., Tse, J. Y. H., and Luk, K. D. K. (2014). Time-varying surface electromyography topography as a prognostic tool for chronic low back pain rehabilitation. *Spine J.* 14, 1049–1056. doi: 10.1016/j.spinee.2013.11.060

Kallenberg, L. A. C., and Hermens, H. J. (2011). Motor unit properties of biceps brachii during dynamic contractions in chronic stroke patients. *Muscle Nerve* 43, 112–119. doi: 10.1002/mus.21803

Kamavuako, E. N., Farina, D., Yoshida, K., and Jensen, W. (2012). Estimation of grasping force from features of intramuscular EMG signals with mirrored bilateral training. *Anna. Biomed. Engin.* 40, 648–656. doi: 10.1007/s10439-011-0438-7

Kim, D. Y., Park, C., Il, Chon, J. S., Ohn, S. H., Park, T. H., et al. (2005). Biomechanical assessment with electromyography of post-stroke ankle plantar flexor spasticity. *Yonsei Med. J.* 46, 546–554. doi: 10.3349/ymj.2005.46.4.546

Kosar, A. C., Candow, D. G., and Putland, J. T. (2012). Potentialbeneficialeffects of whole-body vibration for muscle recovery after exercise. *J. Stren. Condit. Res.* 26, 2907–2911.

Lance, J. W. (1980). The control of muscle tone, reflexes, and movement: Robert Wartenbeg Lecture. *Neurology* 30, 1303–1303. doi: 10.1212/wnl.30.12.1303

Lee, H. M., Huang, Y. Z., Chen, J. J. J., and Hwang, I. S. (2002). Quantitative analysis of the velocity related pathophysiology of spasticity and rigidity in the elbow flexors. *J. Neurol. Neurosurg. Psych.* 72, 621–629. doi: 10.1136/jnnp.72.5.621

Li, S., Shin, H., Zhou, P., and Li, X. (2017). Different effects of cold stimulation on reflex and non-reflex components of poststroke spastic hypertonia. *Front. Neurol.* 8, 6–11. doi: 10.3389/fneur.2017.00169

Lindberg, P. G., Gäverth, J., Islam, M., Fagergren, A., Borg, J., and Forssberg, H. (2011). Validation of a new biomechanical model to measure muscle tone in spastic muscles. *Neurorehabilit. Neural Rep.* 25, 617–625. doi: 10.1177/1545968311403494

Pierce, S. R., Lauer, R. T., Shewokis, P. A., Rubertone, J. A., and Orlin, M. N. (2006). Test-Retest Reliability of Isokinetic Dynamometry for the Assessment of Spasticity of the Knee Flexors and Knee Extensors in Children With Cerebral Palsy. *Archiv. Phys. Med. Rehabilit.* 87, 697–702. doi: 10.1016/j.apmr.2006.01.020

Rojas-Martínez, M., Mañanas, M. A., Alonso, J. F., and Merletti, R. (2013). Identification of isometric contractions based on High Density EMG maps. *J. Electromyogr. Kinesiol.* 23, 33–42. doi: 10.1016/j.jelekin.2012.06.009

Rojas-Martínez, Monica, Mañanas, M. A., and Alonso, J. F. (2012). High-density surface EMG maps from upper-arm and forearm muscles. *J. NeuroEngin. Rehabilit.* 9, 1–17. doi: 10.1186/1743-0003-9-85

Schuurmans, J., De Vlugt, E., Schouten, A. C., Meskers, C. G. M., De Groot, J. H., and Van Der Helm, F. C. T. (2009). The monosynaptic Ia afferent pathway can largely explain the stretch duration effect of the long latency M2 response. *Exper. Brain Res.* 193, 491–500. doi: 10.1007/s00221-008-1647-7

Sheean, G., and McGuire, J. R. (2009). Spastic Hypertonia and Movement Disorders: Pathophysiology, Clinical Presentation, and Quantification. *PM and R* 1, 827–833. doi: 10.1016/j.pmrj.2009.08.002

Sin, M., Kim, W. S., Cho, K., and Paik, N. J. (2019). Isokinetic robotic device to improve test-retest and inter-rater reliability for stretch reflex measurements in stroke patients with spasticity. *J. Visual. Exper.* 2019, 1–13. doi: 10.3791/59814

Sommerfeld, D. K., Eek, E. U. B., Svensson, A. K., Holmqvist, L. W., and Von Arbin, M. H. (2004). Spasticity after Stroke: Its Occurrence and Association with Motor Impairments and Activity Limitations. *Stroke* 35, 134–139. doi: 10.1161/01.STR.0000105386.05173.5E

Sorinola, I. O., White, C. M., Rushton, D. N., and Newham, D. J. (2009). Electromyographic response to manual passive stretch of the hemiplegic wrist: Accuracy, reliability, and correlation with clinical spasticity assessment and function. *Neurorehabilit. Neural Rep.* 23, 287–294. doi: 10.1177/1545968308321778

Starsky, A. J., Sangani, S. G., McGuire, J. R., Logan, B., and Schmit, B. D. (2005). Reliability of biomechanical spasticity measurements at the elbow of people poststroke. *Archiv. Phys. Med. Rehabilit.* 86, 1648–1654. doi: 10.1016/j.apmr.2005.03.015

Tian, N., and Song, R. (2019). Effects of Different Interventions on Cardiac Regulation Using Fuzzy Entropy. *IEEE Access* 7, 75949–75956. doi: 10.1109/ACCESS.2019.2920911

Trompetto, C., Marinelli, L., Mori, L., Pelosin, E., Currà, A., Molfetta, L., et al. (2014). Pathophysiology of spasticity: Implications for neurorehabilitation. *BioMed. Res. Int.* 2014:354906. doi: 10.1155/2014/354906

Urban, P. P., Wolf, T., Uebele, M., Marx, J. J., Vogt, T., Stoeter, P., et al. (2010). Occurence and clinical predictors of spasticity after ischemic stroke. *Stroke* 41, 2016–2020. doi: 10.1161/STROKEAHA.110.581991

Voerman, G. E., Gregorič, M., and Hermens, H. J. (2005). Neurophysiological methods for the assessment of spasticity: The Hoffman reflex, the tendon reflex, and the stretch reflex. *Disabil. Rehabilit.* 27, 33–68. doi: 10.1080/09638280400014600

Wang, H., Huang, P., Li, X., Samuel, O. W., Xiang, Y., and Li, G. (2019). Spasticity assessment based on the maximum isometrics voluntary contraction of upper limb muscles in post-stroke hemiplegia. *Front. Neurol.* 10:465. doi: 10.3389/fneur.2019.00465

Ward, A. B. (2012). A literature review of the pathophysiology and onset of post-stroke spasticity. *Eur. J. Neurol.* 19, 21–27. doi: 10.1111/j.1468-1331.2011.03448.x

Watkins, C. L., Leathley, M. J., Gregson, J. M., Moore, A. P., Smith, T. L., and Sharma, A. K. (2002). Prevalence of spasticity post stroke. *Clin. Rehabilit.* 16, 515–522. doi: 10.1191/0269215502cr512oa

Welmer, A. K., Von Arbin, M., Holmqvist, L. W., and Sommerfeld, D. K. (2006). Spasticity and its association with functioning and health-related quality of life 18 months after stroke. *Cerebrovascul. Dis.* 21, 247–253. doi: 10.1159/000091222

Wissel, J., Schelosky, L. D., Scott, J., Christe, W., Faiss, J. H., and Mueller, J. (2010). Early development of spasticity following stroke: a prospective, observational trial. *J. Neurol.* 257, 1067–1072. doi: 10.1007/s00415-010-5463-1

Wood, D. E., Burridge, J. H., van Wijck, F. M., Mcfadden, C., Hitchcock, R. A., Pandyan, A. D., et al. (2005). Biomechanical approaches applied to the lower and upper limb for the measurement of spasticity: A systematic review of the literature. *Disabil. Rehabilit.* 27, 19–33. doi: 10.1080/09638280400014683

Wu, Y., Chen, Y., Ye, Y., Yan, T., and Song, R. (2018). Age-Related Differences in Complexity during Handgrip Control Using Multiscale Entropy. *IEEE Access* 6, 45552–45561. doi: 10.1109/ACCESS.2018.2861708

Zhang, X., Tang, X., Zhu, X., Gao, X., Chen, X., and Chen, X. (2019). A regression-based framework for quantitative assessment of muscle spasticity using combined emg and inertial data from wearable sensors. *Front. Neurosci.* 13, 1–12. doi: 10.3389/fnins.2019.00398

Zhou, P., Suresh, N. L., and Rymer, W. Z. (2011). Surface electromyogram analysis of the direction of isometric torque generation by the first dorsal interosseous muscle. *J. Neural Engin.* 8:036028. doi: 10.1088/1741-2560/8/3/036028

Conflict of Interest: The authors declare that the research was conducted in the absence of any commercial or financial relationships that could be construed as a potential conflict of interest.

frontiers in Bioengineering and Biotechnology

ORIGINAL RESEARCH
published: 30 November 2020
doi: 10.3389/fbioe.2020.590013

Rehabilitation Effects of Fatigue-Controlled Treadmill Training After Stroke: A Rat Model Study

Yuchen Xu[1,2], *Yuanfa Yao*[2,3], *Hao Lyu*[4], *Stephanie Ng*[4], *Yingke Xu*[2,3], *Wai Sang Poon*[4], *Yongping Zheng*[5], *Shaomin Zhang*[1,2*] *and Xiaoling Hu*[5*]

[1] Qiushi Academy for Advanced Studies, Zhejiang University, Hangzhou, China, [2] Key Laboratory of Biomedical Engineering of Ministry of Education, Zhejiang Provincial Key Laboratory of Cardio-Cerebral Vascular Detection Technology and Medicinal Effectiveness Appraisal, College of Biomedical Engineering & Instrument Science, Zhejiang University, Hangzhou, China, [3] Department of Endocrinology, The Affiliated Sir Run Run Shaw Hospital, Zhejiang University School of Medicine, Hangzhou, China, [4] Division of Neurosurgery, Department of Surgery, Prince of Wales Hospital, The Chinese University of Hong Kong, ShaTin, Hong Kong, [5] Department of Biomedical Engineering, The Hong Kong Polytechnic University, Kowloon, Hong Kong

OPEN ACCESS

Edited by:
Le Li,
First Affiliated Hospital of Sun Yat-Sen University, China

Reviewed by:
Bo Yao,
Chinese Academy of Medical Sciences and Peking Union Medical College, China
Chi-Wen Lung,
Asia University, Taiwan

***Correspondence:**
Shaomin Zhang
shaomin@zju.edu.cn
Xiaoling Hu
xiaoling.hu@polyu.edu.hk

Specialty section:
This article was submitted to Biomechanics, a section of the journal Frontiers in Bioengineering and Biotechnology

Received: *31 July 2020*
Accepted: *28 October 2020*
Published: *30 November 2020*

Citation:
Xu Y, Yao Y, Lyu H, Ng S, Xu Y, Poon WS, Zheng Y, Zhang S and Hu X (2020) Rehabilitation Effects of Fatigue-Controlled Treadmill Training After Stroke: A Rat Model Study. Front. Bioeng. Biotechnol. 8:590013. doi: 10.3389/fbioe.2020.590013

Background: Traditional rehabilitation with uniformed intensity would ignore individual tolerance and introduce the second injury to stroke survivors due to overloaded training. However, effective control of the training intensity of different stroke survivors is still lacking. The purpose of the study was to investigate the rehabilitative effects of electromyography (EMG)-based fatigue-controlled treadmill training on rat stroke model.

Methods: Sprague–Dawley rats after intracerebral hemorrhage and EMG electrode implantation surgeries were randomly distributed into three groups: the control group (CTRL, $n = 11$), forced training group (FOR-T, $n = 11$), and fatigue-controlled training group (FAT-C, $n = 11$). The rehabilitation interventions were delivered every day from day 2 to day 14 post-stroke. No training was delivered to the CTRL group. The rats in the FOR-T group were forced to run on the treadmill without rest. The fatigue level was monitored in the FAT-C group through the drop rate of EMG mean power frequency, and rest was applied to the rats when the fatigue level exceeded the moderate fatigue threshold. The speed and accumulated running duration were comparable in the FAT-C and the FOR-T groups. Daily evaluation of the motor functions was performed using the modified Neurological Severity Score. Running symmetry was investigated by the symmetry index of EMG bursts collected from both hind limbs during training. The expression level of neurofilament-light in the striatum was measured to evaluate the neuroplasticity.

Results: The FAT-C group showed significantly lower modified Neurological Severity Score compared with the FOR-T ($P \leq 0.003$) and CTRL ($P \leq 0.003$) groups. The FAT-C group showed a significant increase in the symmetry of hind limbs since day 7 ($P = 0.000$), whereas the FOR-T group did not ($P = 0.349$). The FAT-C group showed a higher concentration of neurofilament-light compared to the CTRL group ($P = 0.005$) in the unaffected striatum and the FOR-T group ($P = 0.021$) in the affected striatum.

Conclusion: The treadmill training with moderate fatigue level controlled was more effective in motor restoration than forced training. The fatigue-controlled physical training

also demonstrated positive effects in the striatum neuroplasticity. This study indicated that protocol with individual fatigue-controlled training should be considered in both animal and clinical studies for better stroke rehabilitation.

Keywords: fatigue-controlled, electromyography, training intensity, stroke, motor recovery

INTRODUCTION

Stroke is a leading cause of mortality and disability globally, resulting in substantial costs and long-term healthcare burden on both family and society (Gorelick, 2019). With the fast expansion of stroke populations worldwide and insufficiency of rehabilitation professionals in the public health, more than 50 to 60% of stroke survivors are still experiencing moderate to severe motor impairments, which significantly deteriorates their independence in daily living, even after the routine treatments (Hendricks et al., 2002). More effective post-stroke rehabilitation programs are needed to improve the effectiveness of the current treatments (Donkor, 2018).

Effective post-stroke motor restoration depends on timely physical treatments with necessary intensities, facilitating rehabilitative neuroplasticity after the lesion (Hylin et al., 2017). Both clinical and animal studies showed that post-stroke rehabilitation implemented in the subacute period introduced significantly higher neuroplasticity and better motor function recovery than those achieved in the chronic period (Yang et al., 2003; Biernaskie et al., 2004; Cumming et al., 2011). It was because physical training in the early stage after stroke, e.g., the subacute period, could more effectively induce use-dependent neural rewiring and strengthen the synapses during the spontaneous neurological recovery, compared with the later chronic stage when the neuroplastic activities tend to be stable (Yang et al., 2003; Biernaskie et al., 2004; Murphy and Corbett, 2009; Cumming et al., 2011; Bell et al., 2015). However, it also had been found that overloaded training in the early stage after stroke could inhibit functional motor recovery. For example, clinical studies found that physical practices with higher intensities in daily treatment during the subacute period post-stroke was related to worse motor outcomes with more complications compared with those who received standard training (Dromerick et al., 2009; Andrews et al., 2015). Overloaded physical training could introduce additional fatigue resulting in neurological stress that suppressed neural plasticity, motor relearning, and even enlarged brain lesion after stroke. A previous study demonstrated that fatigue induced by physical exercise could impair neural regeneration in the corticostriatal pathway, which could further deteriorate movement control and limit motor relearning in post-stroke rehabilitation (Ma et al., 2018). It was also found that the detrimental effects on the overall motor skill acquisition after fatigue could carry on to subsequent practicing days, even in the absence of fatigue (Branscheidt et al., 2019). Furthermore, in rodent models, forced training was found to increase the levels of the stress hormone, corticosterone, in serum (Sun et al., 2014), and enlarged brain lesion in the subacute stage after stroke (Kozlowski et al., 1996). Corticosterone could downregulate the concentration of the neuron survival and growth-related proteins, e.g., neurofilament-light (NFL), leading to feebler neuroplasticity (Cereseto et al., 2006).

Fatigue level is an essential parameter that should be managed for an optimized motor outcome in post-stroke rehabilitation. However, the training intensity is usually uniformly administrated to a batch of patients in the traditional physio- and occupational treatments, e.g., grouped training with the same intensity, for an easy management with limited professional manpower. On the other hand, patients might also force themselves to complete the assigned training intensities, even if overloaded, with the expectation of promised motor improvements. The fatigue tolerance of individual patients could be diverse to the same training intensity. There is a lack of regulation on the individualized fatigue level during the physical training after stroke in the current clinical practices.

Although rat models with subacute stroke have been investigated on the effects of varied running intensities on motor outcomes, the fatigue levels based training has not been regulated explicitly in the previous studies (Sun et al., 2014; Chen et al., 2015). For example, Sun et al. (2014) demonstrated that running schemes on a treadmill with gradually increased speeds along with the motor recovery progress and adaptive speeds with intermittent stops in a wheel could achieve better motor outcomes than those with the schemes of constant running speed throughout the training (Chen et al., 2015). The results in these studies implied that physical training with a fatigue level adaptive to the motor recovery progress, or the tolerance of individual rats, could achieve more effective motor recovery in early post-stroke rehabilitation.

The individual fatigue level during physical training could be continuously monitored by electromyography (EMG) on the rehabilitation task-related main contracting muscles (Dobkin, 2008). A drop of mean power frequency (MPF) in EMG could be captured in a fatiguing muscle, which had been used as a biomarker in sports medicine (Cifrek et al., 2009; Li et al., 2011; Wang et al., 2018). However, using EMG MPF to regulate the fatigue level in post-stroke physical rehabilitation has not been carried out previously.

In this work, we established a treadmill running platform with fatigue level controlled by monitoring the EMG MPF during running for individual rats in the subacute stage after stroke, with the purpose of avoiding overloaded physical training. We hypothesized that the fatigue-controlled treadmill training would achieve better rehabilitation effects than those administrated with forced and continuous running with a constant speed, which simulated the batched treatment with uniform intensity. The rehabilitation effects were investigated by behavioral assessments, EMG biomarkers, and NFL expression levels in the brain tissues.

MATERIALS AND METHODS

In this study, a custom-made treadmill training system with the control of fatigue level based on EMG was designed as the experimental platform for post-stroke training. The rats with intracerebral hemorrhage (ICH) received fatigue-controlled or forced treadmill training in this system to investigate the effects of fatigue-controlled training on motor function recovery. The design of the experiment is shown in **Figure 1**. All rats performed a 3 day treadmill accommodation running, followed by surgeries of ICH and EMG electrode implantation. Two days after the operations, the rats were divided into three groups randomly and received fatigue-controlled, forced, or no training during the subacute period (day 2 to day 14 post-stroke) (Forghani et al., 2015). The recovery effects were evaluated by behavioral tests, EMG signal markers, and brain tissue Western blot analysis.

Animal Preparation

Fifty-eight Sprague–Dawley adult rats weighted from 270 to 310 g were included in this study. They were housed in a 12/12 h light/dark vivarium with *ad libitum* access to food and water except for experimental periods. All animals went through a 30 min treadmill running at the speed of 16 m/min per day for 3 consecutive days to get familiar with running on the treadmill (Rezaei et al., 2017). The length of the runway was 50 cm, and the treadmill controller would show the accumulative running duration (ZH-PT animal experiment treadmill, Anhui Zhenghua Biological Instrument, China). Rats with occasional stops during running would receive gentle nudges to help them keep running (Ke et al., 2011). If the rat could not keep running in the middle of the track for more than 15 min on the third day, it would be excluded from the study. Six rats were excluded after the 3 day adaptation running.

Surgeries of Intracerebral Hemorrhage and Electromyography Electrodes Implantation

Fifty-two rats passed through the running adaptation and received the surgeries of ICH and EMG electrode implantation. The rat was anesthetized by propofol (1.2 mg/kg, intraperitoneally, and 0.02 mg/kg subsequently) to achieve a 3 h around narcotism for the ICH surgery and the consecutive EMG electrode implantation.

Intracerebral Hemorrhage Surgery

ICH surgery is a common model adopted for investigations on post-stroke motor recovery (Kelly et al., 2003; Park et al., 2010; Bai et al., 2012). It disrupts the blood vessels of the basal lamina and leads to bleeding and contralesional hemiplegia in rats

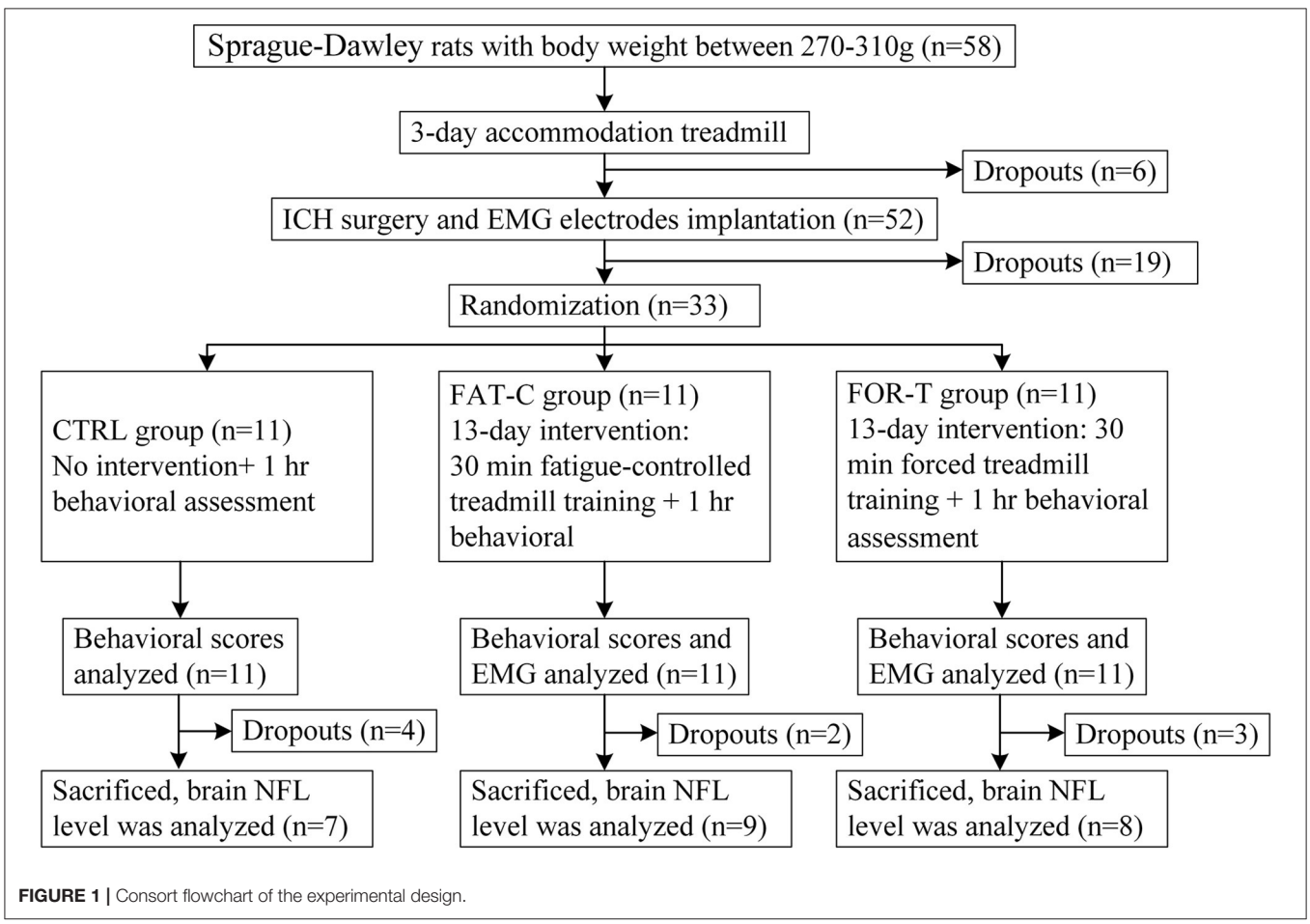

FIGURE 1 | Consort flowchart of the experimental design.

(Chesney et al., 1995). The surgery was guided by a stereotaxic system, and the ICH lesion was introduced by intrastriatal administration of bacterial collagenase according to the method in MacLellan et al. (2006), with the anatomical illustration shown in **Figure 2A**. The brain slices in the previous study showed similar bleeding lesion sizes according to the surgical protocol (Liu et al., 2013). During the operation, the rat was secured prone onto a stereotaxic apparatus (68005, RWD Life Science, China) with a heating pad to keep body temperature maintained at 36–37°C (Wangfischer, 2009). After making an incision over the scalp, the striatum in the right hemisphere was located through stereotaxic coordinates: 0.2 mm anterior, 3.0 mm lateral (**Figure 2A**, red dot), and 6.0 mm ventral to the Bregma. A 1 mm diameter borehole was drilled (**Figure 2A**, red dot) by trephine (78001, RWD Life Science, China), and the 26 gauge, 5 μl syringe (Hamilton syringe 700, Hamilton, USA) was inserted into the striatum. Type IV collagenase (1.2 μl, 0.25 U in 1 μl NaCl 0.9%, C5138, Sigma, USA) was infused using a micro-infusion pump (Micro 4, World Precision Instruments, Inc., USA) for 5 min. The syringe was made to remain in place for 10 min to avoid backflow and subsequently withdrawn slowly (Liu et al., 2013). Then, the hole was sealed by medical glue. The wound on the scalp was left for the following EMG electrode implantation.

Electromyography Electrode Implantation

After the ICH surgery, the intramuscular electrodes were implanted on the AF and UN medial gastrocnemius muscles (MG) (Li et al., 2013). A differential electrode configuration was adopted for the measurement of EMG activity of the target muscles. A skin incision was made on the dorsal side of the calf to expose the MG. The insulation was stripped off from the end of the Teflon-coated stainless steel wires (AS632, Cooner Wire, USA) by 2 cm (Li et al., 2011). After separating the skin from the muscular layer through blunt dissection, the two wires were inserted and looped around the belly and cauda of the MG (Barroso et al., 2019) (**Figure 2B**). The four implanted electrodes were tunneled subcutaneously from both hind limbs to the exposed skull and soldered with a five-pin head connector (**Figure 2B**). The fifth pin was connected to the common ground screw on the skull (0.0 mm anterior and 0.0 mm lateral to Lambda, **Figure 2A**, yellow dot) through a silver wire. Four screws were anchored firmly to the skull (2.0 mm anterior and ±2.0 mm lateral to the Bregma, 2.0 mm anterior and ±3.0 mm lateral to the Lambda, **Figure 2A**, black dots) as a foundation of the head connector. The connector was fixed on the skull by screws with dental cement. After the suturing of the wounds, the rat was put in a warm box [45 cm (length) × 35 cm (width) × 30 cm (height)] to maintain the body temperature at 36–37° (Wangfischer, 2009) with *ad libitum* access to food and water till waking up. Fifteen rats dropped out within the first 2 days after ICH surgery, mainly due to severe cerebral hemorrhage.

Randomization

Two days (48 h) after the ICH and EMG electrode implantation surgeries, 37 rats survived. Thirty-three rats with modified neurological severity score (mNSS) > 6 on day 2 post-stroke were recruited to guarantee the comparable degree of motor impairments. They were distributed randomly into three groups, i.e., the CTRL ($n = 11$), the FAT-C ($n = 11$), and the FOR-T groups ($n = 11$).

Rehabilitation Intervention

Fatigue-Controlled System

In this study, we integrated the treadmill with an EMG analysis system based on a customized MATLAB graphical user interface (GUI) (Matlab, 2016a) to facilitate the fatigue-controlled treadmill training. The structure diagram of the training system is illustrated in **Figure 3**, including three parts: (1) a multitrack treadmill, (2) EMG amplification and acquisition system, and (3) an online signal processing module with GUI.

The EMG signals from the MG muscles in both hind limbs were amplified with a gain of 1,750 by a neural signal acquisition system (OmniPlex Neural Signal Acquisition System, Plexon Inc., USA), with a sampling rate of 40 kHz and band-pass filtered with a fourth-order Butterworth filter (60–2,000 Hz). **Figure 4A** shows the representative EMG trials during the treadmill running.

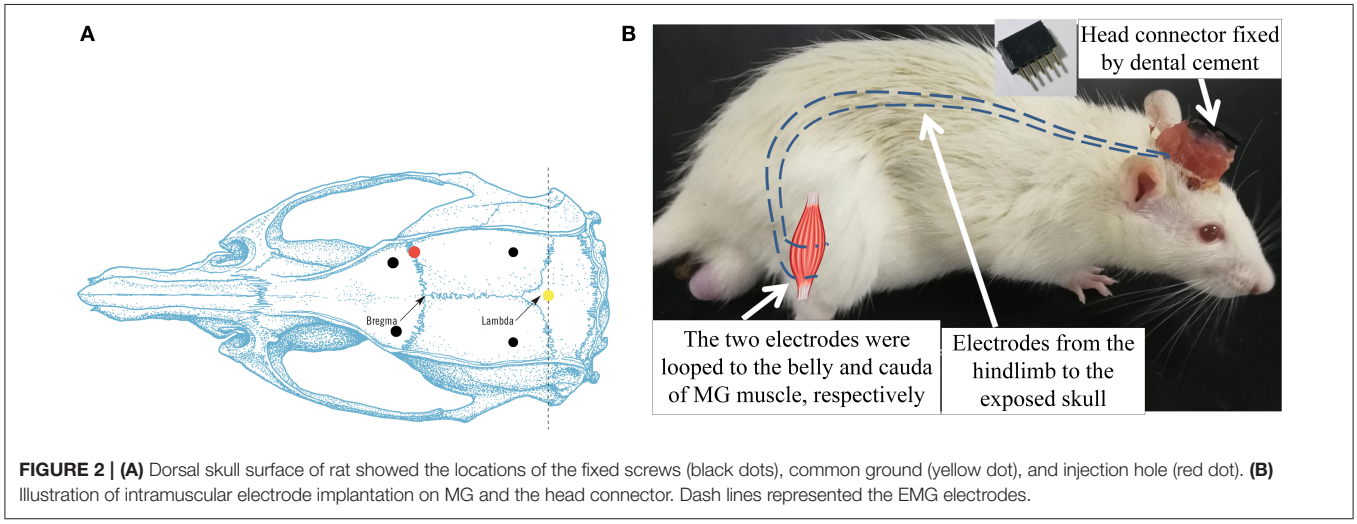

FIGURE 2 | (A) Dorsal skull surface of rat showed the locations of the fixed screws (black dots), common ground (yellow dot), and injection hole (red dot). **(B)** Illustration of intramuscular electrode implantation on MG and the head connector. Dash lines represented the EMG electrodes.

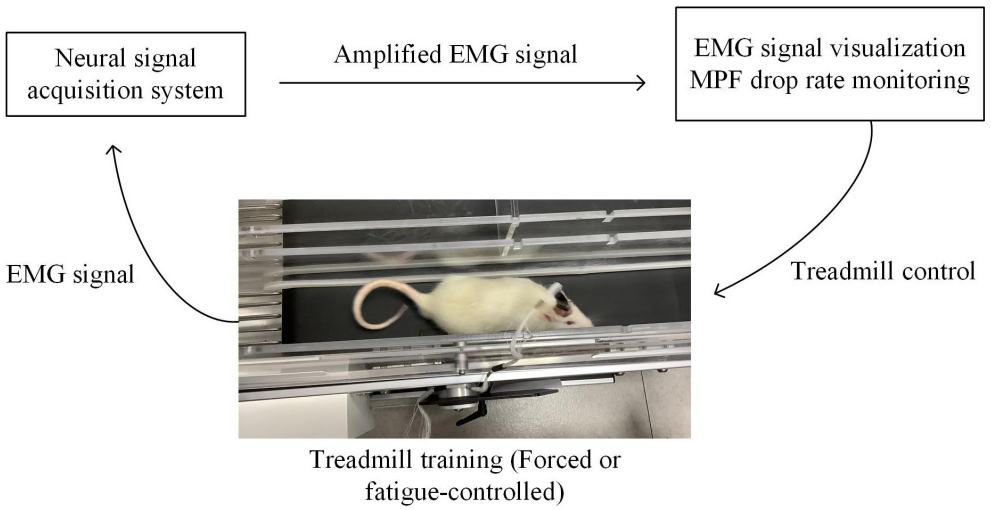

FIGURE 3 | Fatigue-controlled experimental platform. Rat was running on the treadmill; its EMG signal was acquired and amplified by a neural data acquisition system (Plexon Inc., USA) and transmitted to the computer. EMG signal was real-time visualized on the computer screen. The Matlab GUI-based fatigue-controlled software calculated MPF drop rate during treadmill training, and the on/off state of the treadmill was controlled by the MPF drop rate.

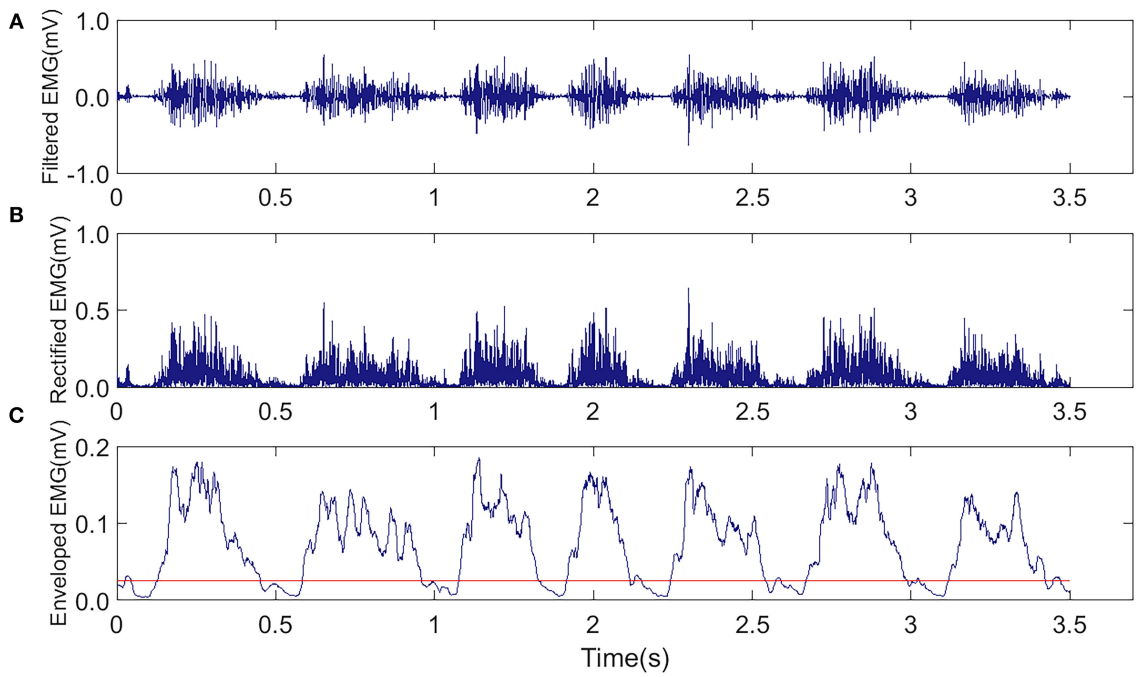

FIGURE 4 | Representative EMG trials were captured from the MG muscle in the AF side of a rat during the treadmill running in the FAT-C group. **(A)** Raw EMG after band-pass filtering (60–2,000 Hz). **(B)** Rectified EMG. **(C)** Enveloped EMG, the red line was the threshold of EMG bursts.

The recorded EMG signals went through visual inspection for removing motion artifacts. Then, the filtered raw EMG signals were further rectified (**Figure 4B**). Moving average window with a length of 25 ms was applied to obtain the envelope of the rectified EMG (**Figure 4C**). The onset and end of a burst duration related to muscle contraction were identified by the threshold (**Figure 4C**, red line), which was defined as the mean value of the enveloped EMG plus 1.5 standard deviations during the resting period (Li et al., 2013).

The EMG signals were displayed in real-time for monitoring the quality and imported to the computer for storage through the MATLAB GUI via the Plexon Control and Server software

(OmniPlexVersion 1.16.1, Plexon Inc., USA) supplied by MATLAB Online Client Development Kit (Plexon Inc., USA). The GUI-based software also visualized the MPF drop rate by calculating the following:

$$MPF = \frac{\int_0^\infty f \bullet s(f)\, df}{\int_0^\infty s(f)\, df} \quad (1)$$

where *s(f)* was the power spectrum density of the EMG signal. The *MPF* value was calculated every 4 s during treadmill training, which was sufficient and stable to represent the change of muscle fatigue.

The *MPF drop rate* was defined as (Li et al., 2011),

$$MPF\ drop\ rate = \frac{baselineMPF - runningMPF}{baselineMPF} \cdot 100\% \quad (2)$$

where the *baseline MPF* was the average *MPF* values in the first 20 s in the 30 min treadmill training. The *running MPF* was the *MPF* values calculated based on the EMG of the target hind limb during treadmill training. Once the *MPF drop rate* exceeded a preset threshold, the software triggered an audio alarm.

Training Protocol

Different rehabilitation interventions were delivered to the three groups from day 2 to day 14 post-stroke. No rehabilitation training was conducted for the CTRL group. For the FOR-T group, the rats were forced to run on the treadmill at a speed of 16 m/min with a duration of 30 min each day without rest (Sun et al., 2014; Chen et al., 2015; Rezaei et al., 2017). If the rats stayed at the end of the treadmill track and failed to catch up with the treadmill, the experimenters would give gentle pushes in the back of rats to force them to continue the running.

For the FAT-C group, the MPF drop rate of the AF hind limb was monitored by the fatigue-controlled system during the treadmill training. Once the MPF drop rate exceeded the threshold, the treadmill would be stopped, and a 3 min rest was applied to the rat, as 3 min rest was enough to ease the fatigue (Carroll et al., 2017). The speed of the treadmill was 16 m/min, and the accumulated running duration was 30 min/day for the FAT-C group. In this work, the fatigue level of the AF hind limb was adopted, with the main purpose to monitor the usage of the paretic hind limb and to minimize the compensatory effects in the UN hind limb (Pin-Barre and Laurin, 2015). A moderate training intensity achieved better motor function recovery in post-stroke rehabilitation, and the MG MPF drop rate was around 11% during moderate treadmill training (Li et al., 2013), so an 11% MPF drop rate was used as the fatigue level threshold of FAT-C group. Three rats (FOR-T: $n = 2$, FAT-C: $n = 1$) dropped out because of EMG electrodes broken during treadmill training, and two rats in the CTRL group dropped out due to severe hemorrhage during day 2 to day 5.

Before collecting EMG, we first checked the noise level of the EMG in both the time and frequency domains to ensure the close connection between the recording headstage and the electrode connector on the head of a rat during training. We also fastened the connection with tape to minimize the motion artifacts.

Evaluation

In this study, the mNSS was applied to evaluate the effects of fatigue-controlled training on post-stroke motor function recovery. The symmetry index (SI) of hind limbs based on EMG was used to evaluate the balance during running. The expression of protein NFL in the striatum was measured to explore the degree of axonal plasticity after the 13 day rehabilitative interventions.

Modified Neurological Severity Score

The mNSS has been used to assess the neurologic deficits of stroke rats (Schaar et al., 2010; Liu et al., 2013), based on behavioral tests. Assessments were conducted by an experimenter blinded to the training protocol and group information of the rats from day 2 to day 14 before daily rehabilitation intervention. Neurologic function was graded on a scale of 0–18, with 0 indicating normal neurologic function and 18 maximum functional deficits (Liu et al., 2013). The mNSS was further decomposed into motor (muscle status and abnormal movement, maximum 6), sensory (visual, tactile and proprioceptive, maximum 2), beam balance (maximum 6), and reflexes/abnormal movements (maximum 4) (Schaar et al., 2010).

Symmetry Index

The SI was used to quantify the balance function between the two hind limbs during the running on the treadmill by EMG (Li et al., 2011). It was calculated by the burst duration of the enveloped EMG on the AF and UN side muscles during treadmill training:

$$SI = \frac{BurstDuration_{AF} - BurstDuration_{UN}}{BurstDuration_{AF} + BurstDuration_{UN}} \cdot 200\% \quad (3)$$

When SI was zero, it represented a perfect balance between the hind limbs. In contrast, a negative SI that represented the UN hind limb showed a longer burst duration than the AF hind limb, vice versa.

Expression Level of Neurofilament-Light in the Striatum

The rehabilitative effects were also evaluated by the level of neurofilaments in the brain tissue after the treadmill training. Neurofilaments are elastic and fibrous proteins (Mages et al., 2018) and are highly related to regeneration and plasticity in axons (Yuan et al., 2012; Bragina and Conti, 2018). In this study, the expression level of NFL in the striatum was evaluated as a biomarker for the axonal plasticity, as the NFL was the backbone of the neurofilaments (Gaetani et al., 2019) and the striatum was the lesion area after ICH (Joseph et al., 2016).

The rats were killed at day 14 post-stroke. The tissue preparation and Western blot analysis were conducted according to the protocol in the previous study (Mages et al., 2018). Four rats dropped out due to blur boundaries of the striatum (CTRL: $n = 2$, FOR-T: $n = 1$, and FAT-C: $n = 1$). Twenty-four rats were used in this test (CTRL: $n = 7$, FOR-T: $n = 8$, and FAT-C: $n = 9$). After transcardial perfusion with saline, the brain tissue was removed. We extracted the striatum from both the hemispheres. These specimens were homogenized and lysed in lysis solution (P0013B, radioimmunoprecipitation assay lysis buffer, Beyotime,

China) with protease inhibitor cocktail (04693132001, complete inhibitor cocktail, Roche, USA) on ice. The lysate was then centrifugated at 13,000 revolutions per minute at 4°C for 10 min. The supernatant was mixed with loading buffer and denatured at 95°C for 5 min. The proteins were separated through 5% spacer gel and 10% separation gel at 100 and 120 V, respectively. Then proteins were transferred to the polyvinylidene fluoride membrane at 200 mA for 2 h. After that, the membrane was blocked by bovine serum albumin for 30 min and incubated with primary antibodies for NFL and glyceraldehyde-3-phosphate dehydrogenase (GAPDH) (NFL: 1:1,000, C28E10; GAPDH: 1:1,000, D16H11, Cell Signaling Technology, USA) at 4°C overnight and incubated with secondary antibody for 2 h at room temperature. The proteins were detected by Tanon software (TanonImage, V1.00, China) using the enhanced chemiluminescent kit (UB279013, Thermo Scientific, USA). The relative protein expression was analyzed with Image J software (1.43u, National Institutes of Health, USA) and controlled with the corresponding expression level of GAPDH.

Statistical Analysis

The normality test was performed on all data samples by the Kolmogorov–Smirnov test with a significant level of 0.05, and all data samples had normal distributions ($P > 0.05$). Differences in the MPF drop rate between the FOR-T and FAT-C groups were evaluated using a two-way analysis of variance (ANOVA). The intragroup changes of MPF drop rate at different time points and intergroup differences of MPF drop rate at the same time point were evaluated using one-way ANOVA followed by *post hoc* Bonferroni tests. Behavioral scores among the three groups were evaluated by two-way analysis of covariance (ANCOVA). The intragroup changes of behavioral scores at different time points and intergroup differences of behavioral scores at the same time point were evaluated using one-way ANOVA and one-way ANCOVA, respectively, followed by *post hoc* Bonferroni tests. The covariate was the behavioral score on day 2 post-stroke to exclude the possible deviations of initial motor impairment among the groups. Two-way ANCOVA evaluated the differences of SI between the FOR-T and FAT-C groups, and the intragroup differences were evaluated through one-way ANOVA followed by *post hoc* Bonferroni tests. The covariate was the SI on day 2 post-stroke to exclude the possible deviations of the initial ability of hind limb balance between the groups. The protein level of NFL among the three groups was investigated by one-way ANOVA followed by *post hoc* Bonferroni tests. $P < 0.05$ was adopted as a statistically significant level in this study. Significant levels of $P<0.005$ and <0.001 were also indicated. All statistical analyses were performed using SPSS (version 20, IBM, USA).

RESULTS

Electromyography Mean Power Frequency Drop Rate During Treadmill Training

In this work, the fatigue level was monitored through the EMG MPF drop rate during treadmill training in both the FOR-T and FAT-C groups. The representative trials on the MPF drop rates paired with EMG signals obtained in the FOR-T and FAT-C groups are shown in **Figures 5A**,**B,** respectively. **Figure 6** shows the daily MPF drop rates of both the hind limbs in the FOR-T and FAT-C groups. **Table 1** summarizes the mean values and 95% confidence intervals of the MPF drop rates in **Figure 6** and the results of two-way ANOVA with effect sizes (EFs), concerning the factors of timepoint and group. The probabilities for the MPF drop rate varying over the time in each group and those for the intergroup comparison on each different timepoints analyzed by one-way ANOVA are also included in **Table 1**.

In the FOR-T group, the MPF drop rate kept increasing from the beginning of the running and exceeded 11% of the initial MPF value after about 10 min. The MPF drop rate reached a plateau and kept around 18% till the end, as shown in **Figure 5A**. On the other hand, the rats in the FAT-C group would take a 3 min rest

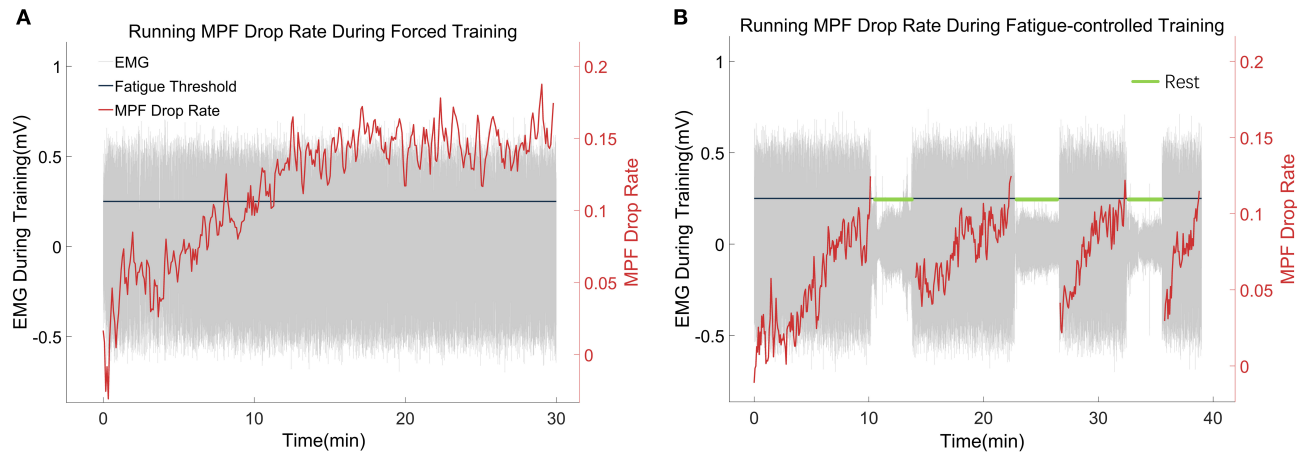

FIGURE 5 | (A,B) Representative trials of the MPF drop rate during treadmill training in the FOR-T group and FAT-C groups. The red lines were real-time MPF drop rates. The gray parts were EMG thumbnails, and the amplitude around ±0.5 mV stood for scuttle, while the amplitude around 0 mV represented the 3 min rest. The black line was the MPF threshold for the FAT-C group.

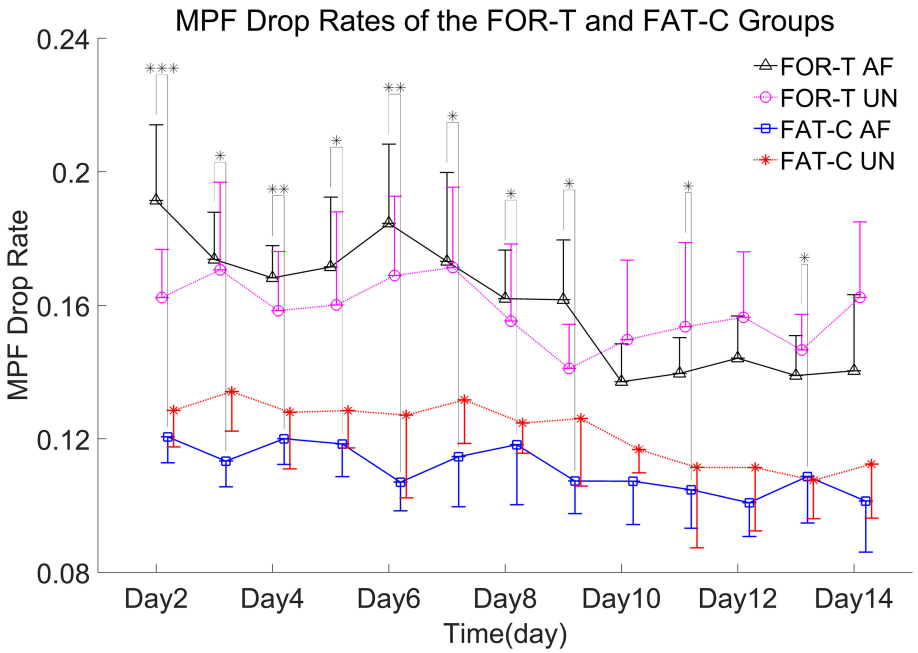

FIGURE 6 | MPF drop rates of the AF/UN hind limbs in the FOR-T and FAT-C groups from day 2 to day 14 post-stroke. Values were represented by mean and 0.5*SD (error bars) at each time point. Significant differences between the MPF drop rates in the AF hind limb of FAT-C and FOR-T groups were indicated by "*". Significant levels were indicated as 1 superscript for <0.05, 2 superscripts for <0.005, and 3 superscripts for <0.001.

once their MPF drop rate exceeded 11% and then continue the running. The MPF drop rate was reduced after the intermittent rest and kept increasing after training started again, as shown in **Figure 5B**. **Figure 6** demonstrated that the MPF drop rates varied significantly with respect to the time point and group factors (two-way ANOVA, time point: $P = 0.006$, EF $= 0.070$, group: $P = 0.006$, EF $= 0.295$, **Table 1**). For the FOR-T AF hind limb group, a significant reduction in the MPF drop rate was observed over the time points (one-way ANOVA, $P = 0.005$, EF $= 0.227$, **Table 1**). There was no significant MPF drop rate variation in other groups. Significant MPF drop rate differences were found from day 2 to day 13 (one-way ANOVAs, $P \leq 0.037$, EF ≥ 0.236, **Table 1**) among the AF and UN hind limbs of the FAT-C and FOR-T groups. The *post hoc* results indicated that the FOR-T AF group demonstrated a significantly higher MPF drop rate compared with the FAT-C AF group from day 2 to day 9 (one-way ANOVAs, $P \leq 0.02$, EF ≥ 0.262, Bonferroni *post hoc* tests $P \leq 0.048$, **Table 1**). In contrast, on day 10 and day 12, a significantly higher MPF drop rate was found in the FOR-T UN group compared with that in the FAT-C AF group (one-way ANOVAs, $P \leq 0.018$, EF ≥ 0.237, Bonferroni *post hoc* tests $P \leq 0.025$, **Table 1**).

Behavioral Scores

The behavioral tests were conducted from day 2 to day 14 post-stroke. In this study, ICH resulted in sensorimotor impairments captured by the motor, sensory, and beam balance assessments in the mNSS. The comparisons on the behavior scores of the CTRL, FOR-T, and FAT-C groups during the rehabilitation are shown in **Figure 7**. In relation to **Figure 7**, the detailed probabilities of the comparisons by two-way ANCOVA on the time point and group factors, one-way ANOVA in each group over the timepoint, and one-way ANCOVA of different groups at the same time point are summarized in **Table 2**.

Overall Modified Neurological Severity Score

Figure 7A shows the variations of the overall mNSS for the CTRL, FOR-T, and FAT-C groups over the time points. Two-way ANCOVA suggested that the overall mNSS varied significantly with respect to the time point and group factors (two-way ANCOVA, timepoint: $P = 0.000$, EF $= 0.576$, group: $P = 0.000$, EF $= 0.456$, **Table 2**). The CTRL group showed a significant reduction in mNSS since day 7 (one-way ANOVA, $P = 0.000$, EF $= 0.433$, Bonferroni *post hoc* test $P \leq 0.021$, **Table 2**). For the FOR-T and FAT-C groups, the significant reduction in mNSS appeared since day 5 (one-way ANOVA, $P = 0.000$, EF $= 0.612$, Bonferroni *post hoc* tests $P \leq 0.011$, **Table 2**) and day 4 (one-way ANOVA, $P = 0.000$, EF $= 0.692$, Bonferroni *post hoc* tests $P \leq 0.000$, **Table 2**). The FAT-C group showed significantly lower mNSS compared with the CTRL group (day 3 to day 14, one-way ANCOVAs, $P \leq 0.003$, EF ≥ 0.286, Bonferroni *post hoc* tests, $P \leq 0.005$, **Table 2**) and the FOR-T group (day 4, day 8, day 10 to day 14, one-way ANCOVAs, $P \leq 0.003$, EF ≥ 0.286, Bonferroni *post hoc* tests, $P \leq 0.042$, **Table 2**). The FOR-T group showed significantly lower mNSS compared with the CTRL group (day 6 to day 14, one-way ANCOVAs, $P \leq 0.000$, EF ≥ 0.413, Bonferroni *post hoc* tests, $P \leq 0.030$, **Table 2**).

TABLE 1 | Comparison of the MPF drop rate with respect to the independent factors of the time point and group.

Time point (Day)	MPF drop rate, mean (95% confidence interval)				One-way ANOVA, *P*-value (EF)	Two-way ANOVA, *P*-value (EF)		
	FAT-C	FOR-T	FAT-C	FOR-T		Time point	Group	Time point*Group
	AF		UN					
Day 2	0.121 (0.099–0.142)	0.191 (0.168–0.214)	0.128 (0.105–0.152)	0.162 (0.139–0.185)	0.000*** (0.515)	0.006* (0.070)	0.006* (0.295)	0.990 (0.047)
Day 3	0.113 (0.084–0.143)	0.174 (0.146–0.201)	0.134 (0.105–0.164)	0.171 (0.145–0.196)	0.011* (0.376)			
Day 4	0.120 (0.099–0.141)	0.168 (0.151–0.186)	0.128 (0.107–0.149)	0.158 (0.139–0.178)	0.003** (0.391)			
Day 5	0.118 (0.091–0.146)	0.171 (0.147–0.196)	0.128 (0.101–0.156)	0.160 (0.133–0.188)	0.020* (0.275)			
Day 6	0.107 (0.076–0.138)	0.193 (0.162–0.224)	0.127 (0.095–0.160)	0.169 (0.138–0.200)	0.001** (0.391)			
Day 7	0.115 (0.086–0.143)	0.173 (0.147–0.199)	0.132 (0.103–0.160)	0.171 (0.144–0.198)	0.008* (0.285)			
Day 8	0.118 (0.095–0.141)	0.162 (0.140–0.184)	0.125 (0.102–0.148)	0.155 (0.132–0.178)	0.017* (0.262)			
Day 9	0.107 (0.086–0.129)	0.162 (0.140–0.183)	0.126 (0.105–0.148)	0.141 (0.120–0.163)	0.007* (0.309)			
Day 10	0.107 (0.086–0.129)	0.137 (0.118–0.156)	0.117 (0.095–0.138)	0.150 (0.13–0.168)	0.018* (0.237)			
Day 11	0.105 (0.077–0.132)	0.140 (0.115–0.164)	0.111 (0.084–0.139)	0.154 (0.128–0.179)	0.037* (0.236)			
Day 12	0.101 (0.078–0.124)	0.144 (0.123–0.166)	0.111 (0.088–0.134)	0.156 (0.135–0.178)	0.003** (0.368)			
Day 13	0.109 (0.091–0.126)	0.139 (0.122–0.156)	0.108 (0.090–0.125)	0.147 (0.124–0.169)	0.009* (0.357)			
Day 14	0.112 (0.070–0.153)	0.140 (0.107–0.174)	0.112 (0.079–0.146)	0.162 (0.133–0.192)	0.097 (0.265)			
One-way ANOVA, *P*-value (EF)	0.844 (0.074)	0.005* (0.227)	0.843 (0.074)	0.969 (0.044)				

Differences with statistical significance are marked with "" (two-way ANOVA, one-way ANOVA).). Significant levels were indicated as 1 superscript for <0.05, 2 superscripts for <0.005, and 3 superscripts for <0.001.*

Motor Subscore

The motor subscore variations of the CTRL, FOR-T, and FAT-C groups during the rehabilitation are shown in **Figure 7B**. Two-way ANCOVA illustrated significant time point effect and group effect on motor subscore among the three groups (two-way ANCOVA, timepoint: $P = 0.000$, EF $= 0.271$, group: $P = 0.000$, EF $= 0.118$, **Table 2**). No significant motor subscore reduction was found in the CTRL group (one-way ANOVA, $P = 0.120$, EF $= 0.126$, **Table 2**). For the FOR-T group, a significant reduction in motor subscore was observed since day 6 (one-way ANOVA, $P = 0.000$, EF $= 0.416$, Bonferroni *post hoc* tests $P \leq 0.022$, **Table 2**). For the FAT-C group, a significant motor score reduction was observed since day 7 (one-way ANOVA, $P = 0.000$, EF $= 0.365$, Bonferroni *post hoc* tests $P \leq 0.006$, **Table 2**). The CTRL group showed significantly higher scores compared with the FAT-C group (day 11 to day 14, one-way ANCOVAs, $P \leq 0.005$, EF ≥ 0.282, Bonferroni *post hoc* tests $P \leq 0.006$, **Table 2**) and the FOR-T group (day 11 to day 14, one-way ANCOVAs, $P \leq 0.005$, EF ≥ 0.282, Bonferroni *post hoc* tests, $P \leq 0.025$, **Table 2**).

Beam Balance Subscore

The trends of beam balance subscore in the CTRL, FOR-T, and FAT-C groups from day 2 to day 14 are presented in **Figure 7C**. The CTRL group showed significantly lower baseline beam balance subscores compared with the FAT-C group (one-way ANOVA, $P = 0.006$, EF $= 0.253$, Bonferroni *post hoc* tests, $P = 0.007$) and the FOR-T group (one-way ANOVA, $P = 0.006$, EF $= 0.253$, Bonferroni *post hoc* tests, $P = 0.034$). Significant timepoint effect and group effect on beam balance subscores of the three groups (two-way ANCOVA, timepoint: $P = 0.000$, EF $= 0.387$, group: $P = 0.000$, EF $= 0.308$, **Table 2**) were observed. For the CTRL group, a significant reduction in beam

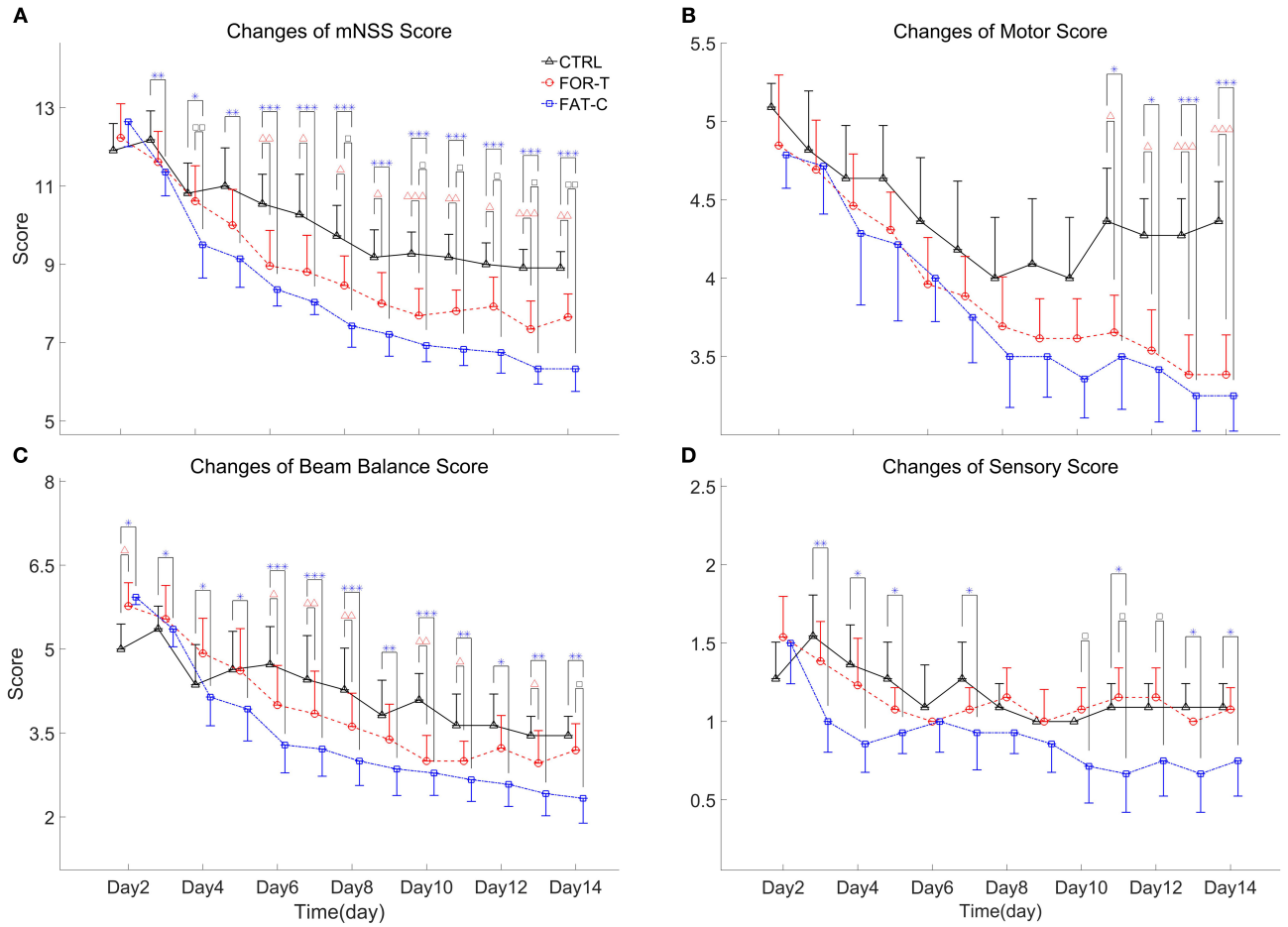

FIGURE 7 | Full mNSS **(A)** and the sub-mNSS on the motor **(B)**, beam balance **(C),** and sensory **(D)** scores for CTRL, FOR-T, and FAT-C groups from day 2 to day 14 post-stroke were presented as mean value with 0.5*SD (error bar). Significant differences between CTRL and FOR-T groups were indicated by "Δ" and the significant differences between the CTRL and the FAT-C groups were indicated by "*". Significant differences between the FOR-T and the FAT-C groups were indicated by "□". Significant levels were indicated as 1 superscript for <0.05, 2 superscripts for <0.005, and 3 superscripts for <0.001.

balance subscore was found since day 9 (one-way ANOVA, $P = 0.000$, EF $= 0.315$, Bonferroni *post hoc* tests, $P \leq 0.004$). The significant score reduction appeared since day 6 in the FOR-T group (one-way ANOVA, $P = 0.000$, EF $= 0.417$, Bonferroni *post hoc* tests $P \leq 0.009$). The FAT-C group showed a significant reduction in the beam balance subscore since day 4 (one-way ANOVA, $P = 0.000$, EF $= 0.486$, Bonferroni *post hoc* tests, $P \leq 0.034$, **Table 2**). The FAT-C group exhibited significantly lower scores compared with the CTRL group (day 3 to day 14, one-way ANCOVAs, $P \leq 0.023$, EF ≥ 0.2, Bonferroni *post hoc* tests $P \leq 0.046$, **Table 2**) and the FOR-T group (day 14, one-way ANCOVA, $P = 0.002$, EF $= 0.334$, with Bonferroni *post hoc* tests, $P = 0.026$, **Table 2**). The FOR-T group showed significantly lower scores compared with the CTRL group (day 6 to day 13, except day 9 and day 12, one-way ANCOVAs, $P \leq 0.001$, EF ≥ 0.339, Bonferroni *post hoc* tests, $P \leq 0.045$, **Table 2**).

Sensory Subscore

The variations of sensory subscore in the CTRL, FOR-T, and FAT-C groups during rehabilitation training are shown in **Figure 7D**. Two-way ANCOVA revealed significant time point effect and group effect on the three groups (two-way ANCOVA, timepoint: $P = 0.000$, EF $= 0.084$, group: $P = 0.000$, EF $= 0.166$, **Table 2**). The CTRL group showed a significant reduction in sensory subscore on day 9 and day 10 (one-way ANOVA, $P = 0.007$, EF $= 0.188$, Bonferroni *post hoc* tests $P \leq 0.019$, **Table 2**). No significant sensory subscore reduction was found in FOR-T and FAT-C groups (one-way ANOVA, $P > 0.05$, **Table 2**). The FAT-C group exhibited significantly lower sensory subscores compared with the CTRL group (day 3 to day 5, day 7, day 11, day 13, and day 14, one-way ANCOVAs, $P \leq 0.034$, EF ≥ 0.181, Bonferroni *post hoc* tests, P$\leq$0.036, **Table 2**) and the FOR-T group (day 10 to day 12, one-way ANCOVAs, $P \leq 0.027$, EF ≥ 0.203, Bonferroni *post hoc* tests, $P \leq 0.042$, **Table 2**).

TABLE 2 | Comparison of behavior scores with respect to the independent factors of the timepoint and group, behavior scores on day 2 as covariate.

	One-way ANCOVA, *P*-value (EF)											
Behavior test	**mNSS**			**Motor**			**Beam Balance**			**Sensory**		
Group / Time point	**CTRL**	**FOR-T**	**FAT-C**	**CTRL**	**FOR-T**	**FAT-C**	**CTRL**	**FOR-T**	**FAT-C**	**CTRL**	**FOR-T**	**FAT-C**
Day 3		0.002**(0.305)			0.937(0.004)			0.023*(0.2)			0.003**(0.286)	
Day 4		0.003**(0.286)			0.738(0.018)			0.022*(0.201)			0.021*(0.203)	
Day 5		0.001**(0.323)			0.531(0.037)			0.007*(0.253)			0.017*(0.213)	
Day 6		0.000***(0.498)			0.464(0.044)			0.000***(0.438)			0.593(0.030)	
Day 7		0.000***(0.413)			0.437(0.047)			0.000***(0.452)			0.034*(0.181)	
Day 8		0.000***(0.517)			0.314(0.066)			0.000***(0.463)			0.113(0.120)	
Day 9		0.000***(0.430)			0.124(0.115)			0.006*(0.262)			0.386(0.054)	
Day 10		0.000***(0.587)			0.081(0.137)			0.000***(0.389)			0.018*(0.209)	
Day 11		0.000***(0.560)			0.005*(0.282)			0.001**(0.339)			0.007*(0.266)	
Day 12		0.000***(0.501)			0.004**(0.295)			0.008*(0.26)			0.027*(0.203)	
Day 13		0.000***(0.651)			0.000***(0.464)			0.001**(0.342)			0.008*(0.258)	
Day 14		0.000***(0.641)			0.000***(0.501)			0.002**(0.334)			0.023*(0.210)	
One-way ANOVA, *P*-value (EF)	0.000*** (0.433)	0.000*** (0.612)	0.000*** (0.692)	0.120 (0.126)	0.000*** (0.416)	0.000*** (0.365)	0.000*** (0.315)	0.000*** (0.417)	0.000*** (0.486)	0.007* (0.188)	0.143 (0.103)	0.304 (0.081)
Two-way ANOVA, *P*-value (EF)	**Time point**											
	0.000***(0.576)			0.000***(0.271)			0.000***(0.387)			0.000***(0.084)		
	Group											
	0.000***(0.456)			0.000***(0.118)			0.000***(0.308)			0.000***(0.166)		
	Time point*Group											
	0.589(0.046)			0.535(0.048)			0.49(0.05)			0.722(0.041)		

Differences with statistical significance are marked with "" (two-way ANCOVA, one-way ANCOVA, one-way ANOVA). Significant levels were indicated as 1 superscript for <0.05, 2 superscripts for <0.005, 3 and superscripts for <0.001.*

Symmetry Index

The trends of SI in the FOR-T and FAT-C groups during treadmill training are shown in **Figure 8**. **Table 3** shows the two-way ANCOVA results of SI and predicted EFs, with independent factors of time point and group. The probabilities for the SI varying over the time in the FOR-T and FAT-C groups analyzed by one-way ANOVA are also included in **Table 3**. The results suggested a significant time point effect and group effect on the SI of the two groups (two-way ANCOVA, timepoint: $P = 0.000$, EF $= 0.224$, group: $P = 0.001$, EF $= 0.065$, **Table 3**). For intragroup analysis, the FAT-C group showed significantly higher SI compared with baseline SI since day 7 ($P = 0.000$, EF $= 0.35$, one-way ANOVA with Bonferroni *post hoc* tests $P \leq 0.046$, **Table 3**). No significant SI variation was observed in the FOR-T group during the training (one-way ANOVA, $P = 0.349$, EF $= 0.121$, **Table 3**).

Neurofilament-light Concentration in the Striatum

The relative protein levels of NFL in the AF and UN striatums of the CTRL, FOR-T, and FAT-C groups measured by Western blot are shown in **Figure 9**. **Table 4** shows the mean values and 95% confidence intervals of the expression level of the NFL and one-way ANOVA probabilities with the predicted EFs on NFL concentration in the AF and UN striatums for the three groups. In the UN striatum, a significantly higher concentration was found in the FAT-C group compared with the CTRL group (one-way ANOVA, $P = 0.005$, EF $= 0.412$, Bonferroni *post hoc* tests $P = 0.004$, **Table 4**). In contrast, for the FOR-T group, no significant difference was found in the FAT-C and CTRL groups (one-way ANOVA, $P = 0.005$, EF $= 0.412$, Bonferroni *post hoc* tests $P > 0.05$, **Table 4**) in the UN side striatum. In the AF striatum, the FAT-C group showed a significantly higher NFL protein level compared with the FOR-T group (one-way ANOVA, $P = 0.021$, EF $= 0.484$, Bonferroni *post hoc* tests, $P = 0.019$, **Table 4**). Compared with the CTRL group, no significant difference was found in the FOR-T and FAT-C groups (one-way ANOVA, $P = 0.021$, EF $= 0.484$, Bonferroni *post hoc* tests, $P > 0.05$, **Table 4**).

DISCUSSION

In this study, the rehabilitation effects of fatigue-controlled training on post-stroke rehabilitation were investigated and evaluated by mNSS, EMG biomarker, and expression level of the NFL. We set up three rehabilitation training strategies, including

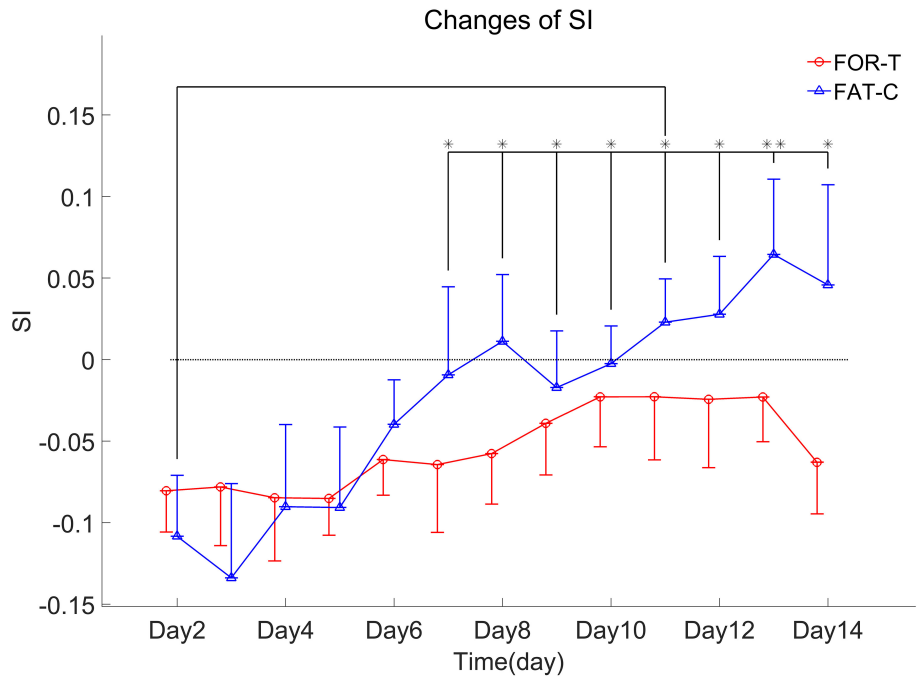

FIGURE 8 | SI values of the FOR-T and FAT-C groups from day 2 to day 14 post-stroke were presented as mean value with 0.5*SD (error bar). Significant differences between day 2 and other time points are indicated by "*". Significant levels were indicated as 1 superscript for <0.05, 2 superscripts for <0.005.

no training, fatigue-controlled training, and forced training. The FAT-C group achieved a significantly lower mNSS and higher NFL level in the striatum than the CTRL and the FOR-T groups did. These results demonstrated that treadmill training with controlled muscular fatigue at a moderate level, i.e., 11% MPF drop in the AF side MG muscle, would lead to better post-stroke recovery in motor function and higher level neuroplasticity in the striatum compared with the traditional forced training.

Electromyography-Based Real-Time Fatigue-Controlled Training

The fatigue-controlled platform could well manage the muscular fatigue level in the FAT-C group based on the monitoring of the EMG MPF drop rates during the running. The real-time fatiguing process in the MG muscles could be captured by the EMG MPF drop rates in both the FAT-C and FOR-T groups during the treadmill training (**Figures 5A,B**). The real-time MPF drop rates showed an increase followed by a plateau in the FOR-T group (**Figure 5A**), which suggested a maximum peripheral fatigue level maintained during the running. In contrast, the fatigue level of the FAT-C group was controlled and alleviated by the 3 min rest, as shown in the real-time MPF drop rate in **Figure 5B**, which demonstrated the fatigue level was controlled during training in the FAT-C group. The MPF drop rate in the AF hind limb of the FAT-C group was maintained at around 11% across sessions, and the significantly lower MPF drop rate was found in the FAT-C group compared with the FOR-T group (**Figure 6**). These cross-sessional MPF drop rates demonstrated that successful fatigue-controlled training was delivered to the FAT-C group.

To our knowledge, although individualized rehabilitative strategies have been attempted in previous studies (Pohl et al., 2002; Lau and Mak, 2011; Chen et al., 2015, 2019), this work was the first study to manage the individual treadmill training according to the real-time fatigue level obtained from the specific muscles of individuals. The fatigue-controlled training method could provide the real-time visualization and evaluation of the fatigue level through the EMG MPF drop rate. It could appropriately adjust the training or rest state for the rats based on the fatigue level. Our method was able to reduce the stress level and accomplished a more precise rehabilitation treatment. In addition, more thresholds of different muscles could be applied in the fatigue-controlled training platform to optimize the strategy for post-stroke rehabilitation in future studies.

Different Fatigue Patterns Found in the Forced Training and Fatigue-Controlled Training Groups

The results that the FAT-C group outperformed the FOR-T group implied that individual training strategies possibly brought different effects on the fatigue of the hind limbs during the treadmill training and resulted in different rehabilitation mechanism adapted by the rats during the motor function recovery. Therefore, we further investigated the patterns of the MPF drop rate in the FAT-C and FOR-T groups.

Lower fatigue level was observed in the FAT-C group compared with the FOR-T group from day 2 to day 14

TABLE 3 | Comparison of SI with respect to the independent factors of the time points and groups, SI on day 2 as covariate.

Time point	SI, mean (95% confidence interval)		One-way ANCOVA, *P*-value (EF)	Two-way ANCOVA, *P*-value (EF)		
	FOR-T	FAT-C		Time point	Group	Time point*Group
Day 2	−0.0804 (−0.1432 to −0.0176)	−0.108 (−0.184 to −0.032)				
Day 3	−0.0781 (−0.1382 to −0.0179)	−0.134 (−0.198 to −0.070)	0.245 (0.217)	0.000*** (0.224)	0.001** (0.065)	0.246 (0.077)
Day 4	−0.0847 (−0.1443 to −0.0250)	−0.09 (−0.160 to −0.021)	0.862 (0.003)			
Day 5	−0.0799 (−0.1145 to −0.0452)	−0.091 (−0.151 to −0.031)	0.729 (0.010)			
Day 6	−0.0613 (−0.0979 to −0.0246)	−0.04 (−0.104 to 0.025)	0.233 (0.116)			
Day 7	−0.063 (−0.1161 to −0.0098)	−0.009 (−0.069 to 0.051)	0.207 (0.104)			
Day 8	−0.0576 (−0.1053 to −0.0099)	0.011 (−0.049 to 0.071)	0.063 (0.226)			
Day 9	−0.0391 (−0.0844 to 0.0063)	−0.017 (−0.077 to 0.043)	0.550 (0.024)			
Day 10	−0.0228 (−0.0667 to 0.0211)	−0.002 (−0.063 to 0.058)	0.542 (0.025)			
Day 11	−0.0228 (−0.0823 to 0.0368)	0.023 (−0.037 to 0.083)	0.249 (0.094)			
Day 12	−0.0243 (−0.0888 to 0.0402)	0.028 (−0.036 to 0.092)	0.238 (0.105)			
Day 13	−0.0229 (−0.0737 to 0.0279)	0.064 (−0.005 to 0.134)	0.051 (0.329)			
Day 14	−0.063 (−0.1214 to −0.0045)	0.046 (−0.030 to 0.122)	0.083 (0.297)			
One-way ANOVA, *P*-Value (EF)	0.349 (0.121)	0.000*** (0.35)				

Differences with statistical significance are marked with "" (two-way ANCOVA, one-way ANCOVA, one-way ANOVA). Significant levels are indicated as 2 superscripts for <0.005, 3 superscripts for <0.001.*

(**Figure 6**), and the decrease trends of training-induced fatigue were found in both the hind limbs of the FAT-C and FOR-T groups (**Figure 6**). For the FAT-C group, lower MPF drop rates were found in the AF hind limb compared with the UN hind limb (**Figure 6**) throughout the rehabilitation interventions. However, for the FOR-T group, lower MPF drop rates were found in the UN hind limb compared with the AF hind limb from day 2 to day 9 (**Figure 6**).

In the FAT-C group, the fatigue was controlled at a moderate level from day 2 to day 14. It was possible that the rats in the FAT-C group would prefer to use the UN hind limb when they were at a moderate fatigue level. In post-stroke moderate-intensity training, a less fatigue-related decrease in median frequency of EMG was also observed in humans at the paretic side compared with the non-paretic side during the same intensity voluntary contractions and locomotor activity (Riley and Bilodeau, 2002).

In contrast, in the FOR-T group, the MPF drop rate of the AF and UN hind limbs reached the maximum peripheral fatigue level because of overloaded usage. In high-intensity treadmill training, lower MPF drop rates were found in the UN hind limb compared with the AF hind limb (Li et al., 2011). This pattern was opposite to the situation found in the FAT-C group. However, lower MPF drop rates were observed in the AF hind limb compared with the UN hind limb from day 10 to day 14 in the FOR-T group. It might be related to increasing tolerance in the 30 min forced treadmill training, and the fatigue could be reduced by exercise-induced strengthening in muscle groups (Dobkin, 2008; Li et al., 2013).

Fatigue-Controlled Training Group Showed Better Motor Function Recovery Compared With the Forced Training Group

The CTRL, FOR-T, and FAT-C groups showed significant motor function recovery at the end of rehabilitation interventions, but the FOR-T and FAT-C groups showed significantly better motor recovery compared with the CTRL group (**Figure 7A**). The FAT-C group showed significantly better motor function compared with the FOR-T group since day 10 (**Figure 7A**). Significant

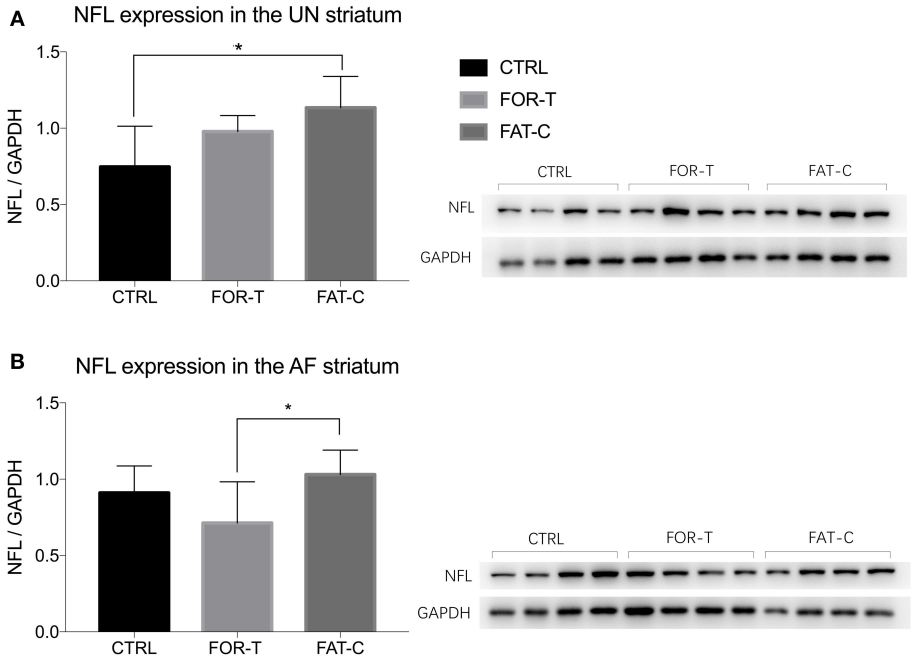

FIGURE 9 | Concentration levels of NFL in the UN **(A)** and AF **(B)** striatum of the CTRL, FOR-T, and FAT-C groups measured by Western blot were presented as mean value with SD (error bar). Significant differences were indicated by "*". Significant levels are indicated as 1 superscript for <0.05.

TABLE 4 | Comparison of NFL concentration on the UN and AF striatum.

Tissue location	Group	NFL concentration, mean (95% confidence interval)	One-way ANOVA, *P*-value (EF)
UN striatum	CTRL	0.747(0.579–0.914)	0.005*(0.412)
	FOR-T	0.978(0.834–1.123)	
	FAT-C	1.134(0.9997–1.270)	
AF striatum	CTRL	0.910(0.800–1.021)	0.021*(0.484)
	FOR-T	0.712(0.557–0.868)	
	FAT-C	1.034(0.878–1.189)	

Differences with statistical significance are marked with "" (one-way ANOVA). Significant levels are indicated as, 1 superscript for <0.05.*

differences were observed in the late stage of rehabilitation intervention in the beam balance subscore (day 14, **Figure 7C**) and the sensory subscore (day 10 to day 12; day 13: $P = 0.055$; day 14: $P = 0.079$, **Figure 7D**). However, no significant difference was found between the FAT-C and FOR-T groups in the motor subscore (**Figure 7B**).

The motor function improvement in the CTRL group could be mainly due to the self-recovery after stroke, which was also observed in other studies (Takamatsu et al., 2010; Sun et al., 2014). The mortality rates in the three groups were 2/11 (CTRL), 0/11 (FOR-T), and 0/11 (FAT-C). The two rats in the CTRL group died in the early period post-stroke. The higher mortality rate implied the importance of post-stroke rehabilitation in the early stage. The behavior scores showed poorer motor function recovery at the early period of rehabilitation in the CTRL group compared with the FOR-T and FAT-C groups, which might account for the higher mortality rate in the CTRL group.

Treadmill training would benefit the motor function recovery, whereas the individual EMG MPF drop rate based fatigue-controlled training showed higher efficiency in motor recovery compared with the traditional forced training. Similar results were reported that the moderate or self-adapted rehabilitation training led to better motor function than high intensity forced training (Pohl et al., 2002; Ke et al., 2011; Lau and Mak, 2011; Li et al., 2013; Chen et al., 2019). Furthermore, recovery plateaus were found in the mNSS of CTRL (day 9 to day 14) and FOR-T (day 10 to day 14) groups but not in the FAT-C group. It might demonstrate that the maximum motor function recovery of the FAT-C group was higher than those of the CTRL and FOR-T groups. The CTRL and FOR-T groups had achieved their maximum motor function recovery, but there still would be a great potential for further motor recovery in the FAT-C group.

Different Fatigue Patterns Led to the Differences in Both Symmetry Index and Motor Function Recovery

Both the FAT-C and FOR-T groups showed negative values of SI at the beginning of rehabilitation and increasing trends along with rehabilitation interventions (**Figure 8**). However, only the FAT-C group achieved significant balance improvement in the late stage of rehabilitation (day 7 to day 14, **Figure 8**). The negative values of SI represented more usage in the UN hind limb and the imbalance of hind limbs post-stroke. The motor deficits were also observed in the behavioral scores (**Figure 7**). The increasing trend of SI implied a more balanced usage of hind

limbs and accompanied by the recovery of beam balance function (**Figure 7C**). The increase of SI paired with motor function recovery was also observed in previous studies (Li et al., 2011, 2013).

A significantly better beam balance subscore was found in the FAT-C group compared with the FOR-T group on day 14 (**Figure 7C**). The plateau of the beam balance subscore was observed in the FOR-T group since day 10, but no plateau of the beam balance subscore was found in the FAT-C group (**Figure 7C**). It implied a potential for further improvement on beam balance subscore in the FAT-C group. The beam balance score was related to the symmetry of limbs and trunk. The significant increase of the SI found in the FAT-C group (**Figure 8**) that indicated the improvement in beam balance in the FAT-C group was mainly related to the recovery of the AF hind limb, whereas the improvement of beam balance in the FOR-T group might be related to the compensation by other limbs or trunk. It was possibly caused by the different fatigue patterns and training strategies. In the FAT-C group, the less fatigue level was found in the AF hind limb compared with the UN hind limb (**Figure 6**). It was possible that moderate fatigue-controlled training promoted more usage on the AF hind limb and led to a better balance. Much more motor recovery was found in speed-dependent treadmill training compared with the steady-speed training in stroke survivors (Pohl et al., 2002; Lau and Mak, 2011). In the FOR-T group, the rats kept running at a maximum peripheral fatigue level (**Figures 5A**, **6**) and could lead to the overloaded usage of the hind limbs. The extreme fatigue might cause the rat to fail to activate the AF hind limb and eventually lead to slower motor function recovery and poorer balance of hind limbs. It also implied that although both the treadmill training groups resulted in motor function recovery, the recovery mechanism might be different. The recovery mechanism of the FOR-T group might mainly be related to the compensation effects of the UN hind limb because overloaded treadmill training did not contribute significantly to the improvement of the balance of locomotion. In contrast, the recovery mechanism of moderate fatigue-controlled training might be related to the improvement of the motor function of AF hind limb and the balance of hind limbs.

Different Training Strategies Caused the Different Neurofilament-Light Concentration and Resulted in Different Motor Function Recovery

Physical training in the subacute post-stroke period facilitated neuron plasticity and rewiring, but overloaded training-induced fatigue might minimize the plasticity. In this study, we found that the concentration of NFL in the UN striatum of the FAT-C group was significantly higher than that in the CTRL group (**Figure 9A**), and the concentration of NFL in the AF striatum of the FAT-C group was significantly higher than that in the FOR-T group (**Figure 9B**).

The increased concentration of NFL in the UN striatum (**Figure 9A**) and better motor function recovery (**Figure 7**) were found in the FOR-T and the FAT-C groups compared with the CTRL group. It might be related to the use-dependent dendritic growth and the compensation effects in the contralesional hemisphere caused by treadmill training. Treadmill training-related repetitive activation of cortical inputs could lead to long-term changes of synaptic plasticity in the related pathway (Zhang et al., 2013) and increase activation of cortico-subcortical networks (Luft et al., 2008), which were regarded as the cellular substrate for motor learning. The previous study also showed that the enhanced motor recovery was associated with significant increases in striatum volume, dendritic arbor in the contralesional striatum (Qin et al., 2014).

More importantly, we found a significantly higher NFL concentration in the FAT-C group compared with the FOR-T group in the AF striatum (**Figure 9B**). In contrast, a lower fatigue level of the AF hind limb (**Figure 6**) and better motor function (**Figure 7**) were found in the FAT-C group compared with the FOR-T group. The results indicated that physical training at a moderate fatigue level during the post-stroke subacute period would facilitate neuron plasticity and rewiring, but overloaded training-induced fatigue might harm the plasticity and lead to a poorer motor function recovery. Simultaneously, the excessive usage of AF hind limb would increase the stress and corticosterone secretion, which would reduce the protein level of the NFL and suppress the plasticity (Cereseto et al., 2006; Zhao et al., 2009). Overreliance on the AF forelimb after unilateral lesions of the forelimb representation area of the rat sensorimotor cortex led to an exaggeration of the initial cortical injury (Humm et al., 1999). So, rehabilitation training with controlled fatigue level in the AF hind limb would benefit the neuroplasticity and improve the efficiency of motor function recovery.

In this study, we measured the concentration of the NFL as a biomarker for post-stroke neuroplasticity. More neuroplasticity related indexes such as long-term depression and long-term potentiation will be included in our future studies to investigate the effects of fatigue-controlled rehabilitation.

CONCLUSION

In this study, the EMG-based real-time fatigue-controlled training platform was established. Our results demonstrated that fatigue-controlled training was the most effective intervention in motor recovery compared to the forced training and the control groups. The EMG activation symmetry in the hind limbs also demonstrated that the treadmill training at a moderate fatigue level would facilitate the motor recovery of the AF hind limb and the balance between the hind limbs. This study also showed that fatigue-controlled training could upregulate the NFL level in the striatum and benefit neuroplasticity after stroke. We extended the understanding of the importance of fatigue-controlled training in rehabilitation after stroke. A training protocol that includes individual fatigue-controlled could be beneficial in both animal studies and clinical trials.

DATA AVAILABILITY STATEMENT

The raw data supporting the conclusions of this article will be made available by the authors, without undue reservation.

ETHICS STATEMENT

The animal study was reviewed and approved by Animal Care Committee of Zhejiang University and the Animal Subjects Ethics Sub-committee, Hong Kong Polytechnic University.

AUTHOR CONTRIBUTIONS

YX contributed to the experiment design, data collection and analysis, and manuscript drafting. YY and HL contributed to the experiment design and data analysis. SN, YX, WP, and YZ contributed to the experiment design and manuscript editing. SZ and XH conceived the study and coordinated the whole project, including the experiment design, system design, and manuscript drafting. All authors contributed to the article and approved the submitted version.

FUNDING

This project was financially supported by the Chinese National Key R&D Program (2017YFC1308501, 2017YFE9125500) and the National Natural Science Foundation of China (81771959, 31627802, 31371001).

ACKNOWLEDGMENTS

The authors thank Prof. Jingsong Li and Dr. Tianshu Zhou for technical supports and Christine Luk, Peter Kun, Yonghong Sun, Chaonan Yu, and Jiacheng Zhang for animal experiments.

REFERENCES

Andrews, A. W., Li, D., and Freburger, J. K. (2015). Association of rehabilitation intensity for stroke and risk of hospital readmission. *Phys. Ther.* 95, 1660–1667. doi: 10.2522/ptj.20140610

Bai, Y., Hu, Y., Wu, Y., Zhu, Y., He, Q., Jiang, C., et al. (2012). A prospective, randomized, single-blinded trial on the effect of early rehabilitation on daily activities and motor function of patients with hemorrhagic stroke. *J Clin Neurosci.* 19, 1376–1379. doi: 10.1016/j.jocn.2011.10.021

Barroso, F. O., Alessandro, C., and Tresch, M. C. (2019). Adaptation of muscle activation after patellar loading demonstrates neural control of joint variables. *Sci. Rep.* 9:20370. doi: 10.1038/s41598-019-56888-9

Bell, J. A., Wolke, M. L., Ortez, R. C., Jones, T. A., and Kerr, A. L. (2015). Training intensity affects motor rehabilitation efficacy following unilateral ischemic insult of the sensorimotor cortex in c57bl/6 mice. *Neurorehabil. Neural Repair* 29, 590–598. doi: 10.1177/1545968314553031

Biernaskie, J., Chernenko, G., and Corbett, D. (2004). Efficacy of rehabilitative experience declines with time after focal ischemic brain injury. *J. Neurosci.* 24, 1245–1254. doi: 10.1523/JNEUROSCI.3834-03.2004

Bragina, L., and Conti, F. (2018). Expression of neurofilament subunits at neocortical glutamatergic and gabaergic synapses. *Front. Neuroanat.* 12:74. doi: 10.3389/fnana.2018.00074

Branscheidt, M., Kassavetis, P., Anaya, M., Rogers, D., Huang, H. D., Lindquist, M. A., et al. (2019). Fatigue induces long-lasting detrimental changes in motor-skill learning. *Elife* 8:e40578. doi: 10.7554/eLife.40578.022

Carroll, T. J., Taylor, J. L., and Gandevia, S. C. (2017). Recovery of central and peripheral neuromuscular fatigue after exercise. *J. Appl. Physiol.* 122, 1068–1076. doi: 10.1152/japplphysiol.00775.2016

Cereseto, M., Reinés, A., Ferrero, A., Sifonios, L., Rubio, M., and Wikinski, S. (2006). Chronic treatment with high doses of corticosterone decreases cytoskeletal proteins in the rat hippocampus. *Eur. J. Neurosci.* 24, 3354–3364. doi: 10.1111/j.1460-9568.2006.05232.x

Chen, C. C., Chang, M. W., Chang, C. P., Chang, W. Y., Chang, S. C., Lin, M. T., et al. (2015). Improved infrared-sensing running wheel systems with an effective exercise activity indicator. *PLoS ONE* 10:e122394. doi: 10.1371/journal.pone.0122394

Chen, C. C., Wang, Y. L., and Chang, C. P. (2019). Remarkable cell recovery from cerebral ischemia in rats using an adaptive escalator-based rehabilitation mechanism. *PLoS ONE* 14:e223820. doi: 10.1371/journal.pone.0223820

Chesney, J. A., Kondoh, T., Conrad, J. A., and Low, W. C. (1995). Collagenase-induced intrastriatal hemorrhage in rats results in long-term locomotor deficits. *Stroke* 26, 312–316. doi: 10.1161/01.STR.26.2.312

Cifrek, M., Medved, V., Tonković, S., and Ostojić, S. (2009). Surface emg based muscle fatigue evaluation in biomechanics. *Clin. Biomech.* 24, 327–340. doi: 10.1016/j.clinbiomech.2009.01.010

Cumming, T. B., Thrift, A. G., Collier, J. M., Churilov, L., Dewey, H. M., Donnan, G. A., et al. (2011). Very early mobilization after stroke fast-tracks return to walking: further results from the phase ii avert randomized controlled trial. *Stroke* 42, 153–158. doi: 10.1161/STROKEAHA.110.594598

Dobkin, B. H. (2008). Training and exercise to drive poststroke recovery. *Nat. Clin. Pract. Neurol.* 4, 76–85. doi: 10.1038/ncpneuro0709

Donkor, E. S. (2018). Stroke in the 21(st) century: a snapshot of the burden, epidemiology, and quality of life. *Stroke Res. Treat.* 2018:3238165. doi: 10.1155/2018/3238165

Dromerick, A. W., Lang, C. E., Birkenmeier, R. L., Wagner, J. M., Miller, J. P., Videen, T. O., et al. (2009). Very early constraint-induced movement during stroke rehabilitation (vectors): a single-center rct. *Neurology* 73, 195–201. doi: 10.1212/WNL.0b013e3181ab2b27

Forghani, R., Kim, H. J., Wojtkiewicz, G. R., Bure, L., Wu, Y., Hayase, M., et al. (2015). Myeloperoxidase propagates damage and is a potential therapeutic target for subacute stroke. *J. Cereb. Blood Flow Metab.* 35, 485–493. doi: 10.1038/jcbfm.2014.222

Gaetani, L., Blennow, K., Calabresi, P., Di Filippo, M., Parnetti, L., and Zetterberg, H. (2019). Neurofilament light chain as a biomarker in neurological disorders. *J. Neurol. Neurosurg. Psychiatr.* 90, 870–881. doi: 10.1136/jnnp-2018-320106

Gorelick, P. B. (2019). The global burden of stroke: persistent and disabling. *Lancet Neurol.* 18, 417–418. doi: 10.1016/S1474-4422(19)30030-4

Hendricks, H. T., van Limbeek, J., Geurts, A. C., and Zwarts, M. J. (2002). Motor recovery after stroke: a systematic review of the literature. *Arch. Phys. Med. Rehabil.* 83, 1629–1637. doi: 10.1053/apmr.2002.35473

Humm, J. L., Kozlowski, D. A., Bland, S. T., James, D. C., and Schallert, T. (1999). Use-dependent exaggeration of brain injury: is glutamate involved? *Exp. Neurol.* 157, 349–358. doi: 10.1006/exnr.1999.7061

Hylin, M. J., Kerr, A. L., and Holden, R. (2017). Understanding the mechanisms of recovery and/or compensation following injury. *Neural Plast.* 2017:7125057. doi: 10.1155/2017/7125057

Joseph, M. J., Caliaperumal, J., and Schlichter, L. C. (2016). After intracerebral hemorrhage, oligodendrocyte precursors proliferate and differentiate inside white-matter tracts in the rat striatum. *Transl. Stroke Res.* 7, 192–208. doi: 10.1007/s12975-015-0445-3

Ke, Z., Yip, S. P., Li, L., Zheng, X. X., and Tong, K. Y. (2011). The effects of voluntary, involuntary, and forced exercises on brain-derived neurotrophic factor and motor function recovery: a rat brain ischemia model. *PLoS ONE* 6:e16643. doi: 10.1371/journal.pone.0016643

Kelly, P. J., Furie, K. L., Shafqat, S., Rallis, N., Chang, Y., and Stein, J. (2003). Functional recovery following rehabilitation after hemorrhagic and ischemic stroke. *Arch. Phys. Med. Rehabil.* 84, 968–972. doi: 10.1016/S0003-9993(03)00040-6

Kozlowski, D. A., James, D. C., and Schallert, T. (1996). Use-dependent exaggeration of neuronal injury after unilateral sensorimotor cortex lesions. *J. Neurosci.* 16, 4776–4786. doi: 10.1523/JNEUROSCI.16-15-04776.1996

Lau, K. W., and Mak, M. K. (2011). Speed-dependent treadmill training is effective to improve gait and balance performance in patients with sub-acute stroke. *J. Rehabil. Med.* 43, 709–713. doi: 10.2340/16501977-0838

Li, L., Rong, W., Ke, Z., Hu, X., and Tong, K. Y. (2013). The effects of training intensities on motor recovery and gait symmetry in a rat model of ischemia. *Brain Inj.* 27, 408–416. doi: 10.3109/02699052.2012.750750

Li, L., Rong, W., Ke, Z., Hu, X., Yip, S. P., and Tong, K. Y. (2011). Muscle activation changes during body weight support treadmill training after focal cortical ischemia: a rat hindlimb model. *J. Electromyogr. Kinesiol.* 21, 318–326. doi: 10.1016/j.jelekin.2010.09.008

Liu, Y., Ao, L. J., Lu, G., Leong, E., Liu, Q., Wang, X. H., et al. (2013). Quantitative gait analysis of long-term locomotion deficits in classical unilateral striatal intracerebral hemorrhage rat model. *Behav. Brain Res.* 257, 166–177. doi: 10.1016/j.bbr.2013.10.007

Luft, A. R., Macko, R. F., Forrester, L. W., Villagra, F., Ivey, F., Sorkin, J. D., et al. (2008). Treadmill exercise activates subcortical neural networks and improves walking after stroke: a randomized controlled trial. *Stroke* 39, 3341–3350. doi: 10.1161/STROKEAHA.108.527531

Ma, J., Chen, H., Liu, X., Zhang, L., and Qiao, D. (2018). Exercise-induced fatigue impairs bidirectional corticostriatal synaptic plasticity. *Front. Cell. Neurosci.* 12:14. doi: 10.3389/fncel.2018.00014

MacLellan, C. L., Auriat, A. M., McGie, S. C., Yan, R. H., Huynh, H. D., De Butte, M. F., et al. (2006). Gauging recovery after hemorrhagic stroke in rats: implications for cytoprotection studies. *J. Cereb. Blood Flow Metab.* 26, 1031–1042. doi: 10.1038/sj.jcbfm.9600255

Mages, B., Aleithe, S., Altmann, S., Blietz, A., Nitzsche, B., Barthel, H., et al. (2018). Impaired neurofilament integrity and neuronal morphology in different models of focal cerebral ischemia and human stroke tissue. *Front. Cell. Neurosci.* 12:161. doi: 10.3389/fncel.2018.00161

Murphy, T. H., and Corbett, D. (2009). Plasticity during stroke recovery: from synapse to behaviour. *Nat. Rev. Neurosci.* 10, 861–872. doi: 10.1038/nrn2735

Park, J. W., Bang, M. S., Kwon, B. S., Park, Y. K., Kim, D. W., Shon, S. M., et al. (2010). Early treadmill training promotes motor function after hemorrhagic stroke in rats. *Neurosci. Lett.* 471, 104–108. doi: 10.1016/j.neulet.2010.01.020

Pin-Barre, C., and Laurin, J. (2015). Physical exercise as a diagnostic, rehabilitation, and preventive tool: influence on neuroplasticity and motor recovery after stroke. *Neural Plast.* 2015:608581. doi: 10.1155/2015/608581

Pohl, M., Mehrholz, J., Ritschel, C., and Rückriem, S. (2002). Speed-dependent treadmill training in ambulatory hemiparetic stroke patients: a randomized controlled trial. *Stroke* 33, 553–558. doi: 10.1161/hs0202.102365

Qin, L., Jing, D., Parauda, S., Carmel, J., Ratan, R. R., Lee, F. S., et al. (2014). An adaptive role for bdnf val66met polymorphism in motor recovery in chronic stroke. *J. Neurosci.* 34, 2493–2502. doi: 10.1523/JNEUROSCI.4140-13.2014

Rezaei, S., Agha-Alinejad, H., Molanouri, S. M., Jafari, M., Azevedo, V. F., Naderi, A., et al. (2017). Evaluation of efforts in untrained wistar rats following exercise on forced running wheel at maximal lactate steady state. *J. Exerc. Nutr. Biochem.* 21, 26–32. doi: 10.20463/jenb.2017.0040

Riley, N. A., and Bilodeau, M. (2002). Changes in upper limb joint torque patterns and emg signals with fatigue following a stroke. *Disabil. Rehabil.* 24, 961–969. doi: 10.1080/0963828021000007932

Schaar, K. L., Brenneman, M. M., and Savitz, S. I. (2010). Functional assessments in the rodent stroke model. *Exp. Transl. Stroke Med.* 2:13. doi: 10.1186/2040-7378-2-13

Sun, J., Ke, Z., Yip, S. P., Hu, X. L., Zheng, X. X., Tong, K. Y., et al. (2014). Gradually increased training intensity benefits rehabilitation outcome after stroke by bdnf upregulation and stress suppression. *Biomed Res. Int.* 2014:925762. doi: 10.1155/2014/925762

Takamatsu, Y., Ishida, A., Hamakawa, M., Tamakoshi, K., Jung, C. G., and Ishida, K. (2010). Treadmill running improves motor function and alters dendritic morphology in the striatum after collagenase-induced intracerebral hemorrhage in rats. *Brain Res.* 1355, 165–173. doi: 10.1016/j.brainres.2010.07.070

Wang, L., Wang, Y., Ma, A., Ma, G., Ye, Y., Li, R., et al. (2018). A comparative study of emg indices in muscle fatigue evaluation based on grey relational analysis during all-out cycling exercise. *Biomed Res. Int.* 2018:9341215. doi: 10.1155/2018/9341215

Wangfischer, Y. (2009). *Manual of Stroke Models in Rats*. Boca Raton, FL: CRC Press.

Yang, Y. R., Wang, R. Y., and Wang, P. S. (2003). Early and late treadmill training after focal brain ischemia in rats. *Neurosci. Lett.* 339, 91–94. doi: 10.1016/S0304-3940(03)00010-7

Yuan, A., Rao, M. V., Veeranna, and Nixon, R. A. (2012). Neurofilaments at a glance. *J. Cell Sci.* 125, 3257–3263. doi: 10.1242/jcs.104729

Zhang, Q. W., Deng, X. X., Sun, X., Xu, J. X., and Sun, F. Y. (2013). Exercise promotes axon regeneration of newborn striatonigral and corticonigral projection neurons in rats after ischemic stroke. *PLoS ONE* 8:e80139. doi: 10.1371/journal.pone.0080139

Zhao, Y., Xie, W., Dai, J., Wang, Z., and Huang, Y. (2009). The varying effects of short-term and long-term corticosterone injections on depression-like behavior in mice. *Brain Res.* 1261, 82–90. doi: 10.1016/j.brainres.2008.12.083

Conflict of Interest: The authors declare that the research was conducted in the absence of any commercial or financial relationships that could be construed as a potential conflict of interest.

frontiers in Bioengineering and Biotechnology

ORIGINAL RESEARCH
published: 18 December 2020
doi: 10.3389/fbioe.2020.592637

Verification of Finger Joint Stiffness Estimation Method With Soft Robotic Actuator

Xiang Qian Shi[1†], Ho Lam Heung[1†], Zhi Qiang Tang[1], Kai Yu Tong[1] and Zheng Li[2]**

[1] Department of Biomedical Engineering, The Chinese University of Hong Kong, Shatin, Hong Kong, [2] Department of Surgery, The Chinese University of Hong Kong, Shatin, Hong Kong

Stroke has been the leading cause of disability due to the induced spasticity in the upper extremity. The constant flexion of spastic fingers following stroke has not been well described. Accurate measurements for joint stiffness help clinicians have a better access to the level of impairment after stroke. Previously, we conducted a method for quantifying the passive finger joint stiffness based on the pressure-angle relationship between the spastic fingers and the soft-elastic composite actuator (SECA). However, it lacks a ground-truth to demonstrate the compatibility between the SECA-facilitated stiffness estimation and standard joint stiffness quantification procedure. In this study, we compare the passive metacarpophalangeal (MCP) joint stiffness measured using the SECA with the results from our designed standalone mechatronics device, which measures the passive metacarpophalangeal joint torque and angle during passive finger rotation. Results obtained from the fitting model that concludes the stiffness characteristic are further compared with the results obtained from SECA-Finger model, as well as the clinical score of Modified Ashworth Scale (MAS) for grading spasticity. These findings suggest the possibility of passive MCP joint stiffness quantification using the soft robotic actuator during the performance of different tasks in hand rehabilitation.

Keywords: soft-elastic composite actuator (SECA), SECA-finger modeling, passive joint stiffness, metacarpophalangeal joint, stroke, spasticity

OPEN ACCESS

Edited by:
Le Li,
First Affiliated Hospital of Sun Yat-sen University, China

Reviewed by:
Chuanxin Minos Niu,
Shanghai Jiao Tong University, China
Zhendong Dai,
Nanjing University of Aeronautics and Astronautics, China

****Correspondence:***
Kai Yu Tong
kytong@cuhk.edu.hk
Zheng Li
lizheng@cuhk.edu.hk

[†] These authors have contributed equally to this work

Specialty section:
This article was submitted to Biomechanics, a section of the journal Frontiers in Bioengineering and Biotechnology

Received: *07 August 2020*
Accepted: *03 December 2020*
Published: *18 December 2020*

Citation:
Shi XQ, Heung HL, Tang ZQ, Tong KY and Li Z (2020) Verification of Finger Joint Stiffness Estimation Method With Soft Robotic Actuator. Front. Bioeng. Biotechnol. 8:592637. doi: 10.3389/fbioe.2020.592637

INTRODUCTION

Spasticity, commonly known as a symptom with a broad range of neurological disorders, is frequently found in subjects after stroke. Previous studies indicated that about 40% of subjects with stroke suffer from spasticity (Francisco and McGuire, 2012; Huang and Patton, 2016), leading to a huge burden on those subjects and challenges to the nursing staff (Yi et al., 2013). Finger flexor spasticity, usually characterized by hyper-resistance in the finger joint, which is a result of pathological neuromuscular activation and biomechanical changes in muscles and soft tissues overlying the joint. Distribution and level of these neural and non-neural components may diverge between individual subjects, and it may change during the time course of post stroke (Andringa et al., 2019). In other words, this spasticity increases stiffness of the finger joints and furthermore leads to a decrease of their range-of-motion (ROM), creating severe reduction to hand function (Sadarangani et al., 2017). To treat subjects with spasticity, several different approaches such as local botulinum toxin injection, physical and occupational therapies, electrical neuro stimulation, and

surgical interventions, have been commonly used in clinic. Despite those approaches have shown their effectiveness in clinical spasticity treatments, the mechanisms that underlie and the influences of spasticity on functional movement are still not well understood. Previous clinical studies rarely focused on the changes of passive finger joint stiffness opposing the joint rotation, though it may reflect the spasticity of the finger flexors (Kamper and Rymer, 2000). Hence, management of spasticity includes reliable and accurate assessments of passive finger joint stiffness is needed for better identification of treatment strategies and goals.

However, the only assessments regularly incorporated into neurorehabilitation are through clinical measures (Fugl-Meyer et al., 1975; Gregson et al., 1999), which are typically subjective, labor intensive, and graded on an ordinal scale. Nevertheless, result subjectivity and rater reliability have been continuously questioned by researchers since the measurement is dependent on clinicians' experience (Damiano et al., 2002; Fleuren et al., 2010). Modified Ashworth Scale (MAS), for example, the most popularly used scale has a relatively simple protocol (Blackburn et al., 2002; Mehrholz et al., 2005). Junior clinicians learn the MAS from the instruction first and develop their own standard through their clinical experiences (Park et al., 2017). There are no common standards to train the clinicians. Therefore, it would be satisfied to propose an objective and effective way to assess the spasticity of finger flexors. In contrast, robotic measures offer the possibility for objective, efficient, and descriptive assessments (Lambercy et al., 2012; Maggioni et al., 2016).

The most common clinical examination of spasticity includes assessment of exaggerated tendon tap reflexes by passive muscle stretch. Several rehabilitation instruments have been built in laboratories to quantitatively examine joint resistance to passive stretch. The evaluation of biomechanical joint properties (Nalam and Lee, 2019), such as passive joint stiffness and the range of motion (ROM), is hopefully achieved through an instrument-aided assessment. Rehabilitation robot commonly provides a relatively objective and stable platform for the analysis on the biomechanical behavior of fingers for subjects with stroke and no neurological deficit. Many clinical studies have investigated the passive joint stiffness of the index finger metacarpophalangeal (MCP) joint, due to its prominent role in many hand functions (Minami et al., 1983; Esteki and Mansour, 1996; Kamper et al., 2002; Kuo and Deshpande, 2012). Various mechatronic devices are thereby designed for standalone passive finger joint stiffness measurement after stroke (Milner and Franklin, 1998; Kamper et al., 2006; Yap et al., 2016). These measurements focus on the changes in passive stiffness opposing MCP rotation to further quantify the spasticity of finger flexors. However, due to the bulky size of all components, mechatronic devices are hard to be used to examine the stiffness of other joints across different fingers, e.g., proximal interphalangeal (PIP) joints that the stiffness is comparable to MCP joints after contracture (Prosser, 1996; Tang et al., 2019), in each finger. In addition, current measurements are separated from activities of daily living (ADL) and therapeutic training. Regular joint stiffness measurement as an indication of the performance of finger function during rehabilitation would be ineffective, and thereby only pre-determined training exercises could be offered to subjects regardless of their joint stiffness condition (Kamper et al., 2006). Continuous assessment of finger stiffness would be helpful and valuable to provide information for physiotherapists to adjust the rehabilitation models and formulate timely and accurate treatment plans that are suitable to subjects' condition (Kamper et al., 2006).

Previously, we introduced the first 3D printed soft-elastic composite actuator (SECA) for hand rehabilitation that quantifies stiffness of the impaired fingers (Heung et al., 2020). We further demonstrated the methodology of applying this soft actuator to finger stiffness evaluation using its static models. The accuracy of the models was validated both in free space bending and on phantom fingers. Experimental results showing the joint stiffness of subjects with chronic stroke and no neurological deficit were obtained using the static model, which are supportive to existing clinical measures. However, validation of our method feasibility and compatibility in our previous study (Heung et al., 2020) only involved experiments performed on mannequin hands with different torsion springs with preset stiffness values. It would be necessary to compare the results obtained from our new method with existing ground-truth joint stiffness values based on the well-validated stiffness quantification methods in existing literatures.

In this work, we replicated the standalone stiffness measurement device proposed by Esteki and Mansour (1996) and Kuo and Deshpande (2012) for measuring the passive joint moment and angle for the MCP joint in the index finger. Ground-truth values of MCP joint stiffness would be obtained by taking derivative of the double exponential function-based model for finger kinematics (Esteki and Mansour, 1996; Silder et al., 2007; Deshpande et al., 2011) that fitted with collected joint torque and angle data, which has been the standard procedures in existing literatures of presenting the torque-angle relationship (Milner and Franklin, 1998; Kamper et al., 2006; Yap et al., 2016). Previous studies already showed that torque required to extend the hypertonic MCP joint was nearly linear with respect to the joint angle, thus showing an almost constant rotational stiffness as soon as the effect of joint capsule-ligament complex (CLC) that would increase the passive resistance upon closing to full flexion or extension was not considered (Kamper and Rymer, 2000; Kamper et al., 2003; Kuo and Deshpande, 2012). Accuracy of the mechatronics device we replicated, and the stiffness quantification method, was also already demonstrated in their study with their thirteen subjects (Esteki and Mansour, 1996) and (Kuo and Deshpande, 2012). In our study, eight subjects (four subjects with chronic stroke and four subjects with no neurological deficit) are recruited for the evaluation of MCP joint stiffness in their index fingers using our method and existing standardized method. Results of MCP joint stiffness are compared with each other, as well as the MAS scores, for reflecting the clinical potential of our method. This effort is undertaken with the intent to improve our understanding of the change of finger stiffness during among subjects with different levels of impairment after stroke in an objective manner, together with the expectation of assisting in the guidance of more effective hand rehabilitation training in the future.

SECA-Finger Modeling for Stiffness Evaluation

System Description

We have designed the 3D printed SECA that can actively control flexion and extension of a spastic finger. MCP segment on the SECA corresponds to actuation of the MCP joint of the spastic finger, which joint flexion is controlled on pressurization and extension is controlled on depressurization (Heung et al., 2019). Flex sensor (Flex-point Sensor System, Draper, UT, United States) is placed beneath the MCP segment for measuring the bending angle. Besides, we have developed the SECA-Finger model for predicting the bending performance of SECA on spastic finger, as illustrated in **Figure 1** (Tang et al., 2019; Heung et al., 2020). The influence of spastic fingers to SECA actuation is also addressed by the model, allowing us to obtain indicative results regarding the stiffness of MCP joint.

Static Modeling

Previously, we have already derived the SECA-Finger model that presents the bending performance of SECA on a spastic finger (Heung et al., 2020). As only the joint stiffness due to flexor tone is of our interest, we only consider the joint angle range between the fully extended position and the initial resting position (i.e., $\theta \geq 0$ and $\theta < \theta_0$, θ is the bending angle that θ_m is for the current bending angle of MCP joint and θ_0 is the resting angle of the joint and always less than 90°). To demonstrate the pressure-angle relationship, we have obtained the following equation of (Heung et al., 2020)

$$P = \frac{2w_m aL^2(a + \pi(a+b) + 2r) + EI\theta^2 - kL(\theta - \theta_0)^2}{2L\left(\frac{\pi}{2}\left(\frac{t}{2} + a + b\right)r^2 + eb\left(\frac{t}{2} + a\right) + \frac{eb^2}{2} + \frac{2r^3}{3}\right)\theta} \quad (1)$$

in which a is the actuator wall thickness, b is the actuator internal rectangular height, e is the actuator internal chamber width, r is the actuator internal circular radius, t is the layer thickness, L is the actuator internal chamber length (L_m for MCP segment), w_m is the actuator strain energy density function, P is the input pressure, E is the layer Young's modulus, I is the layer second moment of area, k is the joint stiffness (k_m for MCP joint), θ is the joint angle (θ_m for MCP joint, in radian) (Heung et al., 2020).

Rearranging the analytical model of equation (1) in the region of $\theta \in [0^0, \theta_0]$, the joint stiffness equation is

$$k_m = \frac{A + EI\theta_m^2 - B\theta_m}{L(\theta - \theta_0)^2} \quad (2)$$

which

$$A = 2w_m aL^2(a + \pi(a+b) + 2r)$$

$$B = 2PL\left(\frac{\pi}{2}\left(\frac{t}{2} + a + b\right)r^2 + eb\left(\frac{t}{2} + a\right) + \frac{eb^2}{2} + \frac{2r^3}{3}\right)$$

Furthermore, γ is an empirical coefficient defined for MCP joint angle. The value is set to be 0.7 to avoid reaching singularity (i.e., only small difference between the bending angle of SECA θ and the resting angle of finger joint θ_0) and generating inaccurate results. Therefore, the possible ranges of MCP joint angle and input pressures for stiffness evaluation using equation (2) become

$$\theta_m \in [\theta_{i\_m}, \gamma\theta_{0\_m}], 0 < \gamma < 1 \quad (3)$$

$$P = cutoff, \quad when\ (\theta_m > \gamma\theta_{0\_m}) \quad (4)$$

where θ_{i_m} is the extended MCP joint angle upon wearing of the SECA in a unpressurized state (i.e., $P = 0$ and $\theta_{i\_m} > 0$, since the SECA would not be able to fully extend the spastic MCP joint, as discussed previously when we were presenting the principle of SECA; Heung et al., 2020), θ_{0_m} is the resting angle of MCP joint, $\gamma\theta_{0\_m}$ is the upper limit of MCP joint angle.

Resting angle of MCP joint θ_{0_m} with bare hand only is measured prior to the experiment. Then, the ROM for stiffness evaluation begins from the initial extended MCP joint angle facilitated by the SECA. The end of ROM is set as 70% of the resting angle θ_{0_m}, as we previously discovered that the range between θ_{i_m} and $\gamma\theta_{0\_m}$ ($\gamma = 0.7$) would provide the most stable stiffness results for finger joints and prevent model singularity (Heung et al., 2020). Here, $\gamma = 0.7$ was established as an empirical value from our previous research work for the upper limit of MCP joint angle (Heung et al., 2020). As soon as the measured MCP joint angle exceeds this limit, the SECA will not be further actuated. Eventually, the average of all the stiffness values calculated at different pressure points is the final MCP joint stiffness measured by the SECA.

Ground-Truth Stiffness Evaluation With Standard Mechatronic Devices

System Description

To obtain the ground-truth value of MCP joint stiffness for verifying the accuracy of our method, we rebuilt the standard MCP joint stiffness measurement device. The device was demonstrated and confirmed accurate and effective previously by other research groups in Esteki and Mansour (1996) and Kuo and Deshpande (2012), as shown in **Figure 2**. The results from the measurement device is compared with the results obtained by our method for validation.

The device mainly consists of an arm rest, a finger splint, two load cells (Model 1021, Range 0-100 N, Arizon Inc., China), and a DC servomotor (RDS5160, Torque 60 kg.cm, DSservo Inc., China), as illustrated in **Figure 2**. The forearm of subjects is vertically clamped to the arm rest for maintaining the palm in vertical plane and the finger moving in horizontal plane. The arm rest can also prevent any lateral and rotational displacement of forearm during the test. The distal interphalangeal (DIP) and proximal interphalangeal (PIP) joints in the finger are clamped to the finger splint, such that the rotation of MCP joint can be coupled to the servomotor through the shaft. The sensor box that contains the two load cells is also placed on the shaft, allowing the tip of the finger splint to be embedded inside the box for measuring the force tangential to the circular path upon rotation of the finger.

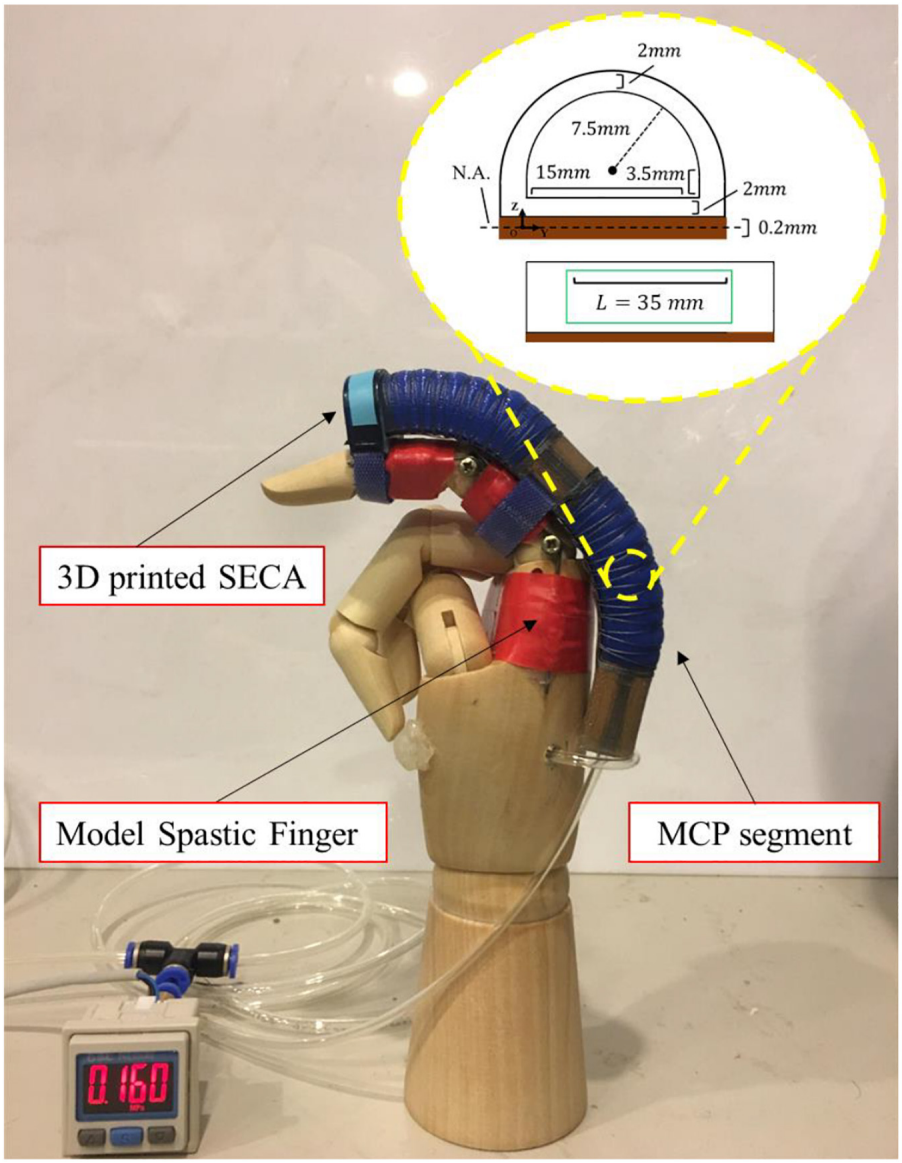

FIGURE 1 | Demonstration of actuated movement of the 3D printed SECA on a model spastic finger. Example actuated state of the MCP joint bound with the MCP segment of the SECA at 160 kPa pressure. Size of the MCP segment is labeled in the figure.

MCP Stiffness Measurement

Prior to the measurement, the distance between the MCP joint and the tip of the finger splint is measured. Then, the MCP joint is passively moved by the servomotor at specific positions, as instructed by Esteki and Mansour (1996); Kamper and Rymer (2000), and Kuo and Deshpande (2012) and will be discussed in the following section. Upon each rotation, the passive tip force at the finger splint is measured and multiplied by the measured distance, resulting in the calculated passive MCP joint torque, as presented by

$$\tau_{passive} = l_{fin} \times F_{passive} \tag{5}$$

which l_{fin} is the distance between the MCP joint and the tip of the finger splint (load cells), $F_{passive}$ is the measured tangential force to the circular rotation of index finger, and $\tau_{passive}$ is the MCP joint torque. A classic double exponential function-based model developed for finger kinematics is further used to describe the relationship between the passive MCP joint moment and its corresponding joint angle (Esteki and Mansour, 1996; Silder et al., 2007; Deshpande et al., 2011), which is given by

$$\tau_{passive}(\theta_m) = A(e^{-B(\theta_m - E)} - 1) - C(e^{D(\theta_m - F)} - 1) \tag{6}$$

that

$$\theta_m \in [\theta_{i\_m}, \gamma\theta_{0\_m}], \gamma = 0.7$$

which θ_m is the MCP joint angle (in degree), and A to F are the fitting parameters for the model. They are estimated

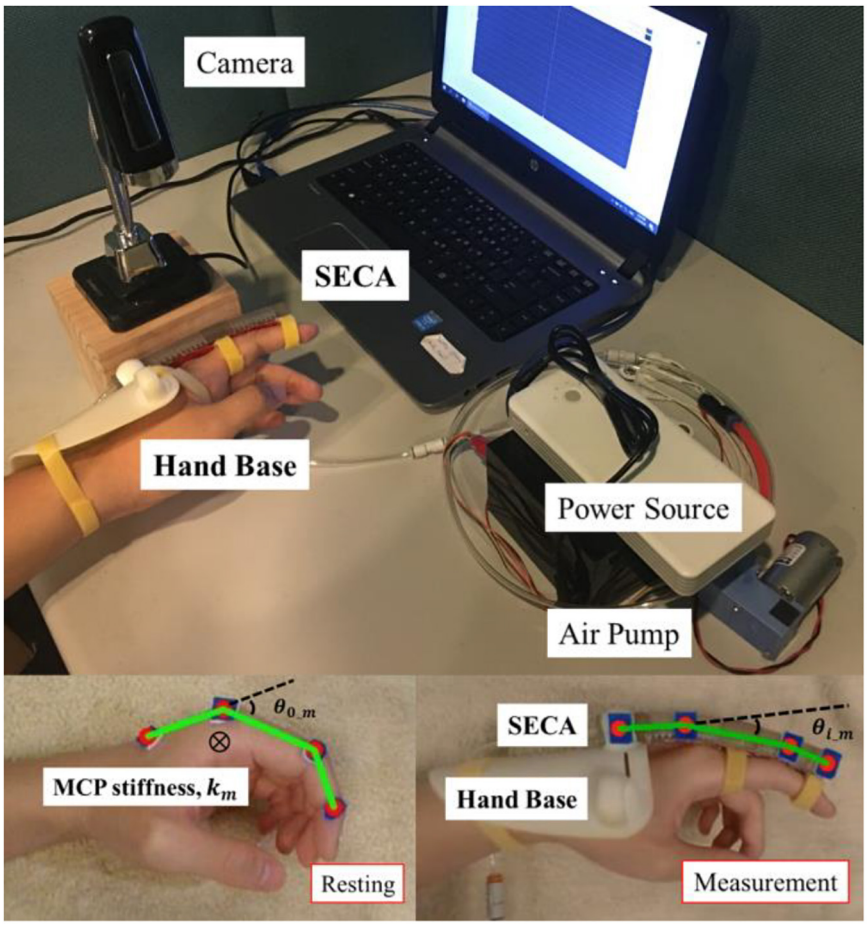

FIGURE 2 | Attachment of the SECA to finger with the hand base during MCP joint stiffness measurement. θ_{0_m} is the initial resting angle of MCP joint, θ_{i_m} is the extended MCP joint angle upon wearing of the SECA in a unpressurized state, and k_m is the measured MCP joint stiffness. The hardware setup followed our previous work in Heung et al. (2020). The movement of SECA is controlled by input pneumatic pressure. A camera remains on top of the index finger for recording the passive MCP joint rotation.

using the Non-linear least squares (NLS) method in MATLAB based on the minimization of sum of squared differences (SSD) between the experimental values and the fitting model (Kuo and Deshpande, 2012). The MCP joint stiffness is obtained by taking derivative of equation (6) within the angle range of θ_{i_m} and $\gamma\theta_{0\_m}$.

$$k_m = |-CDe^{-D(\theta_m - F)} - ABe^{-B(\theta_m - E)}| \quad (7)$$

In equation (7), θ_m is substituted with the angle values located in the range between θ_{i_m} and $\gamma\theta_{0\_m}$, such that stable stiffness values can be ensured and be not obscured by the torque increase upon closing to full flexion and extension of the MCP joint, which will be explained in the following section. Eventually, six joint angles are selected by portion, as suggested by Kamper and Rymer (2000), from the defined range and substituted into the stiffness equation (7). The average of all six calculated joint stiffness at different angle points is the final MCP joint stiffness measured by the device.

MATERIALS AND METHODS

Subjects

Four subjects with chronic stroke who had demonstrated weak hand strength with moderate level of finger flexor spasticity was recruited. Four subjects with no neurological deficit from the laboratory also participated in the study to serve as the control. Both have given their informed consents. The clinical evaluation was registered to the Joint Chinese University of Hong Kong-New Territories East Cluster (CUHK-NTEC) Clinical Research Ethics Committee (Ref. ID: NCT03286309). **Table 1** listed the demographic information of all the recruited subjects with stroke.

Experimental Configuration

The subjects are first examined with our stiffness evaluation method. Then, the subjects are further assessed with the replicated stiffness measurement device. Stiffness values obtained from two methods are compared with each other for validation.

TABLE 1 | Demographic information of the recruited subjects.

Subjects	Age	Gender	Stroke onset	Stroke type	Hemiplegic side	MAS	ARAT[3]	FMA-UE[4]
S1	65	Male	11 years	Hemorrhagic	Left	1+	25	27
S2	32	Male	48 months	Hemorrhagic	Left	2	3	16
S3	72	Female	62 months	Ischemic	Left	3	0	8
S4	59	Female	59 months	Ischemic	Left	1+	10	16
H1[1]	24	Male	–	–	– (Left)[2]	–	57	66
H2[1]	25	Male	–	–	– (Right)[2]	–	57	66
H3[1]	25	Male	–	–	– (Right)[2]	–	57	66
H4[1]	25	Male	–	–	– (Right)[2]	–	57	66

[1]*Subjects without neurological impairment as control group.*
[2]*MCP joints on the index fingers in the dominant hands were chosen for the assessment.*
[3]*ARAT (Action Research Arm Test) is a continuous measurement for the changes in upper limb function among hemiplegic subjects with no categorical cutoff scores. Full score is 57. Higher score indicates better upper limb performance.*
[4]*FMA-UE (Fugl-Meyer Assessment for Upper Extremity) is designed as performance-based impairment index to assess the motor function, balance, sensations, and joint functions in hemiplegic subjects with chronic stroke. In this work, FMA-UE refers only to the upper extremity motor function part with a total score of 66.*

SECA-Finger Modeling for Stiffness Evaluation

Index finger is selected as a stiffness indicator of the hand, similar to the approaches from different research groups (Kamper and Rymer, 2000; Heung et al., 2019, 2020). Examination of MCP joint stiffness in index finger is conducted from the pressure-angle relationship during the actuated flexion and extension of MCP joint with the SECA, as described in equation (1) – (4).

The SECA contains MCP segment for the actuation of MCP joint. It is attached to a hand base and secured to the index finger using Velcro Strap, as shown in **Figure 2** already. To ensure result consistency, the posture of the upper limb needs to be defined during experiments, as already described in our previous work (Heung et al., 2020). The hand base of the soft robotic hand covers the wrist to maintain it in a neutral position (0° of flexion and extension) with respect to the forearm, while the forearm is also being held in its neutral position (0° of supination and pronation). The elbow is flexed 90° and supported on the desk. The subjects need to sit vertically to the table and relax the whole time during the experiment to ensure the collected MCP joint angle is solely due to the passive rotation driven by the SECA.

Ground-Truth Stiffness Evaluation With Standard Mechatronic Devices

Index finger is also selected as a stiffness indicator of the hand. The standard stiffness measurement device for measuring passive MCP joint angle and torque in index finger is replicated and used for obtaining the ground-truth stiffness values, as shown in **Figure 3**. Previous study already demonstrated the effectiveness of this device in quantifying the MCP joint stiffness in index finger (Esteki and Mansour, 1996) and (Kuo and Deshpande, 2012).

The DIP and PIP joints in the index finger are clamped by the finger splint, allowing solely the MCP joint to be rotated by the servomotor in horizontal plane. Passive extension force at the splint tip is measured by the load cells in the sensor box with the sampling rate of 80 Hz during passive rotation of MCP joint. The force is multiplied by the distance between the MCP joint and the splint tip, thereby obtaining the final values of passive MCP joint stiffness. The posture of upper limb follows the settings in the experiment using SECA, as elaborated previously. A hand holder is placed in the arm rest for holding the other four fingers in vertical plane. Velcro Straps are used to fix the forearm (0° of supination and pronation) and wrist (0° of flexion and extension) at the natural position, as illustrated in **Figure 3**. The subjects need to sit vertically with the elbow being flexed at 90° and supported on the desk. The subjects are required to stay relax the whole time as well to ensure the collected force is solely due to the passive extension driven by the servomotor.

Protocol

A brief physical examination of MAS is first performed on assessing the flexor tone in the spastic finger. The degree of spasticity is assessed by a trained clinical assessor who is blind to the experimental condition. For the subjects with no neurological deficit, the examination of spasticity with MAS is not conducted, and the result can be classified as "no increase in flexor muscle tone" (MAS score = 0) (Kamper and Rymer, 2000). After confirming their MAS grades, the evaluation of MCP joint stiffness in the index fingers will be conducted.

Preparation procedures are required for the subjects prior to both experiments using our SECA and the standard measurement device. To maintain the assessed muscle tone being consistent and stably presented on subjects in two tests, they are instructed to sit vertically for 30 min with the elbow at 90° and supported on the desk to relax the forearm muscles prior to each test. Any passive mobilization to extend the fingers, or any generated movement (either passive or active) on the fingers that will greatly alter the muscle tone is not allowed during the relaxation time. The 30 min resting time before the spasticity measurement was suggested by Kakebeeke et al. (2005) to minimize the effect of any movement or mobilization taken before the test.

In the first stiffness test using the SECA, unreliable MCP stiffness results due to model singularity (i.e., small difference between the resting angle of MCP joint and the current bending angle of MCP joint) and the extra passive MCP joint resistance provided by the joint CLC upon closing to full flexion or extension can be excluded by setting the angle range between

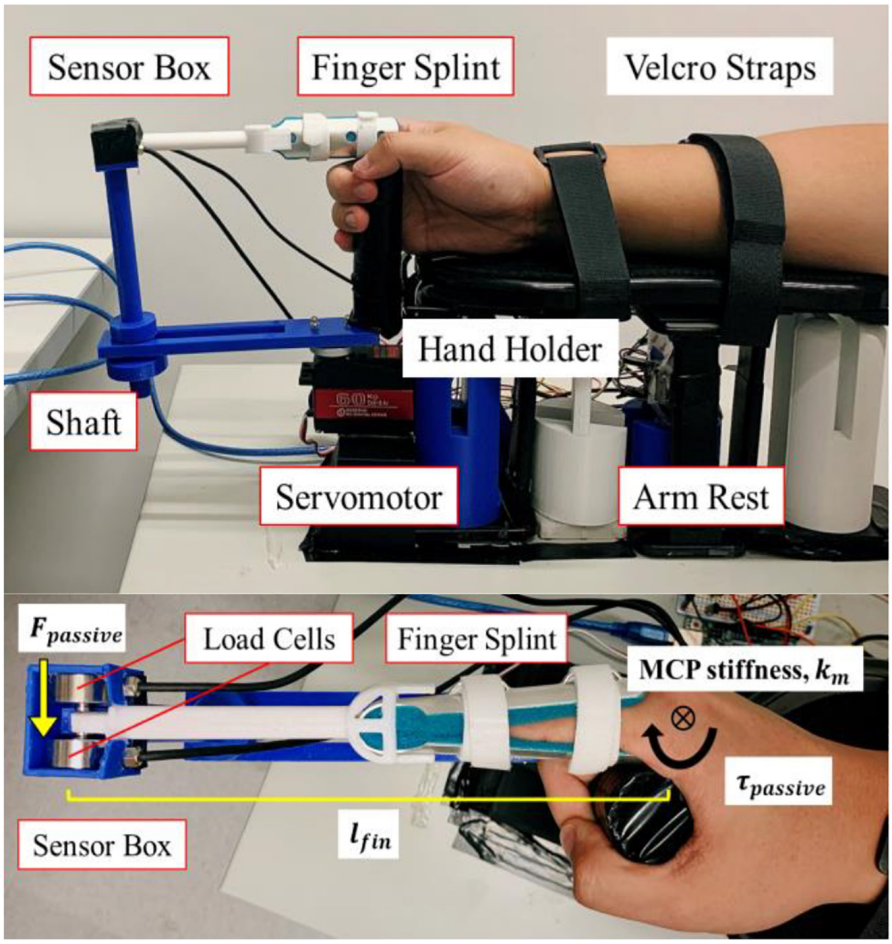

FIGURE 3 | Stiffness measurement device replicated from Esteki and Mansour (1996) and Kuo and Deshpande (2012) for MCP joint stiffness testing in index finger. Two load cells are placed in the sensor box. The finger splint is embedded in the sensor box. The MCP joint is rotated by the DC servomotor. The forearm is secured on the arm rest, which includes Velcro straps and a hand holder.

θ_{i_m} and $\gamma\theta_{0\_m}(\gamma = 0.7)$. Stable stiffness results can be ensured within the defined angle range. Also, only three repetitions are performed to measure the passive MCP joint angle, as it has been suggested that short-term effect of any stretch, e.g., loosening the joints and reducing the muscle tone, may occur if more than three times (Charalambous, 2014; Levine, 2018).

During the measurement, the SECA is placed on the index finger in an unpressurized state. Pressure is then increased step by step from zero by 20 kPa one at a time to move the MCP joint to different angles, which the measured angles and the corresponding pressure values are recorded. The SECA holds the MCP joint at each position for 30 s to ensure stable angle values can be collected (Esteki and Mansour, 1996). As soon as the MCP angle reaches its upper limit $\gamma\theta_{0\_m}$, the MCP joint will slowly (2° per second) return to the extended position θ_{i_m} with the SECA, such that the dynamics of SECA-Finger model can be ignored. This whole process is defined as one complete repetition. Upon completion of all three repetitions, three MCP joint angle values would have been recorded at each specific pressure input, e.g., at 0, 20 kPa, etc., respectively. Average MCP joint angle at each pressure input is taken from the three measured angle values and substituted into the static model in equation (1) – (4) to obtain the measured stiffness value at each specific pressure input. Eventually, the final MCP joint stiffness is determined from the average of all measured stiffness values.

On the other hand, the standard stiffness measurement device is used in the second stiffness test. Previous study used the measurement device to rotate the MCP joint from the flexed position (50°) to the fully extended position (−40°), i.e., ROM of 90°, and obtain the passive MCP stiffness values for this overall range (Kamper et al., 2006). With sufficient data collected from this range, a linear pattern of stiffness values could be observed in the range from 0° to 50°. To reduce any potential discomfort due to full extension of the joint (−40° to 0°), we adjusted the testing ROM from the range of −40° to 50° to the range of 0° to 90°. The device therefore rotates the MCP joint step by step from 90° (flexion) to 0° (extension) by 10° one at a time. The speed during each rotation is 2° per second, such that the dynamics of fingers can be ignored. The servomotor holds the MCP joint at each position for 30 s to ensure stable tip force values can be

collected (Esteki and Mansour, 1996). As soon as the MCP joint angle reaches extension (0°), the MCP joint will slowly (2° per second) return to the flexed position (90°) with the servomotor. This whole process is defined as one complete repetition. Another reason of rotating the joint with the device in one repetition is that we want to further demonstrate the existence of extra passive MCP joint resistance due to the joint CLC in full flexion or extension (Kuo and Deshpande, 2012), which further supported to define the angle range. Besides, during the fitting of the double exponential function-based model for describing finger kinematics, it is suggested that torque values measured from full ROM are required and necessary, as mentioned previously (Kuo and Deshpande, 2012).

Similar to the stiffness test using SECA, upon completion of all three repetitions, three measured MCP joint torque values would have been recorded at each specific joint position, e.g., at 90°, 80°, etc., respectively. Average MCP joint torque at each joint position is taken from the three measured torque values and fitted into the double exponential function-based model in equation (6) for getting the parameters. The parameters are then substituted into equation (7) for the stiffness equation. Six joint angles are selected by portion, as suggested by Esteki and Mansour (1996); Kamper and Rymer (2000), and (Kuo and Deshpande, 2012), from the defined angle range between θ_{i_m} and $\gamma\theta_{0\_m}(\gamma = 0.7)$ and substituted into the stiffness equation (7). Eventually, the average of all six calculated joint stiffness is the final MCP joint stiffness measured by the stiffness measurement device. Throughout all the tests, subjects did not indicate any discomfort and pain upon the stretch of their MCP joints.

EXPERIMENTAL RESULTS

Stiffness From the SECA

Quantification of MCP joint stiffness is conducted. Pressures of 0, 20, 40, and 60 kPa are applied to the SECA. Bending angles of MCP segment, and the corresponding actuation pressures, are recorded for the calculation of stiffness values using equation (2). To avoid singularity, it should be noted again that the maximum MCP joint angle cannot exceed their pre-defined upper limits. **Table 2** shows the MCP joint stiffness of all eight subjects measured by the SECA. The data from subject S1 with chronic stroke and subject H1 with no neurological deficit is also plotted in **Figure 4** as well as an example to demonstrate the stiffness evaluation for S1 and H1, which the stiffness of 0.0809 Nm/rad and 0.0316 Nm/rad is obtained respectively from the average of different measured stiffness values at different pressure values.

Stiffness From the Standard Stiffness Measurement Device

Table 2 presents the MCP joint stiffness of all eight subjects measured by the standard stiffness measurement device. The data from subject S1 and with chronic stroke and subject H1 with no neurological deficit is also plotted in **Figure 4** as an example to demonstrate the stiffness evaluation for S1 and H1, which the stiffness of 0.0849 Nm/rad and 0.0377 Nm/rad is obtained respectively from the average of different measured stiffness values at different joint angles. In **Figure 4**, it is worth to note that the MCP joint is stretched in full range to obtain complete set of torque values with respect to the joint positions for the fitting of the double exponential model. The calibrated model parameters are then substituted into equation (7) for the measured stiffness values at different joint angles. However, to minimize the effect of the CLC to the MCP joint stiffness, only the joint angles within the range listed in **Table 2** are adopted to stiffness evaluation. **Table 3** also shows the fitting parameters for the double exponential model and the MCP joint stiffness equation.

Comparison Between Two Approaches

The results from two different approaches are similar with each other. Upon the increase of muscle tone (spasticity), the MCP joint stiffness further increases. Only a maximum stiffness difference of 0.021 Nm/rad is observed in subject S2 with chronic stroke, and minimum difference of 0.004 Nm/rad in subject S4 with chronic stroke. From our data, it is also observed that the stiffness from our SECA would be slightly smaller than the actual joint stiffness. Here, we believe that the stiffness evaluation method using our SECA is feasible for finger joint stiffness quantification during any rehabilitation training. It

TABLE 2 | Summarization of MCP joint stiffness characteristic with different measurement approaches.

	MAS	θ_{0_m} [1]	$[\theta_{i\_m}, \gamma\theta_{0\_m}]$[2]	Ground-truth k_m (Nm/rad) [3]	k_m from SECA (Nm/rad) [4]	Difference
S1	1+	54°	[18°, 38°]	0.0849 (±0.0158)	0.0809 (±0.0025)	0.004 (±0.0066)
S2	2	64°	[34°, 45°]	0.5217 (±0.0436)	0.5011 (±0.0408)	0.021 (±0.0271)
S3	3	51°	[30°, 36°]	0.6362 (±0.0173)	0.6255 (±0.0231)	0.011 (±0.0135)
S4	1+	35°	[13°, 25°]	0.0930 (±0.0099)	0.0857 (±0.0106)	0.007 (±0.0067)
H1	–	45°	[10°, 32°]	0.0377 (±0.0032)	0.0316 (±0.0003)	0.006 (±0.0013)
H2	–	46°	[9°, 32°]	0.0328 (±0.0183)	0.0277 (±0.0004)	0.005 (±0.0077)
H3	–	40°	[10°, 28°]	0.0466 (±0.0057)	0.0408 (±0.0006)	0.006 (±0.0037)
H4	–	58°	[11°, 41°]	0.0393 (±0.0059)	0.0295 (±0.0026)	0.010 (±0.0027)

[1] *The resting MCP joint angle upon wearing of the SECA onto the index finger at zero pressure.*
[2] *The angle range for the calculation of MCP joint stiffness with the standard stiffness measurement device and our SECA.*
[3] *MCP joint stiffness measured by the standard stiffness measurement device.*
[4] *MCP joint stiffness measured by our SECA.*

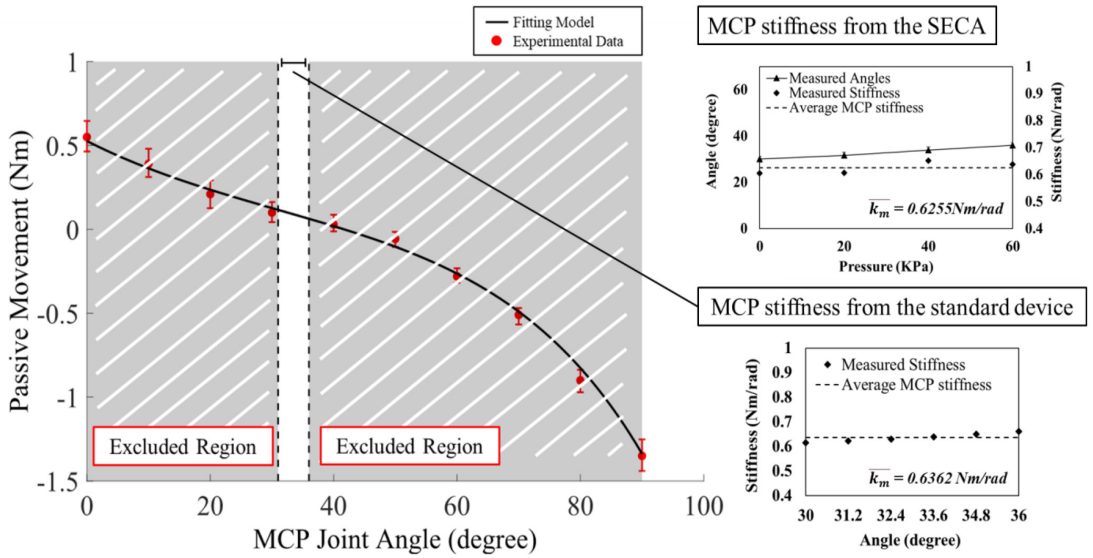

FIGURE 4 | Examples of the experimental data and model fitting results for subject S3 with chronic stroke with MAS = 3. The torque and angle of the MCP joint in S3 is collected from the ROM of 0° to 90° for model fitting. Results of MCP joint stiffness in S3 are presented by two different estimation methods. Using the SECA, pressure is increased by 20 kPa until the angle reaches the upper limit. Using the standard device, six joint angles are selected by portion in the angle range for estimation of MCP joint stiffness. Error bar presents the different between the maximum and minimum measured stiffness values. Final joint stiffness is taken by the average of all measured values.

would be possible to extend the quantification to the proximal interphalangeal (PIP) or distal interphalangeal joints (DIP) joints as well using our SECA, which has been hard to be accomplished by the standard stiffness measurement device.

DISCUSSION

Spasticity is a well-known symptom seen in subjects after suffering a stroke. Hand function is severely affected due to the excessive flexor tone in muscles. The purpose of this study was to validate the compatibility of our stiffness quantification method in clinical practices. We quantified the passive MCP joint stiffness in subjects with chronic stroke and no neurological deficit. We also investigated the difference of stiffness results obtained from our SECA and the standard stiffness measurement device. The results between using our approach with the SECA and the standard device were consistent, which only a difference of 0.0044 Nm/rad was observed in the MCP stiffness. The results were also supportive when comparing with MAS.

TABLE 3 | Fitting model parameters.

	A	*B*	*C*	*D*	*E*	*F*	R^2
S1	0.005	0.073	0.130	0.045	21.88	63.58	0.88
S2	0.006	0.050	0.065	0.041	30.75	10.64	0.91
S3	0.015	0.028	0.230	0.038	21.79	68.11	0.88
S4	0.030	0.035	0.082	0.044	80.46	25.33	0.89
H1	0.001	0.097	0.100	0.032	19.23	75.34	0.91
H2	0.006	0.077	0.016	0.081	17.33	60.25	0.90
H3	0.005	0.080	0.038	0.046	17.57	55.16	0.89
H4	0.003	0.081	0.055	0.042	20.81	67.87	0.93

The passive MCP stiffness evaluation was conducted with the replicated standard device to collect the passive joint torque and ROM in each subject. The double exponential function-based model fitted well with the collected finger kinematic data, which the performance was similar to previous research (Knutson et al., 2000; Kuo and Deshpande, 2012). From the results obtained from existing research and using the standard stiffness measurement device, it was disclosed that the measured passive MCP joint extension torque significantly increased as soon as the joint angle was approaching to its limit of rotation. All the subjects exhibited larger joint stiffness upon closing to full flexion or extension of MCP joints, which is suggested due to the extra resistance provided by the joint CLC apart from the finger flexors for maintaining finger joint stability (Kuo and Deshpande, 2012). In spasticity assessments, the assessors would also leave the fingers some space without fully extending them because of safety concerns and not creating discomfort. Passive resistance due to CLC would not be assessed and considered as part of the muscle tone at all. Therefore, ROM of MCP joints during stiffness evaluation would be restricted around the resting position based on the range defined in equation (3) and (4). This would mainly assess the MCP stiffness due to finger flexor tone and the values would tend to be stable within the defined range around the resting position.

Common clinical examinations of spasticity include the Ashworth Scale (AS) and Tardieu Scale (TS). To further quantify the MCP stiffness after stroke, there is not a lot of studies conducted the quantify the stiffness of spastic finger joint to the best of our knowledge. We have concluded the results from some

TABLE 4 | Existing studies about the quantification of MCP joint stiffness on both subjects with chronic stroke and no neurological deficit.

Test subjects	Studies	MAS	Estimated MCP stiffness k_m (*Nm/rad*)
Subjects with chronic stroke	Towles et al., 2010	1 – 3[1]	∼ 0.09337 to ∼1.12894 ($n = 12$)
	Kamper and Rymer, 2000	3	∼0.60733 to ∼ 0.88236 ($n = 3$)
		2	∼0.22345 to ∼ 0.55004 ($n = 6$)
	Brokaw et al., 2011	2	∼0.53476 ($n = 1$)
		1+	∼0.14323 ($n = 1$)
Subjects with no neurological deficit	Kuo and Deshpande, 2012	–	∼0.01578 to ∼ 0.21046 ($n = 10$)[2]
	Esteki and Mansour, 1996	–	∼0.02535 to ∼0.05792 ($n = 3$)[2]

[1] *Joint stiffness values were organized as a whole group without classification with respect to different MAS.*
[2] *Values were estimated in the angle region between 0° and resting angle θ_{0_m}. Stiffness increase when approaching full MCP joint flexion and extension was not considered.*

existing conclusive studies and presented in **Table 4**. Results of MCP stiffness values from our and existing research reflected the possible similar joint properties between subjects having MAS of 0, 1, and 1+ and subjects with no neurological deficit. For subjects with no neurological deficit, depending on their body characteristics, e.g., age, weight, gender, muscle strength, etc. (Dionysian et al., 2005), their MCP joint stiffness could vary greatly, e.g., from around 0.02 Nm/rad to 0.2 Nm/rad, as reviewed in **Table 4**, among each individual. In our four subjects with no neurological deficit, their MCP stiffness ranged from 0.03 Nm/rad to 0.05 Nm/rad, which was also located in the range in **Table 4**. For subjects with chronic stroke having MAS of 0, 1, and 1+, their MCP joint stiffness was observed to be closed to some subjects with no neurological deficit, as comparing the 1+ grade and the 1–3 grade range with subjects with no neurological deficit in **Table 4**. In our subjects with chronic stroke with MAS of 1+ grade, the MCP stiffness was around 0.09 Nm/rad, which was also located in the range of MAS between 1 and 3, e.g., from around 0.09 Nm/rad to 1.13 Nm/rad, and closed to the value of 1+ grade in **Table 4**. The stiffness value was also located in the range of subjects with no neurological deficit, e.g., from around 0.02 Nm/rad to 0.2 Nm/rad. Indeed, more cautions should be taken to assess subjects with mild spasticity as their finger characteristics in terms of post-stroke stiffness would be similar. One possible way to optimize the assessment in an objective manner would be to classify the joint stiffness range for the mapping of each MAS grade with more test subjects with chronic stroke in the future (Pandyan et al., 1999; Towles et al., 2010; Brokaw et al., 2011; Zakaria et al., 2015).

As soon as excessive muscle tone further increases in finger flexors, larger MCP stiffness values could eventually be observed. For subjects with chronic stroke having MAS of 2 and 3, their MCP joint stiffness was observed to be much larger than that of subjects with no neurological deficit, e.g., from around 0.22 Nm/rad to 1.12 Nm/rad in **Table 4**. In our subject with chronic stroke having the MAS of 2 grade, the MCP stiffness was around 0.5 Nm/rad, which was higher than that of subjects having lower MAS grade. Stiffness values for subjects having MAS higher than 2 would be higher than subjects having lower MAS and subjects with no neurological deficit. For subjects having MAS of the 3 grade, stiffness values could be up to 1 Nm/rad and obviously higher than that of other subjects with less spasticity. From the MCP stiffness results, we might also know that assessors would be easier to distinguish the condition of subjects having stronger spasticity (MAS $\geq$ 2) comparing with subjects having less spasticity (MAS $<$ 2), as more marked increase of resistance against passive joint movement would be more easier for assessors to recognize during assessment. Overall, larger stiffness results would be observed in subjects with higher MAS grade. Values of their MCP joint stiffness in both subjects with chronic stroke and no neurological deficit were also found to be near the stiffness ranges presented by previous studies, as summarized in **Tables 3**, **4** already. This shows the potentials of our quantification method based on the SECA-Finger model and integrating it into hand rehabilitation training in future studies for observing the possible recovery process of finger stiffness.

This work explored the difference of passive MCP joint stiffness among subjects who experienced a stroke or remain neurologically intact. Experimental results provided some evidence of quantifying the MCP stiffness using our SECA. In the future, our proposed methods could be applied to our rehabilitation robotic hand that reflects the stiffness for individual finger. With the stiffness information, optimal training tasks might be planned for each individual with stroke depending on the finger stiffness condition. Therapeutic progress might also be indicated in detail to motivate patients for achieving better improvement during rehabilitation training.

DATA AVAILABILITY STATEMENT

The raw data supporting the conclusions of this article will be made available by the authors, without undue reservation.

ETHICS STATEMENT

The studies involving human participants were reviewed and approved by Joint Chinese University of Hong Kong-New Territories East Cluster (CUHK-NTEC) Clinical Research Ethics Committee (Ref. ID: NCT03286309). The patients/participants provided their written informed consent to participate in this study. Written informed consent was obtained from the individual(s) for the publication of any potentially identifiable images or data included in this article.

AUTHOR CONTRIBUTIONS

XS and HH developed the mathematical theories, designed the experimental devices and experimental protocols, implemented the data collection software, performed the experiments, analyzed the experimental results, and participated in manuscript preparation. HH, XS, and ZT performed the experiments, contributed to discussions, analysis, and participated in manuscript revisions. KT and ZL supervised the project, contributed to discussions, analysis, and participated in manuscript revisions. All the authors have approved the submitted manuscript.

FUNDING

This material is based on the work supported by the Hong Kong Innovation and Technology Fund (ITS/065/18FP).

REFERENCES

Andringa, A., van Wegen, E., van de Port, I., Kwakkel, G., and Meskers, C. (2019). Measurement properties of the NeuroFlexor device for quantifying neural and non-neural components of wrist hyper-resistance in chronic stroke. *Front. Neurol.* 10:730. doi: 10.3389/fneur.2019.00730

Blackburn, M., van Vliet, P., and Mockett, S. P. (2002). Reliability of measurements obtained with the modified Ashworth scale in the lower extremities of people with stroke. *Phys. Ther.* 82, 25–34. doi: 10.1093/ptj/82.1.25

Brokaw, E. B., Black, I., Holley, R. J., and Lum, P. S. (2011). Hand spring operated movement enhancer (HandSOME): a portable, passive hand exoskeleton for stroke rehabilitation. *IEEE Trans. Neural Syst. Rehabil. Eng.* 19, 391–399. doi: 10.1109/tnsre.2011.2157705

Charalambous, C. P. (2014). "Interrater reliability of a modified Ashworth scale of muscle spasticity," in *Classic Papers in Orthopaedics*, eds D. F. Kader and P. A. Banaszkiewicz (London: Springer), 415–417. doi: 10.1007/978-1-4471-5451-8_105

Damiano, D. L., Quinlivan, J. M., Owen, B. F., Payne, P., Nelson, K. C., and Abel, M. F. (2002). What does the Ashworth scale really measure and are instrumented measures more valid and precise? *Dev. Med. Child Neurol.* 44, 112–118. doi: 10.1017/s0012162201001761

Deshpande, A. D., Gialias, N., and Matsuoka, Y. (2011). Contributions of intrinsic visco-elastic torques during planar index finger and wrist movements. *IEEE Trans. Biomed. Eng.* 59, 586–594. doi: 10.1109/tbme.2011.2178240

Dionysian, E., Kabo, J. M., Dorey, F. J., and Meals, R. A. (2005). Proximal interphalangeal joint stiffness: measurement and analysis. *J. Hand Surg.* 30, 573–579. doi: 10.1016/j.jhsa.2004.10.010

Esteki, A., and Mansour, J. (1996). An experimentally based nonlinear viscoelastic model of joint passive moment. *J. Biomech.* 29, 443–450. doi: 10.1016/0021-9290(95)00081-x

Fleuren, J. F., Voerman, G. E., Erren-Wolters, C. V., Snoek, G. J., Rietman, J. S., Hermens, H. J., et al. (2010). Stop using the Ashworth Scale for the assessment of spasticity. *J. Neurol.* 81, 46–52. doi: 10.1136/jnnp.2009.177071

Francisco, G. E., and McGuire, J. R. (2012). Poststroke spasticity management. *Stroke* 43, 3132–3136. doi: 10.1161/strokeaha.111.639831

Fugl-Meyer, A. R., Jääskö, L., Leyman, I., Olsson, S., and Steglind, S. (1975). The post-stroke hemiplegic patient. 1. a method for evaluation of physical performance. *Scand. J. Rehabil. Med.* 7, 13–31.

Gregson, J. M., Leathley, M., Moore, A. P., Sharma, A. K., Smith, T. L., and Watkins, C. L. (1999). Reliability of the tone assessment scale and the modified Ashworth scale as clinical tools for assessing poststroke spasticity. *Arch. Phys. Med. Rehabil.* 80, 1013–1016. doi: 10.1016/s0003-9993(99)90053-9

Heung, H. L., Tang, Z. Q., Shi, X. Q., Tong, K. Y., and Li, Z. (2020). Soft rehabilitation actuator with integrated post-stroke finger spasticity evaluation. *Front. Bioeng. Biotechnol.* 8:111. doi: 10.3389/fbioe.2020.00111

Heung, K. H., Tong, R. K. Y., Lau, A. T. H., and Li, Z. (2019). Robotic glove with soft-elastic composite actuators for assisting activities of daily living. *Soft Robot.* 6, 289–304. doi: 10.1089/soro.2017.0125

Huang, F. C., and Patton, J. L. (2016). Movement distributions of stroke survivors exhibit distinct patterns that evolve with training. *J. Neuroeng. Rehabil.* 13:23.

Kakebeeke, T. H., Lechner, H. E., and Knapp, P. A. (2005). The effect of passive cycling movements on spasticity after spinal cord injury: preliminary results. *Spinal Cord* 43, 483–488. doi: 10.1038/sj.sc.3101747

Kamper, D. G., and Rymer, W. Z. (2000). Quantitative features of the stretch response of extrinsic finger muscles in hemiparetic stroke. *Muscle Nerve* 23, 954–961. doi: 10.1002/(sici)1097-4598(200006)23:6<954::aid-mus17>3.0.co;2-0

Kamper, D. G., Fischer, H. C., Cruz, E. G., and Rymer, W. Z. (2006). Weakness is the primary contributor to finger impairment in chronic stroke. *Arch. Phys. Med. Rehabil.* 87, 1262–1269. doi: 10.1016/j.apmr.2006.05.013

Kamper, D. G., Hornby, T. G., and Rymer, W. Z. (2002). Extrinsic flexor muscles generate concurrent flexion of all three finger joints. *J. Biomech.* 35, 1581–1589. doi: 10.1016/s0021-9290(02)00229-4

Kamper, D., Harvey, R. L., Suresh, S., and Rymer, W. Z. (2003). Relative contributions of neural mechanisms versus muscle mechanics in promoting finger extension deficits following stroke. *Muscle Nerve* 28, 309–318. doi: 10.1002/mus.10443

Knutson, J. S., Kilgore, K. L., Mansour, J. M., and Crago, P. E. (2000). Intrinsic and extrinsic contributions to the passive moment at the metacarpophalangeal joint. *J. Biomech.* 33, 1675–1681. doi: 10.1016/s0021-9290(00)00159-7

Kuo, P.-H., and Deshpande, A. D. (2012). Muscle-tendon units provide limited contributions to the passive stiffness of the index finger metacarpophalangeal joint. *J. Biomech.* 45, 2531–2538. doi: 10.1016/j.jbiomech.2012.07.034

Lambercy, O., Lünenburger, L., Gassert, R., and Bolliger, M. (2012). "Robots for measurement/clinical assessment," in *Neurorehabilitation Technology*, eds D. J. Reinkensmeyer and V. Dietz (Cham: Springer), 443–456. doi: 10.1007/978-1-4471-2277-7_24

Levine, P. G. (2018). *Stronger After Stroke: Your Roadmap to Recovery*. New York, NY: Springer Publishing Company.

Maggioni, S., Melendez-Calderon, A., van Asseldonk, E., Klamroth-Marganska, V., Lünenburger, L., Riener, R., et al. (2016). Robot-aided assessment of lower extremity functions: a review. *J. Neuroeng. Rehabil.* 13:72.

Mehrholz, J., Wagner, K., Meissner, D., Grundmann, K., Zange, C., Koch, R., et al. (2005). Reliability of the modified Tardieu scale and the modified Ashworth scale in adult patients with severe brain injury: a comparison study. *Clin. Rehabil.* 19, 751–759. doi: 10.1191/0269215505cr889oa

Milner, T. E., and Franklin, D. W. (1998). Characterization of multijoint finger stiffness: dependence on finger posture and force direction. *IEEE Trans. Biomed. Eng.* 45, 1363–1375. doi: 10.1109/10.725333

Minami, A., An, K.-N., Cooney, W. P. III, Linscheid, R. L., and Chao, E. Y. S. (1983). Ligamentous structures of the metacarpophalangeal joint: a quantitative anatomic study. *J. Orthop. Res.* 1, 361–368. doi: 10.1002/jor.1100010404

Nalam, V., and Lee, H. (2019). Development of a two-axis robotic platform for the characterization of two-dimensional ankle mechanics. *IEEE/ASME Trans. Mechatron.* 24, 459–470. doi: 10.1109/tmech.2019.2892472

Pandyan, A. D., Johnson, G. R., Price, C. I., Curless, R. H., Barnes, M. P., and Rodgers, H. (1999). A review of the properties and limitations of the Ashworth and modified Ashworth scales as measures of spasticity. *Clin. Rehabil.* 13, 373–383. doi: 10.1191/026921599677595404

Park, J.-H., Lee, K.-J., Yoon, Y.-S., Son, E.-J., Oh, J.-S., Kang, S. H., et al. (2017). "Development of elbow spasticity model for objective training of spasticity assessment of patients post stroke," in *Proceedings of the 2017 International Conference on Rehabilitation Robotics (ICORR)*, London (Piscataway, NJ: IEEE).

Prosser, R. (1996). Splinting in the management of proximal interphalangeal joint flexion contracture. *J. Hand Ther.* 9, 378–386. doi: 10.1016/s0894-1130(96)80045-7

Sadarangani, G. P., Jiang, X., Simpson, L. A., Eng, J. J., and Menon, C. (2017). Force myography for monitoring grasping in individuals with stroke with

mild to moderate upper-extremity impairments: a preliminary investigation in a controlled environment. *Front. Bioeng. Biotechnol.* 5:42. doi: 10.3389/fbioe.2017.00042

Silder, A., Whittington, B., Heiderscheit, B., and Thelen, D. G. (2007). Identification of passive elastic joint moment–angle relationships in the lower extremity. *J. Biomech.* 40, 2628–2635. doi: 10.1016/j.jbiomech.2006.12.017

Tang, Z. Q., Heung, H. L., Tong, K. Y., and Li, Z. (2019). Model-based online learning and adaptive control for a "human-wearable soft robot" integrated system. *Int. J. Robot. Res.* doi: 10.1177/0278364919873379

Towles, J. D., Kamper, D. G., and Rymer, W. Z. (2010). Lack of hypertonia in thumb muscles after stroke. *J. Neurophysiol.* 104, 2139–2146. doi: 10.1152/jn.00423.2009

Yap, H. K., Lim, J. H., Goh, J. C. H., and Yeow, C.-H. (2016). Design of a soft robotic glove for hand rehabilitation of stroke patients with clenched fist deformity using inflatable plastic actuators. *J. Med. Devices* 10:044504.

Yi, X., Zhou, Q., Lin, J., and Chi, L. (2013). Aspirin resistance in Chinese stroke patients increased the rate of recurrent stroke and other vascular events. *Int. J. Stroke* 8, 535–539. doi: 10.1111/j.1747-4949.2012.00929.x

Zakaria, N. A. C., Komeda, T., Low, C. Y., Hanapiah, F. A., and Inoue, K. (2015). "Spasticity mathematical modelling in compliance with modified Ashworth scale and modified Tardieu scales," in *Proceedings of the 2015 15th International Conference on Control, Automation and Systems (ICCAS)*, Busan (Piscataway, NJ: IEEE).

Conflict of Interest: The authors declare that the research was conducted in the absence of any commercial or financial relationships that could be construed as a potential conflict of interest.

frontiers in Neuroscience

ORIGINAL RESEARCH
published: 21 January 2021
doi: 10.3389/fnins.2020.580762

The Effects of Extracorporeal Shock Wave Therapy on Spastic Muscle of the Wrist Joint in Stroke Survivors: Evidence From Neuromechanical Analysis

Yan Leng[1†], *Wai Leung Ambrose Lo*[1†], *Chengpeng Hu*[1], *Ruihao Bian*[1], *Zhiqin Xu*[1], *Xiyao Shan*[1], *Dongfeng Huang*[2*] and *Le Li*[1,3*]

[1] Department of Rehabilitation Medicine, The First Affiliated Hospital, Sun Yat-sen University, Guangzhou, China, [2] Department of Rehabilitation Medicine, The Seventh Affiliated Hospital, Sun Yat-sen University, Shenzhen, China, [3] Institute of Medical Research, Northwestern Polytechnical University, Xi'an, China

OPEN ACCESS

Edited by:
Nicola Smania,
University of Verona, Italy

Reviewed by:
Lucio Marinelli,
University of Genoa, Italy
Robert Dymarek,
Wroclaw Medical University, Poland

***Correspondence:**
Dongfeng Huang
huangdf@mail.sysu.edu.cn
Le Li
lile5@mail.sysu.edu.cn

[†]These authors have contributed equally to this work

Specialty section:
This article was submitted to Neural Technology, a section of the journal Frontiers in Neuroscience

Received: 09 October 2020
Accepted: 21 December 2020
Published: 21 January 2021

Citation:
Leng Y, Lo WLA, Hu C, Bian R, Xu Z, Shan X, Huang D and Li L (2021) The Effects of Extracorporeal Shock Wave Therapy on Spastic Muscle of the Wrist Joint in Stroke Survivors: Evidence From Neuromechanical Analysis. Front. Neurosci. 14:580762. doi: 10.3389/fnins.2020.580762

Background: This study combined neuromechanical modeling analysis, muscle tone measurement from mechanical indentation and electrical impedance myography to assess the neural and peripheral contribution to spasticity post stroke at wrist joint. It also investigated the training effects and explored the underlying mechanism of radial extracorporeal shock wave (rESW) on spasticity.

Methods: People with first occurrence of stroke were randomly allocated to rESW intervention or control group. The intervention group received one session of rESW therapy, followed by routine therapy which was the same frequency and intensity as the control group. Outcome measures were: (1) NeuroFlexor method measured neural component (NC), elastic component (EC) and viscosity component (VC), and (2) myotonometer measured muscle tone (F) and stiffness (S), (3) electrical impedance myography measured resistance (R), reactance (X) and phase angle (θ); (4) modified Asworth scale; (5) Fugl Meyer Upper limb scale. All outcome measures were recorded at baseline, immediately post rESW and at 1-week follow-up. The differences between the paretic and non-paretic side were assessed by *t*-test. The effectiveness of rESW treatment were analyzed by repeated-measures one-way analysis of variance (ANOVA) at different time points.

Results: Twenty-seven participants completed the study. NC, EC, and VC of the Neuroflexor method, F and S from myotonometer were all significantly higher on the paretic side than those from the non-paretic side. R, X, and θ from electrical impedance were significantly lower on the paretic side than the non-paretic side. Immediately after rESW intervention, VC, F, and S were significantly reduced, and X was significantly increased. The clinical scores showed improvements immediate post rESW and at 1-week follow-up.

Conclusions: The observed changes in upper limb muscle properties adds further support to the theory that both the neural and peripheral components play a role in

muscle spasticity. ESW intervention may be more effective in addressing the peripheral component of spasticity in terms of muscle mechanical properties changes. The clinical management of post stroke spasticity should take into consideration of both the neural and non-neural factors in order to identify optimal intervention regime.

Keywords: stroke, spasticity, extracorporeal shock ware therapy, muscle mechanical properties, upper extremities, neurorehabilitation

INTRODUCTION

Spasticity is a clinical sign frequently appears in patients with stroke (Katoozian et al., 2018). Spasticity contributes to complications such as pain, altered posture, anchylosis or deformities and osteoporosis which affects the recovery of motor function and quality of lives of stroke survivors (Malhotra et al., 2011). The stretch reflex arc impairment has been considered as a main contributing factor to spasticity. However, the structural and component changes in muscle fibers and tendon, including muscle atrophy (e.g., fiber size reduction, fiber loss, lean muscle decline), muscle cross-sectional area shrinking and intramuscular fat accumulation, along with concomitant mechanical or morphological alterations of the intra- and extracellular components also played an important role in the development of spasticity (Lieber et al., 2004; Li and Francisco, 2015). The current management regimens for spasticity include physical therapy (such as neuromuscular stimulation, functional electrical stimulation, or ultrasound therapy), oral anti-spasticity drugs, intrathecal baclofen, chemical nerve block and motor point block. However, spasticity cannot always be adequately managed despite the diversity of treatment regimens. The common side effects of drugs and the invasiveness of local treatment are undesirable. Thus, effective and non-invasive intervention methods for spasticity are urgently needed, particularly for the intervention that target the peripheral muscular factor that contributes to muscle spasticity (Yelnik et al., 2010). The application of quantitative evaluation techniques of muscle properties will facilitate the understanding of the underpinning mechanisms and the effectiveness of new intervention strategy of post stroke spasticity management (Lindberg et al., 2011; Chuang et al., 2012; Pennati et al., 2016).

Previous studies showed that extracorporeal shock wave (ESW) could increase the efficiency of the tissue regeneration process by promoting blood microcirculation and tissue rheology (Goertz et al., 2012; Link et al., 2013). Other study demonstrated the neuronal effects of ESW therapy to increase the expression of neuronal nitric oxide synthase and creates new axons (Lee and Kim, 2015) which indicated that ESW might be a promising modality to treat spasticity caused by the upper motor neuron (UMN) lesion non-invasively(Manganotti and Amelio, 2005; Sohn et al., 2011). Based on the propagation pattern, there are the two different types of ESW stimulus: focused extracorporeal shock wave (fESW) and radial extracorporeal shock wave (rESW). The fESW is generated electromagnetically, electrohydraulically and piezoelectrically with rapidly increased pressure that means more invasive with the highest energy exposure in the focal area of deep zones. The pressure of rESW is pneumatically generated by the ballistic device that slowly increases. The wave is absorbed to a depth of 3 cm which is less invasive and better tolerance (Dymarek et al., 2014, 2016a). Previous studies reported that both types of ESW could successfully treat spasticity. Significant effectiveness of ESW was observed in patients suffering from cerebral palsy (Amelio and Manganotti, 2010), multiple sclerosis(Marinelli et al., 2015) and stroke (Daliri et al., 2015). ESW therapy was considered as a useful tool to treat spasticity and to improve joint range of motion and gait pattern in neurorehabilitation. It was reported that ESW could reduce pain and muscle tone in MS patients through acting on the non-reflex hypertonia, such as reducing muscle fibrosis. A total of six studies (Manganotti and Amelio, 2005; Santamato et al., 2013; Troncati et al., 2013; Daliri et al., 2015; Li et al., 2016; Wu et al., 2018) that utilized ESW intervention to treat upper limb spasticity in stroke patients reported significant reductions in MAS, increased of elbow passive range of movement and Fugl-Meyer score (Wu et al., 2018). The authors of these studies concluded that ESW therapy was at least as effective as botulinum toxin type A (BoNT-A) for the treatment of post stroke upper limb spasticity. Daliri et al. (2015) reported a significant improvement in post-stroke spasticity of the wrist flexor muscles as assessed by the α motor neuron excitability and the H-reflex (HMR, Hmax/Mmax ratio) of electromyography (EMG) post ESW intervention. However, Manganotti et al. (Manganotti and Amelio, 2005) reported no significant alterations on the motor nerve conduction parameters of nEMG examination after ESW treatment. In two studies that investigated the effect of ESW treatment on lower limb post-stroke muscles spasticity, the authors reported no statistically significant change in all EMG parameters (F wave, H-reflex, and H/M ratio) was observed. These findings confirm that the effect of ESW is not related to spinal excitability modifications (Sohn et al., 2011; Santamato et al., 2014). These contradictory results cast some uncertainties on the underpinning mechanism of ESW intervention for spasticity, which add some support to the hypothesis that ESW affects rheological properties of the hypertonic muscles, in particular on its impact on altering the periphery biomechanical properties of muscles that contribute to spasticity. This is partly related to the current status of the application of clinical scales for subjective measurements, or rely on a single type of assessment method to evaluate spasticity.

A recently published review discussed several advanced quantitative measurement technologies to assess spasticity (Luo et al., 2019). The authors emphasized the importance to

apply different measurement techniques to assess spasticity quantitatively and objectively, given the neural and peripheral components that contribute to spasticity. It is therefore logical to assess the mechanism of ESW intervention with a combination of assessment techniques to clarify its effects on the neural and peripheral contribution of muscle spasticity. The Neuroflexor (NF) method is a recently developed instrument based on the biomechanical modeling method (Lindberg et al., 2011; Gäverth et al., 2013). Resistant force during passive extension of the wrist joint was measured to estimate the neural and non-neural contribution to spasticity. Three parameters are derived: neural component (NC), elasticity component (EC), and viscosity component (VC) (Lindberg et al., 2011; Gäverth et al., 2013). The NF was validated in people with Parkinson's disease, cerebral palsy and stroke (Gäverth et al., 2014; Zetterberg et al., 2015; Kachmar et al., 2016). Our previously published study confirmed the feasibility to assess muscle stiffness, elasticity and viscosity characteristic of upper extremity spastic muscle in patients with stroke using the NF technique (Leng et al., 2019). A systematic review published recently encouraged the application of measuring technique to, including myotonometer, to assess the changes of muscle properties induced by ESW in spastic muscle (Dymarek et al., 2020). This would facilitate further understanding and new insights into the mechanism that underpins the intervention.

Myotonometer is a handheld instrument to objectively quantify muscle biomechanical properties. It applies multiple short impulses over the muscle bulk via the testing probe to generate vertical oscillations in the muscle fibers (Gapeyeva and Vain, 2008). The oscillation waveform is reflective of the viscoelastic properties of the muscle including muscle tone, elasticity, and stiffness (Gapeyeva and Vain, 2008; Lo et al., 2017). Published studies have indicated that the myotonometer is reliable and valid to measure skeletal muscle viscoelastic parameters in individuals with stroke (Rydahl and Brouwer, 2004; Chuang et al., 2012; Lo et al., 2017). Electrical impedance myography (EIM) is considered as a biomarker to assess neuromuscular disease progress and response to therapy. EIM measures the inherent muscle properties by sending an alternating sine wave current to the tissue and detecting the surface voltage, acquiring the parameters of resistance (R), reactance (X), and Phase angle [$\theta = \arctan(X/R)$]. These parameters are associated with the muscle's component, extracellular and intracellular fluids, the cell membrane integrity, and tissue interfaces, respectively (Esper et al., 2006). EIM is supposed to reflect on muscle composition and structure rather than its electrical activity (Tarulli et al., 2006). To date, there is limited number of study that investigated the changes of mechanical and electrical properties after ESW intervention in stroke survivors (Lo and Li, 2020).

Therefore, the present study aimed to assess the neural and peripheral contribution to spasticity post stroke by combining biomechanical modeling method with mechanical muscle properties and muscle composition information from electrical impedance measurement. This was followed by an investigation of the effects and underlying mechanism of rESW on spasticity.

MATERIALS AND METHODS

Study Design

This study was a single-blinded randomized controlled study. All participants were randomly allocated to ESW intervention group or control group. An overview of the study is illustrated in the CONSORT flow diagram (**Figure 1**). Data collection took place at the Department of Rehabilitation of the First Affiliated Hospital of Sun Yat-Sen University between June 2019 and January 2020. A randomization schedule was pre-generated in SPSS by an independent statistician. The sequence of allocation was kept in sealed envelope. The randomization process allocated each participant an identification number which appeared on all report forms to maintain confidentiality.

Sample Population

The inclusion criteria were as follows: (1) the first occurrence of stroke as confirmed by computed tomography or magnetic resonance imaging which resulted in unilateral hemiparesis; (2) at least 1 month of stroke onset; (3) the passive range of wrist joint was between -20° palmar flexion and 30° dorsiflexion; and (4) the MAS score for the radiocarpal joint $\geq$1. The exclusion criteria were as follows: (1) medically unstable; (2) receiving muscle relaxant or anti-spastic medication; (3)infraction at the cerebellum region; (4) coagulation disorders, electronic and metal implants or skin lesion of the upper extremity; (5) cognitive dysfunction as assessed by Mini Mental State Examination (score >26); (6) upper limb fracture or non-muscle spasm related restriction of joint movement.

Ethics Consideration

This study was approved by the Ethics Committee of the First Affiliated Hospital, Sun Yat-sen University [Ethics Number: (2017).143]. In addition, the trial had been prospectively registered at Chinese Clinical Trial Registry (ChiCTR- IOR-17012299). All participants provided written consent prior to enrollment. Study procedures were conducted according to the Declaration of Helsinki.

Outcome Measures

Outcome measures were recorded by independent assessors who were blinded to the group allocation of participants. Neural and peripheral contribution of spasticity were assessed by the parameters of Neural component (NC), Elastic component (EC) and Viscosity component (VC) measured by the NeuroFlexor. Mechanical muscle properties of tone (F) and stiffness (S) were assessed by myotonometer. EIM measured the parameters of resistance (R), reactance (X), and Phase angle (θ) [$\theta = \arctan(X/R)$]. Severity of muscle spasm was clinically assessed by the Modified Ashworth Scale (MAS). Upper limb function was assessed the Fugl-Meyer Assessment (FMA) scale.

Study Procedures

Anthropometric characteristics of the sample population including age, gender, paretic side and stroke onset time, were collected before the experiment began. Baseline assessment

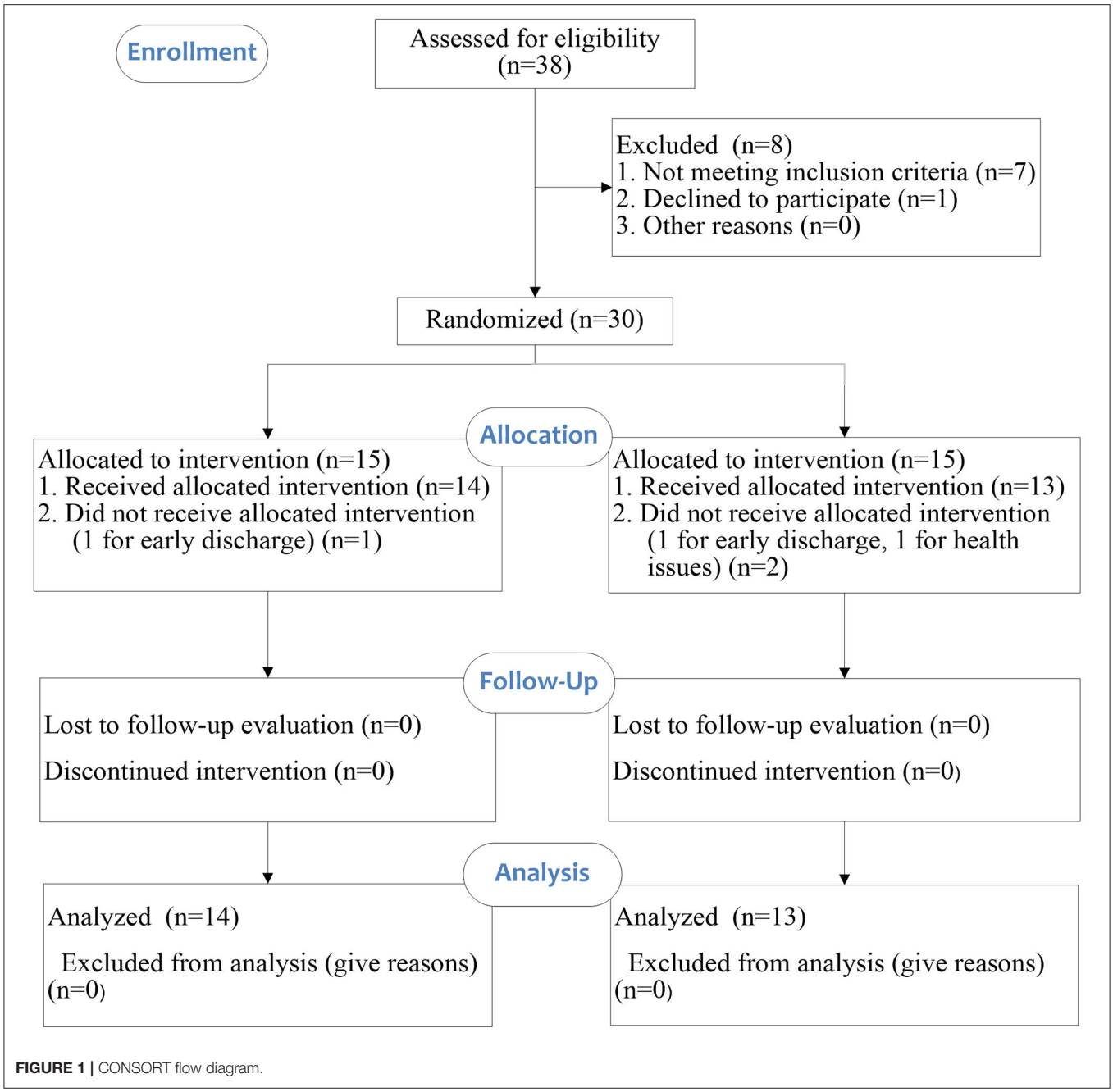

FIGURE 1 | CONSORT flow diagram.

was then conducted (t0). For the intervention group, ESW was administered immediately after baseline assessment and outcome measures were recorded right after ESW (t1). Participants then received 1 week of routine rehabilitation therapy at the same frequency and intensity with the control group. Participants in the control group received 5 sessions of regular rehabilitation treatment within a week. Each session lasted for 1.5 h and included stretching exercise therapy, occupational therapy and neurodevelopmental facilitation techniques. Outcome measures were then recorded immediately by the end of the intervention period (7 days) for both groups (t2).

Instruments

NeuroFlexor

The NeuroFlexor (Aggro MedTech AB, Solna, Sweden) produces passive movement at constant speed and records the passive resisting forces from the wrist joint in real time by the force sensor under the moveable platform (**Figure 2A**). During passive joint movement, time, angle and resisting forces were recorded simultaneously. The NF instrument ran 7 times at slow mode of 5°/s and 12 times at fast mode of 236°/s. The range of wrist movement was 50° with a starting position at −20° palmar flexion and an end position at 30° extension (7, 21). Three

components of NC, EC and VC were calculated based on a biomechanical model which was described in detailed in previous study (Lindberg et al., 2011; Pennati et al., 2016; Leng et al., 2019). EC represents the length-dependent resistant force and VC represents the viscosity-dependent resistant force. NC is estimated at maximal extension at the end of the fast passive movement by subtracting the EC and VC from the total force.

Myotonometer

A handheld myotonometer (MyotonPRO®, Estonia) was used to quantify the flexor carpi radialis muscle tone and stiffness. The test location as the thickest part of the flexor carpi radialis, which originates from the medial epicondyle of the humerus and inserts at the surface of the palm at the base of the second metacarpal bone (Garten, 2013). The patient laid in supine with upper extremity relaxed on the side. The wrist joint was kept in the neutral position with finger slightly flexed. B-mode ultrasound scan was then conducted to confirm the location of the thickest part of the muscle bulk. The testing probe of the myotonometer was placed perpendicularly to the skin surface of the tested location. The probe was first loaded by pushing against the skin surface to the required depth. Once the required depth

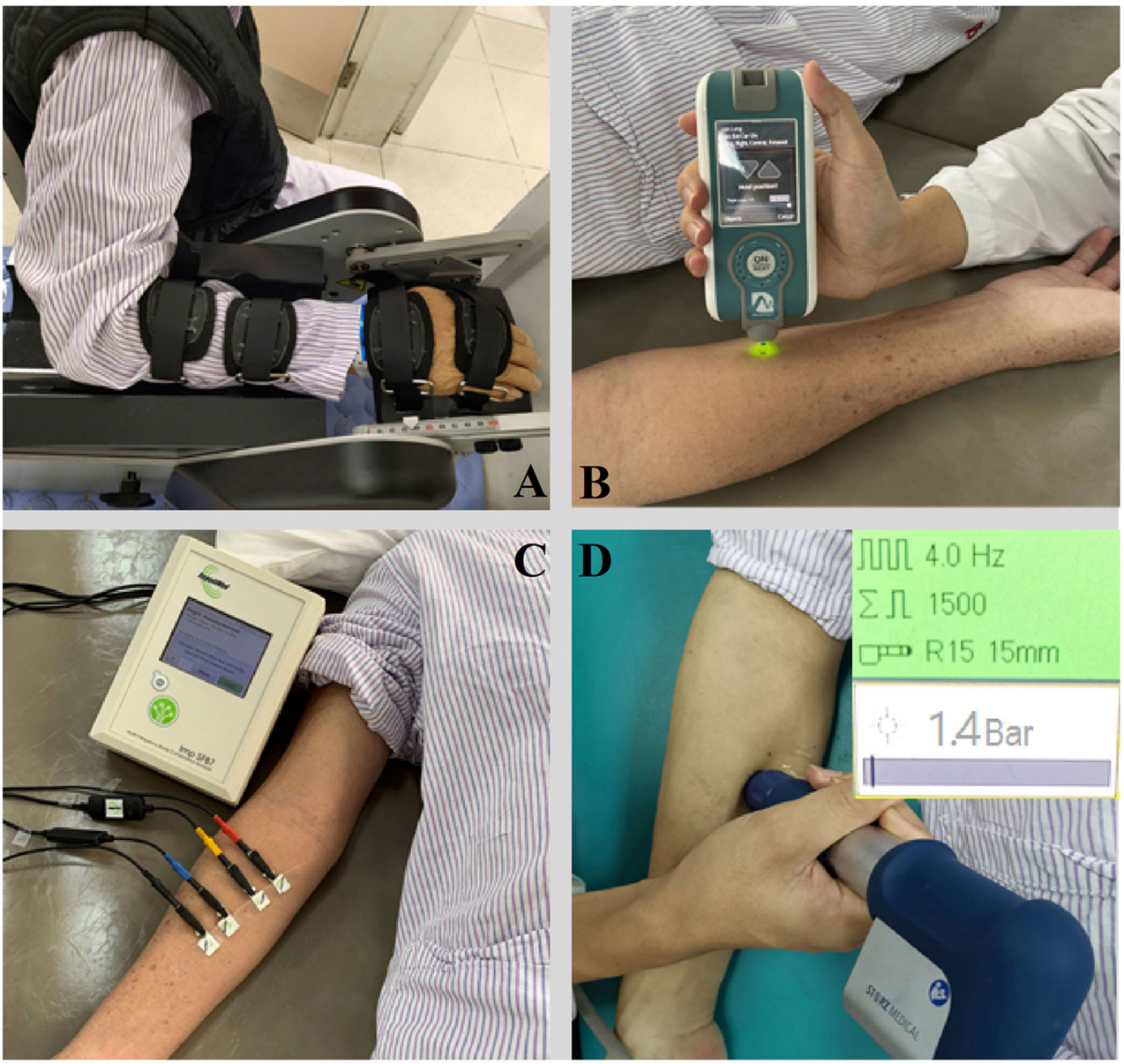

FIGURE 2 | The apparatus for measurement and therapy adopted in the study. **(A)** NeuroFlexor; **(B)** Myotonometer; **(C)** Electrical impedance myography; **(D)** Extracorporeal shock wave therapy.

TABLE 1 | The characteristic of the sample populations.

Characteristic	Experimental group	Control group	Inter-group *P*-value
Patients (*n*)	14	13	
Age (years)	51.14 ± 13.68	58.92 ± 10.08	0.107
Gender (M/F)	11/3	11/2	0.686
Weight (kg)	64.21 ± 10.53	66.08 ± 7.01	0.596
Height (m)	1.65 ± 6.90	1.69 ± 5.03	0.141
Stroke subtype (IS/HS)	8/6	10/3	0.276
Affected site(R/L)	9/5	10/3	0.472
Time since onset (months)	17.39 ± 29.18	24.42 ±37.09	0.588
MAS (score)	2.00 ± 0.78	1.85 ± 0.80	0.268
FMA (score)	22.79 ± 14.37	30.23 ± 20.73	0.285

*F, female; M, male; R, right; L, left; IS, ischaemicstroke; HS, haemorrhagicstroke; n, number. FMA, Fugl-Meyer assessment scale of the motor function in paretic upper-extremity; MAS, Modified Ashworth Score. *Statistically significant between experimental group and control group.*

was reached (indicated by a change of indicator light from red to green), the device then applied three short impulses (1 s apart) to induce damped oscillations within the muscle bulk (**Figure 2B**). The oscillation pattern recorded by the transducer was used to calculate the muscle mechanical properties of tone and stiffness (Lo et al., 2017, 2019).

Electrical Impedance Myography

The muscle electrical resistance properties that reflect the muscle composition and structure of the flexor carpi radialis was assessed by EIM (Imp SFB7 Impedimed, Inc., Sydney, NSW, Australia). The center point of the electrodes was identified as the upper third between the medial epicondyle of the humerus and the second metacarpal bone at the radial side of the wrist. B-mode ultrasound scan was conducted to confirm the location of the muscle belly and the direction of the muscle fibers of flexor carpi radialis. Two pairs of electrodes were linearly arranged along the muscle fibers direction, including one pair of voltage electrodes on the inner regions and an outer pair of current electrodes (30). Each pair of electrodes was distributed symmetrically along the center point marked in advance. The distance between the two outer current electrodes and the two inner voltage electrodes was 60 and 20 mm, respectively. The dimension of the electrodes was 13 × 10 mm (**Figure 2C**). Three measurements were recorded at each assessment and the mean value of the measurement was used for statistical analysis. The data obtained by the device was exported for offline analysis by the bespoke software Bioimp. The parameters of resistance, reactance, and phase angle were recorded across multiple frequencies of between 5 and 1,000 kHz, and those parameters obtained at 50 kHz was chosen to analysis.

Extracorporeal Shock Wave

A radial ESW (rESW) pneumatic device (Chattanooga, DJO Global Inc., Guildford, United Kingdom) was adopted to provide a single session of shock wave intervention to the radial carpi flexor muscle (**Figure 2D**). The treatment protocol of ESW was follow: 1,500 shots with a pressure of 1.5 bars and wave irradiation of 4 Hz (Dymarek et al., 2020). The treating area was focused on the muscle belly of the radial carpi flexor. The energy applied was 0.038 mJ/mm^2.

Statistical Analysis

Statistical analyses were conducted using SPSS 22 (IBM, United States). Descriptive statistics were calculated for all dependent variables. The data between the experimental group and the control group were analyzed with independent *t*-test or corresponding non-parametric test. The differences of all recorded parameter between the paretic and non-paretic side were assessed by independent *t*-test. The correlations between the different parameters as measured by difference device and clinical outcome measures were determined using Pearson correlations for normally distributed data, or Spearman's correlations for non-normally distributed data. The effectiveness of rESW treatment in the intervention group at different time points were analyzed by repeated-measures one-way analysis of variance (ANOVA) and LSD *post-hoc* test. The significant level of all statistical tests was set at 0.05.

RESULTS

Thirty stroke survivors participated in the current study and 27 of them completed all assessments. Three participants (one from the intervention group and two from the control group) did not complete the final assessment (t2) due to personal reasons. The clinical characteristics and functional levels of the sample population are presented in **Table 1**. There was no significant difference between the intervention group and control group at baseline.

Bilateral Differences

The three parameters of NC, EC, and VC, on the paretic side were significantly higher than the non-paretic side ($p < 0.05$) (**Figure 3A**). The myotonometer measured muscle tone and stiffness on the paretic side were significantly higher than the non-paretic side ($p < 0.001$) (**Figure 3B**). The EIM measured parameters of resistance, reactance and phase angle were significantly lower on the paretic side than the non-paretic side ($p < 0.001$) (**Figure 3C**). **Table 2** shows a summary of the NF, myotonometer and EIM parameters on the paretic and non-paretic sides.

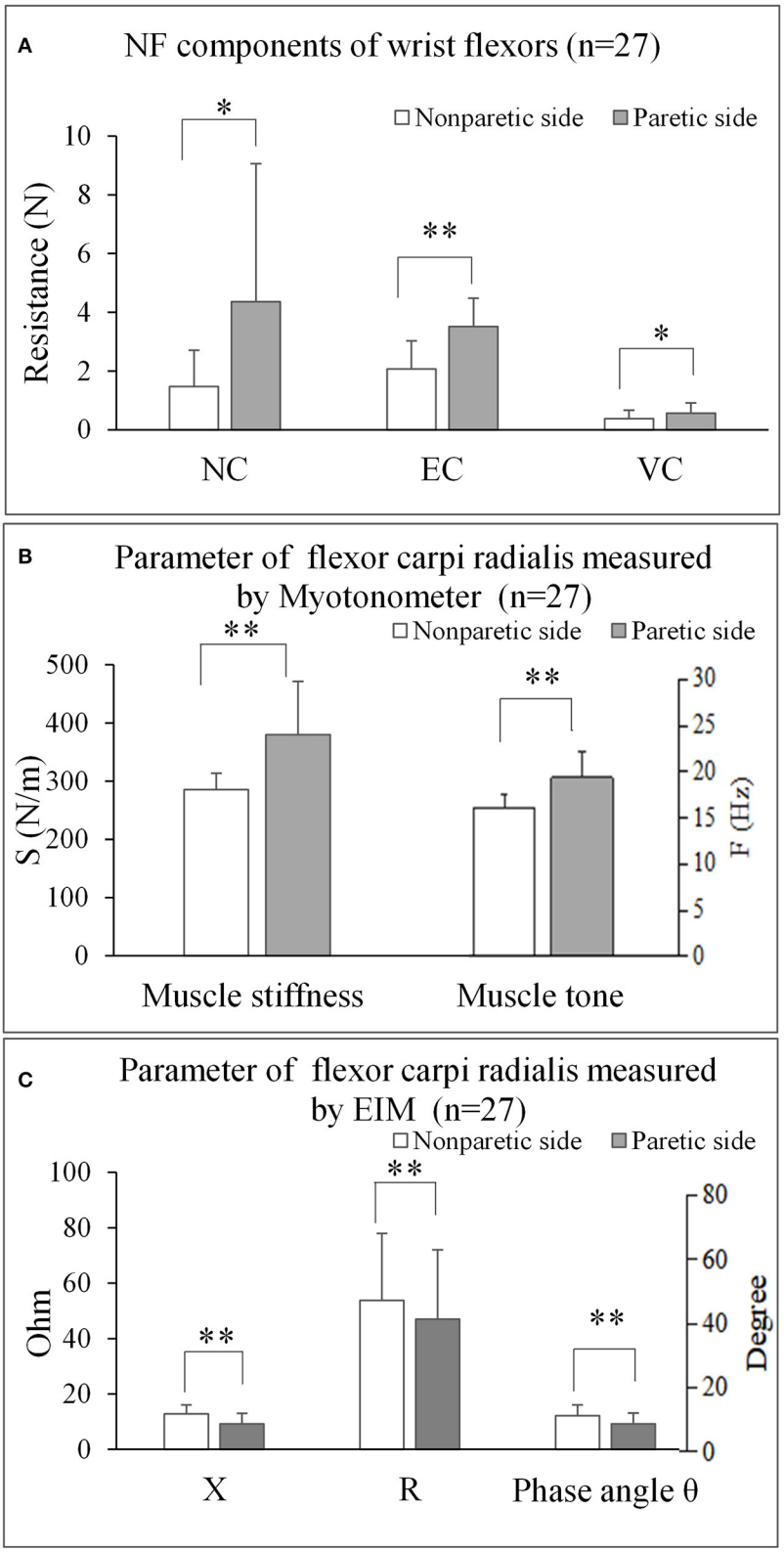

FIGURE 3 | The comparisons of bilateral parameters for each measuring techniques. **(A)** NF components of wrist flexors ($n = 27$). **(B)** Parameter of flexor carpi radialis measured by Myotonometer ($n = 27$). **(C)** Parameter of flexor carpi radialis measured by EIM ($n = 27$). NF, NeuroFlexor; NC, Neural Component; EC, Elasticity Component; VC, Viscosity Component; S, Stiffness; F, Frequency; EIM, Electrical impedance myography; X, Reactance; R, Resistance. *$P < 0.05$; ** $P < 0.001$.

TABLE 2 | Summary of the NF, Myotonometer and EIM parameters on the paretic and non-paretic side.

Measurements	Paretic side	Non-paretic side	Inter-group *P*-value
NeuroFlexor			
NC (N)	4.26± 4.70	1.47 ± 1.24	0.007*
EC (N)	3.51 ± 0.97	2.07 ± 0.96	<0.001**
VC (N)	0.57± 0.34	0.38 ± 0.29	0.041*
Myotonometer			
S (N/m)	379.96 ±91.32	285.19 ± 28.37	<0.001**
F (Hz)	19.34 ± 2.93	16.03 ±1.61	<0.001**
EIM			
R (Ohm)	47.05 ±25.04	53.78 ± 24.21	<0.001**
X (Ohm)	9.18± 3.82	12.85 ± 3.27	<0.001**
Phase angle (Degree)	9.25 ± 3.85	12.23 ±3.91	<0.001**

*NC, Neural Component; EC, Elasticity Component; VC, Viscosity Component; S, Stiffness; F, Frequency; EIM, Electrical impedance myography; X, Reactance; R, Resistance. *P < 0.05; **P < 0.001.*

Correlation Between Parameters

Moderate to high positive correlations were observed between the MAS and NC (**Figure 4A**, $r = 0.764$, $p < 0.001$), between MAS and S (**Figure 4B**, $r = 0.689$, $p < 0.001$) and between MAS and F (**Figure 4C**, $r = 0.543$, $p = 0.003$). Slight positive correlations were also observed between EC and F (**Figure 4D**, $r = 0.382$, $p = 0.049$) and between VC and phase angle (**Figure 4F**, $r = 0.394$, $p = 0.042$) of the paretic forearm flexor muscle, moderate negative correlations were observed between NC and X (**Figure 4E**, $r = -0.428$, $p = 0.026$). No significant correlation was observed between MAS and EIM parameters ($p > 0.05$), and between FMA and any other outcome measures ($p > 0.05$) of the paretic forearm flexor muscle.

Post Intervention

The results of all the outcome measures at baseline (t0), immediately after rESW (t1) and at the end of the intervention period (t2) are presented in **Table 3** and **Figure 6**. The total resistance measured by the NF decreased after intervention compared with pre intervention, but had no significant difference. The typical trend curve is shown in **Figure 5**. In the intervention group, the MAS score (**Figure 6A**) significantly decreased immediately after the rESW (t1: $p = 0.012$) and at the end of the intervention period (t2: $p = 0.021$) when compared to baseline. The MAS scores between the experimental group and the control group were significant different at t2 ($p = 0.030$). The FMA scores (**Figure 6B**) were significantly increased in the experimental group ($p < 0.001$) and the control group ($p < 0.001$) after 1 week of intervention, but the difference between the two group were not significantly different ($p > 0.05$). For the quantitative parameters in the intervention group, S (**Figure 6C**) and F (**Figure 6D**) were significantly reduced at t1 ($pS < 0.001$, $pF < 0.001$) and t2 ($pS = 0.006$, $pF = 0.001$) when compared to baseline. VC (**Figure 6E**) was significantly reduced and X (**Figure 6F**) was significantly increased at t1 (pVC = 0.033, pX = 0.041) with no significant difference at t2 when compared with t0. NC, EC, R, and phase angle were not significantly different at t1 and t2 compared to baseline. In the control group, all quantitative parameters had no significant difference at t2 when compared with baseline. For the comparison between the experimental group and the control group, S was significantly difference at the end of the intervention period (t2: $p = 0.034$). All other quantitative parameters had no statistically significant difference between the experimental group and control group at the end of intervention.

DISCUSSION

This study assessed the neural and peripheral contributing factors to post stroke muscle spasticity by applying passive torque measurement combined with biomechanical modeling, myotonometer measurements and electrical impedance myography. This was followed by the investigation of the effect of ESW intervention on muscle spasticity and upper limb function. Significant differences in several factors and mechanical parameters were observed between the affected and unaffected wrist joint of stroke survivors. Biomechanical characteristic parameters (i.e., muscle tone, stiffness, elasticity, and viscosity) and electrical impedance parameters were significantly improved after ESW intervention, especially at immediate effects right after treatment (t1).

Bilateral Differences and Clinical Relevance

NeuroFlexor Method

Some authors stated that although neural reflex hyperexctibility was a key contributing factor to the increase in resistance torque, the reduction in muscle elasticity and increasing in muscle viscosity must also be considered (7, 35). The results of the present study indicated NC, EC, and VC were significantly higher on the paretic side than the non-paretic side. This supports that theory that both the neural factor and the peripheral muscle factor play a role in spasticity. It is possible that different individuals have different portion of contribution from the neural and peripheral components

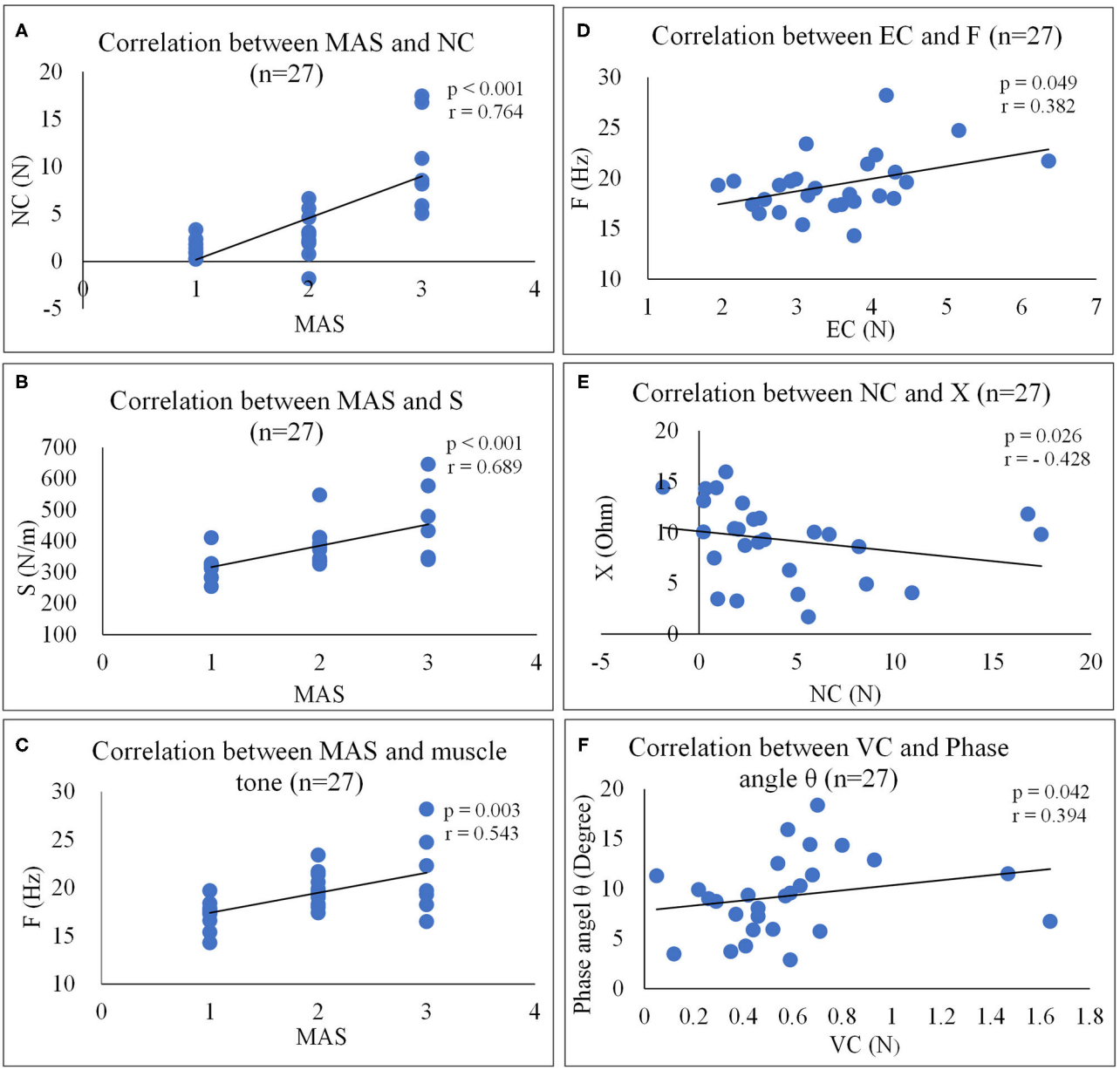

FIGURE 4 | Correlation analyses between outcome measures. **(A)** Correlation between MAS and NC ($n = 27$). **(B)** Correlation between MAS and S ($n = 27$). **(C)** Correlation between MAS and muscle tone ($n = 27$). **(D)** Correlation between EC and F ($n = 27$). **(E)** Correlation between NC and X ($n = 27$). **(F)** Correlation between VC and phase angle θ ($n = 27$). NF, NeuroFlexor; NC, Neural Component; EC, Elasticity Component; VC, Viscosity Component; S, Stiffness; F, Frequency; EIM, Electrical impedance myography; X, Reactance; R, Resistance.

(Leonard et al., 2001; Gäverth et al., 2013; Wang et al., 2017). Previous studies investigated the effect of Botox A injection on spastic elbow flexor using the NeuroFlexor method and reported a significant reduction in the neural factor but not for the non-neural peripheral factor of spasticity (Gäverth et al., 2014; Wang et al., 2018). These results provide evidence to support that individualized intervention is required to address the main spasticity contributing factors in different patients.

Muscle Mechanical Properties Measurement

This study observed significant differences in muscle tone and stiffness between the paretic side and non-paretic side as assessed by myotonometer (**Table 2**). This is consistent with the finding of NeuroFlexor in terms of the involvement of non-neural peripheral muscle factor that contribute to spasticity. The observed differences in muscle tone and stiffness between paretic and non-paretic flexor carpi radialis were consistent with published study which reported differences of 1 Hz and 30

TABLE 3 | All outcome measures at each measuring time point.

Measurement/Time point	t0	t1	t2
MAS			
Experimental group	2.00± 0.78	1.00± 0.78*	1.07± 0.73*
Control group	1.84± 0.80		1.77± 0.73
Inter-group *P*-value	0.605		0.030*
Fugl-Meyer			
Experimental group	22.79 ± 14.37	23.07 ± 14.39	25.50 ± 13.73**
Control group	30.23 ± 20.73		32.76 ± 20.73**
Inter-group *P*-value	0.285		0.310
NF			
VC (N)			
Experimental group	0.61± 0.46	0.41± 0.24*	0.52± 0.31
Control group	0.53± 0.17		0.37± 0.09
Inter-group *P*-value	0.533		0.205
EC (N)			
Experimental group	3.63 ± 1.18	3.86 ± 1.60	3.66 ± 2.18
Control group	3.37 ± 0.70		3.92 ± 1.19
Inter-group *P*-value	0.492		0.704
NC (N)			
Experimental group	5.32 ± 5.44	4.75 ± 4.58	4.35 ± 4.49
Control group	3.13 ± 3.65		3.32 ± 3.11
Inter-group *P*-value	0.234		0.499
Myotonometer			
F (Hz)			
Experimental group	19.66 ± 2.38	16.76 ± 2.11**	16.79 ± 1.81*
Control group	19.01 ± 3.49		18.12 ± 2.72
Inter-group *P*-value	0.576		0.147
S (N/m)			
Experimental group	385.50 ± 88.15	308.46 ± 61.09**	303.57 ± 42.05*
Control group	374.00 ± 97.86		351.46 ± 67.03
Inter-group *P*-value	0.751		0.034*
EIM			
X (Ohm)			
Experimental group	9.93 ± 3.51	10.51 ± 3.56*	10.11 ± 5.22
Control group	8.59 ± 4.22		8.44 ± 3.83
Inter-group *P*-value	0.378		0.355
R (Ohm)			
Experimental group	50.40 ± 21.49	52.67 ± 22.03	51.76 ± 19.36
Control group	43.84 ± 29.72		44.05 ± 29.38
Inter-group *P*-value	0.515		0.425
Phase angle (Degree)			
Experimental group	9.80 ± 3.23	10.01 ± 3.27	10.03 ± 4.45
Control group	8.71 ± 4.63		8.59 ± 4.62
Inter-group *P*-value	0.485		0.418

*Values of assessments for MAS and Fugl-Meyer scoring, F and S parameters of Myotonometer, VC parameters of NF and X parameters of EIM at the different time points shown as mean ± SD. MAS, Modified Ashworth Score; NF, NeuroFlexor; NC, Neural Component; EC, Elasticity Component; VC, Viscosity Component; S, Stiffness; F, Frequency; EIM, Electrical impedance myography; X, Reactance; R, Resistance. *P < 0.05; **P < 0.001.*

N/m in gastrocnemius in stroke survivors (Park et al., 2019). Our previously published study indicated that spastic the flexor carpi radialis (FCR) tend to have higher stiffness value, as measured by value of shear wave elastography, and the stiffness tend to increase as the stretching angle increased (Leng et al., 2019). These findings add further support the alteration of mechanical properties of spastic muscle post stroke and their contribution to spasticity. Previous studies proposed that changes

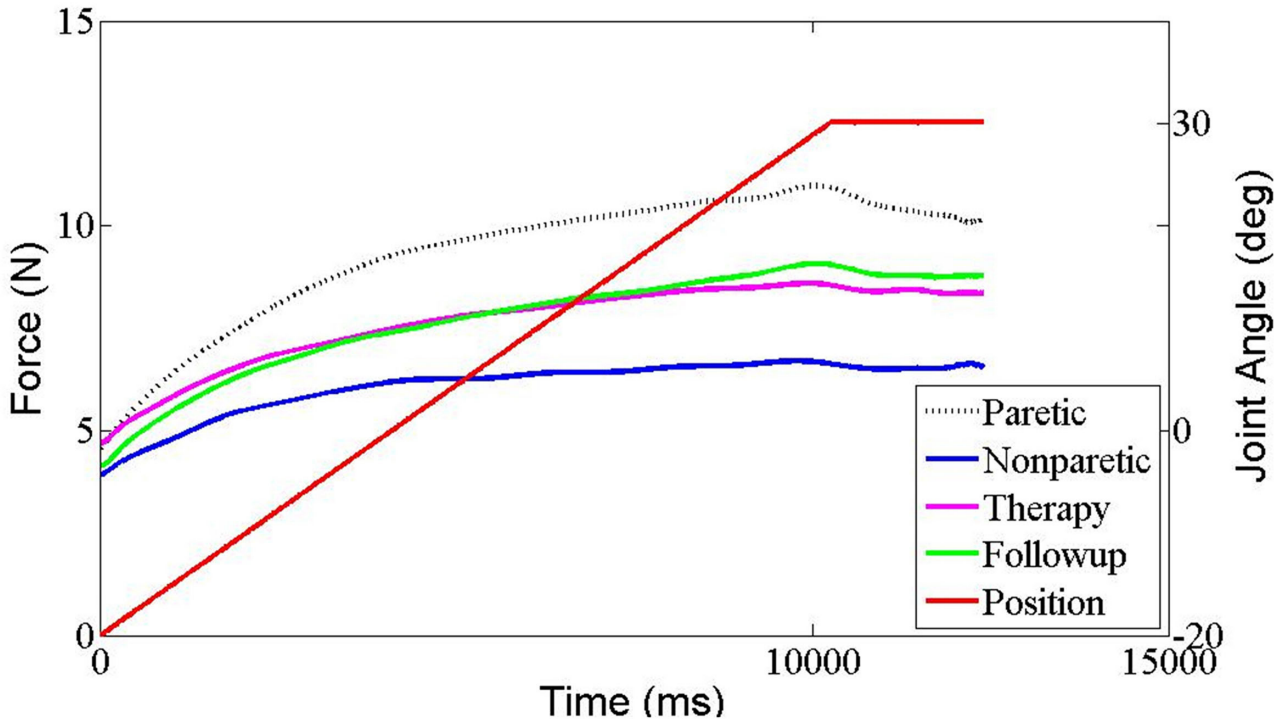

FIGURE 5 | The typical resistant force trend curve in each measurement situation recorded by Neuroflexor in one stroke patient. Red trace represents the angle of wrist movement (from flexion to extension). Black dashed trace represents resistant force of paretic side, Blue trace represents resistant force of non-paretic side, pink trace represents resistant force immediately after ESW intervention of paretic side and green trace represents resistant force at 1 week later of paretic side.

in biomechanical characteristics after stroke occurrence were related to the changes in muscle morphology, composition and extracellular matrix (Li et al., 2007; Lieber and Ward, 2013). These changes include muscle atrophy, fat infiltration, and increase of fascicular membrane thickness (De Bruin et al., 2014) and a reduction in cross-sectional area and volume (Sions et al., 2012). The movement dysfunction on the affected limb leads to the deposition of extracellular matrix, especially hyaluronic acid (Piehl-Aulin et al., 1991), which in turn contribute to an increase in viscosity between muscle fibers and the difficulty in the sliding of muscle fibers. In the development of the course of disease, if the extracellular matrix deposition is not treated in time, irreversible collagen accumulation will form and lead to increase in muscle fibrosis, muscle stiffness, and reduction in muscle elasticity (Lieber et al., 2003; Raghavan et al., 2016).

Electrical Impedance Myography

Previous studies have reported the alteration of muscle impedance of the biceps brachii (Li et al., 2017) and the hypothenar muscle (Zong et al., 2018) after the occurrence of stroke. These findings supported that reactance (X) and phase angle (θ) were stable and sensitive biomarkers in the assessment of muscle intrinsic properties. Resistance and reactance are both related to muscle mass and geometry, as well as tissue quality including extracellular and intracellular water, and the properties of cell membranes (Shiffman et al., 1999). Reduced impedance parameters are related to abnormal muscle fiber structure and damaged membrane integrities, which is induced by the loss of muscle fibers, reduced fiber cross-sectional area, or increased intramuscular extracellular matrix (Rutkove et al., 2002; Li et al., 2014). Metoki et al. (2003) revealed that paretic lower extremity muscles to have an approximate 20% reduction in muscle area and volume compared to the affected side. The contribution of muscle intrinsic property as measured by EIM to spasticity need further investigation.

Extracorporeal Shock Wave on Spasticity

The results showed that the MAS scores immediately after the ESW intervention (t1) and by the end of the intervention period (t2) were significantly lower, which was consistent with the results of previous studies (Santamato et al., 2013; Troncati et al., 2013; Daliri et al., 2015; Li et al., 2016; Guo et al., 2019). The Fulg-meyer of upper limb scores were significantly increased by the end of the intervention period (t2) in both groups, but no significant difference was observed between groups. This suggested that ESW may not be superior to conventional intervention in promoting the recovery of upper limb motor function. The long-term effect on motor function remains to be studied in the future.

Our results showed that there was a significant decrease in muscle tone, stiffness and viscosity of the wrist flexor on the affected side post ESW intervention (**Table 3** and **Figure 6**). This decreasing corresponds with a significant

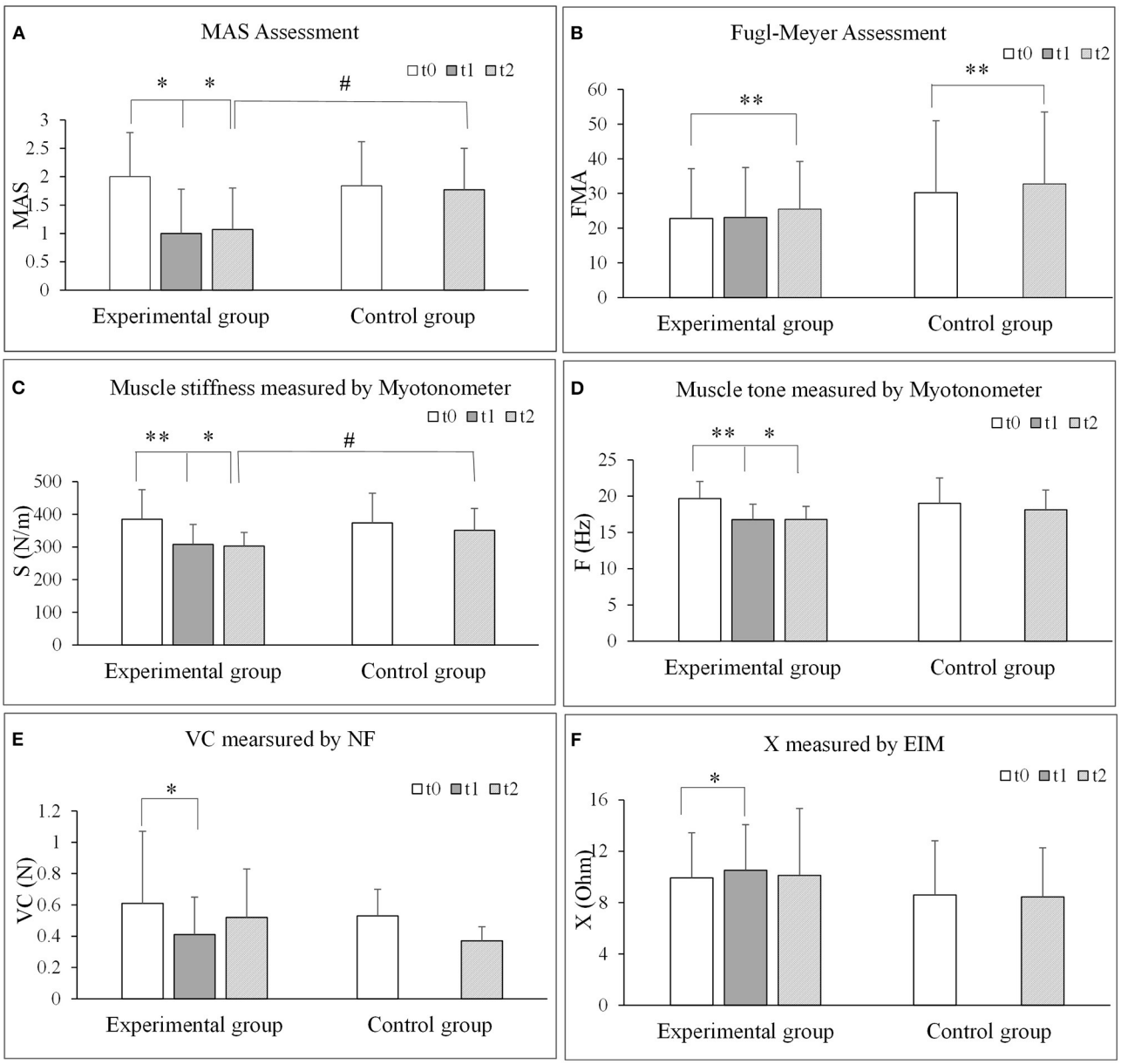

FIGURE 6 | Comparisons of each outcome measures before and after extracorporeal shock wave therapy. **(A)** MAS assessment. **(B)** Fugl-Meyer assessment. **(C)** Muscle stiffness measured by Myotonometer. **(D)** Muscle tone measured by Myotonometer. **(E)** VC measured by NF. **(F)** X measured by EIM. NF, NeuroFlexor; NC, Neural Component; EC, Elasticity Component; VC, Viscosity Component; S, Stiffness; F, Frequency; EIM, Electrical impedance myography; X, Reactance; R, Resistance. *$P < 0.05$; **$P < 0.001$.

reduction in MAS score. In previous studies, most reports focused on neuromuscular denervation rather than the structure or biomechanical characteristics of spastic muscle tissue after ESW intervention (Dymarek et al., 2014; Jia et al., 2020). Dymarek et al. (2016b) observed an improvement in trophic condition (electrophysiological and thermal effect) of the spastic muscles post rESW intervention when assessed by infrared thermal (IRT) imaging. Results of the present study observed a reduction in muscle biomechanical characteristics parameters immediately post ESW intervention and continued to be lower by the end of the intervention week. Moon investigated the effects of ESW on spastic muscle by isokinetic dynamometer (Moon et al., 2013). They found that a reduction in the peak eccentric torque, an indicator of muscle stiffness, immediately after rESW intervention and at 1 week follow up. The authors proposed that ESW affects the mechanical muscles stiffness rather than the stretch reflex hyper excitability. Park et al. (2018) investigated the effect of ESW on muscle tone and stiffness

with myotonomter in patients with stroke. The study reported a significant reduction of muscle tone (5.1 and 5.7 Hz), and muscle stiffness (17.8 and 22.5 N/m for the muscle flexor carpi radials and flexor digitorum, respectively. The present study observed similar level of reduction of muscle tone and muscle stiffness post ESW. These findings further support that ESW is beneficial in treating spasticity related alteration of muscle mechanical properties.

The VC component of the NeuroFlexor method significantly declined immediately post intervention in the ESW group. Some authors reported that the low energy mechanical vibration induced by the sonic impulse of ESW acts on spastic muscle differently from normal vibrationary stimulation (Romeo et al., 2014). However, the exact mechanism that underpins the alteration of mechanical properties induced by ESW is unclear. The majority of early literature suggested that the benefit of ESW on spasticity was by reducing the hyperexcitability of the alpha motor neuron (Leone and Kukulka, 1988) or the shock wave pressure act on the golgi tendon organ to suppress motor nerve excitability (Bae et al., 2010). However, studies that investigated the underpinning mechanism of ESW by electrophysiological measures of such as Hmax/Mmax (Daliri et al., 2015), F wave (Manganotti et al., 2012), and EMG muscle activities at rest (Dymarek et al., 2014) did not report significant difference in spastic muscle. The neural effects of ESW intervention in spasm are still controversial, recently published systematic review (Dymarek et al., 2014) suggested the neuronal effects were unlikely to be the primarily mechanism to intervene with muscle tone and stiffness since most studies did not observe a reduction in EMG activities (Dymarek et al., 2014). The lack of difference in NC component between the ESW group and the control group observed in the present study adds further support that ESW may address the peripheral muscle factor that contribute to spasticity (Manganotti and Amelio, 2005; Sohn et al., 2011; Santamato et al., 2013). Therefore, it is more likely that the biological response induced by ESW, including increase in blood flow, oxygenation, metabolic process activation and proliferative effect (Notarnicola et al., 2018) may affect the fibrosis and rheological components of muscle tissue, promoting the degradation and absorption of extracellular matrix and decreasing the muscle viscosity and stiffness (Lohse-Busch et al., 2014).

The increase in X after intervention, as measured by EIM, is related to the increase in the number of cell and cell membrane area (Shiffman and Rutkove, 2013). We proposed that the mechanical vibration produced by ESW may result in myofibers to arrange more closely and in more orderly arrangement, which in turn promote the metabolism or redistribution of extracellular matrix, allowing an increase in current resistant passes through under the same unit volume through the myofiber cell member.

Correlation Between Clinical Scales and Muscle Properties

The present study observed a significant correlation between MAS and NeuroFlexor parameters, and between MAS and myotonometer parameters. MAS score was found to be highly positively correlated with NC value but not the EC and VC values as assessed by the Neuroflexor. This result may reflect the association between the clinical symptoms of spasticity and the stretch reflex excitability (indicated by NC of NeuroFlexor), and the muscle properties (indicated by F and S of myotonometer). The changes observed in the mechanical muscle properties measured by Myotonometer are related to muscle atrophy, fiber composition and extracellular matrix deposition (Aaron et al., 2006). These changes play a role in the increase in resistant torque thus it might reflect the level of spasticity measured by MAS during passive movement. This study provided a novel interpretation about spasticity by combining with muscle intrinsic properties. The correlation between EC (measured by NeuroFlexor) and F (measured by Myotonomter) indicated a positive correlation which provide further support for the feasibility to assess the biomechanical feature of muscle spasticity by these methods.

EIM measured impedance parameters were not correlated to MAS scores (**Figure 3**). Impedance parameters is reflective of the intrinsic muscle properties which include the quality of cell membranes and connective tissues of the muscles. The lack of association may be related to the core of MAS measurement that is to assess the joint resistant during passive movement (Bohannon and Smith, 1987), while the EIM parameters measured the intrinsic muscle properties of a particular muscle group. In addition, the MAS is suggested to be more related to an increase in neural stretch reflex activity (Malhotra et al., 2009; Fleuren et al., 2010) rather than considering the non-neural mechanical properties of the resistance (Dietz and Sinkjaer, 2007). There is no significant correlation between FMA and muscle intrinsic properties as measured by the NeuroFlexor, myotonometer or EIM. FMA is more related to motor functional recovery of the entire upper limb, rather than the function of a single muscle group. Thus, in future study, a technique that focused on function assessment after intervention of one particular muscle such as sEMG, shear wave elasticity should be correlated to motor function to further reveal the correlation between muscle function and intrinsic properties.

LIMITATIONS

The findings of the present study should be interpreted with cautious due to its limitations. First, this study administered ESW for a single session (Sohn et al., 2011; Santamato et al., 2014) and outcome measures were recorded by the end of the 1-week intervention period. Thus, it is unclear the optimal intensity and frequency of ESW intervention, or if the observed benefit may persist through medium long term. In addition, the lack of a placebo treatment to compare with rESW is another limitation of this study to interpretate post intervention changes. Since the placebo effects may not be null, we will include the sham rESW as previous studies (Manganotti and Amelio, 2005; Daliri et al., 2015) in the future study. The contribution of neural factor was assessed by the NC parameters of the NeuroFlexor, which was based on published biomechanical

modeling method (Lindberg et al., 2011; Wang et al., 2017). Further studies that involve other means to assess neural activities, such as EMG on F-wave and H-flex, is recommended to substantiate the findings of ESW on muscle spasticity. This study could not ascertain if the tested muscle was completely relaxed during myotonometer assessment, despite the wrist joint was placed in a neutral or apparently relaxed position. While devices such as EMG could assess the muscle relaxation state, it was not be feasible to simultaneously apply EMG and myotonometer. This was due to the placement of the electrodes on the skin surface would affect the myotonometer's measurements. Last, the lack of pain assessment is another limitation of this study since pain was reported to have a reciprocal connection with spasticity that may also be affected by rESW.

CONCLUSION

This study reported quantifiable changes in upper limb muscle properties in post stroke muscle spasticity which adds further support to the theory that both neural component and peripheral component play a role in muscle spasticity. ESW intervention may be more effective in addressing the peripheral component of spasticity. The clinical management of post stroke spasticity should consider both the neural and non-neural factors in order to identify optimal intervention regime.

DATA AVAILABILITY STATEMENT

The datasets analyzed during the current study are available from the corresponding authors upon reasonable request.

ETHICS STATEMENT

The studies involving human participants were reviewed and approved by the Ethics Committee of the First Affiliated Hospital, Sun Yat-sen University [Ethics Number: (2017).143]. The patients/participants provided their written informed consent to participate in this study.

AUTHOR CONTRIBUTIONS

YL, LL, and DH conceived and designed the study. YL, CH, RB, and ZX performed the experiments. YL and WL wrote the paper. WL, XS, DH, and LL made contributions to the experiments. WL, DH, and LL reviewed and edited the manuscript. All authors had read and approved the manuscript.

FUNDING

This study was supported by Natural Science Foundation of China (Nos. 31771016, 32071316, and 81971224), the National Key Research and Development Program of China (No. 2020YFC2004304), and 5010 Planning Project of Sun Yat-sen University of China (No. 2014001), and partly supported by Science and Technology Planning Project of Guangdong Province (No. 2017B010110015), Guangdong Basic and Applied Basic Research Foundation (No. 2020A1515011356), and Guangzhou Research Collaborative Innovation Projects (No. 201604020108).

ACKNOWLEDGMENTS

The authors would like to thank all the participants of this study.

REFERENCES

Aaron, R., Esper, G. J., Shiffman, C. A., Bradonjic, K., Lee, K. S., and Rutkove, S. B. (2006). Effects of age on muscle as measured by electrical impedance myography. *Physiol. Meas.* 27, 953–959. doi: 10.1088/0967-3334/27/10/002

Amelio, E., and Manganotti, P. (2010). Effect of shock wave stimulation on hypertonic plantar flexor muscles in patients with cerebral palsy: a placebo-controlled study. *J. Rehabil. Med.* 42, 339–343. doi: 10.2340/16501977-0522

Bae, H., Lee, J. M., and Lee, K. H. (2010). The effects of extracorporeal shock wave therapy on spasticity in chronic stroke patients. *J. Korean Acad. Rehabil. Med.* 34, 663–669.

Bohannon, R. W., and Smith, M. B. (1987). Interrater reliability of a modified Ashworth scale of muscle spasticity. *Phys. Ther.* 67, 206–207. doi: 10.1093/ptj/67.2.206

Chuang, L. L., Wu, C. Y., and Lin, K. C. (2012). Reliability, validity, and responsiveness of myotonometric measurement of muscle tone, elasticity, and stiffness in patients with stroke. *Arch. Phys. Med. Rehabil.* 93, 532–540. doi: 10.1016/j.apmr.2011.09.014

Daliri, S. S., Forogh, B., Emami Razavi, S. Z., Ahadi, T., Madjlesi, F., and Ansari, N. N. (2015). A single blind, clinical trial to investigate the effects of a single session extracorporeal shock wave therapy on wrist flexor spasticity after stroke. *Neurorehabilitation* 36, 67–72. doi: 10.3233/NRE-141193

De Bruin, M., Van De Giessen, M., Vroemen, J. C., Veeger, H. E., Maas, M., Strackee, S. D., et al. (2014). Geometrical adaptation in ulna and radius of cerebral palsy patients: measures and consequences. *Clin. Biomech.* 29, 451–457. doi: 10.1016/j.clinbiomech.2014.01.003

Dietz, V., and Sinkjaer, T. (2007). Spastic movement disorder: impaired reflex function and altered muscle mechanics. *Lancet Neurol.* 6, 725–733. doi: 10.1016/S1474-4422(07)70193-X

Dymarek, R., Halski, T., Ptaszkowski, K., Slupska, L., Rosinczuk, J., and Taradaj, J. (2014). Extracorporeal shock wave therapy as an adjunct wound treatment: a systematic review of the literature. *Ostomy Wound Manage* 60, 26–39.

Dymarek, R., Ptaszkowski, K., Ptaszkowska, L., Kowal, M., Sopel, M., Taradaj, J., et al. (2020). Shock waves as a treatment modality for spasticity reduction and recovery improvement in post-stroke adults - current evidence and qualitative systematic review. *Clin. Interv. Aging* 15, 9–28. doi: 10.2147/CIA.S221032

Dymarek, R., Taradaj, J., and Rosińczuk, J. (2016a). The effect of radial extracorporeal shock wave stimulation on upper limb spasticity in chronic stroke patients: a single-blind, randomized, placebo-controlled study. *Ultrasound Med. Biol.* 42, 1862–1875. doi: 10.1016/j.ultrasmedbio.2016.03.006

Dymarek, R., Taradaj, J., and Rosińczuk, J. (2016b). Extracorporeal shock wave stimulation as alternative treatment modality for wrist and fingers spasticity in poststroke patients: a prospective, open-label, preliminary clinical trial. *Evid. Based Complement. Alternat. Med.* 2016:4648101. doi: 10.1155/2016/4648101

Esper, G. J., Shiffman, C. A., Aaron, R., Lee, K. S., and Rutkove, S. B. (2006). Assessing neuromuscular disease with multifrequency electrical impedance myography. *Muscle Nerve* 34, 595–602. doi: 10.1002/mus.20626

Fleuren, J. F., Voerman, G. E., Erren-Wolters, C. V., Snoek, G. J., Rietman, J. S., Hermens, H. J., et al. (2010). Stop using the Ashworth Scale for the assessment of spasticity. *J. Neurol. Neurosurg. Psychiatry* 81, 46–52. doi: 10.1136/jnnp.2009.177071

Gapeyeva, H., and Vain, A. (2008). *Methodological Guide: Principles of Applying Myoton in Physical Medicine and Rehabilitation*. Tartu: Muomeetria Ltd.

Garten, H. (2013). "*M. flexor* carpi radialis," in *The Muscle Test Handbook,* ed H. Garten (Munich: Churchill Livingstone), 72–73. doi: 10.1016/B978-0-7020-3739-9.00036-5

Gäverth, J., Eliasson, A. C., Kullander, K., Borg, J., Lindberg, P. G., and Forssberg, H. (2014). Sensitivity of the NeuroFlexor method to measure change in spasticity after treatment with botulinum toxin A in wrist and finger muscles. *J. Rehabil. Med.* 46, 629–634. doi: 10.2340/16501977-1824

Gäverth, J., Sandgren, M., Lindberg, P. G., Forssberg, H., and Eliasson, A. C. (2013). Test-retest and inter-rater reliability of a method to measure wrist and finger spasticity. *J. Rehabil. Med.* 45, 630–636. doi: 10.2340/16501977-1160

Goertz, O., Lauer, H., Hirsch, T., Ring, A., Lehnhardt, M., Langer, S., et al. (2012). Extracorporeal shock waves improve angiogenesis after full thickness burn. *Burns* 38, 1010–1018. doi: 10.1016/j.burns.2012.02.018

Guo, J., Qian, S., Wang, Y., and Xu, A. (2019). Clinical study of combined mirror and extracorporeal shock wave therapy on upper limb spasticity in poststroke patients. *Int. J. Rehabil. Res.* 42, 31–35. doi: 10.1097/MRR.0000000000000316

Jia, G., Ma, J., Wang, S., Wu, D., Tan, B., Yin, Y., et al. (2020). Long-term effects of extracorporeal shock wave therapy on poststroke spasticity: a meta-analysis of randomized controlled trials. *J. Stroke Cerebrovasc. Dis.* 29:104591. doi: 10.1016/j.jstrokecerebrovasdis.2019.104591

Kachmar, O., Voloshyn, T., and Hordiyevych, M. (2016). Changes in muscle spasticity in patients with cerebral palsy after spinal manipulation: case series. *J. Chiropr. Med.* 15, 299–304. doi: 10.1016/j.jcm.2016.07.003

Katoozian, L., Tahan, N., Zoghi, M., and Bakhshayesh, B. (2018). The onset and frequency of spasticity after first ever stroke. *J. Natl. Med. Assoc.* 110, 547–552. doi: 10.1016/j.jnma.2018.01.008

Lee, J. H., and Kim, S. G. (2015). Effects of extracorporeal shock wave therapy on functional recovery and neurotrophin-3 expression in the spinal cord after crushed sciatic nerve injury in rats. *Ultrasound Med. Biol.* 41, 790–796. doi: 10.1016/j.ultrasmedbio.2014.10.015

Leng, Y., Wang, Z., Bian, R., Lo, W. L. A., Xie, X., Wang, R., et al. (2019). Alterations of elastic property of spastic muscle with its joint resistance evaluated from shear wave elastography and biomechanical model. *Front. Neurol.* 10:736. doi: 10.3389/fneur.2019.00736

Leonard, C. T., Stephens, J. U., and Stroppel, S. L. (2001). Assessing the spastic condition of individuals with upper motoneuron involvement: validity of the myotonometer. *Arch. Phys. Med. Rehabil.* 82, 1416–1420. doi: 10.1053/apmr.2001.26070

Leone, J. A., and Kukulka, C. G. (1988). Effects of tendon pressure on alpha motoneuron excitability in patients with stroke. *Phys. Ther.* 68, 475–80. doi: 10.1093/ptj/68.4.475

Li, J., Geisbush, T. R., Rosen, G. D., Lachey, J., Mulivor, A., and Rutkove, S. B. (2014). Electrical impedance myography for the *in vivo* and *ex vivo* assessment of muscular dystrophy (MDX) mouse muscle. *Muscle Nerve* 49, 829–35. doi: 10.1002/mus.24086

Li, L., Tong, K. Y., and Hu, X. (2007). The effect of poststroke impairments on brachialis muscle architecture as measured by ultrasound. *Arch. Phys. Med. Rehabil.* 88, 243–50. doi: 10.1016/j.apmr.2006.11.013

Li, S., and Francisco, G. E. (2015). New insights into the pathophysiology of post-stroke spasticity. *Front. Hum. Neurosci.* 9:192. doi: 10.3389/fnhum.2015.00192

Li, T. Y., Chang, C. Y., Chou, Y. C., Chen, L. C., Chu, H. Y., Chiang, S. L., et al. (2016). Effect of radial shock wave therapy on spasticity of the upper limb in patients with chronic stroke: a prospective, randomized, single blind, controlled trial. *Medicine* 95:e3544. doi: 10.1097/MD.0000000000003544

Li, X., Li, L., Shin, H., Li, S., and Zhou, P. (2017). Electrical impedance myography for evaluating paretic muscle changes after stroke. *IEEE Trans. Neural Syst. Rehabil. Eng.* 25, 2113–2121. doi: 10.1109/TNSRE.2017.2707403

Lieber, R. L., Runesson, E., Einarsson, F., and Frid, N., J. (2003). Inferior mechanical properties of spastic muscle bundles due to hypertrophic but compromised extracellular matrix material. *Muscle Nerve* 28, 464–471. doi: 10.1002/mus.10446

Lieber, R. L., Steinman, S., Barash, I. A., and Chambers, H. (2004). Structural and functional changes in spastic skeletal muscle. *Muscle Nerve* 29, 615–627. doi: 10.1002/mus.20059

Lieber, R. L., and Ward, S. R. (2013). Cellular mechanisms of tissue fibrosis. 4. Structural and functional consequences of skeletal muscle fibrosis. *Am. J. Physiol. Cell Physiol.* 305, C241–C252. doi: 10.1152/ajpcell.00173.2013

Lindberg, P. G., Gäverth, J., Islam, M., Fagergren, A., Borg, J., and Forssberg, H. (2011). Validation of a new biomechanical model to measure muscle tone in spastic muscles. *Neurorehabil. Neural Repair* 25, 617–25. doi: 10.1177/1545968311403494

Link, K. A., Koenig, J. B., Silveira, A., Plattner, B. L., and Lillie, B. N. (2013). Effect of unfocused extracorporeal shock wave therapy on growth factor gene expression in wounds and intact skin of horses. *Am. J. Vet. Res.* 74, 324–32. doi: 10.2460/ajvr.74.2.324

Lo, W. L. A., and Li, L. (2020). "Chapter 12: Quantitative evaluation," in *Intelligent Biomechatronics in Neurorehabilitation,* ed X. Hu (London: Academic Press), 72–73. doi: 10.1016/B978-0-12-814942-3.00012-X

Lo, W. L. A., Yu, Q., Mao, Y., Li, W., Hu, C., and Li, L. (2019). Lumbar muscles biomechanical characteristics in young people with chronic spinal pain. *BMC Musculoskelet. Disord.* 20:559. doi: 10.1186/s12891-019-2935-z

Lo, W. L. A., Zhao, J. L., Li, L., Mao, Y. R., and Huang, D. F. (2017). Relative and absolute interrater reliabilities of a hand-held myotonometer to quantify mechanical muscle properties in patients with acute stroke in an inpatient ward. *Biomed. Res. Int.* 2017:4294028. doi: 10.1155/2017/4294028

Lohse-Busch, H., Marlinghaus, E., Reime, U., and, M., and Wis, U. (2014). Focused low-energy extracorporeal shock waves with distally symmetric polyneuropathy (DSPNP): a pilot study. *Neurorehabilitation* 35, 227–33. doi: 10.3233/NRE-141116

Luo, Z., Lo, W. L. A., Bian, R., Wong, S., and Li, L. (2019). Advanced quantitative estimation methods for spasticity: a literature review. *J. Int. Med. Res.* 48:300060519888425. doi: 10.1177/0300060519888425

Malhotra, S., Pandyan, A. D., Day, C. R., Jones, P. W., and Hermens, H. (2009). Spasticity, an impairment that is poorly defined and poorly measured. *Clin. Rehabil.* 23, 651–8. doi: 10.1177/0269215508101747

Malhotra, S., Pandyan, A. D., Rosewilliam, S., Roffe, C., and Hermens, H. (2011). Spasticity and contractures at the wrist after stroke: time course of development and their association with functional recovery of the upper limb. *Clin. Rehabil.* 25, 184–91. doi: 10.1177/0269215510381620

Manganotti, P., and Amelio, E. (2005). Long-term effect of shock wave therapy on upper limb hypertonia in patients affected by stroke. *Stroke* 36, 1967–1971. doi: 10.1161/01.STR.0000177880.06663.5c

Manganotti, P., Amelio, E., and Guerra, C. (2012). Shock wave over hand muscles: a neurophysiological study on peripheral conduction nerves in normal subjects. *Muscles Ligaments Tendons J.* 2, 104–7.

Marinelli, L., Mori, L., Solaro, C., Uccelli, A., Pelosin, E., Curr, A., et al. (2015). Effect of radial shock wave therapy on pain and muscle hypertonia: a double-blind study in patients with multiple sclerosis. *Mult. Scler. J.* 21, 622–9. doi: 10.1177/1352458514549566

Metoki, N., Sato, Y., Satoh, K., Okumura, K., and Iwamoto, J. (2003). Muscular atrophy in the hemiplegic thigh in patients after stroke. *Am. J. Phys. Med. Rehabil.* 82, 862–5. doi: 10.1097/01.PHM.0000091988.20916.EF

Moon, S. W., Kim, J. H., Jung, M. J., Son, S., Lee, J. H., Shin, H., et al. (2013). The effect of extracorporeal shock wave therapy on lower limb spasticity in subacute stroke patients. *Ann. Rehabil. Med.* 37, 461–70. doi: 10.5535/arm.2013.37.4.461

Notarnicola, A., Covelli, I., Maccagnano, G., Marvulli, R., Mastromauro, L., Ianieri, G., et al. (2018). Extracorporeal shockwave therapy on muscle tissue: the effects on healthy athletes. *J. Biol. Regul. Homeost. Agents* 32, 185–193.

Park, S.-J., Cho, K.-H., and Kim, S.-H. (2019). The immediate effect of interferential current therapy on muscle tone and stiffness in chronic stroke patients. *J. Korean Soc. Phys. Med.* 14, 1–5. doi: 10.13066/kspm.2019.14.1.1

Park, S. K., Yang, D. J., Uhm, Y. H., Yoon, J. H., and Kim, J. H. (2018). Effects of extracorporeal shock wave therapy on upper extremity muscle tone in chronic stroke patients. *J. Phys. Ther. Sci.* 30, 361–364. doi: 10.1589/jpts.30.361

Pennati, G. V., Plantin, J., Borg, J., and Lindberg, P. G. (2016). Normative NeuroFlexor data for detection of spasticity after stroke: a cross-sectional study. *J. Neuroeng. Rehabil.* 13:30. doi: 10.1186/s12984-016-0133-x

Piehl-Aulin, K., Laurent, C., Engstr M-Laurent, A., Hellstr, M., S., and Henriksson, J. (1991). Hyaluronan in human skeletal muscle of lower extremity: concentration, distribution, and effect of exercise. *J. Appl. Physiol.* 71, 2493–2498. doi: 10.1152/jappl.1991.71.6.2493

Raghavan, P., Lu, Y., Mirchandani, M., and Stecco, A. (2016). Human recombinant hyaluronidase injections for upper limb muscle stiffness in individuals with cerebral injury: a case series. *EBioMedicine* 9, 306–313. doi: 10.1016/j.ebiom.2016.05.014

Romeo, P., Lavanga, V., Pagani, D., and Sansone, V. (2014). Extracorporeal shock wave therapy in musculoskeletal disorders: a review. *Med. Princ. Pract*. 23, 7–13. doi: 10.1159/000355472

Rutkove, S. B., Aaron, R., and Shiffman, C. A. (2002). Localized bioimpedance analysis in the evaluation of neuromuscular disease. *Muscle Nerve* 25, 390–7. doi: 10.1002/mus.10048

Rydahl, S. J., and Brouwer, B. J. (2004). Ankle stiffness and tissue compliance in stroke survivors: a validation of Myotonometer measurements. *Arch. Phys. Med. Rehabil.* 85, 1631–1637. doi: 10.1016/j.apmr.2004.01.026

Santamato, A., Micello, M. F., Panza, F., Fortunato, F., Logroscino, G., Picelli, A., et al. (2014). Extracorporeal shock wave therapy for the treatment of poststroke plantar-flexor muscles spasticity: a prospective open-label study. *Top. Stroke Rehabil.* 21(Suppl. 1), S17–S24. doi: 10.1310/tsr21S1-S17

Santamato, A., Notarnicola, A., Panza, F., Ranieri, M., Micello, M. F., Manganotti, P., et al. (2013). SBOTE study: extracorporeal shock wave therapy vs. electrical stimulation after botulinum toxin type a injection for post-stroke spasticity-a prospective randomized trial. *Ultrasound Med. Biol*. 39, 283–91. doi: 10.1016/j.ultrasmedbio.2012.09.019

Shiffman, C. A., Aaron, R., Amoss, V., Therrien, J., and Coomler, K. (1999). Resistivity and phase in localized BIA. *Phys. Med. Biol.* 44, 2409–2429. doi: 10.1088/0031-9155/44/10/304

Shiffman, C. A., and Rutkove, S. B. (2013). Circuit modeling of the electrical impedance: I. *Neuromusc. Dis. Physiol. Meas*. 34, 203–21. doi: 10.1088/0967-3334/34/2/203

Sions, J. M., Tyrell, C. M., Knarr, B. A., Jancosko, A., and Binder-Macleod, S. A. (2012). Age- and stroke-related skeletal muscle changes: a review for the geriatric clinician. *J. Geriatr. Phys. Ther*. 35, 155–61. doi: 10.1519/JPT.0b013e318236db92

Sohn, M. K., Cho, K. H., Kim, Y. J., and Hwang, S. L. (2011). Spasticity and electrophysiologic changes after extracorporeal shock wave therapy on gastrocnemius. *Ann. Rehabil. Med*. 35, 599–604. doi: 10.5535/arm.2011.35.5.599

Tarulli, A. W., Chin, A. B., Partida, R. A., and Rutkove, S. B. (2006). Electrical impedance in bovine skeletal muscle as a model for the study of neuromuscular disease. *Physiol. Meas.* 27, 1269–1279. doi: 10.1088/0967-3334/27/12/002

Troncati, F., Paci, M., Myftari, T., and Lombardi, B. (2013). Extracorporeal Shock Wave Therapy reduces upper limb spasticity and improves motricity in patients with chronic hemiplegia: a case series. *Neurorehabilitation* 33, 399–405. doi: 10.3233/NRE-130970

Wang, R., Gäverth, J., and Herman, P. A. (2018). Changes in the neural and non-neural related properties of the spastic wrist flexors after treatment with botulinum toxin A in post-stroke subjects: an optimization study. *Front. Bioeng. Biotechnol*. 6:73. doi: 10.3389/fbioe.2018.00073

Wang, R., Herman, P., Ekeberg, Ö., Gäverth, J., Fagergren, A., and Forssberg, H. (2017). Neural and non-neural related properties in the spastic wrist flexors: an optimization study. *Med. Eng. Phys*. 47, 198–209. doi: 10.1016/j.medengphy.2017.06.023

Wu, Y. T., Yu, H. K., Chen, L. R., Chang, C. N., Chen, Y. M., and Hu, G. C. (2018). Extracorporeal shock waves vs. botulinum toxin type A in the treatment of poststroke upper limb spasticity: a randomized noninferiority trial. *Arch. Phys. Med. Rehabil*. 99, 2143–2150. doi: 10.1016/j.apmr.2018.05.035

Yelnik, A. P., Simon, O., Parratte, B., and Gracies, J. M. (2010). How to clinically assess and treat muscle overactivity in spastic paresis. *J. Rehabil. Med*. 42, 801–7. doi: 10.2340/16501977-0613

Zetterberg, H., Frykberg, G. E., Gäverth, J., and Lindberg, P. G. (2015). Neural and nonneural contributions to wrist rigidity in Parkinson's disease: an explorative study using the NeuroFlexor. *Biomed. Res. Int.* 2015:276182. doi: 10.1155/2015/276182

Zong, Y., Shin, H. H., Wang, Y. C., Li, S., Zhou, P., and Li, X. (2018). Assessing hand muscle structural modifications in chronic stroke. *Front. Neurol.* 9:296. doi: 10.3389/fneur.2018.00296

Conflict of Interest: The authors declare that the research was conducted in the absence of any commercial or financial relationships that could be construed as a potential conflict of interest.

frontiers in Bioengineering and Biotechnology

ORIGINAL RESEARCH
published: 16 February 2021
doi: 10.3389/fbioe.2020.591004

Applying Stretch to Evoke Hyperreflexia in Spasticity Testing: Velocity vs. Acceleration

Lizeth H. Sloot[1,2], Guido Weide[1,3], Marjolein M. van der Krogt[1], Kaat Desloovere[3], Jaap Harlaar[1,4], Annemieke I. Buizer[1,5] and Lynn Bar-On[1,3]**

[1] Amsterdam UMC, Vrije Universiteit Amsterdam, Department of Rehabilitation Medicine, Amsterdam Movement Sciences, Amsterdam, Netherlands, [2] Institute of Computer Engineering (ZITI), Heidelberg University, Heidelberg, Germany, [3] Department of Rehabilitation Sciences, KU Leuven, Leuven, Belgium, [4] Department of Biomechanical Engineering, TU Delft, Delft, Netherlands, [5] Emma Children's Hospital, Amsterdam UMC, Amsterdam, Netherlands

In neurological diseases, muscles often become hyper-resistant to stretch due to hyperreflexia, an exaggerated stretch reflex response that is considered to primarily depend on the muscle's stretch velocity. However, there is still limited understanding of how different biomechanical triggers applied during clinical tests evoke these reflex responses. We examined the effect of imposing a rotation with increasing velocity vs. increasing acceleration on triceps surae muscle repsonse in children with spastic paresis (SP) and compared the responses to those measured in typically developing (TD) children. A motor-operated ankle manipulator was used to apply different bell-shaped movement profiles, with three levels of maximum velocity (70, 110, and 150°/s) and three levels of maximum acceleration (500, 750, and 1,000°/s^2). For each profile and both groups, we evaluated the amount of evoked triceps surae muscle activation. In SP, we evaluated two additional characteristics: the intensity of the response (peak EMG burst) and the time from movement initiation to onset of the EMG burst. As expected, the amount of evoked muscle activation was larger in SP compared to TD (all muscles: $p < 0.001$) and only sensitive to biomechanical triggers in SP. Further investigation of the responses in SP showed that peak EMG bursts increased in profiles with higher peak velocity (lateral gastrocnemius: $p = 0.04$), which was emphasized by fair correlations with increased velocity at EMG burst onset (all muscles: $r > 0.33$–0.36, $p \leq 0.008$), but showed no significant effect for acceleration. However, the EMG burst was evoked faster with higher peak acceleration (all muscles $p < 0.001$) whereas it was delayed in profiles with higher peak velocity (medial gastrocnemius and soleus: $p < 0.006$). We conclude that while exaggerated response intensity (peak EMG burst) seems linked to stretch velocity, higher accelerations seem to evoke faster responses (time to EMG burst onset) in triceps surae muscles in SP. Understanding and controlling for the distinct effects of different biological triggers, including velocity, acceleration but also length and force of the applied movement, will contribute to the development of more precise clinical measurement tools. This is especially important when aiming to understand the role of hyperreflexia during functional movements where the biomechanical inputs are multiple and changing.

Keywords: spasticity assessment, stretch reflex, hyperreflexia, cerebral palsy, spastic paresis, upper motor neuron

OPEN ACCESS

Edited by:
Philippe Sucosky, Kennesaw State University, United States

Reviewed by:
Jens Bo Nielsen, University of Copenhagen, Denmark
Fan Gao, University of Kentucky, United States

****Correspondence:***
Lizeth H. Sloot
lizeth.sloot@ziti.uni-heidelberg.de
Lynn Bar-On
l.bar-on@amsterdamumc.nl

Specialty section:
This article was submitted to Biomechanics, a section of the journal Frontiers in Bioengineering and Biotechnology

Received: *03 August 2020*
Accepted: *29 December 2020*
Published: *16 February 2021*

Citation:
Sloot LH, Weide G, van der Krogt MM, Desloovere K, Harlaar J, Buizer AI and Bar-On L (2021) Applying Stretch to Evoke Hyperreflexia in Spasticity Testing: Velocity vs. Acceleration. Front. Bioeng. Biotechnol. 8:591004. doi: 10.3389/fbioe.2020.591004

INTRODUCTION

Spastic paresis (SP) is the most commonly diagnosed impairment in children with cerebral palsy or hereditary spastic paraplegia, and the most common cause for physical disability in children (Cans et al., 2002). The goal of treatment of children with SP is to improve function, i.e., activities of daily life such as walking. SP is generally characterized by increased resistance to motion in affected joints, which can be caused by neural- and tissue related impairments (van den Noort et al., 2017). Neural impairments include exaggerated reflex responses and baseline muscle activation (Dietz and Sinkjaer, 2007; van den Noort et al., 2017). Tissue-related impairments often develop over time, and include muscle shortening and increased stiffness of muscle fiber, tendon, or connective tissue (Dietz and Sinkjaer, 2007). Even though the underlying etiology guides treatment selection to manage SP, the ability to accurately measure these impairments and especially the exaggerated reflex responses, remains challenging.

The commonly accepted definition of spasticity refers to a velocity-dependent increase in tonic stretch reflexes (muscle tone) resulting from hyper-excitability of the stretch reflex (Lance, 1980), or hyperreflexia. Following this definition, clinical scales such as the Modified Tardieu Scale provide a qualitative assessment of spasticity by moving a passive joint at low and high velocity while grading the resistance to the movement (Gracies et al., 2010). The resistance during slow movement is suggested to be indicative of increased tissue stiffness and/or baseline muscle activation, while the difference in resistance between slow and fast movement is thought to reflect hyperreflexia. To standardize this procedure and increase the objectivity of the spasticity assessment, instrumented manual and robotic versions have been proposed (Wood et al., 2005; Bar-On et al., 2014). These instrumented tests provide not only quantitative information on evoked muscle activation, but also control or can provide feedback on the applied movement profile to stretch the muscle, yielding better accuracy and reliability than manual subjective scales (Burridge et al., 2005).

Robotic devices are increasingly applied to evoke and record muscle responses while controlling either the applied velocity or the applied torque (Pierce et al., 2006; Poon and Hui-Chan, 2009; de Gooijer-van de Groep et al., 2013; Willerslev-Olsen et al., 2013; Sloot et al., 2015). These standardized tests are an important step toward quantification of evoked abnormal muscle activation, although most setups still operate under the assumption that hyperreflexia is solely dependent on a velocity-driven feedback loop. Different mechanisms however are known to regulate reflex responses: the muscle spindles, which are sensory proprioceptors in the skeletal muscles that sense muscle stretch and rate of change, and Golgi tendon organs that sense force or tension. Despite a multitude of research on hyperreflexia, there is still no consensus on the exact feedback mechanisms responsible for the stretch reflexes measured during clinical tests. One reason is the wide variability in how the motorized movement trajectories are applied even for specifically the ankle joint (Wood et al., 2005). For example, stretches are applied at different starting points or range of ankle angles, while the sensitivity to activate a stretch reflex is found to be dependent on the muscles' starting length (Meinders et al., 1996). Research on hyperreflexia does suggest two main pathophysiological characteristics of recorded muscle activity during the spasticity assessments: a reduced excitability threshold and exaggerated response intensity (Sheean, 2008). The effects of different biomechanical triggers, such as position, velocity, and acceleration of the applied stretch on these characteristics of the evoked muscle response are still unknown.

As motor-controlled devices allow for controlled replication of the movement profiles applied during the clinical examination, they provide a unique testbed to disentangle the effect of different biomechanical triggers on abnormal muscle responses and are thus crucial for correct interpretation of the clinical tests (Wood et al., 2005). Previous research found different amounts of ankle plantar flexor muscle activation during instrumented motor-controlled assessment of hyperreflexia compared to manual techniques (Rabita et al., 2005; Sloot et al., 2017). As dorsiflexion angle and peak velocity did not differ between methods, other differences in movement trajectories were suggested to have affected the muscle's responses. Specifically, bell-shaped velocity profiles were applied during the manual assessments while the robotic assessments applied ramp-and hold movements with high accelerations. Since bell-shaped velocity profiles are found to be more representative of functional movement such as walking, it is relevant to explore the role of velocity vs. acceleration components in evoked muscle responses during standardized motorized assessment.

Thus, it is still speculative what mechanisms are triggered during clinical examination and the role of different movement profiles on evoking abnormal muscle activation. Therefore, the aim of this study was to compare different bell-shaped movement profiles, currently most resembling functional movement, to examine the effect of increasing imposed rotational velocity vs. acceleration on the evoked calf muscle responses. To verify the abnormal characteristics of the muscle response measured in children with SP it was contrasted to the response in typically developing children. This work contributes to the understanding of the influence of the applied movement profile during manual clinical spasticity examination and as such, supports the development of clinically relevant instrumented alternatives.

METHODS

A convenience sample of 13 children with SP [7 female; 11.3 $\pm$ 8.2 yr; 32.4 $\pm$ 10.0 kg; gross motor function classification system (GMFCS, Palisano et al., 1997) level I ($n = 3$), II ($n = 9$), and III ($n = 1$); spasticity test (SPAT, Scholtes et al., 2007) score, executed with extended knee, of 0 ($n = 3$), 1 ($n = 4$), and 2 ($n = 6$)] and 8 typically developing children (5 female; 9.9 $\pm$ 1.6 yr; 29.6 $\pm$ 19.0 kg) were included in the study. Potential participants were excluded when reporting medical problems or sports injuries interfering with lower leg joint mechanics in either group and in the SP group if treatment occurred in the previous 6 months with Botulinum NeuroToxin-A, any neuro- or orthopedic surgery involving the lower-leg, a baclofen pump,

if there was more than 20° knee flexion contracture or severe cognitive deficits. Informed consent was provided by the legal guardians and ascent obtained from the participants. The study was approved by the Dutch central ethical committee on research involving human subjects (CCMO) [NL4441073.000.12].

Protocol

Children were seated in an adjustable chair with the hip and knee joints set to 120° hip flexion and 20° knee flexion for the most affected leg in the SP group (as defined by records of their clinical examination) and the right leg in the TD group (**Figure 1A**). The foot was optimally fixated using an adjustable footplate that allowed stabilization of the subtalar joints (Huijing et al., 2013). The footplate was attached to a motor that applied rotations around the talo-crural joint in the sagittal plane. The rotation was measured using a potentiometer and the position corresponding to the individual's neutral ankle angle was calibrated using a goniometer (MOOG, Nieuw-Vennep, The Netherlands) (Sloot et al., 2015). The axis of the talo-crural joint and the motorized footplate were visually aligned by minimizing knee translation during manual rotation of the ankle in the footplate. Ankle passive range of motion (ROM) was determined by imposing low velocity dorsal (max. 6–10 Nm) and plantar (max. 4–7.5 Nm) flexion moments as measured by an integrated force transducer (Sloot et al., 2015). Surface EMG electrodes were placed on the gastrocnemius medialis (GM), lateralis (GL), soleus (SO), and tibialis anterior (TA) muscles according to SENIAM guidelines (Hermens et al., 2000) and measured with a wired system (Porti7, TMSi, Oldenzaal, The Netherlands).

The experimental measurements consisted of two repetitions of five different bell-shaped movement profiles imposed over 42° of ankle range of motion (**Figure 1B**), lasting between 0.46 and 0.73 s. The profiles had three levels of maximum acceleration (low: 500°/s^2; medium: 750°/s^2; high: 1,000°/s^2) and three levels of maximum velocity (low: 70°/s; medium: 110°/s; high: 150°/s) (see **Supplementary Table 1**). For comparison between movement profiles, the starting ankle plantarflexion orientation was adjusted such that each profile was carried out within the same 42° range (this range was required to reach the highest velocity), to ensure that the peak velocity or acceleration were reached at similar joint positions between profiles (**Figure 1B**). This range ended at the subject-specific maximal ankle dorsiflexion angle, which corresponded to mean ± std: 7.0 ± 16.0° TD vs. −4.6 ± 8.7° SP (**Figure 1B**; see **Supplementary Figure 1** for the variability in absolute ankle angle range between participants and more details about duration of the profiles). With this approach, the movement profiles were always applied over a range that ensured muscle stretch, in contrast to applying the profiles at a certain, non-individualized ankle angle. Measurements started at a random time instant, with at least 20 s rest in between imposed stretches to account for possible time-dependent viscosity effects and to allow participants to return to a relaxed state. The children were instructed to remain relaxed, and a stretch was repeated if any EMG activation of agonist and/or antagonist occurred before or at an unexpected time during stretch.

Analysis

Sagittal ankle angle, foot reaction moment, and muscle activity were measured at 1,024 Hz. EMG data were filtered using a band pass filter (20–500 Hz), a notch filter (45–54 Hz) and a low-pass filter (100 Hz), after which the root-mean-square envelope was extracted. Ankle angle and moment were low-pass filtered at 30 Hz. All filters were 6th order bi-directional Butterworth implementations.

In line with other instrumented tests that mimic clinical examinations (Bar-On et al., 2014; Sloot et al., 2017), the amount of muscle activation was quantified by both the average and peak EMG measured during the imposed movement profile, after subtraction of the baseline (i.e., minimum EMG measured 0.5 s prior to start of the stretch). The peak was taken as the 95th percentile to correct for outliers.

In addition to this general evaluation of the amount of muscle activation, we explored the characteristics of potentially evoked hyperreflexia in SP specifically. First, muscle responses were detected for each triceps surae muscle according to the method of Staude and Wolf (1999) that identifies bursts in the EMG signal, with the additional condition of peak EMG exceeding two standard deviations of the signal (Sloot et al., 2017). The identified EMG bursts were visually inspected and manually corrected if needed. Only trials with the occurrence of an EMG burst were further analyzed. For each detected EMG burst, we evaluated the time until EMG burst onset as well as the intensity of the response. The absolute time to onset was defined from the moment at which the applied movement was initiated until onset of the burst. It should be noted that this is not quantifying the latency of the evoked muscle response, as the timing of the actual threshold that triggers a reflex response is unknown. The intensity of the response was defined as the burst peak EMG, i.e., the maximum EMG after subtraction of the baseline value, recorded in the time window between EMG burst onset plus 50 ms, a sufficient time window to capture stretch reflex activation (Willerslev-Olsen et al., 2014), and normalized to each muscle's peak value found over all profiles to allow for comparison between individuals. To substantiate this analysis, we also identified the velocity and acceleration at the onset of the EMG burst—minus 30 ms, to account for an electromechanical delay (Sinkjaer et al., 1999).

Statistics

To evaluate the effect of velocity and acceleration on the amount of muscle activation, average and peak EMG parameters were averaged over the two repetitions per profile. As these variables did not follow a normal distribution, non-parametric Friedman tests were performed per population (TD and SP) to compare between the velocity profiles (VEL: low, medium, high) and similarly between the acceleration profiles (ACC: low, medium, high). *Post-hoc* testing was performed using Tukey-Kramer multiple comparison correction. To test between TD and SP, data was concatenated over profiles per variable and compared using the non-parametric Wilcoxon sign-rank test.

For the detailed analysis of EMG bursts in the SP group, the effects of acceleration and velocity profiles on both time until

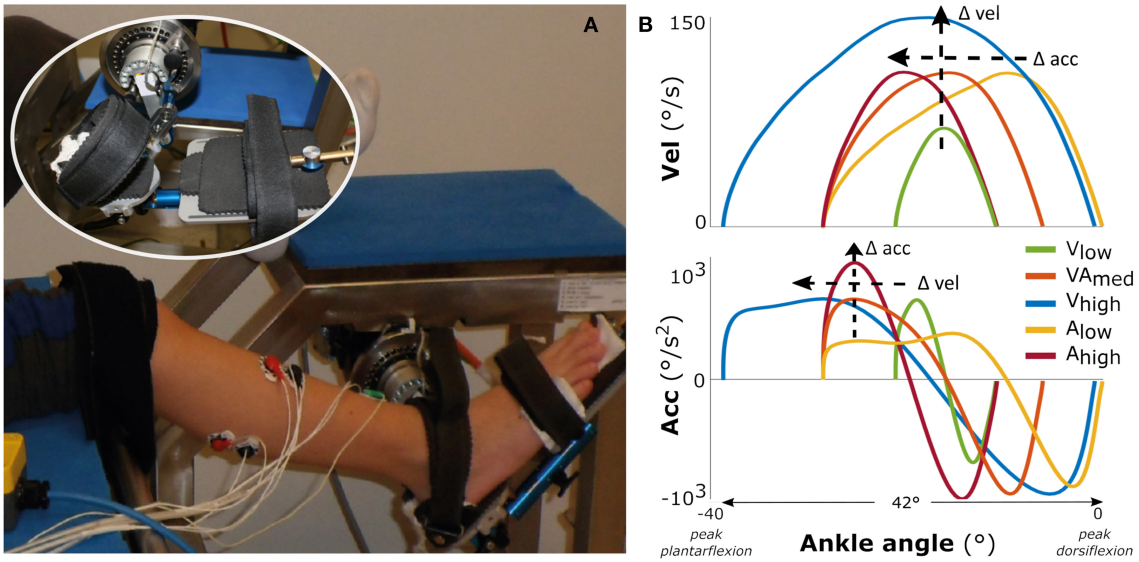

FIGURE 1 | Measurement set-up and movement profiles. On the left **(A)** the motorized footplate with adjustable chair, with the foot fixation enlarged as inset. On the right **(B)** the imposed movement velocity (upper figure) and the imposed movement acceleration (lower figure) vs. the ankle range of motion, averaged over all participants.

onset of the EMG burst and on peak EMG burst were assessed as previously, including *post-hoc* testing. For the assessment of the velocity effect, onsets that occurred after the applied peak velocity plus the electromechanical delay (<4% of the cases) were not considered. Similarly, for the acceleration effect, onsets that occurred after applied peak acceleration plus electromechanical delay (<30% of the cases) were not considered. We confirmed that these exclusions did not affect the conclusions of this analysis. To substantiate the profile analysis for peak EMG bursts, we also correlated the individual peak EMG burst values to both the corresponding velocity and acceleration at the onset of the EMG burst using Spearman's correlation analysis. Correlation values >0.6 were considered good; 0.41–0.60 moderate; 0.21–0.40 fair; and <0.20 poor (Altman, 1991). Level of significance was set at $p = 0.05$. All analyses were performed in Matlab (R2019a, Natick, MA, USA).

RESULTS

Amount of Muscle Activity

The amount of evoked muscle activation was significantly higher for the children with SP compared with TD children in all triceps surae muscles (all $p < 0.001$), underlining the exaggerated response in SP (**Figure 2**). In typically developing children, we did not find an effect of either velocity or acceleration on the amount of muscle activation (all $p > 0.19$).

In SP, larger amounts of muscle activation were found between movement profiles with increasing movement velocity (both peak and average for all muscles: $p < 0.02$, **Figure 2**). The opposite effect was found for acceleration, with a reduced amount of triceps surae muscle activation between movement profiles with increasing movement acceleration, most prominently for GL and SO (GL_{peak}: $p = 0.02$; GL_{mean}: $p = 0.02$ SO_{peak}: $p = 0.008$; SO_{peak}: $p = 0.02$, **Figure 2**). An overview of these parameters and statistical results can be found in **Supplementary Table 2**.

SP: EMG Bursts

EMG bursts were detected in 73–92% of the trials for the three triceps surae muscles in SP, and the percentages were comparable between movement profiles (**Supplementary Table 3**). Comparisons between different movement profiles indicated that peak EMG burst increased with increasing peak velocity for GL ($p = 0.04$) with a similar trend for GM ($p = 0.16$) but showed no significant differences between acceleration profiles (**Figure 3**). The time until EMG burst onset increased between movement profiles with increasing velocity (GM: $p < 0.001$; SO: $p = 0.006$; a trend for GL: $p = 0.07$; **Figure 3**) but decreased between movement profiles with increasing acceleration (all muscles $p < 0.001$). An overview of these parameters and statistical results can be found in **Supplementary Table 4**.

As individual variability combined with reduced power in this EMG burst analysis might have masked a relation between peak EMG burst and applied velocity and acceleration in the profile analysis, as found for the total amount of muscle activation, we performed an additional correlation analysis using individual data points. Increased peak EMG burst was fairly correlated with higher velocity at onset of the EMG burst for all three muscles (GM: $r = 0.35$; GL: $r = 0.36$; SO: $r = 0.33$; all: $p < 0.008$; **Figure 4**). In contrast, there was none or a negative correlation with acceleration at onset of the EMG burst (GL: $r = -0.24$, $p = 0.003$; GM: $r = 0.15$; SO: $r = -0.08$).

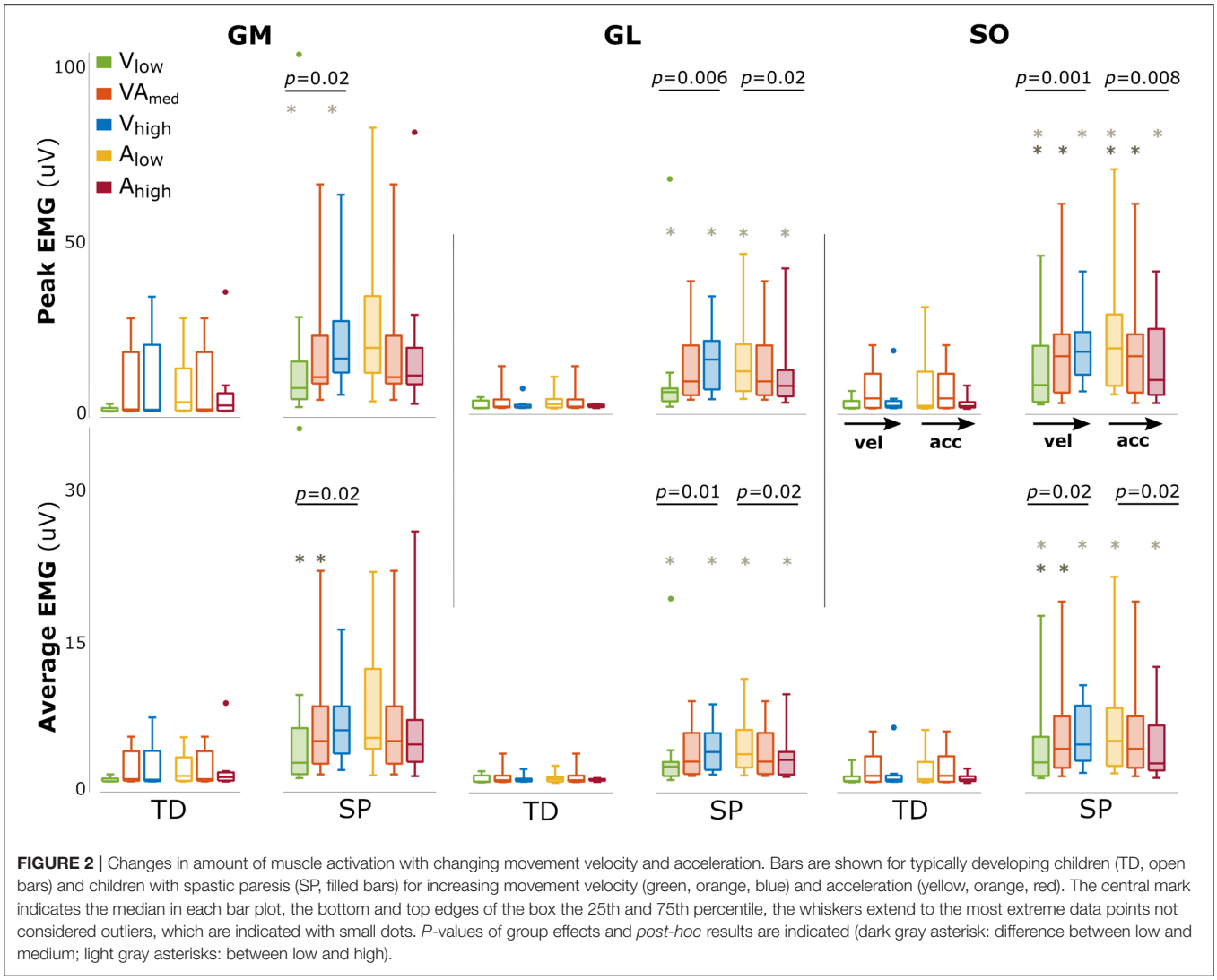

FIGURE 2 | Changes in amount of muscle activation with changing movement velocity and acceleration. Bars are shown for typically developing children (TD, open bars) and children with spastic paresis (SP, filled bars) for increasing movement velocity (green, orange, blue) and acceleration (yellow, orange, red). The central mark indicates the median in each bar plot, the bottom and top edges of the box the 25th and 75th percentile, the whiskers extend to the most extreme data points not considered outliers, which are indicated with small dots. *P*-values of group effects and *post-hoc* results are indicated (dark gray asterisk: difference between low and medium; light gray asterisks: between low and high).

DISCUSSION

Current clinical spasticity assessments impose movements on relaxed muscles to evoke exaggerated stretch reflexes that resist the imposed muscle stretch. Instrumented versions of these tests improve the quantification of the outcome. Yet, it remains the question whether the complex physiological mechanisms underlying the exaggerated reflex responses to stretch are fully understood and thus correctly assessed. As expected, we found that the amount of ankle plantar flexor muscle activation was larger and sensitive to the profiles in SP compared with TD, with the amount increasing with increasing peak velocity but decreasing with increasing peak acceleration. A more detailed analysis of activation bursts in SP revealed that the intensity of the response (peak EMG burst) increased between movement profiles with increasing maximum velocity. This was also confirmed by the correlation analysis of individual data points whereby higher threshold velocities correlated with more intense responses. On the other hand, EMG bursts were evoked faster with higher peak acceleration.

The increase in the amount of muscle activation with increasing stretch velocity in SP suggests the presence of an underlying velocity-dependent increase in tonic stretch reflexes according to the definition of spasticity by Lance (1980). The velocity dependence of stretch reflexes is originally based on findings from animal studies, showing increased velocity-sensitive fusimotor drive at the muscle spindles' gamma motor fibers in spastic muscles. However, fusimotor drive does not seem to be increased in human spastic muscles (Sheean, 2008), and unlike our findings, velocity-related reflex activation in spastic muscles has also been shown to be weak and non-linear (Powers et al., 1989; Blum et al., 2017; Baude et al., 2019). Reduced or dysregulated inhibitory drive to the alpha motor neurons from the spine and brain has also been suggested to underlie spasticity, although the precise relation to changed excitability and sensitivity of the stretch reflex remains unknown. Thus, the

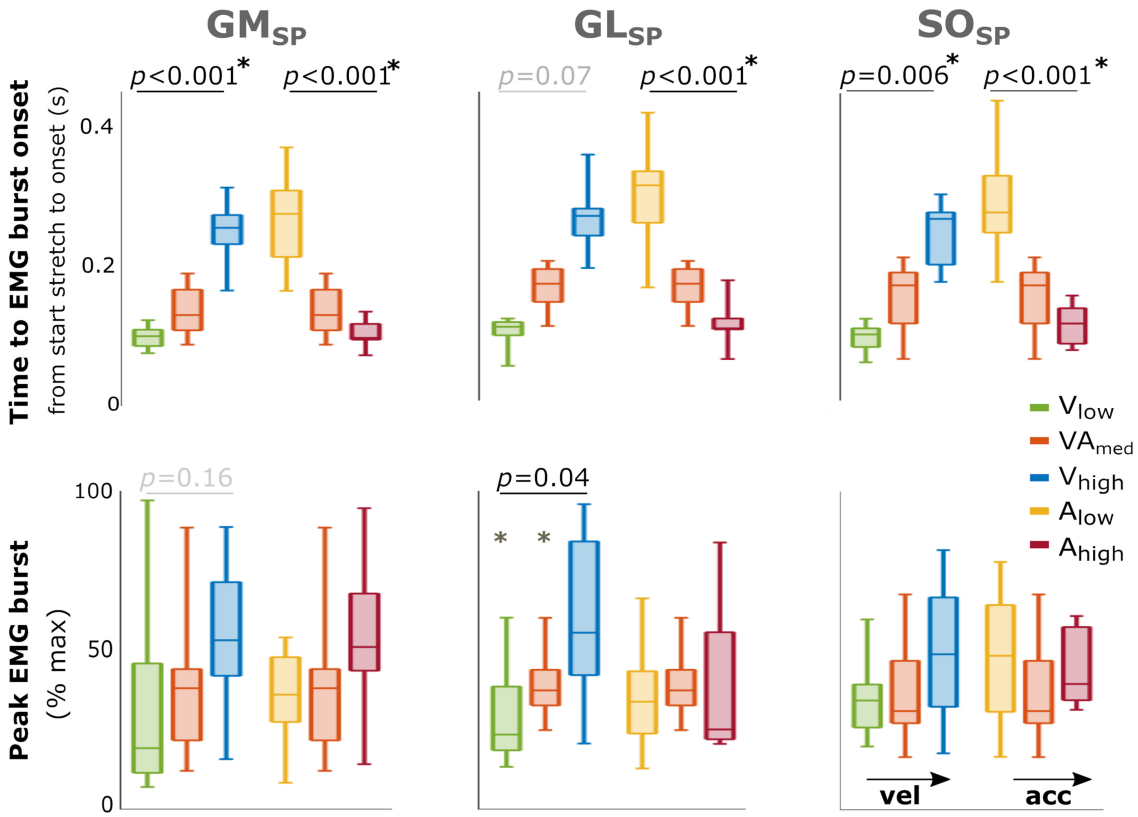

FIGURE 3 | Effect of velocity and acceleration on EMG burst characteristics in SP. Effect of increasing velocity (green, orange, blue) and acceleration (yellow, orange, red) on both total time from start stretch initiation to EMG burst onset (top) and peak EMG burst (bottom). The central mark indicates the median in each bar plot, the bottom and top edges of the box the 25th and 75th percentile, the whiskers extend to the most extreme data points not considered outliers, which are indicated with small dots. *P*-values of group effects and *post-hoc* results are indicated (star next to *p*-value indicates all three conditions are significantly different). With GM gastrocnemius medialis, GL gastrocnemius lateralis and SO soleus muscle.

actual origin of the generally accepted velocity-dependency in spasticity is still unclear.

In our more detailed analysis of EMG bursts in SP we specifically investigated only those trials in which there was a detectable burst in the EMG, commonly regarded as indicative of hyperreflexia. Such EMG bursts were detected in most SP participants and the number of bursts did not seem to be profile- or muscle-dependent. We explored two characteristics of the recorded muscle activity: the time to EMG burst onset (not equivalent to reflex latency), and the intensity of the response represented by the peak EMG burst. In the context of hyperreflexia, the timing may represent hyper-excitability or the susceptibility of the muscle to motor neuron recruitment, while response intensity may represent hypersensitivity, or the number of recruited motor neurons (Bar-On et al., 2015). We found earlier EMG burst onsets in profiles with higher accelerations, while profiles with higher velocities delayed the onsets. On the other hand, we found that the intensity of the response increased in profiles with higher velocity without an effect of acceleration. This was substantiated by the fair correlations indicating more intense responses with higher threshold velocities. These findings suggest that if we indeed measured stretch reflex responses, hyper-sensitivity (peak EMG burst) is velocity-dependent, while hyper-excitability (time to EMG burst onset) of the muscle response is driven by acceleration.

Evidence for acceleration-driven stretch reflex activation has been previously reported in studies investigating triceps surae activity during postural responses. In particular, the onset of EMG bursts following muscle stretch due to standing perturbations have repeatedly been found to be related to acceleration (Schafer, 1967; Finley et al., 2013; Blum et al., 2017). It is interesting to note that while the applied acceleration did affect our reported total amount of evoked muscle activity, which is often analyzed in instrumented spasticity tests, this biomechanical trigger is usually not accounted for. Our reported relation between onset of burst EMG and acceleration also corresponds to a recent study in SP showing that an acceleration-based model accurately predicted the timing of GM EMG burst onset (Falisse et al., 2018). However, these authors also showed that a force-related model accurately predicted both EMG burst onset timing as well as the response intensity. Advocates of the force-feedback mechanism argue that muscle spindle sensitivity depends on the state of the cross-bridges prior to muscle stretch. A greater cross-bridge overlap will increase a muscle's

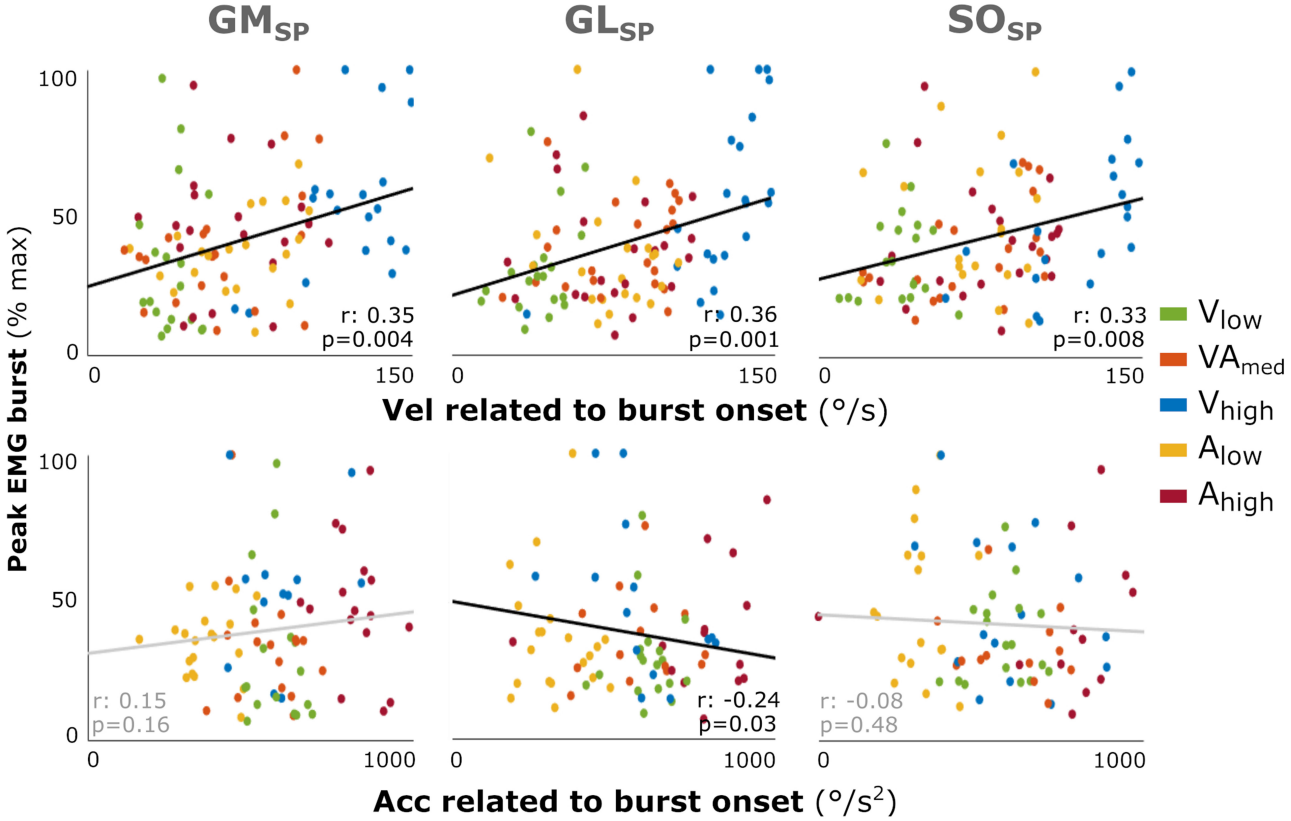

FIGURE 4 | Correlation between the muscle response intensity and velocity or acceleration related to burst onset in SP. Individual intensity peak EMG values are correlated with the acceleration (Acc) or velocity (Vel) values at the time of EMG burst onset minus the electromechanical delay (30 ms). Peak burst EMG values are the maximum EMG minus the baseline, normalized to each muscle's peak over all profiles per participant. Although not affecting the analysis, the color coding for the different movement profiles is used for context. Spearman's rho correlation coefficients and corresponding *p*-values are given. With GM gastrocnemius medialis, GL gastrocnemius lateralis, and SO soleus muscle.

initial tension, affecting the detection and thus response to the proceeding stretch (Blum et al., 2017). Since the velocity-profiles in our study had small differences in starting position (max. 19°), it is possible that this resulted in small variations in pre-tension and thus in muscle activation (De Groote et al., 2018). However, these history-dependent effects on stretch reflex activation are probably more relevant when muscles are active, as the amount of cross-bridge overlap depends on the performed activity. Falisse et al. took a first step at understanding reflexes during walking, showing that modeled force-dependency was also a better predictor of exaggerated gastrocnemius muscle activity recorded during early stance in children with SP (Falisse et al., 2018). Therefore, acceleration and force-related variables may be important to evaluate in addition to velocity when developing accurate instrumented spasticity tests, especially when assessing functional movements.

While we showed relations between the evoked muscle responses and both stretch velocity and acceleration, it is important to note that stretch reflexes are also known to be length-dependent. Wu et al. showed that at faster velocities, the joint was moved further in its position to a longer muscle length at catch (Wu et al., 2010). In the current study, profiles with higher velocities were started more toward plantarflexion such that maximum velocity occurred at a similar joint position (**Figure 1B**). Therefore, the longer time to EMG burst onset with increasing velocity may have been related to it taking longer for the muscle to be sufficiently stretched. In addition, in order to apply each profile over the same angular range, profiles differed in the maximum reached dorsiflexion angle. The profiles of A_{low} and V_{high} both ended at a similar maximum angle and showed similar peak EMG burst responses. Although to a lesser extent, this was also the case for A_{high} and V_{low} profiles. These findings may be indicative of some length-dependency. Meinders et al. argue that at longer lengths, the GM stretch reflexes are reduced (Meinders et al., 1996), possible due to inhibitory actions following stimulation of the Golgi tendon organ. It should be noted that standardizing the joint angle might not precisely standardize the input at the level of the muscle spindles, as the effects of ankle joint displacement in particular in the pennate triceps surea muscles have been shown to not linearly translate to muscle-tendon complex and thus muscle fiber lengthening (Weide et al., 2020). Therefore, we chose to align the peak applied

velocities and accelerations at about the same ankle angle and apply the movement profiles over an ankle range at which an individual's muscles were (sufficiently) lengthened. Nevertheless, given the relevance of length-dependency on stretch reflexes, future investigations applying bell-shaped movement profiles should also vary for muscle length and examine the role of start and end muscle length in current manual clinical spasticity tests, for instance by using a measured passive angle-force relationship during a slow profile to indicate the start of muscle stretch.

The nature of both manual clinical and instrumented tests assumes that the evoked muscle activity reflects involuntary reflex activation rather than voluntary muscle contraction. This requires that the participant actively relaxes, which is a somewhat artificial situation. Also, since longer lasting stretches are applied over a large ROM during these tests, other feedback mechanisms than stretch reflexes, such as via the supraspinal structures, and fast voluntary responses might occur. As we did not apply instantaneous perturbations, the exact biomechanical trigger and thus latency of a possible (reflex) response are unknown. The lack of this information makes it challenging to determine the exact nature of the measured muscle response, given that the shortest voluntary reaction time of 100 ms and supraspinal structure reaction time of 70–80 ms fall within the measured time window (Sinkjaer et al., 1988; Mirbagheri et al., 2000). However, we do have several reasons to assume we are analyzing involuntary muscle responses. First, the children were instructed to relax. Younger children, who had problems actively relaxing their muscles, were enticed to do so by playing a "statue-still" game, also involving their parents. We did monitor the background EMG before and during applied stretch and repeated trials with higher levels of activity prior to stretching. Unfortunately, no study has yet reported an approach to verify or quantify the state of muscle relaxation or the occurrence of voluntary reactions during these types of clinical tests, other than subjective impressions and EMG monitoring. Second, conform the presence of abnormal activation, bursts in muscle responses were more common in SP compared to TD. Voluntary anticipatory responses are expected to result in the opposite effect because lowered sensory drive that is required to produce these movements, has been found in patients with neurological lesions (Nielsen et al., 2020). Some studies have applied very short (up to 50 ms) perturbations to evoke muscle responses, which allows for more accurate determination of the underlying neurophysiological mechanisms of stretch reflexes and the latencies of different peaks (Sinkjaer et al., 1988; Mirbagheri et al., 2000). Such an approach could provide more insight into the relation between the different triggers examined in this study and monosynaptic Ia stretch reflexes (usually referred to as M1, with an onset around 30 ms), indirect spinal pathways (M2, around 60 ms), transcortical reflexes (M3, around 90 ms) or later responses that are not purely reflex in nature. However, as these perturbations are applied at a specific ankle angle or muscle length, their relation to current clinical tests performed over the whole ROM, or to functional movements, are unclear. Understanding the interplay between different biomechanical triggers and the mechanisms underlying hyperreflexia as well as voluntary contractions warrants more emphasis, especially in the light of the development of instrumented tests.

Next to the limitations arising from the nature of functional tests, the current study has some specific limitations. First, we applied lower maximum velocity and acceleration than the values up to 300 and 3,600 deg/s^2 previously reported in literature for manual stretching methods (Berardelli et al., 1983). In our study maximum values were chosen to ensure the children were able to remain relaxed during the measurements and were found to be high enough to evoke stretch reflexes in most of the children with SP. Second, only three different levels of velocity and acceleration were included in the study. While more intermediate steps would have increased the levels of detail, it is not expected to have changed the reported relationships. Third, we did not execute the different movement profiles in random order. However, having found opposite results for the effects of velocity and acceleration on stretch reflex parameters, while both were applied in increasing order, showed that the effect of the biomechanical triggers overruled any potential order effect. Third, the number of subjects included in this clinical study was limited, though large enough to find effects. Having included subjects with varying degrees of clinically diagnosed spasticity, we demonstrated that our findings can be cautiously generalized to a heterogeneous SP population. Our choice to also include mildly involved children with SP meant that not every profile had an EMG burst. Thus, the secondary analyses were carried out on fewer data, which may explain the findings of only fair correlations and may indicate that the reported effects may have even been underestimated. Finally, to ensure the analyses remained hypothesis driven, we excluded those instances when EMG burst onset occurred after peak velocity or acceleration similar as done in other studies (Falisse et al., 2018), but we confirmed that this did not affect the conclusions.

This study is the first to vary and control both the applied velocity and acceleration during an instrumented spasticity assessment. As expected, triceps surae activation was found to be larger and more sensitive to changes in velocity and acceleration in children with SP compared to TD children. In addition, the analysis in SP suggests that the two characteristics of hyperreflexia are affected by different biomechanical triggers: exaggerated response intensity seems linked to stretch velocity while higher acceleration seems to evoke faster responses. As such, this work indicates that biomechanical triggers should be accounted for when developing instruments to quantify spasticity. This becomes even more paramount when studying stretch reflex responses during functional movements in which both velocity and acceleration inputs are highly volatile. The reported differences in evoked muscle response between movement profiles indicate that any feedback provided by a manual instrumented test on applied stretch velocity should ultimately be accompanied by information on characteristics such as the acceleration. As this feedback will be complex and all the biological triggers are difficult to control, algorithms that extract and differentiate the response based on a range of stretches, or motorized alternatives to standardize the

applied stretch, might be desirable. The testbed used in this study could be further refined to better identify the nature of the abnormal responses as well as control other factors affecting the stretch reflex, such as muscle length and force characteristics.

DATA AVAILABILITY STATEMENT

The raw data supporting the conclusions of this article will be made available by the authors, without undue reservation.

ETHICS STATEMENT

The studies involving human participants were reviewed and approved by Dutch central ethical committee on research involving human subjects (CCMO) [NL4441073.000.12]. Written informed consent to participate in this study was provided by the participant's legal guardian/next of kin and ascent given by the participants.

AUTHOR CONTRIBUTIONS

LS, GW, KD, JH, MK, and LB conceptualized the methods. LS, GW, and LB designed the experiments. JH, AB, and LB acquired funding. GW and LB collected the data. LS and LB processed and analyzed the data. LS, MK, AB, and LB interpreted the data. LS and LB wrote the manuscript. LS generated the figures and tables. All authors provided critical feedback on the manuscript.

FUNDING

This research was financially supported by the KNAW Fund Medical Sciences (Ter Meulen Scholarship), the German Carl-Zeiss Foundation project HEIAGE and grants from the Research Foundation Flanders (FWO-12R4215N and IWT-TBM 060799) and from the Netherlands Organization for Scientific Research (NWO-016.186.144).

ACKNOWLEDGMENTS

The authors would like to thank Peter Hordijk for his assistance programming the applied movement profiles.

SUPPLEMENTARY MATERIAL

The Supplementary Material for this article can be found online at: https://www.frontiersin.org/articles/10.3389/fbioe.2020.591004/full#supplementary-material

Supplementary Figure 1 | Imposed movement velocity profiles. **(A)** Variability between participants in the range of ankle angle over which the different movement profiles were applied. The average applied velocity vs. angle is shown for all movement profiles per group, with SP in solid lines and TD in dashed lines. The movement profile of V_high is also shown for each participant, representing the maximum angular range over which the profiles were applied. The zero angle represents the neutral ankle angle, with negative values being plantarflexion and positive values dorsiflexion. **(B)** The average movement profiles of the CP group shown over time, with the total duration of the profiles and timing of peak velocities.

Supplementary Table 1 | Peak velocity and acceleration imposed during different movement profiles for typically developing (TD) children and children with spastic paresis (SP). A slow profile was used to determine the ankle range of motion of participants. With Max. maximum, Med. Medium, vel velocity, acc acceleration.

Supplementary Table 2 | Effects on the amount of muscle activation for typically developing (TD) children and children with spastic paresis (SP). Median and interquartile range values per group as well as statistical outcomes. *Post hoc* results are indicated when $p<0.05$ (with Tukey-Kramer correction for multiple comparison), with lm representing a significant difference between the low and medium conditions and lh a difference between the low and high conditions (no differences were found for mh). Results for testing between the grouped data of TD and SP are also given. With GM, Gastrocnemius Medialis; GL, Gastrocnemius Lateralis; SO, soleus muscles.

Supplementary Table 3 | Percentage of detected EMG onsets in children with spastic paresis (SP). Percentage of onsets taken over all trials in the SP data per profile. With GM, gastrocnemius medialis; GL, gastrocnemius lateralis; SO, soleus muscle.

Supplementary Table 4 | Effects on EMG burst characteristics in children with spastic paresis. Median and interquartile range values for group effects on acceleration and velocity as well as statistical outcomes. *Post hoc* results are indicated when $p<0.05$ (with Tukey-Kramer correction for multiple comparison), with lm representing a significant difference between the low and medium conditions, lh a difference between the low and high conditions and mh between medium and high. With max. GM, Gastrocnemius Medialis; GL, Gastrocnemius Lateralis; SO, soleus muscles.

REFERENCES

Altman, D. G. (1991). *Practical Statistics for Medical Research*. London: CRC press. doi: 10.1201/9780429258589

Bar-On, L., Aertbelien, E., Molenaers, G., Dan, B., and Desloovere, K. (2014). Manually controlled instrumented spasticity assessments: a systematic review of psychometric properties. *Dev. Med. Child Neurol.* 56, 932–950. doi: 10.1111/dmcn.12419

Bar-On, L., Molenaers, G., Aertbelien, E., Van Campenhout, A., Feys, H., Nuttin, B., et al. (2015). Spasticity and its contribution to hypertonia in cerebral palsy. *Biomed Res. Int.* 2015:317047. doi: 10.1155/2015/317047

Baude, M., Nielsen, J. B., and Gracies, J. M. (2019). The neurophysiology of deforming spastic paresis: A revised taxonomy. *Ann. Phys. Rehabil. Med.* 62, 426–430. doi: 10.1016/j.rehab.2018.10.004

Berardelli, A., Sabra, A. F., Hallett, M., Berenberg, W., and Simon, S. R. (1983). Stretch reflexes of triceps surae in patients with upper motor neuron syndromes. *J. Neurol. Neurosurg. Psychiatry* 46, 54–60. doi: 10.1136/jnnp.46.1.54

Blum, K. P., D'Incamps, B. L., Zytnicki, D., and Ting, L. H. (2017). Force encoding in muscle spindles during stretch of passive muscle. *PLoS Comput. Biol.* 13:e1005767. doi: 10.1371/journal.pcbi.1005767

Burridge, J. H., Wood, D. E., Hermens, H. J., Voerman, G. E., Johnson, G. R., Van Wijck, F., et al. (2005). Theoretical and methodological considerations in the measurement of spasticity. *Disabil. Rehabil.* 27, 69–80. doi: 10.1080/09638280400014592

Cans, C., Guillem, P., Arnaud, C., Baille, F., Chalmers, J., McManus, V., et al. (2002). Prevalence and characteristics of children with cerebral palsy in Europe. *Dev. Med. Child Neurol.* 44, 633–640. doi: 10.1017/S0012162201002675

de Gooijer-van de Groep, de Vlugt, E., de Groot, J. H., Heijden-Maessen, H. C. M., Wielheesen, D. H. M., van Wijlen-Hempel, R. S., et al. (2013). Differentiation between non-neural and neural contributors to ankle joint stiffness in cerebral palsy. *J. Neuroeng. Rehabil.* 10, 1–8. doi: 10.1186/1743-0003-10-81

De Groote, F., Blum, K. P., Horslen, B. C., and Ting, L. H. (2018). Interaction between muscle tone, short-range stiffness and increased sensory feedback gains explains key kinematic features of the pendulum test in spastic cerebral palsy: a simulation study. *PLoS ONE* 13:e0205763. doi: 10.1371/journal.pone.0205763

Dietz, V., and Sinkjaer, T. (2007). Spastic movement disorder: impaired reflex function and altered muscle mechanics. *Lancet Neurol.* 6, 725–733. doi: 10.1016/S1474-4422(07)70193-X

Falisse, A., Bar-On, L., Desloovere, K., Jonkers, I., and De Groote, F. (2018). A spasticity model based on feedback from muscle force explains muscle activity during passive stretches and gait in children with cerebral palsy. *PLoS ONE*. 13:e0208811. doi: 10.1371/journal.pone.0208811

Finley, J. M., Dhaher, Y. Y., and Perreault, E. J. (2013). Acceleration dependence and task-specific modulation of short- and medium-latency reflexes in the ankle extensors. *Physiol. Rep*. 1:e00051. doi: 10.1002/phy2.51

Gracies, J. M., Burke, K., Clegg, N. J., Browne, R., Rushing, C., Fehlings, D., et al. (2010). Reliability of the Tardieu Scale for assessing spasticity in children with cerebral palsy. *Arch. Phys. Med. Rehabil*. 91, 421–428. doi: 10.1016/j.apmr.2009.11.017

Hermens, H. J., Freriks, B., Disselhorst-Klug, C., and Rau, G. (2000). Development of recommendations for SEMG sensors and sensor placement procedures. *J. Electromyography Kinesiol*. 10, 361–374. doi: 10.1016/S1050-6411(00)00027-4

Huijing, P. A., Benard, M. R., Harlaar, J., Jaspers, R. T., and Becher, J. G. (2013). Movement within foot and ankle joint in children with spastic cerebral palsy: a 3-dimensional ultrasound analysis of medial gastrocnemius length with correction for effects of foot deformation. *BMC Musculoskelet. Disord*. 14:365. doi: 10.1186/1471-2474-14-365

Lance, J. W. (1980). *Pathophysiology of Spasticity and Clinical Experience With Baclofen. Spasticity: Disordered Motor Control*. Chicago, IL: Year Book Medical Publicers, 185–203.

Meinders, M., Price, R., Lehmann, J. F., and Questad, K. A. (1996). The stretch reflex response in the normal and spastic ankle: effect of ankle position. *Arch. Phys. Med. Rehabil*. 77, 487–492. doi: 10.1016/S0003-9993(96)90038-6

Mirbagheri, M. M., Barbeau, H., and Kearney, R. E. (2000). Intrinsic and reflex contributions to human ankle stiffness: variation with activation level and position. *Exp. Brain Res*. 135, 423–436. doi: 10.1007/s002210000534

Nielsen, J. B., Christensen, M. S., Farmer, S. F., and Lorentzen, J. (2020). Spastic movement disorder: should we forget hyperexcitable stretch reflexes and start talking about inappropriate prediction of sensory consequences of movement? *Exp. Brain Res.* 238, 1627–1636. doi: 10.1007/s00221-020-05792-0

Palisano, R., Rosenbaum, P., Walter, S., Russell, D., Wood, E., and Galuppi, B. (1997). Development and reliability of a system to classify gross motor function in children with cerebral palsy. *Dev. Med. Child Neurol.* 39, 214–223. doi: 10.1111/j.1469-8749.1997.tb07414.x

Pierce, S. R., Lauer, R. T., Shewokis, P. A., Rubertone, J. A., and Orlin, M. N. (2006). Test-retest reliability of isokinetic dynamometry for the assessment of spasticity of the knee flexors and knee extensors in children with cerebral palsy. *Arch. Phys. Med. Rehabil*. 87, 697–702. doi: 10.1016/j.apmr.2006.01.020

Poon, D. M. Y., and Hui-Chan, C. W. Y. (2009). Hyperactive stretch reflexes, co-contraction, and muscle weakness in children with cerebral palsy. *Dev. Med. Child Neurol*. 51, 128–135. doi: 10.1111/j.1469-8749.2008.03122.x

Powers, R. K., Campbell, D. L., and Rymer, W. Z. (1989). Stretch reflex dynamics in spastic elbow flexor muscles. *Ann. Neurol.* 25, 32–42. doi: 10.1002/ana.410250106

Rabita, G., Dupont, L., Thevenon, A., Lensel-Corbeil, G., Perot, C., and Vanvelcenaher, J. (2005). Differences in kinematic parameters and plantarflexor reflex responses between manual (Ashworth) and isokinetic mobilisations in spasticity assessment. *Clin. Neurophysiol.* 116, 93–100. doi: 10.1016/j.clinph.2004.07.029

Schafer, S. S. (1967). Acceleration response of a primary muscle-spindle ending to ramp stretch of extrafusal muscle. *Experientia* 23, 1026–1027. doi: 10.1007/BF02136428

Scholtes, V. A. B., Dallmeijer, A. J., and Becher, J. G. (2007). "The Spasticity Test: a clinical instrument to measure spasticity in children with cerebral palsy," in *The Effectiveness of Multilevel Botulinum Toxin Type A and Comprehensive Rehabilitation in Children With Cerebral Palsy*, ed V. A. B. Scholtes (Amsterdam: Ponsen & Looijen BV), 29–64.

Sheean, G. (2008). "Neurophysiology of spasticity," in *Upper Motor Neurone Syndrome and Spasticity: Clinical Management and Neurophysiology*, eds M. P. Barnes and G. R. Johnson (Cambridge University Press), 9–63.

Sinkjaer, T., Andersen, J. B., Nielsen, J. F., and Hansen, H. J. (1999). Soleus long-latency stretch reflexes during walking in healthy and spastic humans. *Clin. Neurophysiol.* 110, 951–959. doi: 10.1016/S1388-2457(99)00034-6

Sinkjaer, T., Toft, E., Andreassen, S., and Hornemann, B. C. (1988). Muscle-stiffness in human ankle dorsiflexors - intrinsic and reflex components. *J. Neurophysiol.* 60, 1110–1121. doi: 10.1152/jn.1988.60.3.1110

Sloot, L. H., Bar-On, L., van der Krogt, M. M., Aertbelien, E., Buizer, A. I., Desloovere, K., et al. (2017). Motorized versus manual instrumented spasticity assessment in children with cerebral palsy. *Dev. Med. Child Neurol.* 59, 145–151. doi: 10.1111/dmcn.13194

Sloot, L. H., van der Krogt, M. M., de Gooijer-van de Groep, van Eesbeek, S., de Groot, J., Buizer, A. I., et al. (2015). The validity and reliability of modelled neural and tissue properties of the ankle muscles in children with cerebral palsy. *Gait Posture*. 42, 7–15. doi: 10.1016/j.gaitpost.2015.04.006

Staude, G., and Wolf, W. (1999). Objective motor response onset detection in surface myoelectric signals. *Med. Eng. Phys.* 21, 449–467. doi: 10.1016/S1350-4533(99)00067-3

van den Noort, J. C., Bar-On, L., Aertbelien, E., Bonikowski, M., Braendvik, S. M., Brostrom, E. W., et al. (2017). European consensus on the concepts and measurement of the pathophysiological neuromuscular responses to passive muscle stretch. *Eur. J. Neurol.* 24, 981–e38. doi: 10.1111/ene.13322

Weide, G., Huijing, P. A., Becher, J. G., Jaspers, R. T., and Harlaar, J. (2020). Foot flexibility confounds the assessment of triceps surae extensibility in children with spastic paresis during typical physical examinations. *J. Biomech.* 99:109532. doi: 10.1016/j.jbiomech.2019.109532

Willerslev-Olsen, M., Andersen, J. B., Sinkjaer, T., and Nielsen, J. B. (2014). Sensory feedback to ankle plantar flexors is not exaggerated during gait in spastic hemiplegic children with cerebral palsy. *J. Neurophysiol.* 111, 746–754. doi: 10.1152/jn.00372.2013

Willerslev-Olsen, M., Lorentzen, J., Sinkjaer, T., and Nielsen, J. B. (2013). Passive muscle properties are altered in children with cerebral palsy before the age of 3years and are difficult to distinguish clinically from spasticity. *Dev. Med. Child Neurol.* 55, 617–623. doi: 10.1111/dmcn.12124

Wood, D. E., Burridge, J. H., Van Wijck, F. M., Mcfadden, C., Hitchcock, R. A., Pandyan, A. D., et al. (2005). Biomechanical approaches applied to the lower and upper limb for the measurement of spasticity: a systematic review of the literature. *Disabil. Rehabil.* 27, 19–32. doi: 10.1080/09638280400014683

Wu, Y. N., Ren, Y. P., Goldsmith, A., Gaebler, D., Liu, S. Q., and Zhang, L. Q. (2010). Characterization of spasticity in cerebral palsy: dependence of catch angle on velocity. *Dev. Med. Child Neurol.* 52, 563–569. doi: 10.1111/j.1469-8749.2009.03602.x

Conflict of Interest: The authors declare that the research was conducted in the absence of any commercial or financial relationships that could be construed as a potential conflict of interest.

frontiers in Bioengineering and Biotechnology

ORIGINAL RESEARCH
published: 25 March 2021
doi: 10.3389/fbioe.2021.604071

Increased Ankle Plantar Flexor Stiffness Is Associated With Reduced Mechanical Response to Stretch in Adults With CP

Jakob Lorentzen[1,2], Rasmus Feld Frisk[1,2], Jens Bo Nielsen[1,2]* and Lee Barber[3]*

[1] Department for Neuroscience, University of Copenhagen, Copenhagen, Denmark, [2] Elsass Foundation, Charlottenlund, Denmark, [3] School of Applied Health Sciences, Griffith University, Brisbane, QLD, Australia

Hyperexcitable stretch reflexes are often not present despite of other signs of spasticity in people with brain lesion. Here we looked for evidence that increased resistance to length change of the plantar flexor muscle-fascicles may contribute to a reduction in the stretch reflex response in adults with cerebral palsy (CP). A total of 17 neurologically intact (NI) adults (mean age 36.1; 12 female) and 13 ambulant adults with CP (7 unilateral; mean age 33.1; 5 female) participated in the study. Subjects were seated in a chair with the examined foot attached to a foot plate, which could be moved by a computer-controlled electromotor. An ultrasound probe was placed over the medial aspect of the leg to measure the length of medial gastrocnemius muscle fascicles. Slow (7 deg/s) and fast (200 deg/s) stretches with amplitude 6 deg of the plantar flexors were applied over an ankle range of 70 deg at 10 deg intervals between 60 and 130 deg plantarflexion. It was checked by EMG electrodes that the slow stretches were sufficiently slow not to elicit any activity and that the fast stretches were sufficiently quick to elicit a maximal stretch reflex in both groups. The torque elicited by the stretches was measured together with changes in the length of medial gastrocnemius muscle fascicles. Muscle fascicles increased significantly in length with increasing dorsiflexion position in both populations ($p < 0.001$), but the fascicles were shorter in the CP population at all positions. Slow stretches elicited significantly larger torque and significantly smaller length change of muscle fascicles as the ankle joint position was moved more towards dorsiflexion in CP than in NI ($p < 0.001$). Fast stretches elicited larger torque responses at ankle joint positions of 80–100 deg in the NI than in the CP group ($p < 0.01$). A significant negative correlation was observed between the torque response and muscle fascicle length change to slow stretch in CP ($p < 0.05$), but not in NI. These findings support that increased passive resistance of the ankle plantar flexor muscle-tendon unit and development of contractures may conceal stretch reflex response in adults with CP. We argue that this should be taken into account in the neurological examination of spasticity.

Keywords: ankle stiffness, biomechanical evaluation, cerebral palsy, contractures, electrophysiology, spasticity

OPEN ACCESS

Edited by:
Lynn Bar-On,
Amsterdam University Medical Center, Netherlands

Reviewed by:
Friedl De Groote,
KU Leuven, Belgium
Thomas D. O'Brien,
Liverpool John Moores University, United Kingdom

****Correspondence:***
Jakob Lorentzen
jlorentzen@sund.ku.dk
Jens Bo Nielsen
jbnielsen@sund.ku.dk

Specialty section:
This article was submitted to Biomechanics, a section of the journal Frontiers in Bioengineering and Biotechnology

Received: *08 September 2020*
Accepted: *22 February 2021*
Published: *25 March 2021*

Citation:
Lorentzen J, Frisk RF, Nielsen JB and Barber L (2021) Increased Ankle Plantar Flexor Stiffness Is Associated With Reduced Mechanical Response to Stretch in Adults With CP. Front. Bioeng. Biotechnol. 9:604071. doi: 10.3389/fbioe.2021.604071

INTRODUCTION

Cerebral palsy (CP) is a congenital neurodevelopmental disorder caused by a non-progressive disturbance of the developing brain, which occurs before, at the time of or shortly after birth (Bax et al., 2005; Graham et al., 2016). The disabilities caused by the primary lesion and secondary problems such as contractures and joint deformities continue to be a challenge also in adulthood and recent observations suggest that significant further deterioration of functional abilities are common at relatively young age in adults with CP (Bottos et al., 2001; Morgan and McGinley, 2014; Cremer et al., 2017). Since CP is the most common cause of childhood disability and life expectancy is close to that of the background population, the population of adults with CP, who require health services and social support, is as large as for several other neurological disabilities in adults such as multiple sclerosis and Parkinson's disease (Peterson et al., 2015). Despite of this, there is comparatively little research performed in adults with CP and we therefore have relatively little knowledge of the nature of their functional challenges and problems.

Recent studies using objective electrophysiological and biomechanical techniques have indicated that it is reduced central neural drive, reduced muscle mass and altered muscle mechanics, including increased passive (non-neural) stiffness leading to reduced joint mobility (contractures) and joint deformities, which are the main causes of limited functional capacity and reduced gait ability in the group of ambulant (high-functioning) adults with CP (Geertsen et al., 2015; Gillett et al., 2018; Yamaguchi et al., 2018; Frisk et al., 2019a,b). In contrast, hyperexcitability of stretch reflexes and muscle "over-activity" appear to have no or little significance (Geertsen et al., 2015; Frisk et al., 2017). However, the observation of lack of exaggerated stretch reflexes should be taken with some caution. Several factors influence the size of the stretch reflex when elicited under standardized conditions during a biomechanical and electrophysiological objective examination, but probably the most important is to which extent the stretch reaches the muscle spindles in the investigated muscles and causes a response of the muscle spindle afferents. In healthy muscles that are exercised regularly, muscle spindles respond quickly and effectively to even very small stretches, but muscles in persons with central motor lesions are different in a number of ways that may change this dramatically. When muscles are inactive, the extrafusal muscle fibres undergo atrophy (Bodine, 2013), which may in itself change the mechanical efficiency of a stretch in activating the muscle spindles, which are placed mainly in parallel with the extrafusal muscle fibres (Windhorst, 2008). Atrophy has been shown to alter the pennation angle of the muscle fascicles, which may result in an altered response of the muscle spindles (Narici et al., 2016). The muscle spindles themselves also undergo alternations in structure and composition of their membrane receptors, which may lead to altered responses to stretch (Carrasco et al., 2017). Importantly, the elastic elements in the muscle such as the connective tissue in the extracellular matrix proliferate and become stiffer, which may eventually result in reduced range of movement and manifest contractures (Singer et al., 2001; de Bruin et al., 2014; Jalal et al., 2020). These alterations in the muscles may be demonstrated within a few days after central motor lesions, but develop gradually over weeks, months and even years following the primary lesion – likely depending on complex genetic and environmental factors in the individual case (Jalal et al., 2020). Due to their early occurrence and their significant impact on functional ability, it has been suggested that these alterations in muscle architecture and function should be considered a muscle disease in its own right (Baude et al., 2019).

Clarification of the interaction between these changes in muscle properties and stretch reflex activity is important for directing clinical practice and treatment. Such an interdependence has indeed been found in children with CP (Bar-On et al., 2018).

In the present exploratory study we investigated whether altered muscle architecture and soft tissue resistance may reduce the ability of an applied stretch in reaching muscle spindles and elicit a mechanical response to stretch in adults with CP.

MATERIALS AND METHODS

A total of 13 adults with CP aged 33 ± 7years (5 females, 8 males; 6 GMFCS I, 3 GMFCS II, and 4 GMFCS III) and 17 neurological intact adults (NI) aged 36.1 ± 4.5years (11 females and 6 males) participated in the study. The CP participants were recruited from the Danish Cerebral Palsy organization. Adults diagnosed with spastic type CP were included if they were independent ambulant with/without walking aid (GMFCS I–III), and had reduced range of motion (ROM) in the ankles or increased passive stiffness in plantar flexors. Participants with CP were excluded if they had received lower limb intramuscular injection with Botulinum toxin type-A within 6 month. The TD participants were recruited from the local community to participate in this study, were matched for age and were required to have had no lower limb injury in the six months prior to testing. All participants were excluded if they had received lower limb orthopaedic surgery or injury within the previous two years. However, 11 of the 13 participants with CP had one or more Achilles tendon elongational surgery during their childhood

Three of the 13 participants with CP had been taking antispastic medication (Baclofen) on a daily basis for more than 5 years. However, all participants were asked to omit taking any anti spastic medication prior to the examination on the day of the study.

The study was approved by the local ethics committee (H-2-2014-028) and all procedures were conducted within the standards of the Helsinki declaration. Prior to experiments, all subjects received written and verbal information, and written consent for participation was obtained.

An overview of the participants is given in **Table 1**.

Test Method

Passive and Reflex Torque

In order to objectively assess the passive and reflex mediated stiffness components of the ankle plantar flexors biomechanical and electrophysiological evaluation was performed according to previous methods (Lorentzen et al., 2010).

TABLE 1 | Demographic information about all participant.

	Adults with CP *n* = 13	NI Adults *n* = 17
Age (Years)	33.1 (SD:10.9; range 23–56)	36.1 (SD:4.5; range 26–55)
Gender (% Female)	39	67
Weight (Kg)	63.5 (SD:7.0)	64.4 (SD:9.4)
Height (CM)	169.7 (9.2)	169.8 (8.7)
GMFCS (1-5)	1 = 6; 2 = 3; 3 = 4	
ROM (deg DF deficit)	0 = 3; −10 = 6; −15 = 2; −20 = 2	0 = 17
MAS (PF)	1 = 5; 2 = 5; 3 = 3	
Strength (PF)	2 = 1; 3 = 4; 4 = 6; 5 = 2	5 = 17
Achilles reflex (% hyperactive)	39	0

The first row shows the participants age in Years and standard deviation (SD); the second row shows the representation (in %) of female among the participants; the third row shows the weight in Kg and SD; the fourth row shows the height in CM and (SD); the fifth row shows the participants General Motor Performance Classification Score (GMFCS; 1–5) (first the score and them the number of participants with this score); the sixth row shows the reduction in ankle dorsi flexion (DF) range of motion (ROM) where the number represents the reduction in dorsi flexion in degrees followed by the number of participants with this reduction; the seventh row shows the Modified Ashworth Score (MAS) in the plantar flexor muscles (PF) (first the score and then the number of participants with this score); the eight row shows the strength in plantar flexors measured by the Medical Research Council scale for muscle strength (MRC; 1–5) (first is indicated the score then the number of participants with this score); the nineth row shows the representation of participants with hyperactive Achilles reflex activity (in %).

Briefly, subjects were seated in a stable reclining armchair that was fixated to the floor with the knee joint secured in a stretched position. The examined foot was attached to a footplate, which could be rotated by a motor (CEM model 26) (**Figure 1A**). The medial malleolus was aligned to the rotational center of the device and the ankle position was secured throughout the experiment by two straps. One strap around the proximal part of the foot and the pedal securing that the heel kept contact to the footplate and one strap around the distal part of the foot and the foot plate securing the distal contact between the distal part of the foot and the footplate at all times throughout the experiment. The motor was driven by a DC power amplifier (Brüel&Kjaer; model 2708) and could deliver maintained torques up to 80 Nm and peak torques up to 120 Nm. An electro-goniometer, connected to the foot plate, measured the foot plate angle and a torque meter measured the torque exerted on the foot plate prior to and during the stretch perturbations. The initial position of the talocrural joint angle was set to 90 deg which was measured with a manual goniometer and subsequent positions were adjusted according to this position. The hip joint was positioned in 100 deg flexion and the knee fully extended. The position of the knee was secured by fixation of the lower part of the thigh with 20 cm broad Velcro straps fixed to the floor.

Perturbations of the ankle were made in eight different initial ankle positions in 10 deg increments between 60 and 130 deg plantar flexion. The perturbations consisted of ramp and hold dorsiflexions with an amplitude of 6 deg at two velocities, 7 deg/s (slow; rise time 900 ms) and 200 deg/s (fast; rise time 10 ms) and with a hold time of 460 ms and fall time of 40 ms. The perturbation characteristics were similar for the two groups of participants. However, due to limitations in ankle ROM in some of the participant not all initial stretch positions were possible in all participants. All participants achieved ankle angles from 80 to 120 deg. A total of 130 and 60 deg positions were possible in 15 NI participants but no participants with CP. A total of 70 deg position was possible in all NI participants but only in seven participants with CP. Ten perturbations per velocity were delivered alternately starting with a slow stretch with a 2 s interval between each perturbation. This procedure was used for all positions.

EMG recordings were made in order to ensure that no muscle activity occurred during slow stretches and that stretch reflexes were elicited during fast stretches. EMG activity was recorded using bipolar electrodes (Ambu Blue sensor N-10-A/25, Ambu A/S Ballerup. Recording area 0.5 cm^2 inter-electrode distance, 2 cm) placed over the soleus muscle. Recordings were made from the soleus muscle in order not to interfere with ultrasound measurements (see below) and since stretch reflexes have a lower threshold and larger amplitude in this muscle as compared to the other plantar flexor muscles. The skin was brushed softly with sandpaper (3M red dot; 3M, Glostrup, Denmark). A ground electrode was placed on the distal part of the tibia. EMG signals were filtered (band-pass, 5 Hz–1 kHz), amplified (2,000×), sampled at 2 kHz, and stored on a PC for off-line analysis. Signal processing and analysis was carried out offline. The EMG records were rectified and low-pass filtered at 40 Hz (first order Butterworth). The trials were then ensemble-averaged to produce a single record for all situations.

To be qualified as a stretch reflex, EMG activity in a window 22–100 ms after onset of perturbation had to be more than 50 μV above the background EMG. The window 22–100 ms was chosen since the onset latency of the short-latency reflex is around 40 ms in adults and the voluntary reaction time is around 100 ms. The reflex torque was measured as the peak torque in a 360 ms window starting 100 ms after the end of the incline ramp phase of the perturbation relative to the baseline torque at the end of the hold period (**Figure 1D**; amplitude difference between black arrows). This has previously been shown to give a valid estimate of reflex torque (Toft et al., 1991). Lorentzen et al. (2010) demonstrated that the reflex torque measured in this way was abolished when transmission in large diameter afferents was blocked by ischemia induced by a blood pressure cuff placed around the thigh and inflated to 240 mm Hg (Lorentzen et al., 2010).

Passive torque was the difference between maximum torque during the slow trials (7 deg/s) and the resting torque at each ankle angle (**Figure 1C**; indicated by black arrows). The mean of the 10 perturbations was calculated (Maganaris et al., 2002; Lorentzen et al., 2010; Willerslev-Olsen et al., 2013).

The torque elicited by a stretch reflex depends on the number of cross-bridges between actin and myosin filaments that may be created. Since this is likely to vary between subjects the reflex torque was normalized to the maximal plantarflexion torque elicited by supramaximal stimulation of the tibial nerve at each of the investigated ankle joint positions. The stimulation was applied to the tibial nerve by a ball electrode (cathode) placed

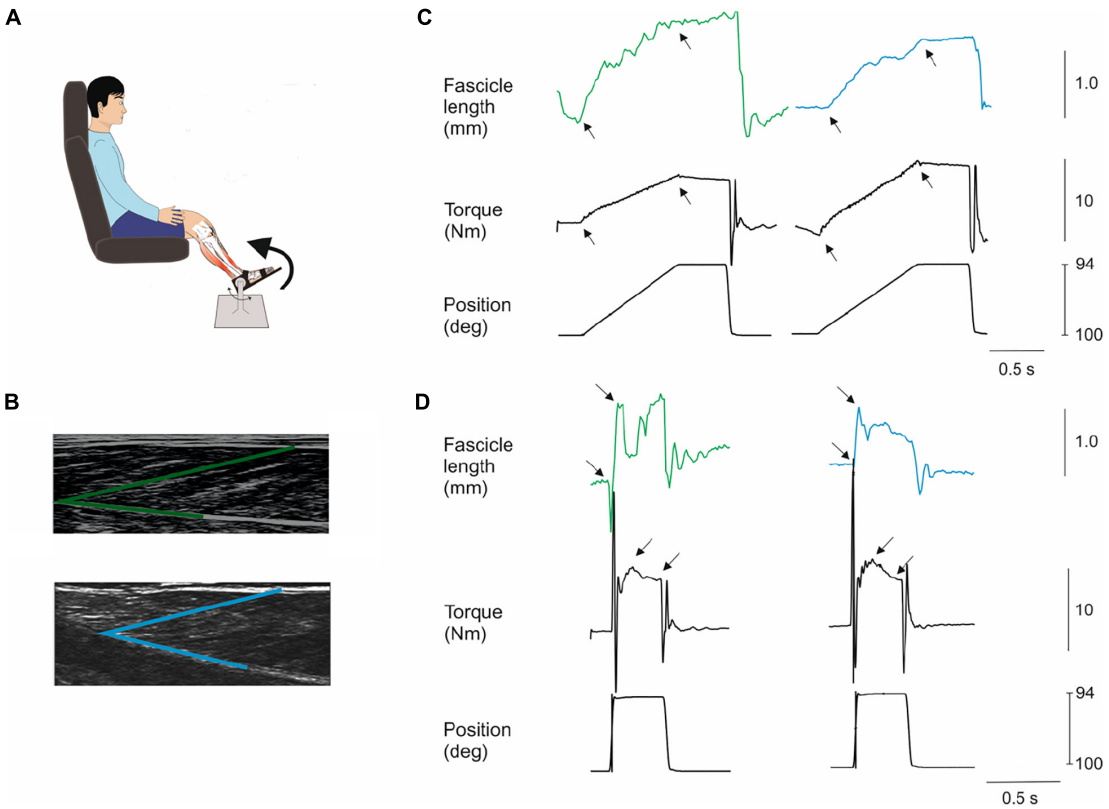

FIGURE 1 | Methods. Subjects were seated in a reclining armchair with the examined leg supported and the foot attached to a plate which could be rotated by a computer-controlled electromotor **(A)**. The hip joint was positioned in 100 deg flexion and the knee fully extended (illustration not true to reality in this respect). Slow (7 deg/s) and fast (200 deg/s) dorsiflexion rotations of the foot plate were applied at different positions of the ankle joint throughout the range of movement at 10 deg. intervals. An ultrasound probe was placed over the medial aspect of the lower limb to monitor the length of medial gastrocnemius muscle fascicles during the stretches **(B)**. A single fascicle was selected (marked in green for an NI individual and in blue for an individual with CP) and its length from the superficial to the deep aponeurosis of the muscle was tracked throughout the experiment. **(C,D)** show examples from an NI individual (left hand graphs) and individual with CP (right hand graphs) of the movement of a fascicle and the torque on the foot plate (black) during a slow **(C)** and a fast stretch **(D)** at 100 deg initial ankle position. Black arrows indicate the interval for measurement of fascicle and torque amplitudes. Note the peak in the torque measurement following the fast stretch in **(D)** indicated by the first arrow. This is the increase of torque elicited by the stretch reflex. The amplitude of this peak was measured in relation to the baseline torque during the holding phase of the stretch as indicated by the second arrow in the torque graphs of **(D)**. All fascicle measurements are in mm, all torque measurements are in Nm and position are in deg.

in the popliteal fossa and a metal plate (anode) placed above the patella using an electrical stimulator (Digitimer DS7AH, United Kingdom). The stimulation was a single shock of 1 ms duration at 300 V and up to 1 A. Since this normalization did not change the findings and since a similar normalization would not make sense in relation to the passive torque (since no cross-bridges are formed in the absence of muscle activity), we have chosen to report only non-normalized data.

Ultrasound

A personal computer-based ultrasound system (LogicScan 128; Telemed, Vilnius, Lithuania) and a 128-element linear probe (B-mode; 7.5 MHz; 60 mm field of view) were used to image the medial gastrocnemius (MG) muscle fascicles at a sampling frequency of 80 Hz (**Figure 1B**). Depth was set to 60 mm, power and gain were both set to 90%. The ultrasound recordings of the MG muscle were performed during the fast and slow stretch perturbations for 10 s which allowed recording of two fast and two slow stretch perturbations at each angle position (**Figures 1C,D**). The probe was positioned over the MG and aligned with the fascicle plane (Bénard et al., 2009) to minimize errors attributable to probe orientation (Klimstra et al., 2007) and secured over the skin surface with a compressive bandage to minimize probe movement relative to the skin. A digital output signal from the ultrasound system was used to synchronize data collection of torque, EMG and changes in fascicles. MG muscle fascicle lengths were determined throughout the slow passive and reflex stiffness trials using a semi-automated fascicle tracking algorithm (Cronin et al., 2011; Gillett et al., 2012). The dynamometer measurements of ankle angle and torque, EMG and ultrasound fascicle length data were integrated using customised Matlab (R2015b, The MathWorks, MA, United States) scripts.

Effort was made to keep the test conditions similar for each of the tests. Special focus was on: seating position according to the above mentioned angles; the room temperature (approximately

20°C); no direct, sharp light from windows; that there was quiet in the room while testing, that the subjects had emptied their bladder prior to the experiments, and that the subjects were sitting relaxed during all measurements.

Clinical Evaluation

On the same day of the biomechanical and electrophysiological test each patient underwent a thorough clinical neurological examination conducted by an experienced physiotherapist specialized in neurology. The neurological examination included evaluation of tonus, ankle ROM, and muscle strength in both lower limbs.

Spasticity was evaluated clinically by use of the Modified Ashworth scale (Bohannon and Smith, 1987) which is a five point ordinal scale from 0 = no increase in tone to 4 = Limb rigid in flexion or extension. The Achilles reflex was evaluated by striking the Achilles tendon with a rubber hammer. The Achilles reflex was categorized as either "normal/no reflex response" or "hyperactive."

The examinations were used to decide which extremity that was most affected by hypertonia and/or hyperreflexia. The most hypertonic leg was subsequently selected for the further biomechanical electrophysiological test.

The main results from the clinical tests are summarized in **Table 1**.

All measurements were carried out either in the morning or in the early afternoon with equal proportions for each of the groups. NI adults were matched with regard to the time of measurement for adults with CP.

Parameters of interest included ankle angle (deg), ankle passive- and reflex torque (Nm), MG fascicle length (mm), fascicle length change (mm), and velocity of fascicle length change (mm/s). Fascicle velocities were determined by differentiating fascicle length with respect to time during fast and slow perturbations (Cronin et al., 2013). Fascicle length change for MG was calculated as the difference in MG fascicle length from beginning (baseline) to end of the fast and slow stretch.

Statistics

All statistical analysis was performed in SPSS 22 and figures were made in Sigmaplot 13.0. MG fascicle length and torque parameters during stretches were analyzed using separate linear mixed model analysis. Significant interaction and main effects of Ankle joint position (70, 80, 90, 100, 110, and 120 deg) and group (CP and NI) were explored. The range 70–120 deg was chosen since a position of 60 deg was not possible in any of the adults with CP and a position of 130 deg was only possible in four adults with CP. A position of 70 and 80 deg was obtained in 7 and 8 of the adults with CP, respectively. It was possible to obtain measurements in all adults with CP for the remaining positions and for all ankle joint positions for NI adults.

With significant main effects *post hoc* pairwise comparisons were performed using one-way ANOVA to detect group differences. Tukey adjustment was used in the *post hoc* comparisons to limit the risk of false positive results.

Correlations between torque and fascicle length measurements were analyzed by Spearman correlation coefficient.

The significance level for all statistical tests was set to 0.05.

RESULTS

Mixed model analysis revealed a significant interaction between ankle joint position and group for the amount of passive torque (**Figure 2A**; $df = 6$; $F = 7.4$; $p < 0.001$), but not for the amount of reflex torque (**Figure 2B**; $df = 6$; $F = 1.9$; $p = 0.099$). Passive torque increased significantly with increasing dorsiflexion position as a main effect in the two populations (**Figure 2A**; $df = 7$; $F = 33.8$; $p < 0.001$). *Post hoc* test revealed significantly larger passive torque in the CP than in the NI group at ankle joint positions of 80 and 90 deg (indicated by asterisks in **Figure 2A**; $p < 0.001$).

Reflex torque varied significantly with ankle joint position in the two populations (**Figure 2B**, $F = 9.4$; $p < 0.001$). *Post hoc* test revealed significantly larger reflex torque in the NI group than in the CP group at 80 and 90 deg ($p < 0.05$). Normalization of the reflex torque to the maximal torque elicited by supramaximal stimulation of the tibial nerve showed similar results.

There was no significant interaction between ankle joint position and group for the baseline muscle fascicle length (**Figure 3A**; $F = 0.3$; $p = 0.93$). However, significantly longer fascicles were observed with increasing dorsiflexion position in the two groups ($df = 7$; $F = 11.6$; $p < 0.001$) and the fascicles were found to be shorter in the CP group than in the NI group ($df = 1$; $F = 33.3$; $p < 0.001$). *Post hoc* test showed that this was the case for all joint positions (**Figure 3A**; significance level indicated by asterisks). There was no difference in the extent of the change in fascicle length from the most plantarflexed to the most dorsiflexed position (slope) in the two populations (0.36 mm/deg in NI vs 0.37 mm/deg in CP).

There was no significant interaction between ankle joint position and group for the change in fascicle length induced by a slow (**Figure 3B**; $df = 6$; $F = 1.6$; $p = 0.16$) or fast stretch (**Figure 3C**; $df = 6$; $F = 1.3$; $p = 0.28$). There was also no significant difference between the two groups for the slow stretch ($df = 1$; $F = 1.5$; $p = 0.22$), whereas a significant difference was found for the fast stretch ($df = 1$; $F = 4.1$; $p < 0.05$). For both types of stretch a significant effect of position was observed (slow stretch: $F = 5.4$; $p < 0.01$; fast stretch: $F = 4.8$; $p < 0.01$). *Post hoc* test showed significantly larger change in fascicle length by the slow stretch in the NI group as compared to the CP group at 80 deg ($p < 0.05$) *Post hoc* test showed significantly larger change in fascicle length with the fast stretch in the NI group as compared to the CP group at ankle joint positions of 70, 80, and 90 deg ($p < 0.05$).

There was no interaction between group and position for the velocity of the change in fascicle length during the slow stretches (**Figure 4A**; $df = 1$; $F = 0.38$; $p = 0.85$). In both groups the velocity varied significantly with the position of the ankle joint ($df = 7$; $F = 15.7$; $p < 0.001$) with the highest velocities around ankle joint positions of 80–90 deg. Significantly lower velocities

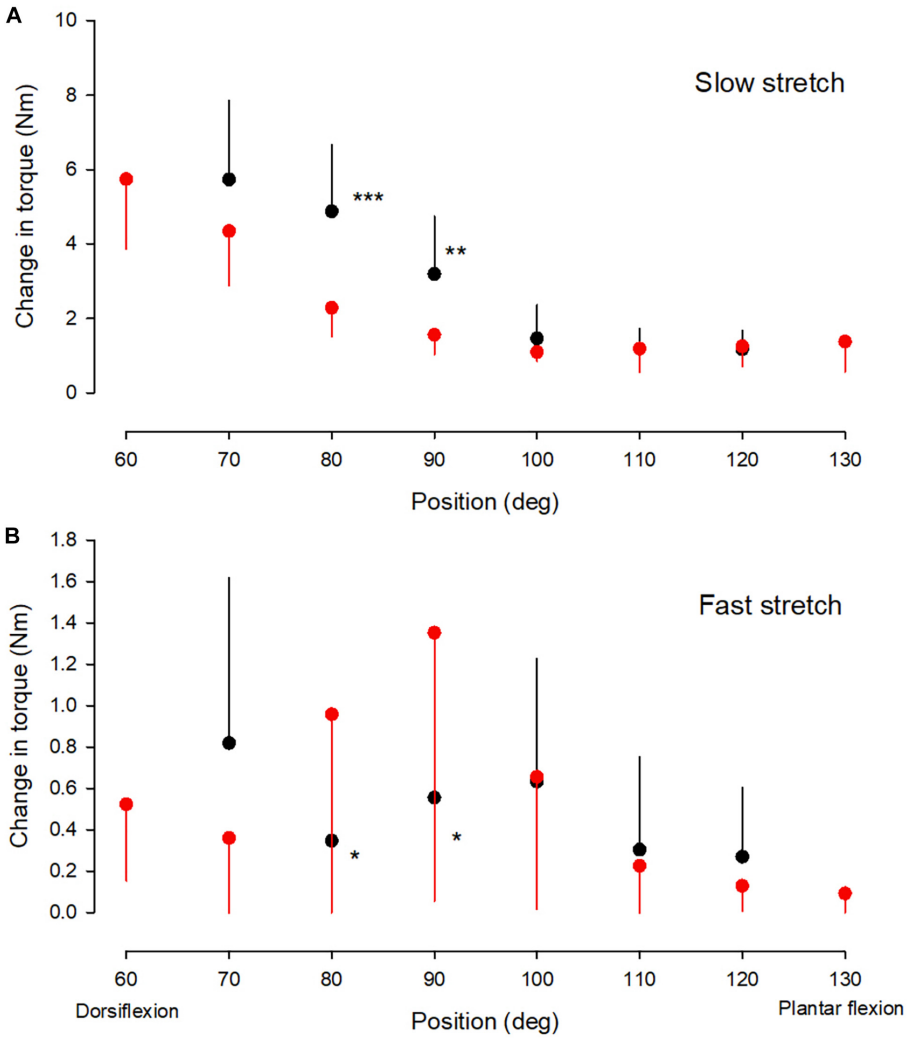

FIGURE 2 | Torque values. The change in passive torque **(A)** and reflex torque **(B)** of the ankle plantarflexor muscle-tendon unit at different ankle joint positions throughout the range of movement in the NI (red circles) and CP group (black circles). It was not possible to obtain measurements at joint positions of 60 and 130 deg in the majority of adults with CP and only measurements from the NI group are therefore shown for these two positions. It was possible to obtain measurements from 7 of the 13 adults with CP at 70 deg and these measurements have therefore also been included. For the remaining positions measurements were obtained from all subjects. Each symbol represents the mean of all measurements in each of the groups at the respective ankle joint positions. Each vertical bar is 1 SD. Statistically significant differences in measurements between the two groups are indicated by stars. *$p < 0.05$, **$p < 0.01$, ***$p < 0.001$.

were observed across all ankle joint positions in the CP group as compared to the NI group ($df = 1$; $F = 38$; $p < 0.001$). *Post hoc* test showed a significant difference between measurements for the two groups at all ankle joint positions except 100 and 120 deg (marked by asterisks in **Figure 4A**).

There was no significant interaction between position and group for the velocity of change in fascicle length during the fast stretches (**Figure 4B**; $df = 5$, $F = 0.3$; $p = 0.85$). The velocity of the change in fascicle length also showed no significant main effect of the position of the ankle joint for the two groups ($df = 6$; $F = 2.5$; $p = 0.1$), but there was a significantly lower velocity in the CP group across all ankle positions ($df = 1$; $F = 19.5$; $p < 0.001$). *Post hoc* test showed a statistically significant difference between measurements in the two groups at ankle joint positions of 90, 100, and 110 deg (marked by asterisks in **Figure 4B**).

In the CP group a significant negative correlation was found between the amount of reflex torque and the amount of passive torque at ankle joint positions of 80 and 90 deg (**Figure 5A**; $r^2 = -0.51$; $p < 0.001$; data at 80 and 90 deg were pooled together). This was not the case in the NI group or at other ankle joint positions in the CP group ($p = 0.15$–0.75). The amplitude of the fascicle length change imposed by fast stretches at ankle joint positions of 80 and 90 deg was also negatively correlated with the amount of passive torque (**Figure 5B**; $r^2 = -0.56$; $p < 0.01$). This was not the case at any other ankle joint positions or in the NI group ($p = 0.2$–0.9). There were also no significant correlations between fascicle length changes and reflex torque in any of the

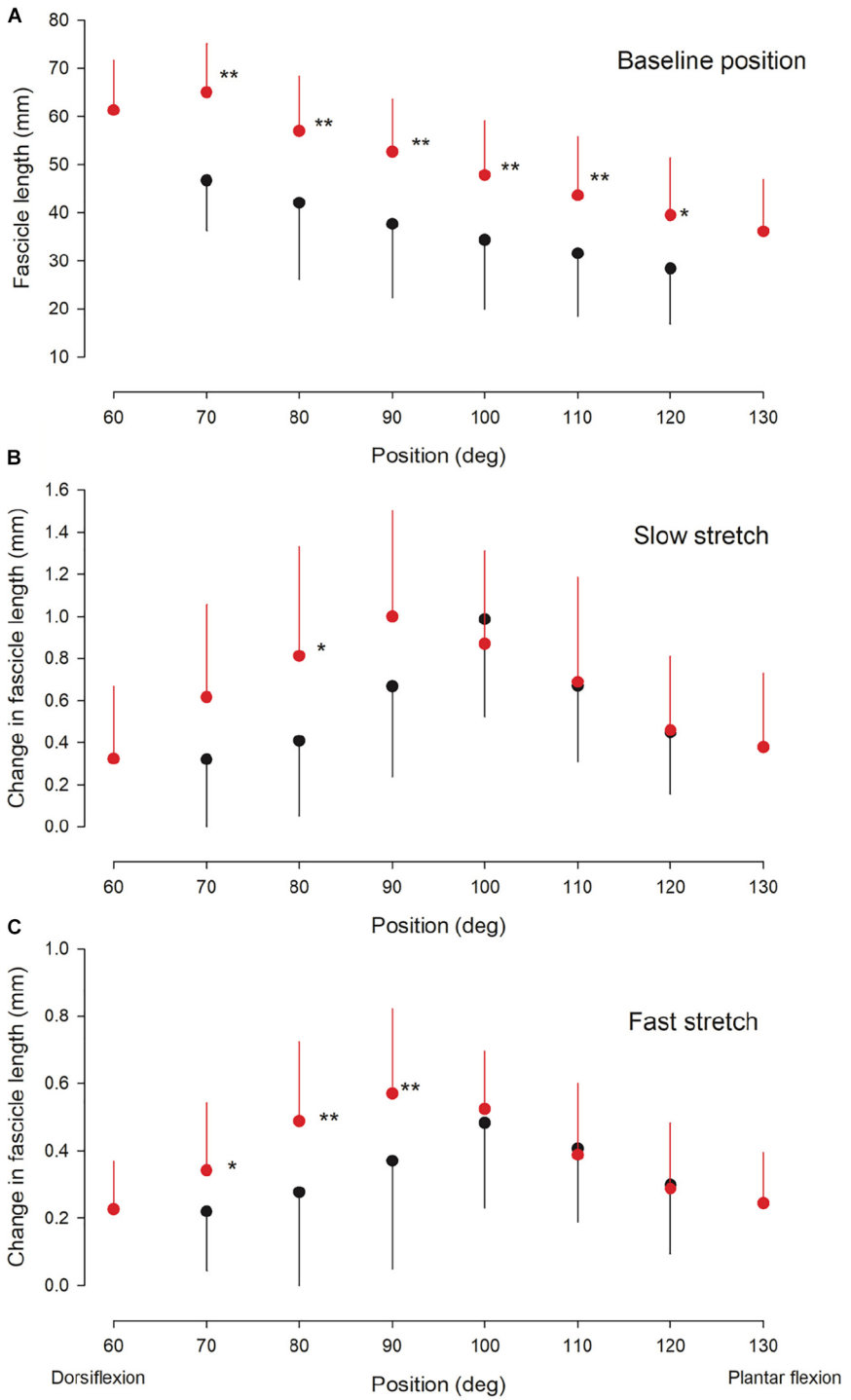

FIGURE 3 | Ultrasound findings. Medial gastrocnemius fascicle length at baseline (rest) **(A)** and the change in medial gastrocnemius muscle fascicle length elicited by a slow **(B)** and fast **(C)** stretch of the ankle plantarflexor muscle-tendon unit at different ankle joint positions throughout the range of movement in the NI (red circles) and CP group (black circles). Otherwise similar legend as for **Figure 2**. Statistically significant differences in measurements between the two groups are indicated by stars. *$p < 0.05$, **$p < 0.01$.

groups ($p > 0.2$). There was also no correlation between the velocity of stretch and the torque measurements at any of the positions or in any of the two groups ($p > 0.1$).

No relation was found between any of the torque measurements and the score on the Modified Ashworth Scale for the adults with CP.

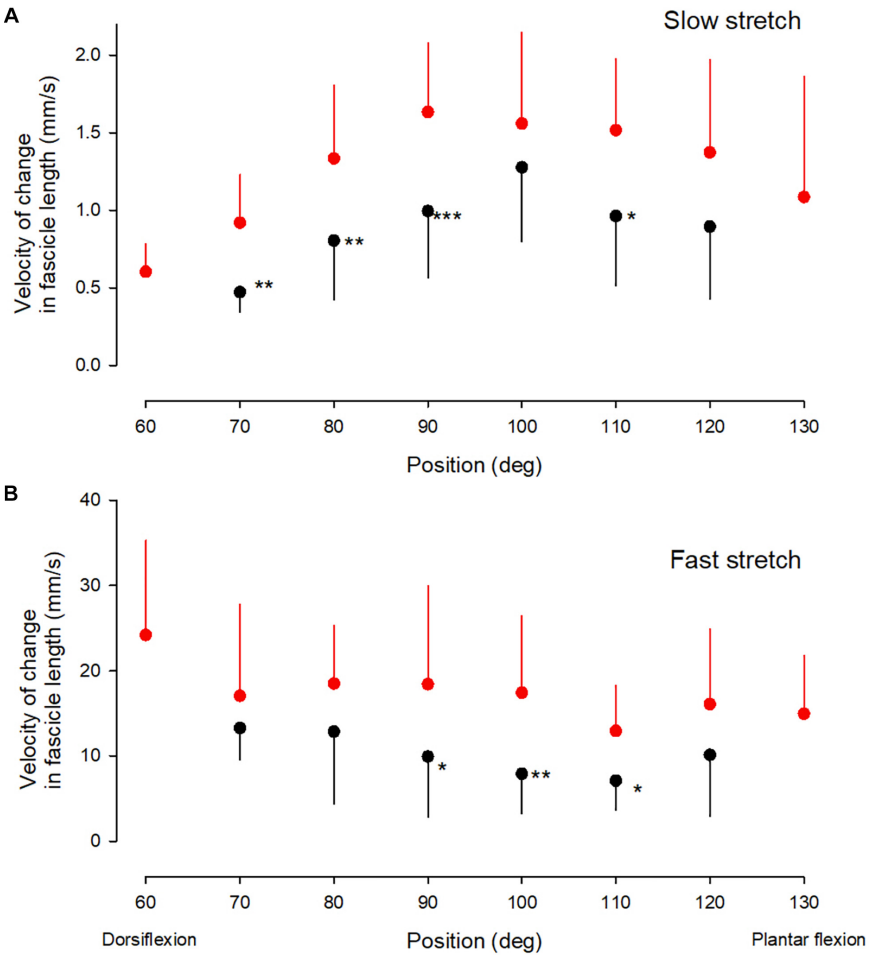

FIGURE 4 | Velocity measurements. Medial gastrocnemius fascicle velocity at different ankle joint positions throughout the range of movement during slow stretch **(A)** and fast stretch **(B)**. Mean, error bar 1 SD. CP, black corcles and NI, red circles. Statistically significant differences in measurements between the two groups are indicated by stars. *$p < 0.05$, **$p < 0.01$, ***$p < 0.001$.

DISCUSSION

In this study, we have found that passive resistance of the ankle plantar flexor joint increases to a larger extent with increasing dorsiflexion position of the ankle joint in a group of adults with CP than in a group of neurologically intact (NI) adults. At the ankle joint positions where larger passive resistance was observed in the CP population, lower reflex torque was elicited by a fast stretch of the ankle plantar flexor muscle unit in the CP group than in the NI group. At the same ankle joint positions, ultrasound measurements showed that the fast stretch lengthened the muscle fascicles less and at a lower velocity in the CP group than in the NI group. These findings indicate that increased passive resistance of the elastic elements in the ankle plantar flexor muscle-tendon unit may diminish the reflex response to a fast stretch and thereby may conceal exaggerated stretch reflexes in people with spasticity.

All individuals in the group of adults with CP had been found to be spastic at some point in their childhood and all referred to themselves as being spastic. In the neurological examination all showed a score on the Modified Ashworth Scale (MAS) of 1 or above 3 used antispastic medication regularly. The finding that the adults with CP did not show larger reflex torque than NI adults – and even showed lower reflex torque than NI adults around the neutral position of the joint – is at variance with the clinical finding of spasticity. This could not be explained by a difference in muscle volume and strength since similar findings were made when the reflex torque measurements were normalized to the maximal muscle torque elicited by supramaximal nerve stimulation.

A number of other studies have similarly failed to demonstrate exaggerated reflexes using objective biomechanical and electrophysiological techniques in patients, who have been diagnosed clinically with spasticity due to multiple sclerosis (Mirbagheri et al., 2008; Lorentzen et al., 2010; Zhang et al., 2014), stroke (Mirbagheri et al., 2008; Lorentzen et al., 2010), spinal cord injury (Lorentzen et al., 2010), or CP (Yamaguchi et al., 2018). As pointed out in several of these

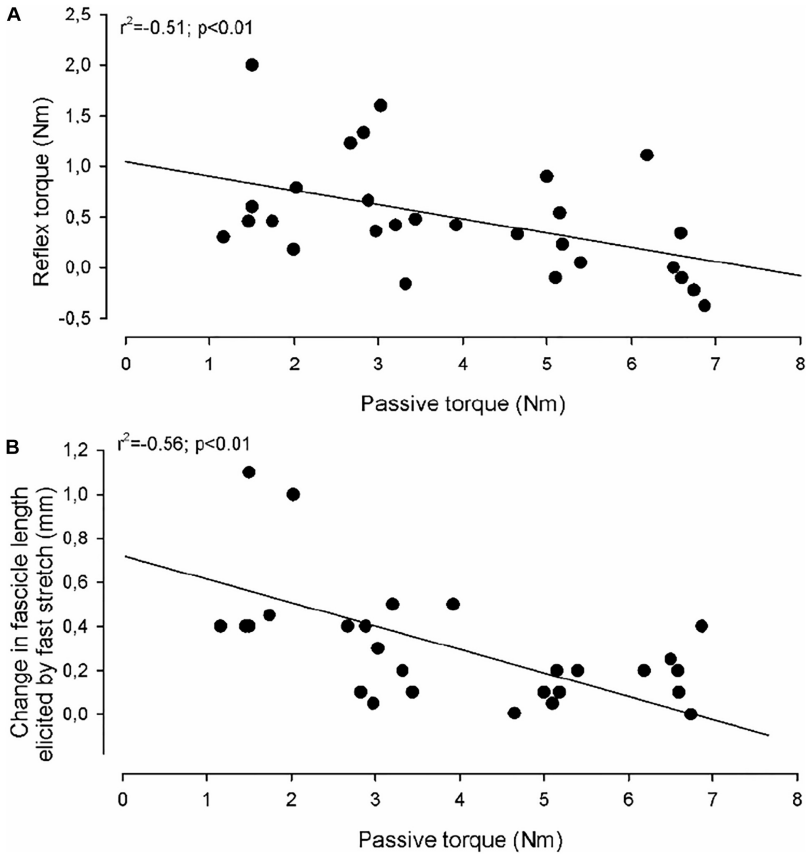

FIGURE 5 | Correlations. In **(A)** the reflex torque in individual adults with CP (elicited by the fast stretch) as a function of the passive torque (elicited by the slow stretch) is shown. **(B)** Shows the change in medial gastrocnemius fascicle length elicited by the fast stretch as a function of the passive torque (elicited by the slow stretch). The full lines indicate the regression lines for the data. The correlation coefficient and statistical significance of the correlation between the measurements using Spearman correlation analysis are given in the upper left part of the graphs.

studies one explanation may be that it is difficult as part of the neurological examination to distinguish whether pathologically increased resistance to movement of a joint is caused by exaggerated reflex (neural) activity or (non-neural) changes in the elastic elements in the muscle, tendon, joint and connective tissue around the joint. This is especially a problem for MAS, which is often used to assess and quantify spasticity clinically, but does not allow a distinction between these two components of resistance to joint manipulation (Biering-Sorensen et al., 2006; Alibiglou et al., 2008; Malhotra et al., 2008). In line with this, no correlation with the MAS score and the torque measurements were observed in the study. Notably some of the adults with CP, who showed a score of 3 or more on MAS showed low reflex torque, but high passive torque.

The observation of a negative correlation between the magnitude of the fascicle length change induced by the fast stretch and the passive torque at joint positions of 80 and 90 deg in the CP populations suggests – together with the observation of a similar negative correlation between passive and reflex torque – that increased resistance of the muscle tissue in the CP group may "protect" the muscle spindles from being stretched sufficiently to cause a significant reflex discharge. Similar findings have been reported previously in children with CP (Bar-On et al., 2018). The findings in our study are therefore not simply explained by the known increase of passive stiffness and decrease of reflex stiffness with age (Geertsen et al., 2017).

The protective effect of increased passive stiffness could theoretically explain why reflexes were not hyperexcitable and even reduced as compared to the NI group at these joint positions in the CP group. However, this is difficult to determine with any certainty since we do not know how large the reflexes would have been in the individual subjects if not for the increased passive stiffness. Furthermore, larger reflexes in the CP group were not observed at joint positions where passive torque was comparable in the two groups. Stretch velocity was somewhat lower at all joint positions in the CP group suggesting that the muscle spindles may have been activated less efficiently in the CP group than in the NI group. Although peripheral factors, such as increased resistance of the elastic tissue in the muscle- or surrounding the spindles, are therefore likely to play some role in the lack of reflex hyperexcitability in the adults with CP, other factors should also be considered. One possible contributing factor is that some of the adults with CP were taking regular antispastic medication and although all were asked to stop medication for a 24 h period

prior to the measurements, it is possible that some effect of the medication still lingered. It is also a possibility that spasticity has simply disappeared in these adults, since they were originally classified as spastic CP early in their childhood. However, all adults in the CP group were found to score at least 1 on the MAS scale and 5 were identified with hyperactive Achilles reflexes.

Our observation of shorter MG fascicle lengths in the CP group than in the NI group is consistent with previous studies in adults with CP (Barber et al., 2011a; Frisk et al., 2019a). Findings in children and youth with CP have been more variable (Malaiya et al., 2007; Mohagheghi et al., 2008; Barber et al., 2011b; Kruse et al., 2018). Some studies have found shorter fascicle lengths (Mohagheghi et al., 2008; Kruse et al., 2018), whereas others have found similar lengths as in age-matched typically developing peers (Malaiya et al., 2007; Barber et al., 2011b). It is likely that differences in normalization or in group selection explains some of this variability in findings. The more consistent findings in adults with CP may indicate progression of atrophy, passive stiffness and contractures with age in the CP population. A history of inactivity and tendon lengthening surgery over several years may contribute to this. However, longitudinal studies are necessary in order to address this issue.

Slow and fast stretch elicited the largest change in fascicle length at ankle joint positions around 90–100 deg; i.e., around the neutral position of the joint, where the maximal amount of voluntary force may also be generated. At more plantar flexed positions significantly smaller length changes were observed with the stretches in both populations suggesting that the muscle was slack at these positions and that more of the imposed stretch was taken up by the tendon and used to tighten the muscle before the fascicle was stretched (Theis et al., 2016; Kalkman et al., 2018). This likely also explains why no significant reflex torque was elicited by the fast stretch at these positions.

The decrease in the fascicle length change and velocity induced by ankle rotation with more dorsiflexed positions than the neutral position of the joint suggests that more force is required to stretch the fascicles at these positions as also evidenced by the increase in the passive torque imposed by the slow stretch. The decrease in the stretch-induced fascicle length change and velocity was observed at slightly more plantar flexed positions in the CP population (i.e., 100 deg in the CP population vs 90 deg in the NI population) and it was accompanied by significantly larger passive torque at these positions. This likely reflects larger passive stiffness of the elastic tissue in the muscle surrounding the muscle spindles at these positions and is likely related to the presence of contractures in the CP population. This is also evidenced by the fact that measurements at 60 deg dorsiflexion was impossible in the CP population and that measurements were only possible in around 50% of the adults with CP at 70 deg.

The lower reflex torque in the CP adults at 80 and 90 deg cannot be explained by a particular low velocity of the fascicle lengthening at those specific positions, since the fascicle length increased at a lower velocity in the CP group than in the NI group at all positions. There was also no significant correlation between the velocity of the fascicle lengthening imposed by the fast stretches and the evoked reflex torque in any of the two groups regardless of normalization. This is surprising since the reflex torque is assumed to be caused by stretch-velocity dependent muscle spindles (Toft, 1995). Evidently other inter-individual factors influence the size of the reflex torque sufficiently to conceal any relation between stretch velocity and reflex size across the different individuals and joint positions.

Functional Implications

The muscle characteristics that we have described in adults with CP in the present study are consistent with previous findings of reduced muscle mass, reduced contractile tissue and infiltration of non-contractile tissue leading to increased passive stiffness and contractures (Gillett et al., 2018; Borg et al., 2019; Frisk et al., 2019a). Reduced muscle mass and muscle strength in combination with reduced mobility of the joint due to the increased stiffness and development of contractures appear to be the main determinants of reduced functional capacity and gait ability in these relatively high functioning and ambulant adults with CP (Geertsen et al., 2015; Gillett et al., 2018; Frisk et al., 2019a). Since the natural history of CP alone is unknown, it is unclear whether antispastic treatment, including botulinum toxin, and surgery, have had a negative or positive impact on the functioning of the group. Nevertheless, the negative correlation between fascicle lengthening and passive stiffness as well as reflex torque indicates that altered muscle properties need to be taken into account when evaluating reflex activity in adults with CP. In contrast, the observation that the mechanical response to fast stretch of the plantar flexor muscles was either reduced or similar to NI individuals depending on the ankle joint position, suggests that hyperexcitability of the spinal stretch reflex circuitry is unlikely to be a major functional challenge for voluntary ankle movement in this group of adults with CP. The increased passive stiffness and decreased reflex stiffness at joint angles of 80 and 90 deg in adults with CP suggests that reduced spindle response to stretch may have acted as an adaptive peripheral countermeasure to increased central excitability of the stretch reflex circuitry. The larger peripheral stiffness may help to ensure stability, but at the cost of larger resistance to movement and reduced movement range. It should also be pointed out that reduced muscle spindle sensitivity does not only affect stretch reflex responses, but probably more importantly from a functional point of view also proprioception and the possibility of integrating information from the spindles into central motor commands.

Clinical Implications

Our findings emphasize the conclusion from several other studies that neural and non-neural components of muscle-tendon stiffness are difficult to tell apart without careful biomechanical and electrophysiological evaluation. Increased resistance of the elastic tissue in the muscles, tendons and joints will require higher and more explosive force in order to stretch the muscles at a sufficiently high velocity to elicit stretch reflex activity and thereby to evaluate the role of reflex hyperexcitability in the clinic. Computer-controlled perturbations using an electromotor as in the present study, guarantees that sufficiently high velocities are reached, but this may not be the case in the clinic where the examiner only have their own ability to generate explosive force to rely on. This emphasizes the need of more precise objective measurement of spasticity in individuals with

CP when initially determining the need for anti-spasticity medication and monitoring change in the relative contribution of hyperexcitability and passive resistance from childhood to adulthood (Lorentzen et al., 2012; Bar-On et al., 2014a,b; Yamaguchi et al., 2018).

DATA AVAILABILITY STATEMENT

The raw data supporting the conclusions of this article will be made available by the authors, without undue reservation.

ETHICS STATEMENT

The studies involving human participants were reviewed and approved by Ethics Committee of the Greater Copenhagen area. The patients/participants provided their written informed consent to participate in this study.

AUTHOR CONTRIBUTIONS

All authors participated in the planning and discussion of the study. JL wrote first draft of the manuscript. All authors read, edited, and commented on the manuscript. All authors accepted the final version of the manuscript for publication. All authors contributed to the article and approved the submitted version.

FUNDING

The study was funded by a grant to JN from the Elsass Foundation, which is a private foundation with the aim of supporting research in cerebral palsy.

REFERENCES

Alibiglou, L., Rymer, W. Z., Harvey, R. L., and Mirbagheri, M. M. (2008). The relation between ashworth scores and neuromechanical measurements of spasticity following stroke. *J. Neuroeng. Rehabil.* 5:18. doi: 10.1186/1743-0003-5-18

Barber, L., Barrett, R., and Lichtwark, G. (2011a). Passive muscle mechanical properties of the medial gastrocnemius in young adults with spastic cerebral palsy. *J. Biomech.* 44, 2496–2500.

Barber, L., Hastings-Ison, T., Baker, R., Barrett, R., and Lichtwark, G. (2011b). Medial gastrocnemius muscle volume and fascicle length in children aged 2 to 5 years with cerebral palsy. *Dev. Med. Child Neurol.* 53, 543–548. doi: 10.1111/j.1469-8749.2011.03913.x

Bar-On, L., Aertbeliën, E., Molenaers, G., Dan, B., and Desloovere, K. (2014a). Manually controlled instrumented spasticity assessments: a systematic review of psychometric properties. *Dev. Med. Child Neurol.* 56, 932–950. doi: 10.1111/dmcn.12419

Bar-On, L., Kalkman, B. M., Cenni, F., Schless, S. H., Molenaers, G., Maganaris, C. N., et al. (2018). The relationship between medial gastrocnemius lengthening properties and stretch reflexes in cerebral palsy. *Front. Pediatr.* 6:259. doi: 10.3389/fped.2018.00259

Bar-On, L., Van Campenhout, A., Desloovere, K., Aertbeliën, E., Huenaerts, C., Vandendoorent, B., et al. (2014b). Is an instrumented spasticity assessment an improvement over clinical spasticity scales in assessing and predicting the response to integrated botulinum toxin type a treatment in children with cerebral palsy? *Arch. Phys. Med. Rehabil.* 95, 515–523. doi: 10.1016/j.apmr.2013.08.010

Baude, M., Nielsen, J. B., and Gracies, J. M. (2019). The neurophysiology of deforming spastic paresis: a revised taxonomy. *Ann. Phys. Rehabil. Med.* 62, 426–430.

Bax, M., Goldstein, M., Rosenbaum, P., Leviton, A., Paneth, N., Dan, B., et al. (2005). Executive committee for the definition of cerebral palsy. proposed definition and classification of cerebral palsy, April 2005. *Dev. Med. Child Neurol.* 47, 571–576. doi: 10.1017/s001216220500112x

Bénard, M. R., Becher, J. G., Harlaar, J., Huijing, P. A., and Jaspers, R. T. (2009). Anatomical information is needed in ultrasound imaging of muscle to avoid potentially substantial errors in measurement of muscle geometry. *Muscle Nerve* 39, 652–665. doi: 10.1002/mus.21287

Biering-Sorensen, F., Nielsen, J. B., and Klinge, K. (2006). Spasticity-assessment: a review. *Spinal Cord* 44, 708–722.

Bodine, S. C. (2013). Disuse-induced muscle wasting. *Int. J. Biochem. Cell Biol.* 45, 2200–2208.

Bohannon, R. W., and Smith, M. B. (1987). Interrater reliability of a modified ashworth scale of muscle spasticity. *Phys. Ther.* 67, 206–207. doi: 10.1093/ptj/67.2.206

Borg, L., Sporring, J., Dam, E. B., Dahl, V. A., Dyrby, T. B., Feidenhans'l, R., et al. (2019). Muscle fibre morphology and microarchitecture in cerebral palsy patients obtained by 3D synchrotron X-ray computed tomography. *Comput. Biol. Med.* 107, 265–269. doi: 10.1016/j.compbiomed.2019.02.008

Bottos, M., Feliciangeli, A., Sciuto, L., Gericke, C., and Vianello, A. (2001). Functional status of adults with cerebral palsy and implications for treatment of children. *Dev. Med. Child Neurol.* 43, 516–528. doi: 10.1017/s0012162201000950

Carrasco, D. I., Vincent, J. A., and Cope, T. C. (2017). Distribution of TTX-sensitive voltage-gated sodium channels in primary sensory endings of mammalian muscle spindles. *J. Neurophysiol.* 117, 1690–1701.

Cremer, N., Hurvitz, E. A., and Peterson, M. D. (2017). Multimorbidity in Middle-Aged adults with cerebral palsy. *Am. J. Med.* 130, 744.e9-744.e15.

Cronin, N. J., Avela, J., Finni, T., and Peltonen, J. (2013). Differences in contractile behaviour between the soleus and medial gastrocnemius muscles during human walking. *J. Exp. Biol.* 216, 909–914. doi: 10.1242/jeb.078196

Cronin, N. J., Carty, C. P., Barrett, R. S., and Lichtwark, G. (2011). Automatic tracking of medial gastrocnemius fascicle length during human locomotion. *J. Appl. Physiol.* 111, 1491–1496. doi: 10.1152/japplphysiol.00530.2011

de Bruin, M., Smeulders, M. J., Kreulen, M., Huijing, P. A., and Jaspers, R. T. (2014). Intramuscular connective tissue differences in spastic and control muscle: a mechanical and histological study. *PLoS One* 9:e101038. doi: 10.1371/journal.pone.0101038

Frisk, R. F., Jensen, P., Kirk, H., Bouyer, L. J., Lorentzen, J., and Nielsen, J. B. (2017). Contribution of sensory feedback to plantar flexor muscle activation during push-off in adults with cerebral palsy. *J. Neurophysiol.* 118, 3165–3174. doi: 10.1152/jn.00508.2017

Frisk, R. F., Lorentzen, J., and Nielsen, J. B. (2019b). Contribution of corticospinal drive to ankle plantar flexor muscle activation during gait in adults with cerebral palsy. *Exp. Brain Res.* 237, 1457–1467. doi: 10.1007/s00221-019-05520-3

Frisk, R. F., Lorentzen, J., Barber, L., and Nielsen, J. B. (2019a). Characterization of torque generating properties of ankle plantar flexor muscles in ambulant adults with cerebral palsy. *Eur. J. Appl. Physiol.* 119, 1127–1136. doi: 10.1007/s00421-019-04102-z

Geertsen, S. S., Kirk, H., Lorentzen, J., Jorsal, M., Johansson, C. B., and Nielsen, J. B. (2015). Impaired gait function in adults with cerebral palsy is associated with reduced rapid force generation and increased passive stiffness. *Clin. Neurophysiol.* 126, 2320–2329. doi: 10.1016/j.clinph.2015.02.005

Geertsen, S. S., Willerslev-Olsen, M., Lorentzen, J., and Nielsen, J. B. (2017). Development and aging of human spinal cord circuitries. *J. Neurophysiol.* 118, 1133–1140. doi: 10.1152/jn.00103.2017

Gillett, J. G., Barrett, R. S., and Lichtwark, G. A. (2012). Reliability and accuracy of an automated tracking algorithm to measure controlled passive and active muscle fascicle length changes from ultrasound. *Comput. Methods Biomech. Biomed. Engin.* 16, 678–687.

Gillett, J. G., Lichtwark, G. A., Boyd, R. N., and Barber, L. A. (2018). Functional capacity in adults with cerebral palsy: lower limb muscle strength matters. *Arch. Phys. Med. Rehabil.* 99:900-906.e1. doi: 10.1016/j.apmr.2018.01.020

Graham, H. K., Rosenbaum, P., Paneth, N., Dan, B., Lin, J. P., Damiano, D. L., et al. (2016). Cerebral palsy. *Nat. Rev. Dis. Primers* 2:15082. doi: 10.1038/nrdp.2015.82

Jalal, N., Gracies, J. M., and Zidi, M. (2020). Mechanical and microstructural changes of skeletal muscle following immobilization and/or stroke. *Biomech. Model Mechanobiol.* 19, 61–80.

Kalkman, B. M., Bar-On, L., Cenni, F., Maganaris, C. N., Bass, A., Holmes, G., et al. (2018). Muscle and tendon lengthening behaviour of the medial gastrocnemius during ankle joint rotation in children with cerebral palsy. *Exp. Physiol.* 103, 1367–1376. doi: 10.1113/EP087053

Klimstra, M., Dowling, J., Durkin, J. L., and MacDonald, M. (2007). The effect of ultrasound probe orientation on muscle architecture measurement. *J. Electromyogr. Kinesiol.* 17, 504–514. doi: 10.1016/j.jelekin.2006.04.011

Kruse, A., Schranz, C., Tilp, M., and Svehlik, M. (2018). Muscle and tendon morphology alterations in children and adolescents with mild forms of spastic cerebral palsy. *BMC Pediatr.* 18:156. doi: 10.1186/s12887-018-1129-4

Lorentzen, J., Grey, M. J., Crone, C., Mazevet, D., Biering-Sørensen, F., and Nielsen, J. B. (2010). Distinguishing active from passive components of ankle plantar flexor stiffness in stroke, spinal cord injury and multiple sclerosis. *Clin. Neurophysiol.* 121, 1939–1951. doi: 10.1016/j.clinph.2010.02.167

Lorentzen, J., Grey, M. J., Geertsen, S. S., Biering-Sørensen, F., Brunton, K., Gorassini, M., et al. (2012). Assessment of a portable device for the quantitative measurement of ankle joint stiffness in spastic individuals. *Clin. Neurophysiol.* 123, 1371–1382. doi: 10.1016/j.clinph.2011.11.001

Maganaris, C. N., Baltzopoulos, V., and Sargeant, A. J. (2002). Repeated contractions alter the geometry of human skeletal muscle. *J. Appl. Physiol.* 93, 2089–2094.

Malaiya, R., McNee, A. E., Fry, N. R., Eve, L. C., Gough, M., and Shortland, A. P. (2007). The morphology of the medial gastrocnemius in typically developing children and children with spastic hemiplegic cerebral palsy. *J. Electromyogr. Kinesiol.* 17, 657–663. doi: 10.1016/j.jelekin.2007.02.009

Malhotra, S., Cousins, E., Ward, A., Day, C., Jones, P., Roffe, C., et al. (2008). An investigation into the agreement between clinical, biomechanical and neurophysiological measures of spasticity. *Clin. Rehabil.* 22, 1105–1115. doi: 10.1177/0269215508095089

Mirbagheri, M. M., Tsao, C., Settle, K., Lilaonitkul, T., and Rymer, W. Z. (2008). Time course of changes in neuromuscular properties following stroke. *Annu. Int. Conf. IEEE Eng. Med. Biol. Soc.* 2008, 5097–5100. doi: 10.1109/IEMBS.2008.4650360

Mohagheghi, A. A., Khan, T., Meadows, T. H., Giannikas, K., Baltzopoulos, V., and Maganaris, C. N. (2008). In vivo gastrocnemius muscle fascicle length in children with and without diplegic cerebral palsy. *Dev. Med. Child Neurol.* 50, 44–50. doi: 10.1111/j.1469-8749.2007.02008.x

Morgan, P., and McGinley, J. (2014). Gait function and decline in adults with cerebral palsy: a systematic review. *Disabil. Rehabil.* 36, 1–9.

Narici, M., Franchi, M., and Maganaris, C. (2016). Muscle structural assembly and functional consequences. *J. Exp. Biol.* 219(Pt. 2), 276–284.

Peterson, M. D., Ryan, J. M., Hurvitz, E. A., and Mahmoudi, E. (2015). Chronic conditions in adults with cerebral palsy. *JAMA* 314, 2303–2305. doi: 10.1001/jama.2015.11025

Singer, B., Dunne, J., and Allison, G. (2001). Reflex and non-reflex elements of hypertonia in triceps surae muscles following acquired brain injury: implications for rehabilitation. *Disabil. Rehabil.* 23, 749–757.

Theis, N., Mohagheghi, A. A., and Korff, T. (2016). Mechanical and material properties of the plantarflexor muscles and Achilles tendon in children with spastic cerebral palsy and typically developing children. *J. Biomech.* 49, 3004–3008.

Toft, E. (1995). Mechanical and electromyographic stretch responses in spastic and healthy subjects. *Acta Neurol. Scand. Suppl.* 163, 1–24.

Toft, E., Sinkjaer, T., Andreassen, S., and Larsen, K. (1991). Mechanical and electromyographic responses to stretch of the human ankle extensors. *J. Neurophysiol.* 65, 1402–1410. doi: 10.1152/jn.1991.65.6.1402

Willerslev-Olsen, M., Lorentzen, J., Sinkjaer, T., and Nielsen, J. B. (2013). Passive muscle properties are altered in children with cerebral palsy before the age of 3 years and are difficult to distinguish clinically from spasticity. *Dev. Med. Child Neurol.* 55, 617–623. doi: 10.1111/dmcn.12124

Windhorst, U. (2008). Muscle spindles are multi-functional. *Brain Res. Bull.* 75, 507–508.

Yamaguchi, T., Hvass Petersen, T., Kirk, H., Forman, C., Svane, C., Kofoed-Hansen, M., et al. (2018). Spasticity in adults with cerebral palsy and multiple sclerosis measured by objective clinically applicable technique. *Clin. Neurophysiol.* 129, 2010–2021. doi: 10.1016/j.clinph.2018.07.004

Zhang, L. Q., Chen, K., Kang, S. H., Sliwa, J. A., Cohen, B. A., Rymer, W. Z., et al. (2014). Characterizations of reflex and nonreflex changes in spastic multiple sclerosis. *J. Neurosci. Methods* 231, 3–8. doi: 10.1016/j.jneumeth.2014.01.014

Conflict of Interest: The authors declare that the research was conducted in the absence of any commercial or financial relationships that could be construed as a potential conflict of interest.

Advantages of publishing in Frontiers

OPEN ACCESS
Articles are free to read for greatest visibility and readership

FAST PUBLICATION
Around 90 days from submission to decision

HIGH QUALITY PEER-REVIEW
Rigorous, collaborative, and constructive peer-review

TRANSPARENT PEER-REVIEW
Editors and reviewers acknowledged by name on published articles

Frontiers
Avenue du Tribunal-Fédéral 34
1005 Lausanne | Switzerland

Visit us: www.frontiersin.org
Contact us: frontiersin.org/about/contact

REPRODUCIBILITY OF RESEARCH
Support open data and methods to enhance research reproducibility

DIGITAL PUBLISHING
Articles designed for optimal readership across devices

FOLLOW US
@frontiersin

IMPACT METRICS
Advanced article metrics track visibility across digital media

EXTENSIVE PROMOTION
Marketing and promotion of impactful research

LOOP RESEARCH NETWORK
Our network increases your article's readership